The Institute of Paper Science and Technology

Atlanta, Georgia

Doctor's Dissertation

A Raman Microspectroscopic Investigation of the Patterns of Molecular Order in the Secondary Cell Walls of Black Spruce and Loblolly Pine Tracheids

James S. Bond

June, 1991

A RAMAN MICROSPECTROSCOPIC INVESTIGATION OF THE PATTERNS OF MOLECULAR ORDER IN THE SECONDARY CELL WALLS OF BLACK SPRUCE AND LOBLOLLY PINE TRACHEIDS

A Thesis submitted by

James S. Bond

B.S. 1981, University of Wisconsin - Green Bay

M.S. 1983, University of Wisconsin - Green Bay

M.S. 1986, Lawrence University

In partial fulfillment of the requirements of
The Institute of Paper Science and Technology for
the degree of Doctor of Philosophy
Atlanta, Georgia

June, 1991

TABLE OF CONTENTS

SUMMARY

Our understanding of the molecular architecture of intact, native plant cell walls is very limited. Traditional methods of investigation rely on techniques which disturb the tissue to varying degrees. Conclusions based on these methods may be intimately related to the techniques used. A promising new technique to study native-state organization and compositional variability in plant cell walls is polarized Raman microspectroscopy. Information obtained from this method should complement that from traditional methods of investigation.

The purpose of this present work was to investigate the macromolecular orientation and compositional variability for both cellulose and lignin in the latewood (S_2) secondary cell walls of loblolly pine and, to a lesser extent, black spruce tracheids using laser Raman spectroscopy. During the early stages of this study, it was recognized that lignin underwent photo-induced changes, i.e., the probe was not entirely nonintrusive. Raman microprobe studies of both black spruce's and loblolly pine's S_2 cell wall layer showed that the intensity of 1595 cm^{-1} aromatic ring-breathing vibrational band of lignin decreased during 514.5 nm laser irradiation. Because of this, the focus of the study changed. The level of detail initially envisioned for the spectral mapping of the biopolymers was not possible without additional foundation work relating to this decay phenomenon.

The first part of this investigation was directed towards understanding the factors which contributed to the photomodification of lignin. Model compound studies and using several excitation frequencies revealed that the 1595 cm^{-1} band was subject to two enhancement mechanisms. The first of these was conjugation enhancement (CE). It arose from aromatic ring conjugated groups in the lignin macromolecule, e.g., α-carbonyls and α-β double bonds that occur in the propyl side chain. Preresonance Raman enhancement (PRRE) was the second mechanism. It was due to the absorption of 514.5 nm photons by structures in lignin. The structural units responsible for this absorption included some of the same lignin subunits that gave rise to CE. For black spruce, approximately 49% of 1595 cm^{-1} band intensity was due to CE, 37% was due to PRRE, and the remainder (14%) due to nonenhanced Raman scattering from an idealized basic phenylpropane unit. For loblolly pine, these percentages were 33%, 56%, and 11%, respectively. The difference in values between the two wood species may reflect differences in the subunits which comprise the lignin macromolecule.

Evidence supported the idea that the decay of the 1595 cm^{-1} band was due to the disruption of these enhancement mechanisms with an accompanying loss of aromaticity. Scanning electron micrographs of the irradiated area revealed a feature whose topography supported the idea that cell wall material, i.e., lignin, was being solubilized. It was felt that phenoxy-type radicals were key players in the decay process.

Attempts to stabilize lignin to laser radiation met with little success. Reduction, oxidation, and substitution reactions of the lignin macromolecule, as well as the use of fluorescence quenchers/radical scavengers failed to stop the decay. The chemical treatments did, however, alter the percent contribution of CE/PRRE to the 1595 cm^{-1} band intensity. Several of the treatments showed promise, but unwanted side reactions prevented their use, e.g., decay was minimized when using a nonaqueous immersion medium (glycerol) but sample burning occurred.

A methodology that was thought to minimize the photomodification of lignin was followed in the spectral mapping studies of cellulose and lignin. This involved a mild acid-chlorite treatment (black spruce) prior to data acquisition, using low laser power levels, keeping acquisition time to a minimum, and treating each acquisition location identically. Sixty neighboring locations were studied for black spruce, fifty for loblolly pine. These locations included three distinct morphological regions: the S_2 cell wall layer of one fiber, the compound middle lamella (CML) between, and the S_2 layer of the adjoining fiber.

Analysis of the data confirmed that in loblolly pine, on the average, cellulose was not uniformly distributed in the three regions. The peak cellulose concentration occurred in the inner S_2 cell wall layer and declined to a minimum near the CML. This trend was also seen for the adjoining fiber, although the peak concentration differed slightly. The data also suggested

that the chain axis of cellulose was more oriented parallel to the cell wall (in a radial section) in the inner S_2 layer and this became less pronounced closer to the CML.

Lignin also showed a nonuniform distribution. The 1595 cm^{-1} lignin peak intensity decreased from a high value near the lumen to a minimum in the outer S_2, and then increased in the CML region. This was paralleled in the adjoining fiber. It was unknown if the data reflected a true lignin concentration gradient or whether the degree of 1595 cm^{-1} band enhancement (reflecting structural differences in lignin macromolecule) varied over these regions. The data also suggested, in general, the aromatic rings of the phenylpropane units in lignin are slightly more oriented parallel to the cell wall (in a radial section) in the inner S_2 regions and thus, parallels the trend seen for cellulose. These data taken together support the idea that during biogenesis, cellulose may act as a template for lignin organization.

The lignin-to-cellulose ratio was fairly flat for both S_2 regions but showed a strong peak in the CML. This peak reflected the lower cellulose concentration and the higher lignin concentration/degree of enhancement in this region.

In addition to these average trends across the three morphological regions, the molecular organization of cellulose and lignin was found to vary along these regions as well. This may be indicative of the occurrence of

nodes in the organization of these components.

The interpretation of the black spruce data was more complex. The mirroring of the trends in organization for the adjoining fibers was not seen. For one fiber (A), on the average, the peak cellulose concentration occurred in the inner S_2 and declined to a minimum in the outer S_2 and remained at that level in the CML. The adjoining fiber (B) showed a flatter cellulose profile. For this fiber, only a slight peak in concentration was seen to occur in the middle of the S_2 cell wall layer. The data suggested that for one of the fibers (A), the chain axis of cellulose was more oriented parallel to the cell wall (radial section) in the inner S_2 and this orientation became less pronounced closer to the CML. This preferential orientation was not as apparent for the adjoining fiber (B).

The trends in the 1595 cm^{-1} band intensity of lignin paralleled those seen for cellulose. The intensification of this band in the CML region that occurred in the loblolly pine data was not seen. It was felt that specific subunits in the CML lignin may have been very sensitive to the acid-chlorite pretreatment and consequently, the enhancement of the 1595 cm^{-1} in this region was disrupted.

The lignin-to-cellulose ratio was fairly flat throughout S_2/CML/S_2 region. The strong peak seen in the loblolly pine data was not apparent; this most probably reflected the disruption of the 1595 cm^{-1} band enhancement

mechanisms.

It is not known to what extent these black spruce data represented the actual native-state cell wall organization, but it was felt that the acid-chlorite pretreatment, as well as the sensitivity of black spruce lignin to 514.5 nm radiation may have biased the (lignin) data.

This present study laid the foundation for future systematic spectral mapping studies of the two major biopolymers, i.e., cellulose and lignin, in secondary plant cell walls in addition to providing a glimpse into the molecular organization of these walls.

PREFACE

As initially envisioned, the purpose of this thesis was to probe the molecular architecture of native plant cell walls using laser Raman spectroscopy. Specifically, investigating the patterns of organization for both cellulose and lignin in the S_2 latewood cell wall layers of loblolly pine and, to a lesser extent, black spruce tracheids was to have been the emphasis of the study. The early experiments revealed that certain substructures in the lignin macromolecule with enhanced Raman scattering coefficients were not stable to 514.5 nm laser radiation but underwent photo-induced changes. The intensity of the 1595 cm^{-1} aromatic ring-breathing vibrational band of lignin decayed with irradiation time under some conditions. A considerable effort was invested in exploring this photodecay, both because it had to be adequately dealt with if the spectral mapping studies of the biopolymers were to reflect their native-state organization, and because of the new insights it provided about species which are constituents of native lignin, but which very likely become fugitive in the course of most preparative procedures.

The thesis thus deals with several distinct but intimately related subjects. These are the photomodification and photostabilization of native-state lignin, Raman intensity enhancement effects, and the molecular architecture of softwood cell walls.

The thesis is divided into three main sections: Introduction, Experimental Material and Methods, and Results and Discussion. The Introduction begins with a brief discussion of the woody cell wall; its components, their organization and methods of investigation are covered. This is followed by a statement of the revised thesis objectives reflecting the transience of intensity in the 1595 cm^{-1} lignin band.

The major portion of the Introduction is devoted to a review of the pertinent literature. The first part of the review is concerned with the photochemistry of wood and related materials. It is subdivided into three sections: near-UV and visible light chromophores, photodegradative reactions, and photostabilization methods. The literature pertaining to enhancement effects on the Raman intensities of aromatic compounds is surveyed in the next part of the review. The review finishes with an in-depth examination of the (woody) plant cell wall; the biogenesis, distribution, and organization of the major components are covered.

The Introduction concludes with a section on theory. The principles of photochemistry are discussed in the first part of this section, while the Raman scattering process and Raman band enhancement effects are addressed in the second. This section provides the reader with the theoretical background that is needed to understand certain aspects of the thesis.

The second major section of the thesis, titled Experimental Material and Methods, is a presentation of the experimental plan, apparatus and procedures which were used. The section is divided into six main areas: Experimental Program, Instrumentation, Species Selection, Sample Preparation, Spectral Enhancement, and Lignin Model Compounds. Instrumentation is further subdivided into two major areas reflecting the two different types of Raman systems which were used in the investigation: macro- and micro-Raman instruments. The classification is based upon the size of the data acquisition region.

The third major section is titled Results and Discussion. In the first part of this section the results of the investigation into understanding the photodecay of the 1595 cm^{-1} aromatic ring-breathing vibrational band of lignin are presented. This initial section is further divided into three main subsections: Cell Wall Feature, Conjugation and Preresonance Raman Enhancement, and Photostabilization of Lignin. The first subsection presents the results of the investigation of the feature which developed at the location on the cell wall where the laser beam was focused while acquiring the Raman spectrum. The results of the study of Raman band intensity enhancement mechanisms using lignin model compounds and native woody tissue are detailed in the second subsection. The subsection titled Photostabilization of Lignin reports on the results of experiments to determine the causes of the photo-induced changes that occurred in the lignin macromolecule during laser irradiation and attempts to achieve photostabilization.

In the second part of the Results and Discussion section, the results of the spectral mapping of the organization of cellulose and lignin in the secondary cell walls of black spruce and loblolly pine are presented. Although complete photostabilization of lignin was not achieved, a methodology that was thought to minimize the bias introduced by lignin photomodification was followed in these studies.

In addition to the three main sections described above are three smaller sections titled: Conclusions, Recommendations, and Appendices. The Conclusions section presents the major findings of this study in a concise form. Recommendations contains suggestions for future work in this area. The Appendices contain representative raw data, the specifics for the chemical treatments, and a published paper reporting on a portion of this work.

INTRODUCTION

PERSPECTIVE

The use of plant fibers is widespread in our society. The pulp and paper industry and, to a lesser extent, the textile industry derive their livelihood from these materials. The suitability of these various fibers for specific applications is closely related to their development and molecular properties.[1] Preston[2] has stated in reference to wood fibers that the hoped-for optimization of these natural materials will require an even more complete knowledge of their properties and development. This notion was echoed by James d'A. Clark[3] when he stated that "the more one knows about the fundamental nature of a material or process, the more likely it is that some improvement can be effected." One area that is lacking in our understanding of the cell wall is the way in which the chemical constituents are structurally organized.

Cellulose, hemicelluloses, and lignin are the major components of plant cell walls and basically establish the chemical and physical nature of the wall (Table 1). As can be seen from this table, cellulose, the β-1,4 linked polymer of anhydroglucose, is the primary component. The principal function of cellulose in the cell wall is to provide a framework while hemicelluloses and lignin serve as matrix materials. The secondary (or minor) components consist of inorganic materials and extractable compounds and typically impart certain characteristics to wood, e.g., color and resistance to disease, but

are not an essential part of the structure of the cell wall.[4]

The cell wall consists of an intricate intermixing of the various components. Figure 1 is a generalized diagram of cell wall organization in a softwood tracheid. The wall consists of concentric lamellae which are organized in a primary wall (P) and a secondary wall in three layers (S_1, S_2, and S_3). The primary wall is laid down in the initial stages of growth. The secondary wall is formed when cell enlargement ceases. The warty layer is believed to consist of a localized thickening of the S_3 layer together with the denatured remnants of the membranous portions of the cytoplasm.[1,4] The exact physical arrangement of cellulose, hemicellulose, and lignin is, for the most part, not known. Most of the investigations have focused on the primary wall; information about the secondary wall is lacking.

Traditional methods of cell wall investigation fall into two major categories.[6,7] The first provides structural information on the molecular level derived from physico-chemical analyses of isolated cell wall components. Techniques using optical and electron microscopy which provide descriptions of cell wall morphology are included in the second category. Although both have been frequently used to elucidate the structure of the cell wall, there are shortcomings associated with each. In the first category, the procedures used to isolate the cell wall components are extremely disruptive of the native-state structures[8] and conclusions drawn from this information are open to question. While the second category has been useful in describing the

Table 1. Schematic Classification of the Chemical Components of Cell Wall Substance in Normal Wood. Percentages Based on Ovendry Weight.[4]

I. Primary Components
   A. Total polysaccharide fractions, expressed as holocellulose -- 60-85%
      1. Cellulose -- 40-50%
         Long-chain polymer generally with low solubility
      2. Hemicellulose -- 20-35%
         Noncellulosic polysaccharides; these are readily soluble in dilute alkali and hydrolyzable by dilute acids to component sugars and uronic acids
   B. Lignin -- 15-35%

II. Secondary Components
   A. Tannins
   B. Volatile oils and resins
   C. Gums, latex, alkaloids, and other complex organic compounds including dyes and coloring materials
   D. Ash -- usually less than 1% (domestic woods)

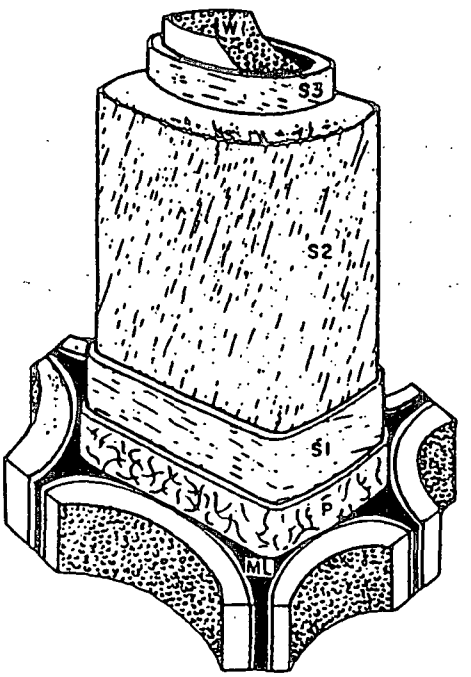

Figure 1. Diagram of cell wall organization. ML - middle lamella, P - primary wall, S - secondary wall, W - warty layer.[5]

morphology of the cell wall, it is very limited in the information it can provide about molecular structure.

Recently developed techniques using electron microscopy, e.g., energy dispersive X-ray analysis (SEM-EDXA), to investigate the distribution of lignin in the cell wall are not well developed and are not without their problems.[9]

Polarized Raman microspectroscopy is a promising new technique to investigate both the orientation and compositional variability of the major cell wall components in undisturbed plant tissue.[10,125] Although the Raman effect was first observed in 1928, it was not until the advent of the intense, monochromatic excitation beam that the laser provided that this vibrational spectroscopy technique advanced. The recent development of the laser Raman microprobe (a combination of a microscope and a Raman spectrometer) has opened up new areas of investigation that were heretofore not possible.[200-202] Information derived from this technique should complement that obtained from the traditional methods of investigation.

The initial purpose of this present work was to examine the organization for both cellulose and lignin in the latewood, secondary cell walls of loblolly pine and, to a lesser extent, black spruce using laser Raman microspectroscopy. As the thesis evolved and it was recognized that certain substructures in the lignin macromolecule were not stable to 514.5 nm laser radiation the

focus, of necessity, changed. Prior to the systematic spectral mapping of the biopolymers' organization, additional foundation work relating to the photo-induced changes in the lignin macromolecule, i.e., the decay of the 1595 cm^{-1} aromatic ring-breathing band during laser irradiation, had to be undertaken.

THESIS OBJECTIVES

The objectives of this thesis as initially envisioned were:

1. Further refine the technique of polarized Raman spectroscopy as applied to the study of both cellulose and lignin in plant cell walls,

2a. Investigate the macromolecular orientation and compositional variability for both cellulose and lignin, as well as their interrelationships in the secondary cell walls of southern pine and, to a lesser extent, black spruce tracheids using Raman microspectroscopy, i.e., conduct a comprehensive mapping study of these biopolymers' patterns of organization,

2b. Correlate the spectral mapping data with cell morphology,

2c. Interpret these findings in light of the present knowledge of cell wall architecture.

Number 2 was to have been the primary objective, but as previously mentioned the early experiments revealed that photomodification of the lignin macromolecule was most likely occurring during 514.5 nm laser irradiation. If

the spectral mapping studies of the biopolymers (particularly lignin) were to reflect their native-state organization then the photodecay of the 1595 cm^{-1} lignin band had to be more fully understood and adequately accounted for in the mapping studies. Therefore, a further objective of the thesis was to investigate this photodecay phenomenon.

LITERATURE SURVEY

This survey is divided into three major parts: Photochemistry Of Wood And Related Materials, Conjugation And Preresonance Raman Effects On Raman Intensities Of Aromatic Compounds, and the Plant Cell Wall. The first two parts deal with the photodecay of the 1595 cm^{-1} aromatic ring-breathing vibrational band of lignin while the latter is concerned with the molecular architecture of (woody) plant cell walls.

Photochemistry Of Wood And Related Material

The aim of this survey is to present a brief overview of the photochemistry of lignocellulosics. Emphasis will be given to the near-UV and visible light photochemistry of woody materials.

Photochemistry is the study of the chemical and/or physical changes that occur in molecules upon absorption of electromagnetic radiation.[11,12] Photochemical reactions occur when molecules absorb this radiation and become photoexcited. These excited molecules are very energetic and have the potential

for internal rearrangement or reaction with other molecular species in the system. The principal regions of the electromagnetic spectrum that are of interest in lignocellulosic photochemistry are the near-ultraviolet (300-400 nm), and the visible region (400-700 nm).[11,12]

Wood Chromophores

Wood is a complex, highly inhomogeneous macromolecular system. The primary chemical constituents besides water are cellulose, hemicelluloses, and lignin, while secondary components include extractives and inorganics. Upon exposure to sunlight, wood and other lignocellulosic products such as paper undergo a complex series of chemical reactions which eventually result in the degradation of these materials. Substantial effort has been directed towards understanding the nature of the chromophores that are responsible for the initial light absorption, as well as those produced during photochemical degradation.

Wood is a fairly good absorber of light and is capable of interacting with a range of wavelengths of electromagnetic radiation because of the wide range of chromophoric groups associated with its basic components.[13-15] Several wood components have been found responsible for the absorption of near UV-visible radiation. Van den Akker *et al.*[16] demonstrated by comparing the light absorption properties of cellulose and lignin, that photochemical reactions are primarily due to chromophoric groups present in lignin. In another

study, Nolan et al.[17] concluded that lignin is the principal contributor to the photoyellowing of wood. They based this conclusion on the similarity in shape between the ultraviolet absorption spectrum of lignin and the photoyellowing spectral sensitivity curve of groundwood, i.e., the degree of photoyellowing of groundwood as a function of exposure wavelength. Norrström[18] showed that the polysaccharides and dichloromethane extracted materials contribute only in a minor way to the light absorption of spruce wood (Picea abies) at 457 nm. Extractives have been mentioned as secondary contributors to the absorption of near UV-visible radiation. They usually have the ability to absorb in the 300 to 400 nm region of the spectrum.[14,15] Although minor constituents, it has been reported that they contribute to the natural yellowish to reddish-brown color of wood[19-22] which indicates that their absorption spectrum extends into the visible region.

As suggested above, the evidence points to the lignin macromolecule as the principal near UV-visible light chromophore in wood. Its absorption spectrum extends beyond 400 nm as shown in Figure 2. The study of this chromophore is an extremely difficult problem. The complexity of its structure, as well as the multitude of possible reaction sites contribute to the difficulty in studying it. In general, the configurations in lignin responsible for light absorption include ring conjugated carbonyls and aliphatic double bonds, quinones, quinone-methides, and free radicals (Figure 3).[24-26]

It has been reported that of all the structural units in spruce lignin

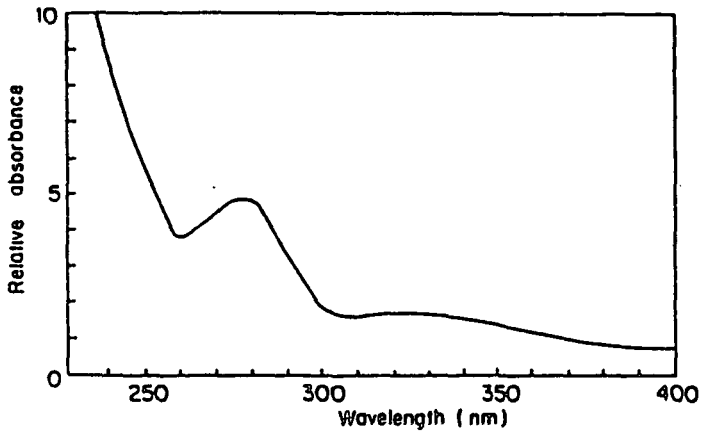

Figure 2. Ultraviolet absorption spectrum of lignin.[23]

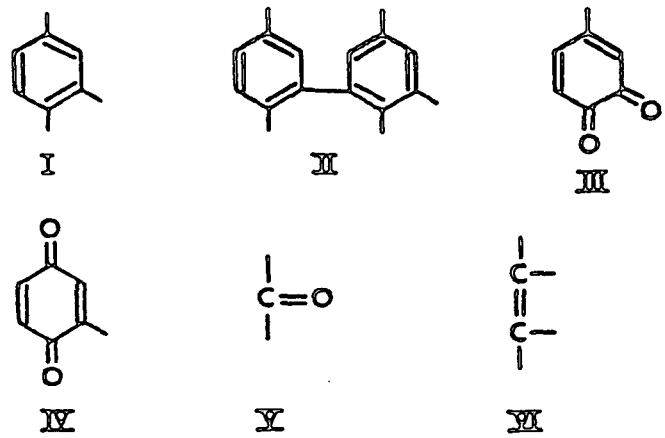

Figure 3. Basic chromophoric structures in lignin.[24-26]

identified so far, only coniferaldehyde may explain the absorption of visible light.[27,28] Approximately 4% of C-9 units[29] in lignin are of the coniferaldehyde-type and 1/4 of these (or 1%) have free phenolic hydroxyl groups.[30] Pew and Connors[31] reported that coniferaldehyde groups are a major contributor to lignin's color in wood. Both carbonyl groups and α-β double bonds have been implicated. (Gellerstedt and Pettersson[32] have shown in lignin model compound studies that conjugated double bonds are susceptible to photooxidative reactions.) Lin and Kringstad[33-36] have reported that the photo-induced degradation and discoloration of lignin are mainly initiated by the absorption of light by α-carbonyl groups.

Quinones and quinonemethides are also mentioned as possible contributors to near UV-visible light absorption. Imsgard et al. have shown in their studies with spruce milled-wood lignin that ortho-quinonoid structures are present in small amounts and that these structures could account for as much as 35-60% of 457 nm light absorption.[38] (It is not known if quinonoid structures are present in native-state lignin, but it is conceivable that a small percentage could remain after lignification is complete and thus contribute to the near UV-visible light absorption of wood.) Harkin[37] suggested that lignin may contain 3 stable quinonemethide groups per 100 C-9 units. Quinonemethides are known to have higher molar extinction in the blue region of the spectrum.[38]

In lignin preparations, it has been reported that phenoxy radicals are present and that these radicals may contribute to lignin's color since they

exhibit absorption in the 500-600 nm region of the electromagnetic spectrum.[42] The existence of intrinsic free radicals in wood is not well established. Rex[39] and Ranby et al.[40] have reported that free radicals do not exist in protolignin. Hon found no evidence for intrinsic free radicals in green loblolly pine wood.[41] He suggested that the customary observed "intrinsic" free radicals may well be an artifact created during mechanical preparations, as well as from exposure to electromagnetic radiation.

There is evidence that transition metal ions are responsible for part of the visible light absorption in wood.[247] (All plant material contains a variety of these ions, as they are necessary for metabolism.[247]) Oxygen atoms or carbon-carbon double bonds that occur in the lignin macromolecule are suitable donor groups that can form ligand-type bonds with transition metals such as manganese.[248] These resulting complexes are capable of absorbing long wavelength radiation.[23]

In summary, Hon and Glasser have classified the potential chromophoric groups in wood and pulp as follows[43]:

1. Chromophoric functional groups: phenolic hydroxyl groups, double bonds, carbonyl groups, etc.
2. Chromophoric systems: quinones, quinonemethides, biphenyls, etc.
3. Leuco chromophoric systems: methylene quinones, phenanthrene quinones, phenylnaphthalenediones, bimethylenequinones, etc.
4. Intermediates: free radicals.

5. Complexes: chelate structures with metal ions.

Photodegradation

Photodegradation describes two general types of degradation processes initiated by light. The first deals with light-initiated reactions in the absence of oxygen. Photooxidation, in which the reactions occur in the presence of oxygen, is the second type. It is generally accepted that the principal reactions in light-induced degradation of wood are photooxidative in nature.[35,44-46]

The main processes involved in the photooxidative degradation of polymers include the following basic steps:

1. Absorption of the incident radiation,
2. Free radical formation,
3. Polymer chain scission,
4. Crosslinking,
5. Secondary oxidative reactions.

The secondary oxidative reactions can include the formation of hydroperoxides and singlet oxygen, both of which are capable of enhancing photodegradation.[47] A detailed discussion of the photooxidative degradation of polymers has been prepared by Rabek.[48]

Photochemical Reactions

Much effort has been directed towards understanding the mechanisms involved in the photodegradation of woody materials. It has been shown that discoloration and photodegradation of wood and high-yield pulps are mainly initiated by the absorption of light.[16,44] Although wood principally absorbs in the UV, visible radiation is known to induce chemical modifications.[17,45,49-51] As was mentioned previously, lignin is believed to be the primary chromophore in wood, and the general consensus is that it plays a key role in photochemical degradation.

Phenolic groups in the lignin molecule are frequently mentioned as possible sites at which the yellowing of lignified material begins. Blocking these sites has been found to increase the stability of lignified material to yellowing under the influence of light and oxygen. Leary[45] suggested that these groups are the reactive centers in the photoyellowing reaction of lignified materials. He speculated that they are first oxidized by hydrogen atom transfer to a neighboring excited molecule or free radical. This leads to the generation of phenoxy radicals which react with oxygen to form yellow and demethoxylated products such as quinones, quinonemethides, and cyclohexadienones (Scheme 1).

Luner[52] has proposed a mechanism for the photo-induced oxidation of wood and lignin-rich pulp. He suggested that colored para-quinone degradation

products are formed through a free radical attack on the lignin macromolecule by oxygen. The α-carbon on the aliphatic side chain of the phenylpropane units containing free phenolic hydroxyl groups is the initial site of attack (Scheme 2).

The production of free radicals thus seems likely to be an integral step in the photochemistry of woody material. Electron spin resonance spectroscopy studies have confirmed the existence of free radials. Kalnins and his coworkers[53] have demonstrated that free radicals are produced in several wood species under the influence of near-UV radiation. Although stable in helium and vacuum, their concentration decreased in the presence of oxygen. This supports the photo-induced mechanism depicted in Scheme 1. Hon[54] reported that wood readily interacts with sunlight, fluorescent light, and artificial UV light to produce free radicals. They were formed in both air and vacuum environments, though larger amounts were generated under vacuum. He concluded that they play a major role in wood surface deterioration and discoloration reactions.

The photo-induced free radicals may be oxidized by atmospheric oxygen, undergo termination reactions, or may be scavenged by phenolic groups in lignin. The scavenging of these free radicals by phenols leads to the production of phenoxy radicals, which may undergo oxidation to produce o-quinones. Support for this comes from the studies of Leary (mentioned above).

Scheme 1.

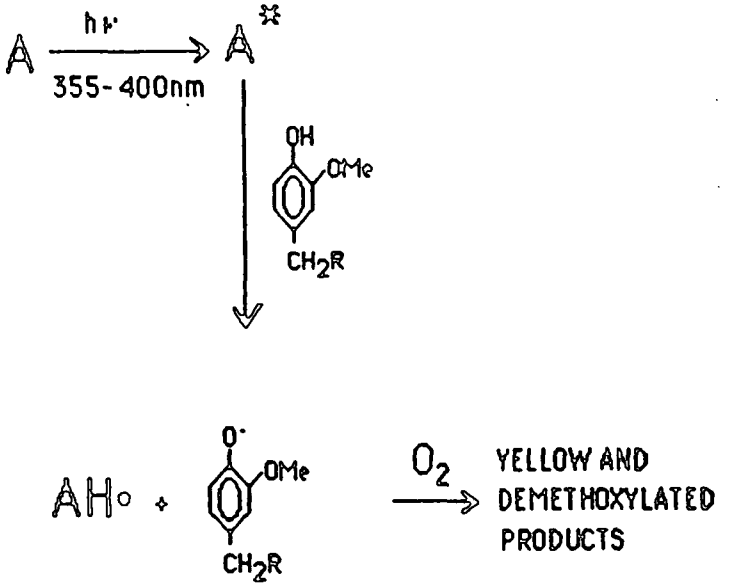

Scheme 2.

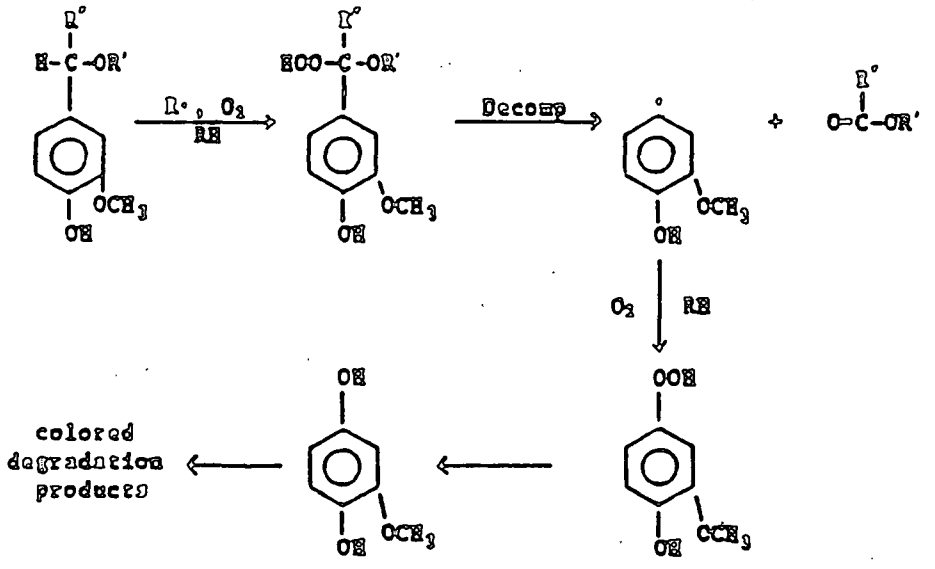

Kringstad and Lin[33] showed that lignin model compounds having α-carbonyl groups can, after excitation to a triplet state, abstract hydrogen from a phenol. They assumed two radicals to be formed in the reaction, a phenoxy radical and a benzyl alcohol radical. The phenoxy radical can react further to form a yellow product while the benzyl alcohol radical was assumed to be reoxidized to the original carbonyl structure in the presence of oxygen (Scheme 3). The α-carbonyl model compound thus acts as a photosensitizer, i.e., it is not consumed in the reaction but only acts as an energy transfer agent.

Scheme 3.

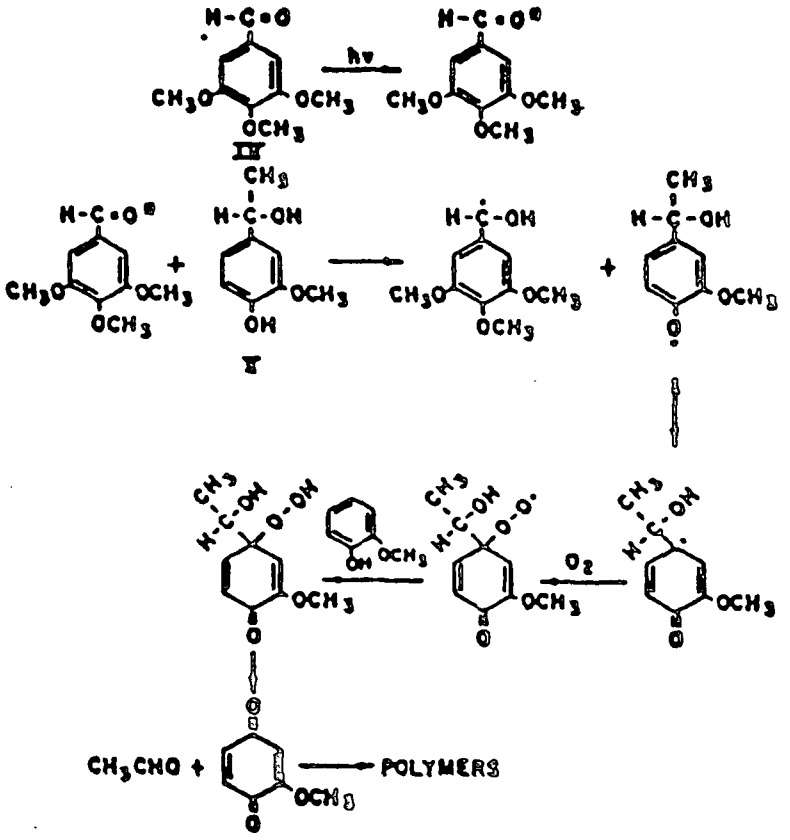

The fate of the phenoxy radicals has been addressed in an article by Gierer and Lin.[55] The authors proposed several pathways which eventually lead to the formation of o-quinones and o-hydroquinones (Scheme 4). Their proposed mechanism supports the hypothesis that phenoxy radical formation is a prerequisite for the reactions leading to discoloration of lignin upon exposure to light and oxygen.

Brunow and Sivonen[56], using α-carbonyl compounds as sensitizers, have suggested that the yellowing of high yield pulp and wood is initiated by excited carbonyl groups. These excited groups may react with molecular oxygen to form singlet oxygen, which then oxidizes the phenolic groups in lignin to form phenoxy radicals. The phenoxy radicals react further and form yellowed products.

Matsuura et al.[57] reached a similar conclusion. They suggested that the excited carbonyl group transfers its energy to an oxygen molecule forming singlet oxygen. The singlet oxygen can then oxidize phenols to phenoxy radicals which can then react further with molecular oxygen to form yellow products (Scheme 5).

Gellerstedt and Pettersson[58], using simple phenolic lignin model compounds with benzophenone as a sensitizer, have proposed that the formation of phenoxy radicals can proceed by either of two pathways (Scheme 6). In the first pathway, photoexcited benzophenone can abstract the phenolic hydrogen,

Scheme 4.

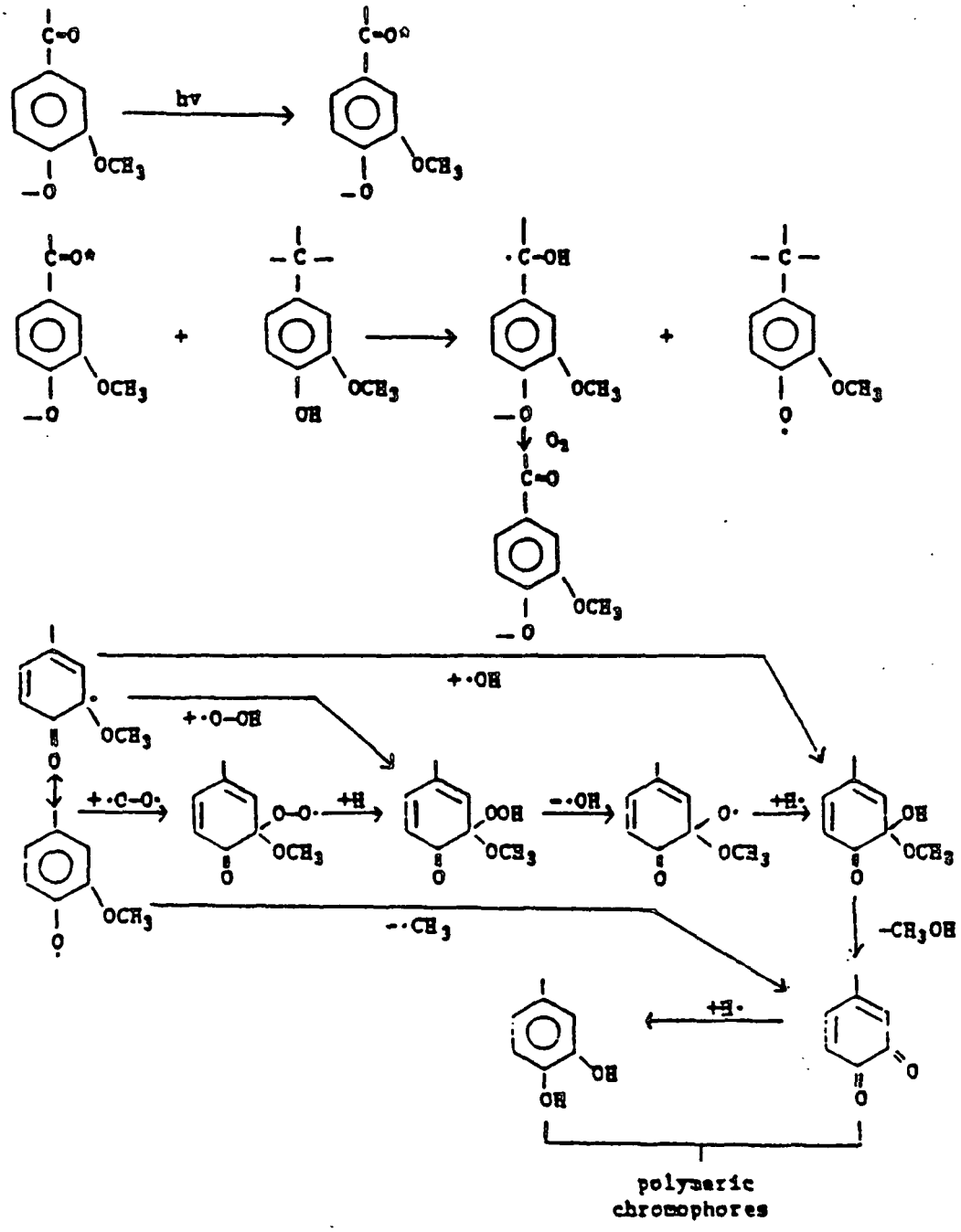
hν
+·OH
+·O–OH
+·C–O·
O–O·
+H
OOH
–·OH
O·
+H·
OH
–·CH₃
–CH₃OH
+H·
polymeric
chromophores

Scheme 5.

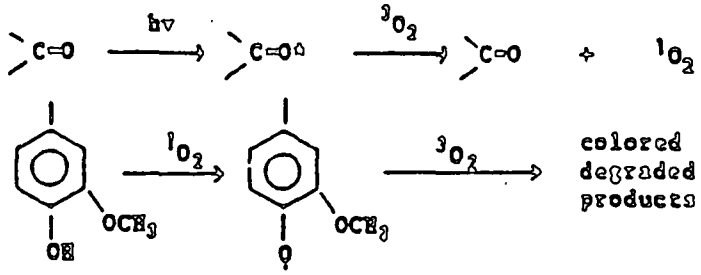

Scheme 6.

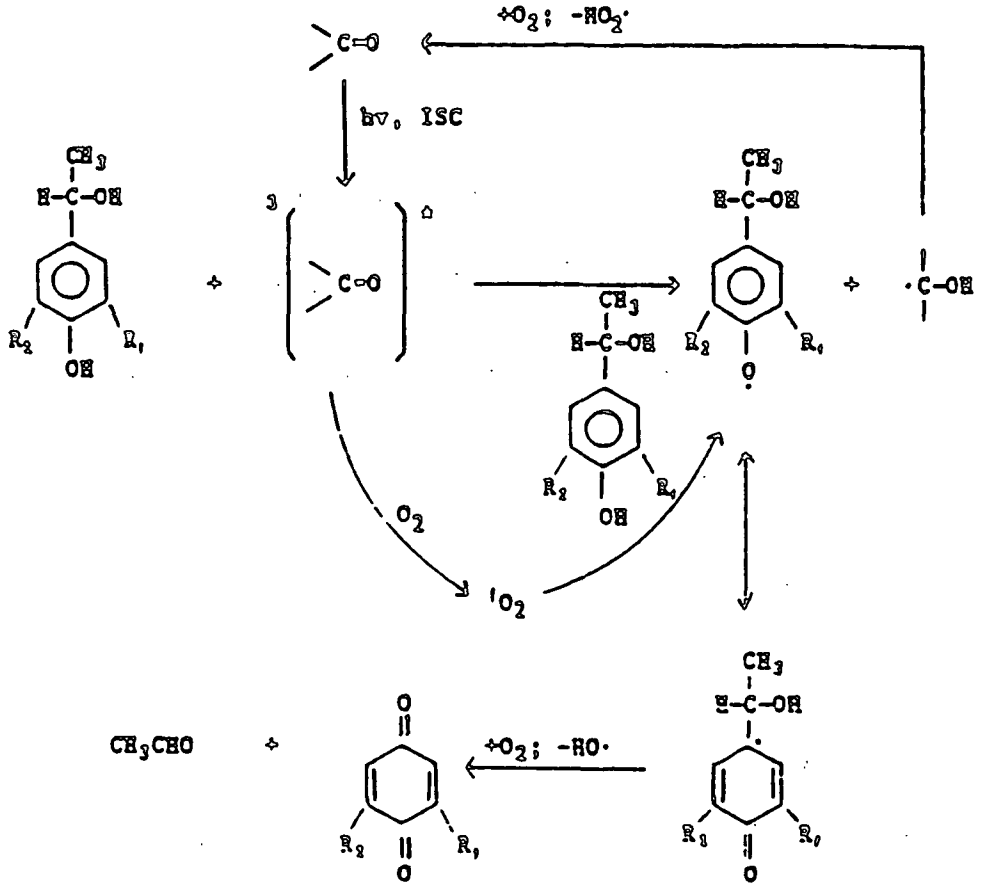

thus creating both phenoxy and benzyl alcohol radicals. Alternatively, the photoexcited benzophenone may transfer its excess energy to ground-state oxygen thus forming singlet oxygen. This can then react with phenolic hydroxyl groups forming phenoxy and hydroperoxy radicals. They suggested that for light-induced oxidation of lignin, the singlet oxygen pathway seems more probable since the distance between carbonyl and phenolic hydroxy groups is of minor importance for the occurrence of the reaction.

Hon et al.[59] have proposed that singlet oxygen is involved in the photodegradation of wood surfaces. In their study, one conclusion was that molecular oxygen may be raised, through interaction with a sensitizer, to an excited state. The singlet oxygen can then interact with wood free radicals to produce hydroperoxide, which is capable of triggering oxidative destruction of cellulose, hemicelluloses, and lignin at the wood surface.

Quenching experiments lend support to the idea that singlet oxygen is involved in degradative reactions, at least for lignin model compounds. Degradation has been retarded in the presence of quenchers such as β-carotene[58-60] and 1,4-diazobicyclo(2,2,2)octane (DABCO)[32,59,61] during irradiation.

Much of the foregoing work has been carried out on lignin model compounds. Whether the results are directly applicable to wood is open to question. Given this uncertainty, the current available knowledge supports the

idea that photochemical oxidation of lignin is the principal reaction in the discoloration and degradation of wood by near-UV and visible radiation. The major steps in the process are:

1. The absorption of light by chromophoric groups most probably part of the lignin macromolecule. These chromophores could include phenolic aryl-propane units containing conjugated α-β double bonds and carbonyl groups, and biphenyl structures.[43]
2. Free radical formation, particularly phenoxy radicals. This could occur by either of two mechanisms: direct hydrogen abstraction by photoexcited α-carbonyl groups or through the generation and subsequent reaction of singlet oxygen.
3. The final step is the reaction between phenoxy radicals and ground-state oxygen to form colored degradation products, particularly quinone-type structures. Figure 4 summarizes these steps.

$$\text{lignin} \xrightarrow{h\nu} \text{lignin}^{*} \xrightarrow[\text{units}]{\text{phenolic}} \text{phenoxy radicals} \xrightarrow{O_2} \text{colored degradation products}$$

Figure 4. Photochemical oxidation of lignin.[47]

Photostabilization

Photostabilization of wood involves the retardation or elimination of unfa-

vorable light-induced degradative pathways. In general, two different approaches have been adopted to stabilize woody material. The first involves chemical modification of the reactive centers in lignin such as α-carbonyl groups and free phenolic hydroxyls. The second method involves the addition of suitable compounds capable of deactivating the photoexcited chromophores and/or preventing the formation of radicals in lignin.

Free phenolic hydroxyl groups have been implicated in discoloration and degradation reactions of woody materials. Much effort has been directed towards blocking these reactive centers. Methylation[62-65], acetylation[65-81], and benzoylation[62,82] reactions have improved wood's stability towards light. These blocking attempts, however, have not been sufficient to achieve total stabilization, which suggests that either alternative degradative pathways exist or the blocking attempts were not 100% effective.

Another successful method of stabilization is eliminating the α-carbonyl groups in lignin which may be partly responsible for the initial light absorption. It has been reported that sodium borohydride reduction of α-carbonyl groups increased the stability of woody materials towards light[55,67,83,84], although photodegradation still occurred. The reason for the partial stabilization may be due to unreacted α-carbonyls and/or the occurrence of other light absorption groups which are not sensitive to sodium borohydride reduction. In addition to sodium borohydride, other reductive agents such as sodium dithionite, thiourea dioxide, and diborane have been tried. Tschirner

and Dence[85] reported that sodium borohydride-treated thermomechanical pulp showed greater light-stability than thermomechanical pulp reduced with dithionite or thiourea dioxide. Treatments designed to remove ring conjugated ethylenic groups were also found to have little effect on the photostability of thermomechanical pulp.[85]

Many compounds are known which can stabilize organic molecules by deactivating the photoactivated states before harmful reactions occur. Deactivation is achieved by energy transfer from the photoexcited molecule to the quencher.[11,12,48] The following types of quenching processes can be distinguished[48]:

1. Collisional quenching,
2. Concentration quenching,
3. Oxygen quenching,
4. Energy transfer quenching,
5. Radiative migration (self quenching).

It has been demonstrated that singlet oxygen quenchers such as β-carotene inhibit degradation and discoloration reactions in inorganic polymer systems to some extent.[32,48,58-61]. Potassium iodide has been cited frequently as an effective fluorescence quencher in inorganic systems[86,87] as have copper (II) ions.[88]

Free radicals are important intermediaries in light-induced reactions.[43,54] These free radicals can undergo photochemical chain reactions which eventually

lead to photodegradation. Reineck et al.[89] were able to show that antioxidants have the ability to reduce the photoyellowing of groundwood when exposed to light. Kringstad[44] has suggested that antioxidants, which can function as effective hydrogen donors, can be used to improve the stability of woody materials. By donating a hydrogen to the free radical, these antioxidants effectively block further radical reactions.

It has been proposed that many of the photostabilizers operate by a combination of mechanisms. For example, hydroxybenzoquinone can act both as a radical scavenger and quencher of excited states.[90-93] In addition, the light-stabilizing efficiency of photostabilization frequently depended on the nature of the polymer and stabilizing system.[48]

Conjugation And Preresonance Raman Effects On Raman Intensities Of Aromatic Compounds

Prior to the onset of this thesis, it was not possible to observe conjugation and preresonance Raman effects because the Raman instrument (scanning spectrometer with a photomultiplier tube detector) being used in our laboratory at that time required very long data acquisition times. A new Raman spectrometer with multichannel detection was acquired at the beginning of the thesis. The data acquisition time of this instrument was short enough to observe the decay of the 1595 cm^{-1} lignin band during laser irradiation of water-immersed woody tissue. This observation eventually led to the knowledge that both of these effects could influence the intensities of specific

Raman bands assigned to (native-state) lignin.

It has been known for some time that the Raman intensities of specific molecular vibrations can be selectively enhanced.[94-99] When the wavelength of light used to excite the Raman scattering falls within or near an electronic absorption band, the intensities of the bands associated with the chromophore are enhanced due to the coupling of the electronic and vibrational transitions. This mechanism is referred to as resonance Raman enhancement (RRE). (If the excitation wavelength falls near the electronic absorption band this mechanism is commonly referred to as preresonance Raman enhancement (PRRE).) The Raman intensity of certain molecular vibrations is also sensitive to the degree of conjugation, i.e., those vibrations arising from bonds which enter into conjugation are selectively enhanced. (Conjugation is defined as the mutual interaction of different pi-electron systems.) This is commonly known as the conjugation effect or conjugation enhancement (CE).

Schmid and coworkers have done an in-depth study of these effects in substituted benzenes and biphenyls.[100-106] In their initial paper, they investigated the effect of substituents on the ≈1600 cm^{-1} aromatic ring-breathing vibration for monosubstituted benzene derivatives.[100] They showed that the Raman intensity of this vibration was determined by the degree of pi-electron conjugation between the aromatic ring and substituents, i.e., the greater the degree of conjugation, the higher the intensity. They also measured the Raman intensity of the carbonyl stretching vibration for those mono-

substituted benzene deviations containing a C=O group. It was again observed that the intensity of the carbonyl band depended on the degree of conjugation between the ring and substituents.

These authors next directed their attention to the relationship between the Raman intensity of the ≈1600 cm^{-1} band of sterically hindered biphenyls and the angle of twist of the coannular (1-1') bond.[101] They observed that when both rings are coplanar, i.e., at maximum conjugation, the intensity was at its largest value. At the other extreme, when the rings were orthogonal, the Raman intensity was the same as that seen for two unsubstituted benzenes because of the interrupted pi-electron conjugation.

In a later paper, they investigated the conjugation and resonance Raman effect on the Raman intensities of diphenylpolyenes.[102] Their major conclusions were that the relative intensities of the ≈1600 cm^{-1} ring vibrations were determined by both CE and (P)RRE, whereas the C=C stretching vibrations of the polyene chain were principally determined only by (P)RRE. In addition, the near-resonance type behavior of both vibrations turned out to be uniform, i.e., both vibrations were subject to the same absorption frequency dependence. In contrast, the CH stretching vibrations of the diphenylpolyenes did not show any RRE and their intensities were not enhanced by CE when the chain length was increased.[106]

Plant Cell Wall

This section provides an in-depth review of the plant cell wall. Emphasis is given to the woody cell wall. The structure, distribution, organization, and biosynthesis of the major components will be covered.

Overview

The woody cell wall is a complex, inhomogeneous structure. Cellulose, hemicelluloses, and lignin are the major components of these walls. The function of cellulose is primarily to provide the framework while hemicelluloses and lignin serve as matrix materials.

This thesis was concerned with the molecular architecture of two of these components, namely cellulose and lignin.

Components

Cellulose

Cellulose is the primary component of plant cell walls and comprises 40-50% of the dry weight of woody plants.[4] It is the major load bearing component in the woody cell wall. Although the structure of cellulose is well documented, many aspects of its organization *in situ* are poorly understood.

Structure

Chemically, cellulose is defined as poly-1,4-β-D-anhydroglucopyranose. It is generally thought that the cellulose chains exist in an extended form and the anhydroglucose rings assume a chair conformation.[107] The methine bonds are perpendicular to the rings and chain axis while the heavy atom linkages are equatorial. The β-1,4 linkage results in a stiff, ribbon-like molecule that is suitable for forming fibrils via hydrogen bonding.

It has been observed that there is a distinct supramolecular ordering to the polysaccharides into stranded aggregates. These aggregates are collectively known as fibrils. A qualifier is usually attached to this term to designate the size of the structure, e.g., microfibrils (Figure 5).

The microfibrils are thought to consist of cellulose crystallites surrounded by paracrystalline cellulose and hemicelluloses. The axis of the cellulose chain is parallel to the axis of the fibrils as shown in Figure 5.

The cell wall is comprised of several concentric layers. In each of these layers, the orientation of the fibrils is different (Figure 6). The orientation ranges from a random arrangement (primary cell wall layer) to highly ordered (secondary cell wall layers - S_{1-3}).

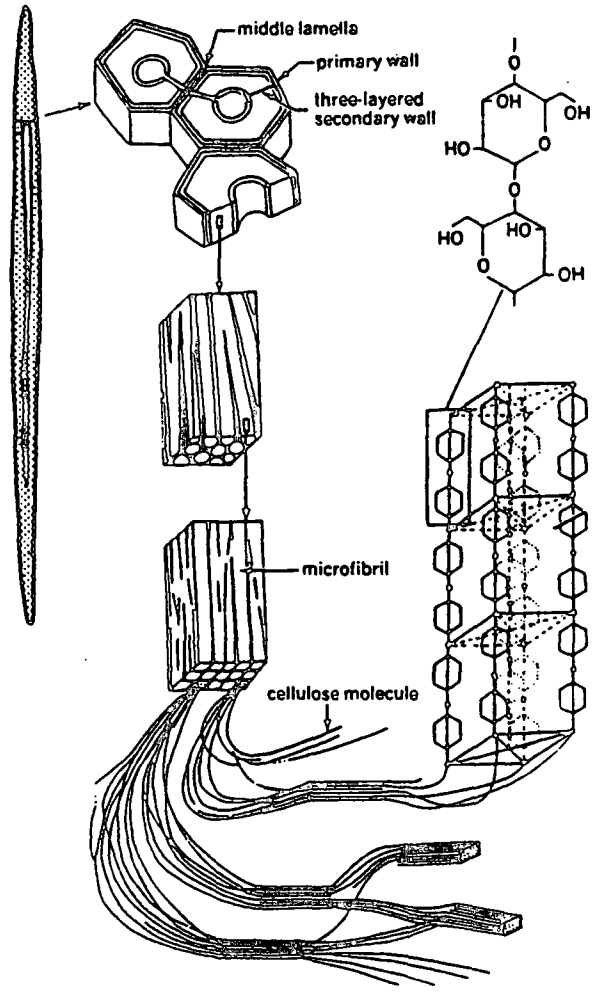

Figure 5. Microscopic and submicroscopic structure of cellulose.[5]

The cellulose content varies with type of plant and the developmental stage. Primary cell walls usually contain 1-10% cellulose while secondary walls of higher plants typically have about 50%.

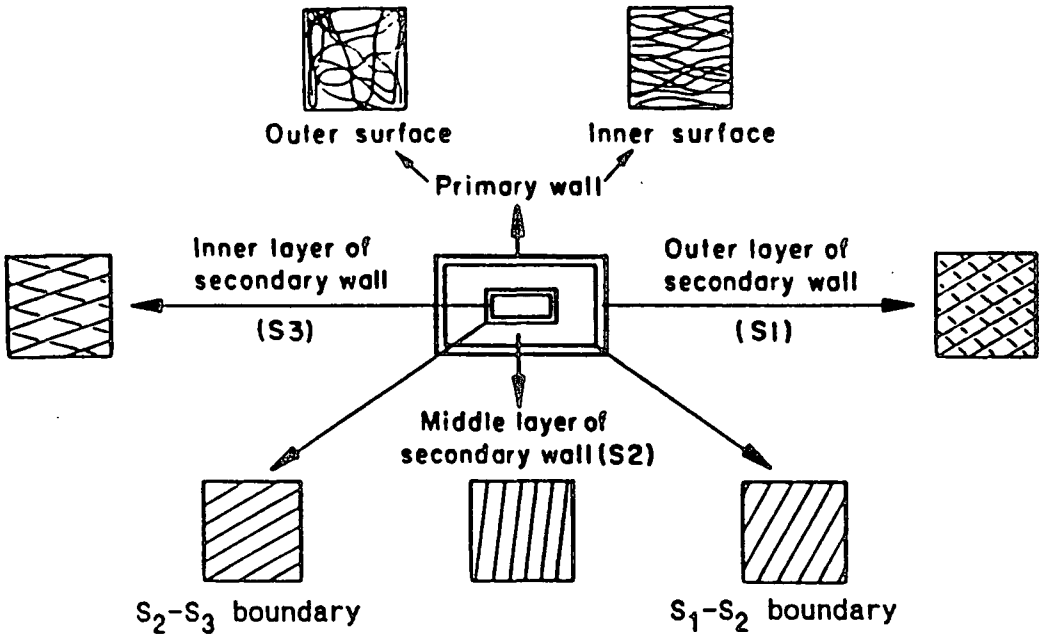

Figure 6. Cell wall organization showing microfibrillar patterns.[108]

The crystallographic form of cellulose synthesized by bacteria and plants is cellulose I. The degree of polymerization (DP; number of glucose residues per molecule) varies depending on the species and location. The DP of cotton cellulose has been estimated to range from 2,000-6,000 in the primary wall and to average about 14,000 in the secondary wall. Similar secondary wall values are reported for wood. In the secondary wall of the algae, Valonia, a more homogeneous DP of 18,000 has been found.[109]

The width of the microfibril varies among different organisms and states of development. Quince seed mucilage microfibrils of low crystallinity have a width in the range of from 1 to 1.5 nm[110] whereas in Valonia the microfibrils are highly crystalline and are about 25 nm wide.[111] The microfibrils can aggregate into larger fibrils, e.g., the bundling of 5.6 nm cotton microfibrils into 60-360 nm macrofibrils.

The debate continues about the substructure of the microfibrils. Various models have been proposed to account for amorphous and crystalline regions in native cellulose. Generally, variations on three basic concepts have been proposed. These concepts are:

1. Continuous chains pass through alternate crystalline and paracrystalline regions along the length of the fibril,
2. Crystallites alternate with paracrystalline regions throughout the width of the fibril,
3. A generally continuous lattice is interrupted by distortions such as those that would occur at randomly located chain ends.

(For a review of these various models, see reference 112.)

Organization

Many different methods exist for probing the organization of cellulose in the cell wall. A brief survey of the most important techniques is presented below.

Polarized Light Microscopy

Microscopy with polarized light was introduced as an analytical method about one hundred years ago, and has since become an important tool in the study of submicroscopic organization. Early studies revealed that the cell wall is optically birefringent, i.e., the index of refraction varies with direction.[6,7]

Bailey[113] observed that regions of the cell wall differed in brightness when viewed between crossed polarizers. He concluded from these studies that the cell wall was a layered structure and that the orientation of cellulose (chain axis) varied within each layer.

Page[114,115] developed a quantitative method for measuring fibril angle by utilizing the birefringent properties of the cell wall. He showed that there was a correlation between fibril angle (in effect the angle formed by the chain axis and the fiber axis) and fiber properties.

Muggli et al.[116,117] derived a theoretical model to predict the intensity distribution of scattered (laser) light from individual wood fibers. They showed that three distinct refractive indices are required to describe the cell wall. Based on these studies, they concluded that both chain axis and methine (CH) bond orientation exist in a fiber cell wall.

Diffraction Methods

X-ray diffraction studies can provide information on crystallite size, shape, perfection, and also can be used as a method of material identification. Sisson et al.[118,119] utilized X-ray diffraction to measure the average cellulose chain axis orientation in fibers. In addition to providing a measure of the angle between chain and fiber axes, their method also provided information concerning the dispersion in the cellulose orientation.

X-ray diffraction studies also revealed that the orientation of the cellulose chains was the same as the orientation of the fibrils seen microscopically. It was concluded from this observation that the axis (chain axis) of the cellulose crystallites was parallel to the fibril axis.[120]

Electron Microscopy

Electron microscopy, particularly transmission electron microscopy (TEM), has been used extensively in the study of cell wall structure. Although TEM per se provides no direct information about cellulose orientation, when combined with X-ray diffraction and wet chemistry, it is possible to deduce the composition and organization of the microfibrils.[6,7,119]

Various schemes have been proposed for cellulose organization.[6,7,50,51] Some authors favor a lamellar organization, while others favor a fibrillar one. (The term lamellae is used to indicate layers of fibrils having the same

orientation.[167]) TEM micrographs of the cell wall indicate that cellulose organization is fibrillar. This orientation is thought to imply a random orientation of the methine bonds.[6,7,121,122] (Although this is not the case for Valonia, the walls appear fibrillar but diffraction studies indicated that methine bond orientations are not random.[6,7,121,122]) This lack of consensus may be due to different sample preparation techniques. The results in electron microscopy are heavily dependent upon the care exercised in sample preparation.[6]

Spectral Studies

Infrared, Raman, and recently NMR spectroscopy have been used to study cellulose organization (infrared, Raman and two-dimensional Fourier transform NMR) and crystal structure and morphology (^{13}C NMR).

Infrared spectroscopy per se has not been used to establish the crystal structure of cellulose and its conformation, although it has aided in conformational studies by providing information about hydrogen-bonding patterns.[123] It has been valuable in establishing the orientation of components in the cell wall.

Morikawa et al.[124] have carried out an infrared analysis of pea stems. Their polarization spectrum measurements of the cell wall indicated that the noncellulosic polysaccharide matrix, as well as cellulose microfibrils have an oriented structure. It was further found that this organization changes

during extensive growth, as well as upon mechanical extension of the walls.

Recently, Raman spectroscopy has been used to investigate cell wall organization in native wood fibers.[10,125] With the use of a Raman microprobe, it was possible to look at domains as small as 1 micron. These studies by Atalla and Agarwal provided direct evidence for the organization of cellulose in the secondary wall. It was found that the pyranose rings of the anhydroglucose repeat units are preferentially oriented in planes perpendicular to the fiber cross section. The methine bonds, on the other hand, were found to be preferentially oriented in planes parallel to the cross section. In this same study, the authors also investigated compositional variability within wood fibers. They found the relative amount of cellulose varied in different locations of the secondary wall.

More recently, Wiley[126] found that cellulose methine bonds are arranged randomly in the plane parallel to the fiber cross section. This study was carried out on both ramie and cotton fibers. He speculated that this arrangement would also hold for wood fibers.[10] It may be that the crystallites are oriented randomly in a single microfibril or, alternately, that they are oriented nonrandomly, but the microfibrils have a random orientation in the lateral direction.

Hatfield, Sardashti, and Maciel[193] reported on the results of an experiment using two-dimensional Fourier transform NMR to investigate the molecular

order of cellulose (and lignin) in Eucalyptus polyanthemus wood. They found that there was no net molecular orientation order of cellulose and lignin over a macroscopic volume of about 0.9 cm^3. (To put this number in context, if the volume were a cube, it would be about 9600 microns on a side. A typical Eucalyptus fiber has a length of 600-700 microns and a 16-21 micron diameter.) The authors do point out that "it may be true that a high degree of molecular orientation order exists for cellulose and lignin within each subdivision of the cell wall ultrastructure, but if that is the case, then the results reported here show that the microscopic orientational characteristics of various subdivisions must be sufficiently randomized over a 0.9 cm^3 sample to yield a zero degree of, i.e., no net, molecular orientational order in the macroscopic NMR experiment." Their results seem disturbing in light of the unquestionable gross order for cellulose in wood. It is conceivable since they were looking at a macroscopic volume (primary and secondary cell wall layers), that a preferential chain axis orientation of cellulose would not be manifested, i.e., the various fibril angles (chain axes) of the different cell wall layers are sufficiently randomized on the macroscopic level to effectively mask the known cellulose order on the microscopic level.

VanderHart and Atalla[278-280] have used solid-state ^{13}C NMR to investigate the microstructure of native celluloses. They proposed that native celluloses are composites of two crystalline forms occurring in different proportions. They designated these I_α and I_β. Their studies suggested that higher plants

celluloses, like cotton and ramie, were rich in I_β while the I_α content was appreciable if not dominant in the algal celluloses and the bacterial cellulose obtained from Acetobacter xylinum. These results in conjunction with Raman spectroscopy studies[281] led the authors to the conclusion that the I_α and I_β forms of cellulose represented lattices with nearly identical conformations of the heavy atom molecular skeletons, but with different hydrogen bonding patterns.

Biogenesis

Biogenesis includes the correlation of biosynthesis with the organelles and functions of the cell, as a programmed sequence of events that is responsible for division, growth, and the differentiation processes.[127] This correlation therefore involves not only the production and molecular properties of cellulose, but also the architecture and function of the cell wall.

Polymerization

Biological and biochemical experiments have shown that cellulose biosynthesis is not a direct enzymatic polymerization of monosaccharides, but an enzymatic transfer reaction in which the activated glucose is transferred to an acceptor.[128] Figure 7 shows this process.

$$\underset{\text{Acceptor}}{(Glc)_n} + \underset{\substack{\text{Donor}\\\text{Substrate}}}{Nu\cdot P\text{-}P\text{-}Glc} \xrightarrow{\text{Enzyme}} (Glc)_{n+1} + Nu\cdot P + P$$

Nu ... Nucleoside P ... energy-rich phosphate group

Figure 7. Enzymatic transfer reaction of glucose.[128]

Much research has been directed towards determining which nucleoside-diphosphate-glucose is involved in cellulose synthesis. Both guanosine-diphosphate-glucose (GDP-glucose) and uridine-diphosphate-glucose (UDP-glucose) have been implicated in higher plants. The evidence does not unequivocally discriminate between the two alternatives. Current opinion favors UDP-glucose as the sugar donor in higher plant cellulose synthesis[129]; GDP-glucose is probably involved in the formation of heteropolysaccharides such as xyloglucan and glucomannan in the Golgi apparatus.[130] There is very little known about the enzymatic steps and intermediate compounds beyond activated glucose and the polymeric cellulose molecule.

Formation Of Microfibrils

The discovery that the bacteria, Acetobacter, forms extracellular pellicles of cellulose raised questions as to the processes involved in the formation of the microfibrils and the extent to which they are influenced by cell organelles or carried out by exogenous chemical interactions and mechanical forces. Ohad et al.[131] suggested that the steps involved may be resolved

into:

1. Polymerization of the activated, monomeric precursor to form cellulose molecules of high molecular weight,
2. Transport of the molecule from the site of synthesis to that of crystallization,
3. Crystallization or fibril formation,
4. Orientation of fibrils during deposition.

Step 1 was addressed in Polymerization. Regarding Step 2, the transport of the basic molecules is still largely unknown. A lipid-D-glucose has been postulated as the form of transport, which is thought to diffuse through the cell wall.[132,133] This concept has been confirmed in bacteria and algae (Protoheca zopfii)[134], but it has not been possible to extend these results to higher plants.

It has been suggested that the enzymes involved in the synthesis of cellulose in Acetobacter are anchored to the cell membrane.[135] In addition, it was reported that cell-free extracts could incorporate D-glucose-1-^{14}C into water- and alkali-insoluble polysaccharides.[133] The alkali-insoluble polysaccharides consisted of aggregates formed from granules of variable size having no well-defined units. It was contended on the basis of these data that individual cellulose molecules are released at cell surfaces as an amorphous or "prefibrous" material that diffuses into the medium and crystallizes to form microfibrils without the necessity of extracellular enzymes.[131] It was

also believed that the orientation of the microfibrils was a mechanical process. The foregoing implies that only the first step (the biosynthesis of cellulose) takes place enzymatically.

An attraction of this theory and its earlier version, the "Intermediate High Polymer Hypothesis"[6,7,131] is that it could explain the formation of amorphous areas in the microfibrils through the entanglement of the preformed polysaccharide chain.

A number of researchers have contested this theory[136-138] for a variety of reasons. Regenerated or recrystallized materials generally adopt a cellulose II structure whereas natural microfibrils show the crystalline structure of cellulose I. Therefore, native fibrils could not be formed by a crystallization process. A second reason for contesting this theory is that cellulose molecules are highly insoluble in water and, as dispersed particles, are unlikely to form well-defined microfibrils. One last reason given is that under the microscope, it could be seen that the microfibrils grow at their tips, which appear smooth and tapered, whereas under the conditions postulated by the foregoing hypothesis, they should be splayed and uneven.[132]

An alternative to the intermediate-polymer theory is the "Endwise Theory." It postulates the transfer or addition and crystallization of the D-glucose units at the growing ends of the microfibrils.[132] This theory supposes simultaneous polymerization and crystallization as the insoluble

polymer is formed. The idea of endwise synthesis is especially attractive as a possible route for the formation of plant cell walls, as it would result in the apposition of the fibrillar structure rather than deposition of the cellulosic materials. Although the "Endwise Theory" adequately answers the objectives raised against the intermediate-polymer hypothesis, it faces some difficulties of its own.[132] One of these is that if the microfibrils contain extended, parallel chains of cellulose, the two ends of the microfibril should show different properties which they do not.[137,139]

Mechanisms Of Orientation In Cell Walls

To what extent microfibril formation and orientation are carried out and controlled by the living cell, or by inanimate, physical forces, are major questions that have been extensively investigated and discussed.

One of the initial hypotheses concerning microfibril orientation suggested that they are oriented by streaming of the flowing cytoplasm over the cell wall.[140] This hypothesis is not feasible because the plasmalemma separates the cytoplasm from the cell wall.

Preston[136], in his ordered granule hypothesis, suggested that cellulose microfibril directions might be determined by the closely packed order of cellulose synthetase granules on the outer plasma membrane. This mechanism could well account for certain specific angular changes between layers of microfibrils, e.g., 60 degrees, 90 degrees, and 120 degrees. It seems unlike-

ly that it could give rise to helicoidal structures that have been shown to occur in the S_1-S_2 and S_2-S_3 transition regions.[141]

A second hypothesis for a microfibril orientation mechanism is the microtubule hypothesis.[142] Microtubules become oriented in specific directions just within the plasma membrane. They are thought to control the direction of the extracellular cellulose microfibrils by somehow acting across the membrane. Microtubules would thus be expected to lie parallel to the most recently deposited layer of microfibrils. Hardham et al.[143] found a second group of microtubules oriented at an angle to the first group in leaf primordia of Graptopetalum paraguayense. They speculated the second group predicted the direction of the next layer of microfibrils to be deposited. As with the first theory, it is unlikely that such a mechanism could give rise to the fan spread, i.e., helicoidal, structures.

A once popular hypothesis for orientation is the multinet growth hypothesis of Roelofsen and Houwink.[144] They proposed that new microfibrils are laid down traversely to the direction of cell elongation. They subsequently become reoriented by growth forces to end up more or less parallel to the length of the cell. The major shortcoming of this theory is that it does not explain the orientation of cellulose microfibrils in cells which are not expanding.

A fourth theory is the terminal complex hypothesis. Freeze-fracture techniques have revealed that microfibrils may be associated with complemen-

tary structures in the cell membrane. These are terminal complexes in the outer (E) face of the membrane and rosettes in the inner (P) membrane face. Mueller and Brown[145] proposed that microfibril direction is controlled by these complexes moving in the plane of the membrane and depositing (and orienting) microfibrils in their wakes.

All of the above hypotheses delegate the problem of microfibril orientation control to the cortical region of the cytoplasm or to the plasma membrane, i.e., they are all cell mediated processes. Several authors contend that self-assembly mechanisms are the major determinants of microfibril formation/orientation.

The existence of an organized system (template) for the production of microfibrils has been suggested by Marx-Figini.[146] Kinetic experiments on cotton cellulose and cellulose from Valonia showed that the degree of polymerization during the biosynthesis of the secondary wall is independent of conversion and reaction conditions. Based on this observation, she hypothesized that the formation of cellulose macromolecules in the secondary wall was controlled by a template or structural mechanism. She stated that, "although the degree of polymerization is genetically controlled, morphology and crystal structure are completely independent from the process of biosynthesis and seem to be only a consequence of the molecular properties of cellulose".[146]

Neville et al.[147] gave the details of such a self-assembly process in trying to explain helicoid (fan spread) structures in plant cell walls. They envisioned the spontaneous positioning of new microfibrils onto the inner surface of the previously deposited wall. The angle between consecutive layers of microfibrils would be determined by the interaction of electrical forces. They stated that these could involve asymmetric patterns of charges on the microfibril surfaces and ionic species in the zone of apposition (periplasm).

Lignin

Lignin is the second most abundant biological material on the planet (exceeded only by cellulose and hemicelluloses) and comprises 15 to 25% of the dry weight of woody plants.[148] Lignin performs multiple functions that are essential to the life of the plant. These functions include: mechanical - it provides rigidity to the lignified plant cell wall, chemical - it acts as an antioxidant and confers resistance against the effects of oxidants, ionizing radiation, etc., and biological - it protects the plant against effects of pathogenic microorganisms[4,6,7,282]. In addition to these major known functions, lignin may have other key functions which are not recognized at this time. Comparatively little is known about the structure and reactions of the biological molecule in situ despite the central role it plays in the structure and physical nature of plants.[148,149]

Structure

Lignin has been described as a three-dimensional network polymer which is deposited between the cells and throughout the cell wall[150]. It is comprised of a variety of phenylpropane monomeric units (Figure 8) that are coupled together irregularly through an assortment of carbon-carbon and ether linkages.[151] The final step in the biosynthesis of lignin is probably not enzyme catalyzed but due to radical coupling reactions, which accounts for the "randomness" of lignin's structure.[152] (This view of random coupling of the lignin precursors is not shared by all lignin chemists. Some scientists believe lignin may have a very ordered nature which is similar to cellulose and proteins.[245])

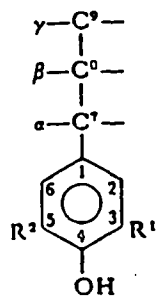

I: $R^1 = R^2 = H$
II: $R^1 = OCH_3$, $R^2 = H$
III: $R^1 = R^2 = OCH_3$

Figure 8. Phenylpropane monomeric unit.[150]

Attempts have been made to classify lignin(s) according to its composition. Gibbs[155] recognized two main classes: guaiacyl and guaiacyl-syringyl lignins. Guaiacyl lignin is composed principally of coniferyl alcohol units (3-methoxy-4-hydroxycinnamyl alcohol) while guaiacyl-syringyl lignin contains monomeric units derived from both coniferyl alcohol and sinapyl alcohol (3,5, dimethoxy-4-hydroxycinnamyl alcohol).[152] In general, the guaiacyl type of lignin is present in the gymnosperms (softwoods) and the guaiacyl-syringyl type is present in the angiosperms (hardwoods).

The nature of the lignin polymerization reactions results in the formation of a three-dimensional, highly branched, interlocking network of essentially infinite molecular weight. This network surrounds and encrusts the polysaccharide fibers in the cell wall, physically connecting each individual cell to its neighboring cells. Covalent linkages between lignin and polysaccharides further cross-link and strengthen the lignocellulose matrix.[153] As a result, it's simply not possible to remove lignin from plant tissue without seriously degrading its structure in the process. Virtually everything known about the chemical structure of lignin has come to light through the study of partially degraded lignin fragments isolated from lignocellulosic materials after chemical or mechanical treatments. These fragments typically have low molecular weight, are soluble in simple organic solvents, are modified chemically, and lack many physical, mechanical and chemical properties of lignin <u>in situ</u>.[150]

Many lignin investigators have tried to ascertain the chemical structure of the lignin macromolecule. Freudenberg and coworkers pioneered the study of its structure.[27] By chemical investigations, they were able to formulate a structural model of Picea lignin. The largest softwood lignin structural model was evaluated by simulating lignin formation by computer. The most recent concept of this model (Glasser and Glasser[154]) is shown in Figure 9 and is composed of 94 phenylpropane units, corresponding to a total molecular weight of more than 17,000. The authors based their model on a wide array of analytical information obtained from investigations of loblolly pine (Pinus taeda) milled wood lignin.

Distribution

An early investigation of lignin distribution was conducted by Ritter.[156] From the appearance of the residue after a 72% sulphuric acid treatment (Klason lignin), he concluded that most of the lignin was located in the intercellular layer (middle lamella). Bailey[157] performed a microanalysis of a fraction of the cell wall (middle lamella and primary walls of adjacent cells). He determined the lignin content to be 71% on a weight basis.

Lange[158], using ultraviolet microspectrophotometry, concluded that the concentration of lignin was 73% in the intercellular layer and 16% in the secondary wall. The lignin content was shown to decrease from the middle lamella to the cell lumen in these investigations. In contrast, Ruch and

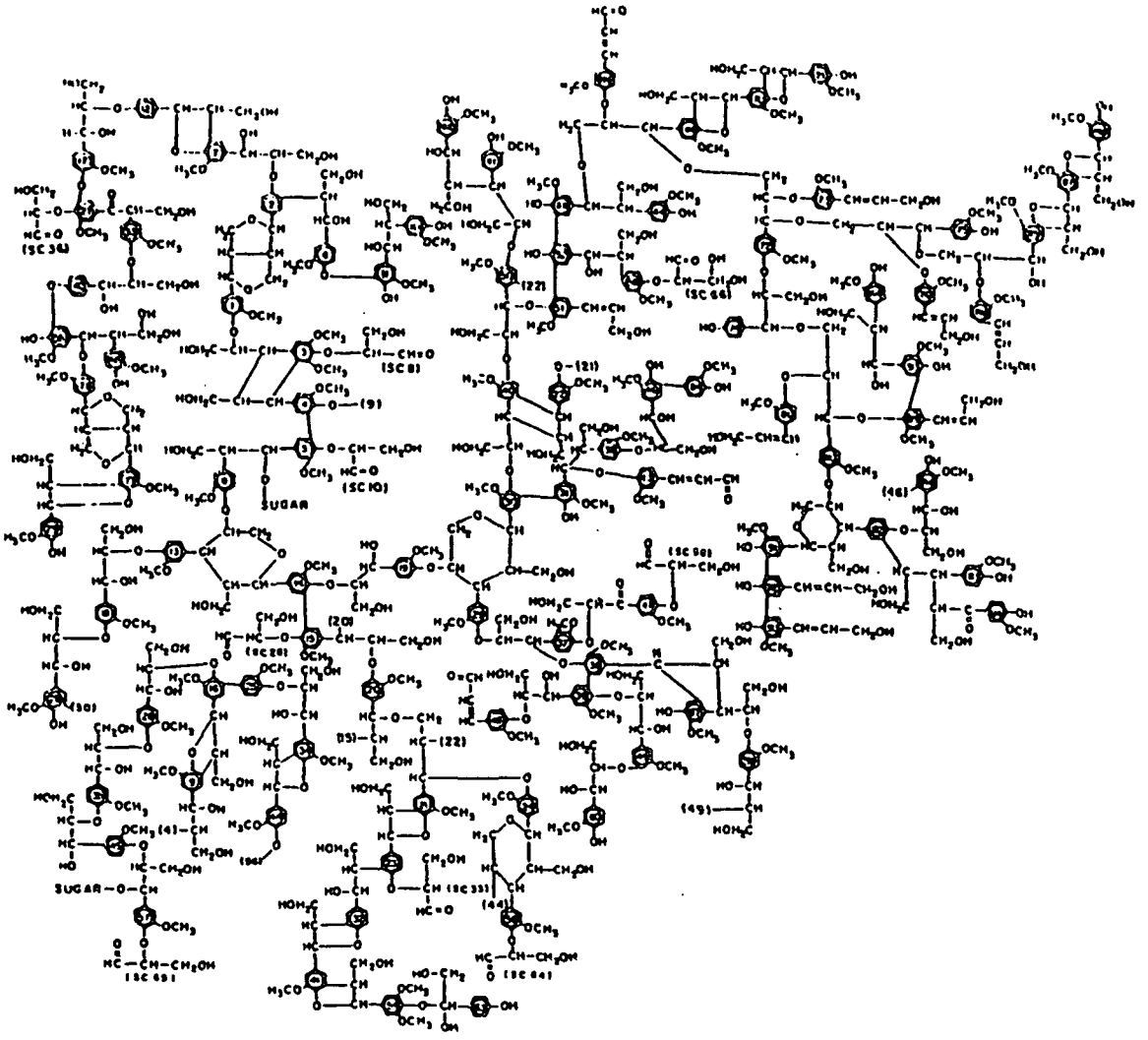

Figure 9. Softwood lignin model designed by computerized evaluation.[154]

Hentgartner, reported by Frey-Wyssling[159], using fluorescence microscopy showed a uniform distribution in the secondary wall of jute fibers. These results were echoed by Fergus et al.[160] who found an approximately uniform lignin distribution in the cell wall of Picea mariana.

The disparity between Lange's observations and those of later investigators has been attributed to the method of illumination, diffraction effects and sample thickness.[159,161]

Although the concentration of lignin in the middle lamella is higher than in the secondary wall, most of the lignin is present in the secondary wall due to its greater volume.[162] Thus for Picea, although the concentration of lignin in the middle lamella (and primary wall) was four times that in the secondary wall, 72% of the lignin was located in the secondary wall while only 28% was located in the middle lamella and primary wall (earlywood).

Saka et al.[163] have used bromination followed by energy dispersive X-ray analysis (EDXA) to determine lignin distribution quantitatively. They found that compared to the results by UV microscopy, the ratio of lignin concentration in the middle lamella to that in the secondary wall was significantly lower. They attributed the discrepancy to different lignin reactivities to bromination; the secondary wall lignin was 1.70 times more reactive than the middle lamella lignin.

Several researchers have investigated the organization of lignin. Stone

et al.[164] using electron microscopy, measured the change in cell wall dimensions during delignification. They concluded from these studies that lignin is arranged in tangentially concentric layers. Kerr and Goring[165], on the other hand, tend to favor an interrupted lamella structure where the dimension of a given lignin (or carbohydrate) entity is greater in the tangential direction of the fiber wall than in the radial direction. In their study, they treated thin wood sections with potassium permanganate. Densitometer traces of electron micrographs of the stained sections indicated the lignin orientation.

In contrast to the above studies, Sacks and coworkers[166] examined wood in which the carbohydrate had been dissolved by acid and found no evidence for lignin lamination. In addition, Heyn[167] conducted an investigation of permanganate stained wood sections. His electron micrographs show a uniform lignin distribution in the cell wall.

Scallan[168] proposed that the disagreement in the literature on cell wall organization is related to the amount of swelling which occurred prior to observation. He developed a model of cell wall organization which provided a common explanation for the variety of observations. Figure 10 shows this model. This structural model allowed for an essentially lamellar distribution of cellulose, but a nonlamellar distribution of lignin. He suggested that if the cell wall was swollen when lignification took place, the lignin would be laid down in disc-shaped, tangentially oriented platelets.

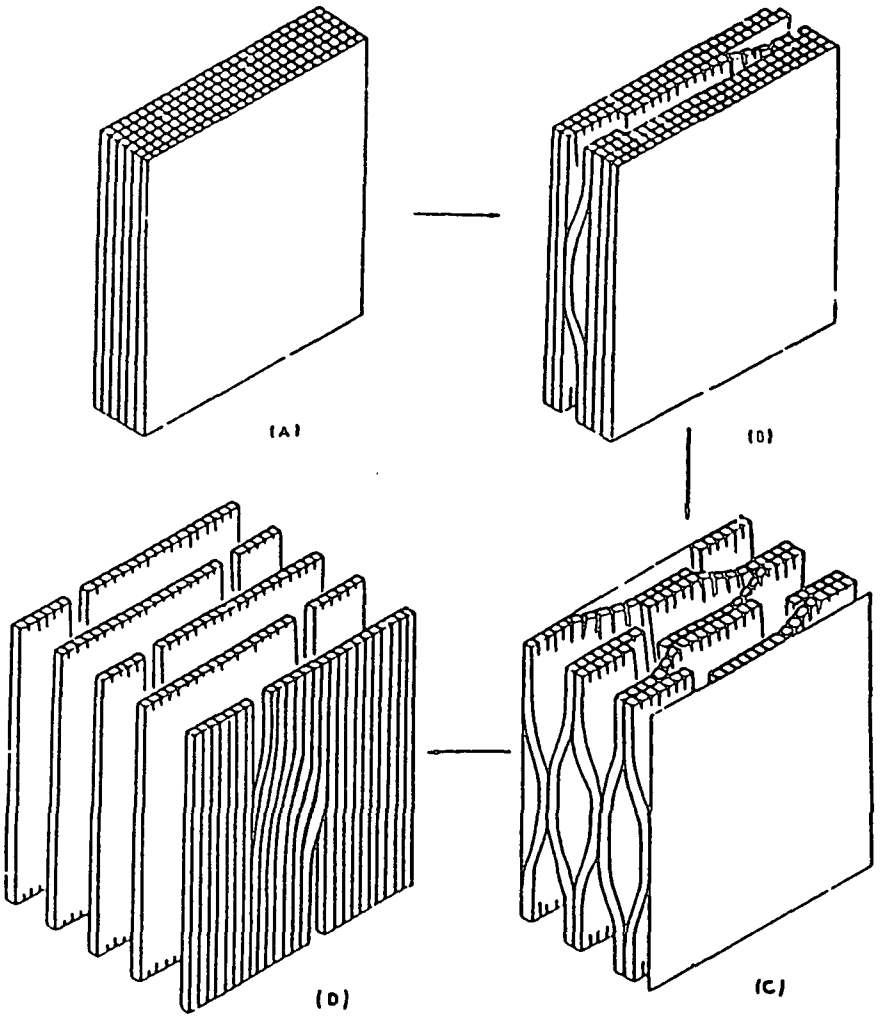

Figure 10. The pattern of internal fibrillation of the cell wall with progressive swelling, as might be expected from the preferential cleavage of tangentially-oriented bonds. The rectangular parallelepipeds represent cellulose fibrils.[168]

Atalla and Agarwal[10,125] used Raman spectroscopy to investigate cell wall organization in native wood fibers. Their studies provided direct evidence for lignin organization in the secondary wall. They found that the aromatic rings of the phenylpropane structural units are parallel to the plane of the cell wall surface. However, they point out, there are regions in the cell wall where this preferential orientation of the aromatic rings is not seen. In the same study, compositional variability within cell walls was investigated. It was found that a substantial variation in lignin content occurred in the secondary wall.

Recently, Terashima[195,196] investigated the higher order structure of protolignin in the cell wall of tree xylem. It was shown by the application of improved tracer methods that lignin was never formed solely in the absence of carbohydrate and that the kind of carbohydrate greatly affected the growing process of the lignin macromolecule. He suggested that anisotropic shrinkage of the random structure of lignin chemically bonded to the hemicellulose gel in the later stages of cell wall formation may cause lignin's aromatic ring to become oriented. He speculated that the aromatic ring orientation seen by Atalla and Agarwal[10,125] could be explained by this anisotropic shrinkage of the swollen honeycomb structure of the lignin - hemicellulose gel. (This is an alternative mechanism for orientation to that proposed by Atalla where the cause is believed to be the adsorption on cellulose microfibrils.[196])

Lignification

Lignification, i.e., the deposition of lignin, is an important aspect in the differentiation of the plant cell wall. This deposition results in cell walls that are extremely rigid and resistant to stress, less permeable to water, and more resistant to pathogenic degradation.[7,169,170] Many techniques exist for investigating lignin deposition. They include the use of specific stains, ultraviolet (UV) microscopy, autoradiography, and scanning electron microscopy-energy dispersive X-ray analysis (SEM-EDXA). (Lignification becomes somewhat operationally defined when using these various techniques. For example, autoradiography is used to study the deposition of lignin precursors whereas UV microscopy is used to investigate the deposition of UV absorbing material [280 nm] and although both techniques are used to study lignification, the "lignin" that they detect may not be identical.)

In an early study on *Pinus radiata*, Wardrop[171], using UV microscopy, suggested that lignification was initiated in the cell corner regions and then extended to the intercellular layer (middle lamella) and primary wall. The process continued towards the lumen through S_1, S_2, and S_3 layers, lagging behind cell wall formation. The same process of lignification was shown to occur in Japanese larch (*Larix leptolepis*) by Imagawa *et al.* using UV microscopy.[172] One notable difference was that lignification was found to take place initially in the middle lamella at the junction of the tracheid cell corners.

Potassium permanganate has been used for lignin detection by many investigators.[173-176] Wardrop[173], using this technique, found that in Pinus radiata the initial lignin deposition took place in the cell corner region of the middle lamella. In some cases, the secondary wall revealed some lignin although the primary wall was unlignified at this point. The process continued to spread through the middle lamella to the primary wall, and subsequently into the secondary wall.

The use of this stain to follow the course of lignification has been brought into question. A number of investigations have suggested that the specificity for lignin is in doubt, and that the staining intensity is not necessarily proportional to lignin content.[177,178]

The pattern of lignification has also been studied using radioactive precursors of lignin. Saleh et al.[179] treated cuttings of Populus trichocarpa, Pseudotsuga menziesii and Triticum vulgaris with tri-tritiated ferulic acid. It was observed that the labeled lignin was first deposited in the primary wall at the cell corners, and was followed by deposition in the intercellular layer. No lignin was detected in the secondary wall, but in a later study by Fujita and Harada[180] using di-tritiated ferulic acid, lignin was found in the secondary cell wall of Cryptomeria japonica. The authors suggested that the failure of Saleh et al. to detect radioactivity in the secondary wall may have been a consequence of the lower lignin concentration in that region.

SEM-EDXA techniques have been applied to the study of lignification in loblolly pine (Pinus taeda) by Saka and Thomas.[181] They found that the process was initiated in the cell corner middle lamella and compound middle lamella regions prior to S_2 formation. A rapid deposition of lignin occurred in these regions. When the middle lamella lignin concentration was approximately 50%, a more gradual deposition in the secondary wall commenced. The S_1 layer was lignified first. The process continued through the S_1 to the S_2, lagging just behind cell wall formation. Finally, the S_3 layer became lignified. It was further found that the concentration of lignin was higher in the S_1 and S_3 layers than the S_2 layer.

A comprehensive study of the deposition of cell wall components in conifer tracheids was undertaken by Takabe using a variety of techniques.[132] Lignification was found to be initiated at the outer surface of the primary wall in the cell corner just before S_1 formation. Lignification of the intercellular layer (middle lamella) and the outermost part of S_1 was begun at the cell corner in the S_1 formation stage and gradually proceeded to the unlignified intercellular layer and the outermost part of S_1, respectively. Lignification of the primary wall occurred at the start of S_2 formation. Lignification of the secondary wall began at the outer part of S_1 and proceeded towards the lumen. Lignin accumulation occurred throughout the secondary wall after S_3 formation. It was also suggested in this study that there were differences in lignin between the compound middle lamella and secondary wall;

the former was found to be richer in the "bulk-polymer" while the later was richer in the "end-polymer." These terms refer to how the monolignol is added to the lignin molecule; all at once in the case of the "bulk-polymer" and slow addition in the "endwise polymer" case.

Biogenesis

Several investigators have attempted to identify particular organelles associated with the process of lignification. Wardrop[173] observed the accumulation of vesicular structures between the plasmalemma and the cell wall during lignification. Similar structures were observed by Hepler et al.[174] between the plasmalemma and developing secondary thickenings of the primary xylem of Coleus. Using tritiated cinnamic acid, Pickett-Heaps[183] found that the radioactivity was associated with the vesicles derived from the Golgi apparatus and possibly from the endoplasmic reticulum.

Fujita et al.[184] working with reaction xylem of Cryptomeria japonica observed what appeared to be Golgi vesicles fusing with the plasmalemma. They speculated that lignin precursors are synthesized and stored in the Golgi vesicles and are incorporated into the wall by fusion of the vesicle membrane and plasmalemma.

Takabe[182] using tritiated phenylalanine observed Golgi bodies, Golgi vesicles, and irregularly swollen smooth endoplasmic reticulum (s-ER) to be associated with the radioactivity. He stated that these results suggest that

the Golgi bodies and s-ER are involved in the biosynthesis and/or transport of lignin precursors.

The final step in lignin biogenesis may not be enzyme catalyzed. The enzymes that initiate lignin biosynthesis are dehydrogenases whose products are free radicals of monomeric lignin precursors. These precursor radicals polymerize spontaneously with other precursor molecules and existing lignin in an autocatalytic radical chain reaction.[185] The random nature of this reaction results in the formation of a three-dimensional, highly branched, interlocking network of essentially "infinite" molecular weight.

Cell Wall Architecture

There are two classes of questions that can be asked about the architecture of plant cell walls. Detailed questions about the nature of the wall polymers, how they are made, assembled, and cross-linked belong to the first class. The second class of questions is harder to define. Questions about the degree and significance of microheterogeneity within the wall, i.e., the spatial distribution of the various cell wall components are included in this class.

Compared with the increasing chemical literature in answer to the first class of questions, answers to the second class are relatively few. There are several reasons for this, but one major one has been the lack of highly specific probes for cell wall components.

Primary Cell Walls

Many models have been put forth to describe the three-dimensional structure of primary plant cell walls. Almost exclusively, they deal with the bonding schemes of the various components. They do not address compositional variability and, for the most part, spatial organization. And, of course, lignin is not included in these models.

Albersheim and his colleagues[186] presented a comprehensive model of the primary wall. From their studies on suspension-cultured sycamore cells they deduced the structure shown diagrammatically in Figure 11. The components of the wall are all interconnected by covalent bonds with the exception of the connection between cellulose and xyloglucan where hydrogen bonding occurs. There have been questions expressed that their model is not acceptable in terms of known wall properties, i.e., the bonding scheme accommodates cell expansion but does not adequately provide for cell elongation.[187]

Monroe, Penny, and Raymond[188] proposed a somewhat similar model (based on data from lupin hypocotyls). This model was based on the known conformation of polysaccharides and on known wall properties. Their model overcame some of the shortcomings of Albersheim's model, specifically in its ability to accommodate bonds of the labilities (guanidinium thiocyanate- and potassium hydroxide-labile bonds) encountered in their study.

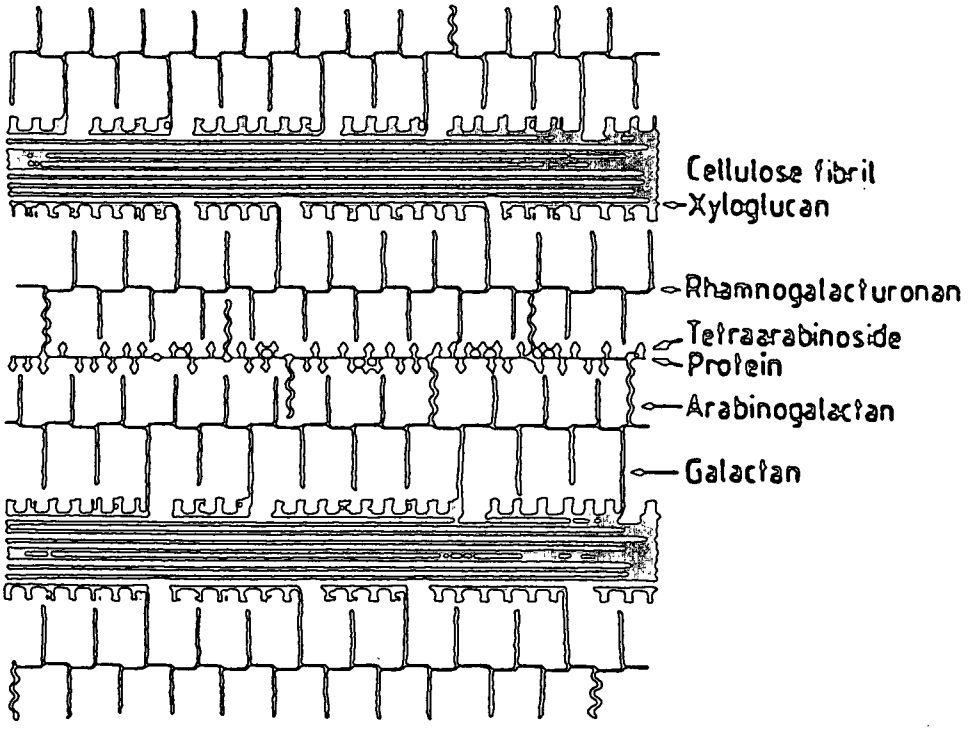

Figure 11. Structural model of the primary cell wall showing the major components as well as their interconnections. This model was based on data from suspension-cultured sycamore cells.[186]

The orientation of cellulose microfibrils has been indirectly addressed in an article by Hayashi et al.[189] These authors suggested that, because of the strong interactions between xyloglucans and cellulose microfibrils, it was possible that the assembly of cellulose molecules into microfibrils could be influenced by the availability of xyloglucans at the assembly sites. It has been stated that this type of control of microfibril formation would have marked architectural consequences.[190]

An in-depth review on plant cell wall architecture has been prepared by Varner and Lin.[190] It is principally concerned with primary cell wall assembly, but does briefly mention lignification.

Secondary Cell Walls

The molecular architecture of woody cell walls is poorly understood. The cellulose component has received a great deal of attention but very little is known of the way in which the microfibrils are held together by the matrix substances or how these themselves are bonded. It is known that some molecular chains of xylan and mannan are bound to the microfibrils and therefore lie parallel to them.[191] It has been claimed that the molecular chains of all hemicelluloses lie parallel to the general run of microfibrils.[192] To this extent, a model of the polysaccharide components of the wall would consist merely of a set of parallel lines, the lines within the cellulose fibrils being regularly spaced but not those outside them (hemicelluloses). (The spacing is a reflection of the region's crystallinity; cellulose is considered to be crystalline in the X-ray diffraction sense whereas hemicelluloses are not.[191])

As was stated previously, there is a lack of consensus about the organization of the components in the cell wall. It is still uncertain whether the organization is lamellar, i.e., a layered structural organization, or not (fibrillar). A cell wall model which takes into account the presence of lignin

was proposed by Fengel[283] In this model, the cellulose fibrils are surrounded by loosely packed hemicellulose molecules (Figure 12). The whole carbohydrate complex is subsequently enclosed by a lignin matrix.

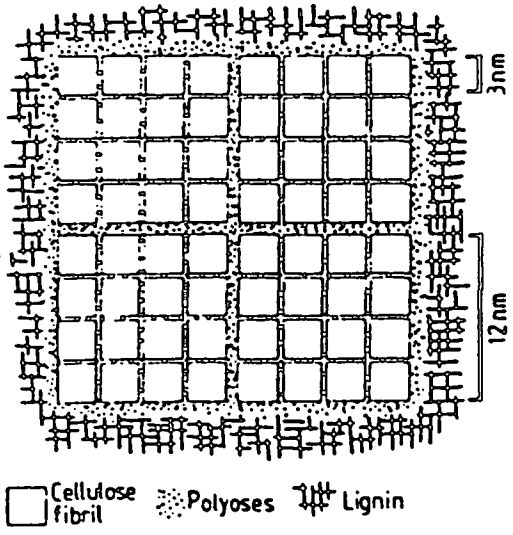

Figure 12. Model of the association of cell wall components according to Fengel.[283]

Figure 13 shows two additional models of the supermolecular organization of the woody cell wall. Figure 13a shows what Page[192] envisioned for the structure of a softwood tracheid cell wall. In his model, hemicelluloses are oriented parallel to the cellulose fibrils and form a single cocrystallized layer around them. (He speculated that the hemicelluloses perform a structural function by providing a link between cellulose and lignin and thus serve as "coupling agents".) Page's model is not appreciably different from that proposed by Fengel mentioned above. The concept that he put forth was that

hemicelluloses function as coupling agents between cellulose and lignin and thus he added a rationale to the structural models of softwoods that was previously lacking.

More recently, Kerr and Goring[165] proposed an interrupted lamella model for the arrangement of the major components as shown in Figure 13b. Their model consists of layers of cellulose-hemicelluloses blocks interrupted in the radial and tangential directions by lignin-hemicelluloses blocks. The model finds some support in the proposal by Scallan.[168] He suggested that if the cell wall was swollen when lignification took place, lignin would be laid down in disc-shaped, tangentially oriented platelets (Figure 10). These platelets are similar to the lignin blocks proposed in the interrupted lamella model.

The interrupted lamella model, although widely published, is not without its opponents. Data obtained from a study of cell wall architecture by Ruel and Barnoud[194] did not agree with the Kerr and Goring model. The authors used the fungus Phanerocheate chrysosporium to degrade the cell wall in spruce wood which permitted the electron microscope visualization of the lignin network. They observed lignin threads 3 to 5 nm in width (as a minimum) mixed with cellulose fibrils but were unable to determine if lignin was continuous or not under their conditions of observation. They noted that their data did not agree with the Kerr and Goring cell wall model. In particular, the longitudinal sections did not show the predicted images corresponding to lignin lamellae seen in transverse sections. They pointed out that their observations are

(a)

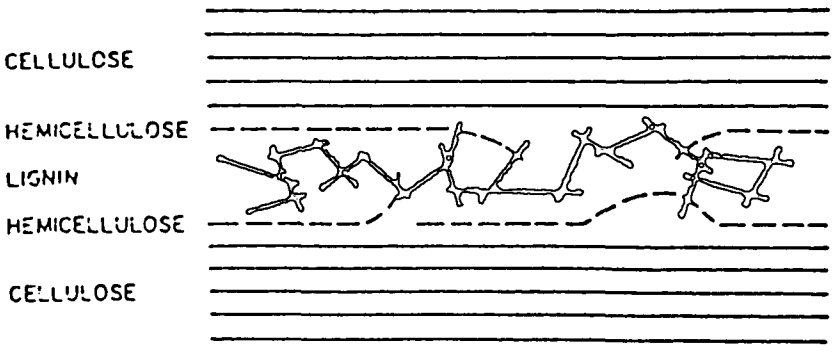

(b)

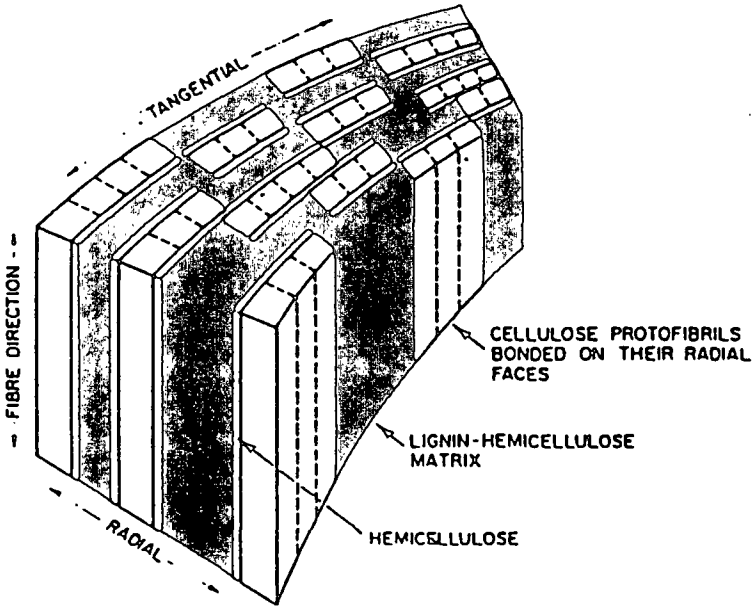

Figure 13. Woody Cell Wall Models. (a) Model for the structure of the softwood tracheid cell wall as proposed by Page.[192] (b) Pictorial representation of the interrupted lamella model for the ultrastructural arrangement of lignin, cellulose, and hemicellulose in the wood cell wall by Kerr and Goring.[165]

more in line with an earlier proposal of Goring[150] where lignin is made *in situ* of a network of short, linear and reticulated chains. (Goring's concept is similar to the lignin network depicted in Figure 13a.)

It has been stated that "an accurate cell wall model must eventually take into account ... orientation of wall components, detailed structure of wall polymers, and the nature of bonds between components. Our knowledge of (primary) cell wall structure is at the moment too inadequate to allow the models proposed now to be other than working hypotheses".[188] It should be added that compositional variability both within and between fibers is another facet that must be included to further our understanding of the architecture of the cell wall.

THEORY

The last major part of the Introduction provides the reader with the theoretical background that is needed to understand certain aspects of this thesis. The principles of photochemistry are discussed in the first part of this section, while the Raman scattering process and Raman band enhancement effects are addressed in the second.

Principles Of Photochemistry[11,12,48]

Photochemistry is the study of the physical or chemical processes which occur in molecules upon the absorption of UV-visible radiation. All photo-

chemical processes are governed by four photochemical laws:

1. The law of Grotthus and Draper[11] states that a photochemical reaction may occur only if light of sufficient energy is absorbed by the system.
2. The law of Stark, Einstein, and Bodenstein[11] states that in the primary step of a photochemical reaction sequence, each photon or quantum absorbed activates only one molecule (this ignores biphotonic excitation).
3. The absorbed photon has a certain probability of populating either the excited singlet or triplet state.
4. The lowest excited singlet and triplet states are the starting levels of most organic photochemical processes.

Photochemical processes usually occur in two stages:

1. Primary photochemical reaction. This reaction is directly due to the absorbed photon and involves electronically excited states.
2. Secondary photochemical reactions (dark reactions). These are the reactions of the various chemical species, i.e., radicals, radical ions, ions and electrons, which are produced by the primary photochemical reaction.

When a molecule absorbs electromagnetic radiation (light) and becomes excited, its energy increases by an amount equal to the energy of the absorbed

photon (E):

$$E = E_2 - E_1 = h\nu = \frac{hc}{\lambda} = hc\tilde{\nu} \qquad [1]$$

where: E_2 = energy of the excited state molecule after light absorption,

E_1 = energy of the ground state molecule before light absorption,

h = Planck's constant = 6.626×10^{-34} Joules·sec.,

ν = frequency of radiation ($sec.^{-1}$),

λ = wavelength of radiation,

c = speed of light = 3×10^8 meters/sec.,

$\tilde{\nu}$ = wavenumber of radiation = $1/\lambda$.

For most organic molecules, the energy difference between the ground and excited states of lowest energy is such that the wavelength of absorbed radiation falls in the ultraviolet-visible region of the electromagnetic spectrum. Some typical values for the energy of UV-visible radiation are given in Table 2. This energy is comparable with bond dissociation energies in organic molecules and in certain inorganic molecules (Figure 14).

Photoexcited molecules are highly energetic and although this facilitates chemical reaction, these molecules are short-lived and can often lose their excess energy and return to the stable ground-state before reactions can occur. The possible paths for the deactivation of an excited state are shown in Figure 15. The first three paths (left-to-right) are intramolecular deac-

tivation processes whereas the latter two are intermolecular. The intramolecular processes are further divided into radiative and non-radiative processes. The intramolecular processes and intermolecular deactivation processes occur concurrently and thus the likelihood of a photochemical reaction is dependent upon the rates of intramolecular energy dissipation processes as compared to the rates of chemical reaction.

Table 2. Energy of Ultraviolet-Visible Radiation.[12]

Region	*Approx. wavelength range* (nm)	*Wave number values* $\bar{\nu}$ (cm^{-1})	*Energy* $\times 10^{-5}$ ($J\ mol^{-1}$)
	200	50 000	5.95
Ultraviolet	↕		
	400	25 000	2.98
Violet	↕		
	450	22 222	2.65
Blue	↕		
	500	20 000	2.39
Green	↕		
	570	17 544	2.09
Yellow	↕		
	590	16 949	2.03
Orange	↕		
	620	16 129	1.93
Red	↕		
	750	13 333	1.59

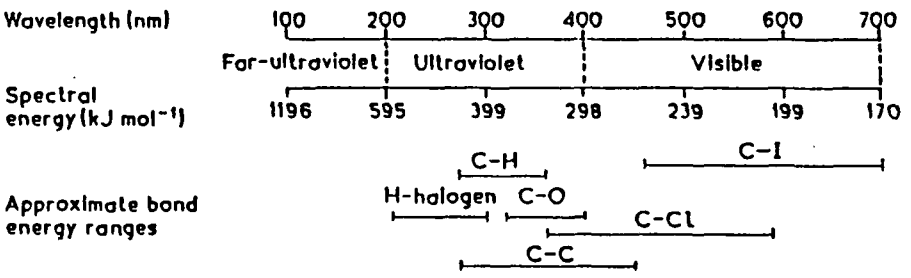

Figure 14. Comparison of the spectral energies in the ultraviolet-visible region with bond dissociation energies.[12]

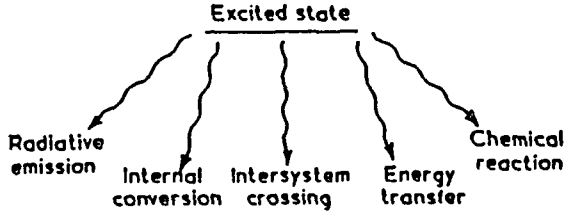

Figure 15. Possible paths for the deactivation of an excited state.[12]

The deactivation processes are best illustrated by a modified "Jablonski" diagram (Figure 16). Absorption (A) of a photon leads to the formation of an excited singlet state (S_1). Generally one of the higher vibrational levels of that state will become excited. Rapid deactivation occurs by vibrational cascade (B) or internal conversion (C) to the lowest vibrational level of the first excited singlet state (S_1).

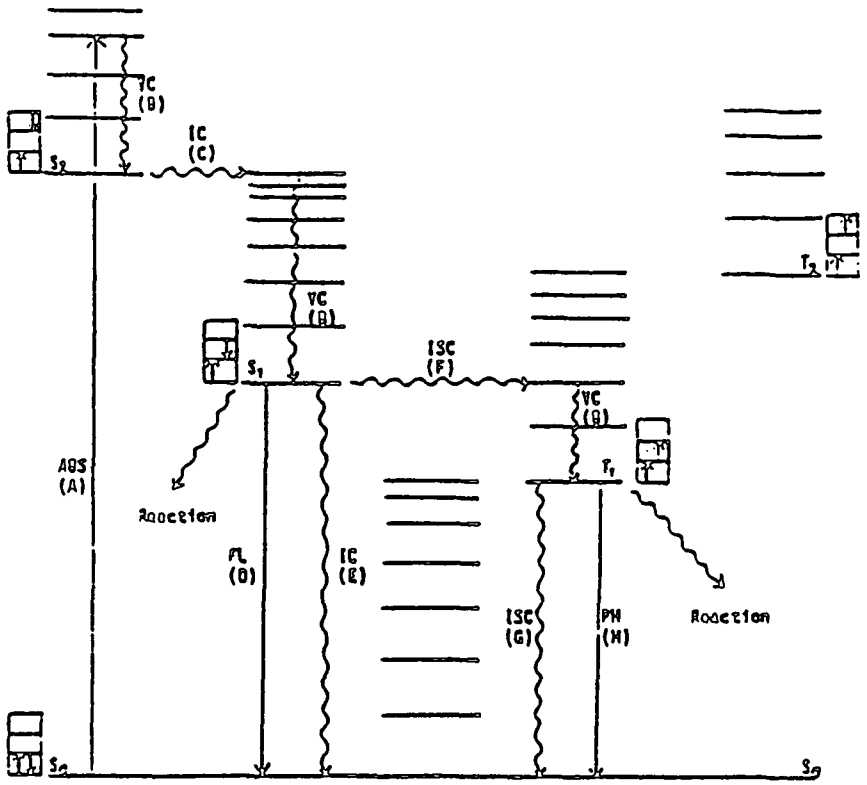

—— Transition with absorption or emission of radiation
≈≈≈ Nonradiative transitions

S_0	: Ground state singlet	VC	: Vibrational cascade
S_1	: First excited singlet	IC	: Internal conversion
S_2	: Second excited singlet	FL	: Fluorescence
T_1	: First excited triplet	PH	: Phosphorescence
T_2	: Second excited triplet	ISC	: Intersystem crossing
ABS	: Absorption		

Figure 16. Modified Jablonski diagram.[47]

Once deactivated to its first excited singlet state, several paths exist for the molecule to return to its initial ground state. It may lose its excess energy by a radiative emission process known as fluorescence (D). Deactivation by non-radiative processes are also possible. Internal conversion (E - a spin-allowed transition between two states of the same multiplicity) to the ground state may occur or, alternatively, intersystem crossing (F - a spin-forbidden transition between two states of different multiplicity) is possible. If a vibrationally excited triplet state is formed, it is rapidly deactivated to the first excited triplet state (T_1). Subsequent deactivation occurs either by intersystem crossing (G - the excess energy is converted to the thermal energy) or by a radiative process referred to as phosphorescence (H).

Energy transfer to an acceptor molecule or chemical reaction are also possible deactivation mechanisms. Energy transfer normally takes place from either the S_1 or T_1 state of the donor with the formation of an S_1 or T_1 state of the acceptor. Energy transfer is commonly referred to as quenching because, if it is sufficiently rapid, all excited state molecules can be deactivated, and thus fluorescence or phosphorescence will be quenched. Chemical reaction can also occur from either the S_1 or T_1 state, and includes such processes as internal rearrangement, fragmentation, and reactions with other molecular species in the system. These processes can result in the formation of free radicals, which are very reactive and can

participate in secondary photochemical reactions.

For a detailed discussion of the mechanisms of photophysical processes and photochemical reactions in polymer systems, see Rabek.[48]

Raman Scattering

Overview[198-202]

Raman scattering was first observed in India in 1928 by C.V. Raman. The Raman effect arises from the interaction of the incident light with the electrons in the illuminated sample and results in changing the molecule from its initial vibrational state to a different vibrational state.

When a molecule interacts with light, the electric field of the photons will exert oppositely directed forces on the electrons and the nuclei. As a result, the electrons will be displaced relative to the nuclei and the polarized molecule will have an induced dipole moment caused by the external field. The induced dipole moment P is proportional to the electric field E:

$$P = \alpha E \qquad [2]$$

The proportionality constant α is the polarizability of the molecule, i.e., the ease with which the electron cloud of the molecule can be distorted.

Following a classical mechanical derivation for polyatomic molecules,

equation 2 becomes:

$$P = E_0\alpha_0 \cos 2\pi\nu_0 t + \frac{1}{2}\sum_{i=1}^{3N-6} E_0 Q_i^0 \left(\frac{\partial\alpha}{\partial Q_i}\right)_0 \times \left[\cos 2\pi(\nu_0 + \nu_i)t + \cos 2\pi(\nu_0 - \nu_i)t\right] \qquad [3]$$

where: ν_0 = excitation frequency,

ν_i = vibrational frequency of molecule,

t = time,

N = number of atoms in the molecule,

Q_i = normal coordinates.

The first term refers to Rayleigh scattering (elastic) which is light unshifted in frequency. If for a particular vibration the polarizability of the molecule changes, then Raman scattering (inelastic) occurs and the incident light frequency is shifted to a higher value (2nd term - antiStokes scattering) and a lower value (3rd term - Stokes scattering). At normal room temperatures, Stokes Raman scattering is more intense and thus is routinely studied and implied in Raman spectroscopy.

Equation 2 is valid for molecules with isotropic polarizability and states that the induced dipole moment P is parallel to the electric field vector E. In general, this is not true as the polarizability of most molecules is anisotropic and the induced dipole moment points in a different direction than the electric vector. The polarizability should, therefore,

properly be expressed as a symmetric matrix (tensor), and equation 2 thus becomes:

$$\begin{aligned} P_x &= a_{xx}E_x + a_{xy}E_y + a_{xz}E_z \\ P_y &= a_{yx}E_x + a_{yy}E_y + a_{yz}E_z \\ P_z &= a_{zx}E_x + a_{zy}E_y + a_{zz}E_z \end{aligned} \qquad [4]$$

where x, y, and z are the axes of an arbitrary coordinate system. This expression relates band intensity (proportional to the square of the induced dipole moment for the vibration) to molecular orientation. It is possible, therefore, to infer information about molecular organization by observing the effect of the polarization of the incident light on Raman band intensities.

Band Enhancement

It has been known for some time that the Raman intensities of certain molecular vibrations are sensitive to both excitation frequency and conjugation. The first effect is usually termed resonance Raman enhancement (RRE), while the latter is referred to as conjugation enhancement (CE).

Preresonance Raman Enhancement[199-204]

When a molecule is excited with incident light whose frequency is within an electronic absorption band, the intensity of some Raman lines is greatly enhanced. This effect (RRE) is due to the coupling of electronic and vibra-

tional transitions and was first predicted by Placzek[203] and later confirmed by Shorygin.[204]

In resonance Raman scattering, the energy of the incident photons coincides with that of an electronic transition. When their energy is close to but not higher than an electronic excitation level of a molecule, the process is referred to as preresonance Raman scattering (PRRE).

The reason for the enhancement can be seen in a theoretical quantum-mechanical expression for the Raman scattering tensor α_{ij}. This tensor is viewed classically as the molecular polarizability and is proportional to the scattered light intensity. The expression is given by:

$$(\alpha_{ij})_{mn} = \frac{1}{h} \sum_{e} \left[\frac{(M_j)_{me}(M_i)_{en}}{\nu_e - \nu_0 + i\Gamma_e} + \frac{(M_i)_{me}(M_j)_{en}}{\nu_e + \nu_s + i\Gamma_e} \right] \qquad [5]$$

where i and j refer to the orthogonal coordinate directions x,y, or z, ν_0 is the excitation frequency, ν_e is the frequency of the transition between the ground and excited electronic state, ν_s is the scattered (Raman) frequency, and $i\Gamma e$ is a damping term related to the width of the excitation state ν_e. The initial and final states of the molecule are represented by m and n, respectively, and the $(M_j)_{me}$ and $(M_i)_{en}$ are electronic dipole transition moments along the directions j and i, from the initial state of m to an

excited state e and from e to the final state n. h is Planck's constant.

In the nonresonance region $\nu_0 << \nu_e$ and α_{ij} is independent of the exciting frequency. When the incident laser frequency ν_0 approaches the excited electronic transition ν_e, the denominator of the right-hand side term becomes very small (the damping term, $i\Gamma_e$ prevents it from reaching zero) and hence the polarizability element α_{ij} becomes very large, i.e., it is subject to preresonance enhancement. This effect can effectively increase the Raman band intensity by many orders of magnitude.

It is important to remember that there are no clear dividing lines between nonresonance, preresonance, and resonance Raman scattering. The intensity of a Raman band is a function of the incident light frequency.

Conjugation Enhancement[99-106,199,204-206]

Raman intensities of certain molecular vibrations are known to depend on conjugation.[99,205,206] Unfortunately, the theoretical background of Raman intensities is not complete, and consequently, most approaches to understanding the relationship between intensity and conjugation are semi-empirical in nature.

Schmid et al.[100-106] have taken this approach in their investigation of Raman intensity and conjugation in aromatic compounds. In an early paper they showed that the degree of band enhancement directly depended on the

amount of pi-electron conjugation between the aromatic ring and substituents.[100] In later papers, they attempted to quantify this relationship. Empirical relationships were derived for intensity and (1) conjugation length[104], and (2) degree of planarity in conjugated systems.[105]

The reason for the enhancement can be inferred from molecular orbital theory together with expressions for Raman intensity. According to molecular orbital theory, conjugation results in the sharing of electrons when the pi-bond is formed, i.e., the pi-electrons are delocalized throughout the conjugated system. As the extent of conjugation increases, the electron density distribution is altered further. Referring to the semi-classical expression for Raman intensity below (Equation 6), conjugation must alter the molecular polarizability (scattering tensor, α_{ij}) to influence Raman intensity. This variable (α_{ij}) relates to the ease with which the electron cloud of the molecular can be distorted.

$$I = \frac{2^7\pi^5}{3^2C^4} I_0 \nu_s^4 \sum_{ij} |\alpha_{ij}|^2 \qquad [6]$$

where: I_0 = intensity of incident light,

ν_s = frequency of scattered light,

α_{ij} = the components of the polarizability tensor.

In a conjugated system, therefore, the electron cloud may be more easily

distorted. This seems reasonable in light of the fact that the electrons are delocalized throughout the conjugated system. To understand this effect further, the quantum mechanical expression for α_{ij} needs to be consulted (Equation 5). For α_{ij} to increase, either the electric dipole transition moments must increase and/or the excited electronic transition frequency (ν_e) must decrease. It is known that as the extent of conjugation increases, the energy difference between the highest occupied molecular orbital (HOMO), and the lowest unoccupied molecular orbital (LUMO) decreases, i.e., ν_e decreases.[210] The effect of conjugation on the electronic dipole transition moments is harder to assess, so the magnitude of the effect is not known.

It thus is likely that conjugation enhancement is due to the change in charge distribution brought about by conjugation (pi-bonds). This delocalization of electrons allows the electron cloud to be more easily distorted by the fluctuating electric field of the incident photons.

A consequence of increased conjugation is that as the wavelength of maximum absorption is shifted to longer wavelength, the effect of preresonance Raman enhancement is increasingly seen. Thus, while the preresonance Raman enhancement contribution can be ascertained by using longer excitation wavelengths, the contribution specifically due to conjugation enhancement cannot be determined with certainty.

Local Temperature Determination At A Sample[199,207,209]

Local heating due to high laser power densities in micro-Raman experiments can easily result in damage or modification to the sample. Various techniques exist to dissipate this thermal energy, such as sample immersion or the use of a heat sink underneath the sample, but at high incident power levels, none of these methods is entirely satisfactory.

A simple method to minimize this unwanted effect is to lower the incident laser power level below the damage threshold. Unfortunately, the signal-to-noise level drops because the intensity of the Raman scattered light, which was low to begin with, is reduced further. In addition, thermal modification may be occurring even though sample burning is not apparent. As will be shown, by measuring the intensity of both Stokes (I_S) and antiStokes (I_{AS}) lines for a particular vibration, the local temperature can be determined and the optimum incident power level ascertained. Furthermore, this determination has important physical-chemical implications.

The intensities of the Stokes and antiStokes lines depend on both the ground and excited state population for a specific vibration. These populations, in turn, are dependent on the temperature of the sample. At thermal equilibrium, the relative occurrence of the ground and excited states follows the Boltzman distribution:

$$I_S/I_{AS} \propto \exp(hc\nu_1/kT) \qquad [7]$$

where: h = Planck's constant = 6.626×10^{-34} Joules·sec.,

c = speed of light = 3×10^8 meters/sec.,

ν_1 = absolute wavenumber of the band (represents the energy difference between the excited and ground states),

k = Boltzman constant = 1.381×10^{23} J/K,

T = absolute temperature.

According to Hayes and Loudon[207], the frequency dependence of the Stokes and antiStokes scattering processes can be described by:

$$I_S \propto \nu_0(\nu_0-\nu_1)^3 \qquad [8]$$

$$I_{AS} \propto \nu_0(\nu_0+\nu_1)^3 \qquad [9]$$

where: ν_0 = excitation frequency,

$\nu_0-\nu_1$ = frequency of the Stokes band,

$\nu_0+\nu_1$ = frequency of the antiStokes band.

Combining equations 7, 8, and 9 results in the following expression:

$$I_S/I_{AS} = \frac{(\nu_0-\nu_1)^3}{(\nu_0+\nu_1)^3} \exp(hc\nu_1/kT) \qquad [10]$$

or solving for T:

$$T(K) = \frac{hc\nu_1}{k} \left[\ln\left(\frac{I_S}{I_{AS}}\right) - 3\ln\left(\frac{\nu_0-\nu_1}{\nu_0+\nu_1}\right)\right]^{-1} \qquad [11]$$

Therefore, by measuring I_S/I_{AS}, one can determine the local temperature of the sample due to the exciting laser beam using equation 11.

EXPERIMENTAL MATERIALS AND METHODS

EXPERIMENTAL PROGRAM

The experimental program can be divided into two main parts. The first part was exploratory in nature and dealt with understanding the decay of the 1595 cm^{-1} aromatic ring-breathing vibrational band of lignin during 514.5 nm laser irradiation of water-immersed woody tissue. The investigation focused on three general areas: understanding the cell wall marking that occurred simultaneously with the 1595 cm^{-1} band decline, Raman band enhancement effects in woody tissue, and stabilizing lignin to 514.5 nm radiation. The experimental approach in this first part consisted of performing a specific experiment, analyzing and interpreting the data, performing a subsequent experiment using the knowledge gained from the preceding experiment(s), etc. The results of this exploratory investigation are discussed in the PHOTOCHEMICAL EFFECTS IN WOODY TISSUE section of the thesis.

The second part of the experimental program was concerned with the spectral mapping of the organization of cellulose and lignin in the secondary cell walls of softwood tracheids. The Raman band at 1098 cm^{-1} (chain axis) was used to explore the organization of cellulose molecules while the 1595 cm^{-1} band was used to determine lignin (aromatic ring) organization. By varying the plane of polarization of the incident laser light relative to the cell wall and observing the changes in the intensities of these bands, it was

possible to argue for or against a particular orientation.[10] (Two electric vector [EV] orientations were used in this study: parallel to the long axis of the cell wall and perpendicular to it.) In order to investigate the compositional variability, the band intensities when the EV was oriented parallel and perpendicular to the cell wall were added together for each component to evaluate the total amount of cellulose/lignin in the particular domain. This was done to ensure orientational effects did not confuse the situation.[10]

The second part of the experimental program consisted of two major steps. The first step was to select an appropriate tree species to investigate. Black spruce has traditionally been used in our laboratory for the Raman microprobe study of plant cell walls. Due to its rather narrow (radial) latewood single wall thickness, it was decided to choose another softwood species with a larger wall thickness to use in addition to black spruce as detailed in the EXPERIMENTAL MATERIAL AND METHODS - SPECIES SELECTION section of the thesis.

The second step dealt with choosing the location, pattern, number, and spacing of the data collection points on the secondary cell wall. The location of the data collection region was somewhat dictated by being able to locate suitable areas on two adjacent fibers. The region needed to have a relatively planar surface and be free of sectioning artifacts, have well defined boundaries between the various morphological regions, and be of adequate length to allow multiple sampling along the fiber's length. (The

occurrence of rays crossing the fiber's long dimension at right angles compounded this latter requirement.) In addition, the secondary single wall thickness of the fibers in the selected region should allow for multiple point sampling in their width direction. Thus, the locations chosen to investigate for the two woody species were found by scanning the fibers through the microscope and selecting regions which met the above criteria. The investigated regions were close to the earlywood/latewood transition (the wall thickness criterion) and somewhere in the middle two-thirds of the fiber's length. This latter position was difficult to determine with any degree of certainty because the ends of the fibers were seldom observed.

The choice of the particular sampling pattern and number of data points was somewhat arbitrary. Information obtained, time to acquire the data from the grid of sampling points, and the effect of biasing the data from a neighboring location (the sphere-of-influence of the laser beam on the lignin macromolecule) entered into the decision. A 10 x 5 grid pattern was chosen after consideration of the above items. This grid area included three distinct morphological regions: the S_2 cell wall layer of one fiber, the compound middle lamella (CML) between, and the S_2 layer of the adjoining fiber. Ten locations along (parallel to the fiber's longitudinal axis - "row") and two (one for the CML) locations across (perpendicular to the axis - "column") each fiber region were studied. (The black spruce data include an additional S_2 row of ten data points. At this spacing it was observed that the photo-

modified region surrounding the data points overlapped and it was decided to reduce the number of S_2 rows from three to two to minimize this. The grid for black spruce is thus 10 x 6: 10 x 3 [S_2], 10 x 1 [CML], and 10 X 2 [S_2].)

The (along the fiber) spacing between the individual data points was governed on one extreme by the minimum step (increment) size of the motorized microscope stage and on the other by the occurrence of suitable cell wall regions of adequate length to accommodate the ten sampling points. One micron was the smallest step size attainable with the motorized stage, but at this spacing the sphere-of-influence of the laser beam, i.e., the photomodified area, overlapped the neighboring data point. A ≈2.5 micron spacing was selected as a compromise between keeping the data points close enough to each other to achieve some degree of correlation and far enough apart so that irradiation at one location did not unduly influence the neighboring location.

As was previously mentioned, it is possible to infer information about molecular orientation by observing the effect of the polarization of the incident light on Raman band intensities. Because of dichroism in the optics of both the microscope and the spectrometer (these components may favor one polarization direction over another), the rotation of the electric vector relative to morphological features is usually accomplished by rotating the sample. This was not practical for the mapping studies because of the sensitivity of lignin to laser radiation and the difficulty in accurately positioning the sample after rotation. In lieu of sample rotation, electric vector

rotation was accomplished by using a laser-line rotator - also known as a half-wave retardation plate. (The half-wave plate is an optical element typically made of mica or quartz that resolves the incident polarized beam of light into two orthogonally polarized components and retards the phase of one component by 180° relative to the other. The sum of the two emergent beams is a beam with linear polarization but rotated twice the angle the incident beam's electric vector made with the optic axis of the retarder. By changing this angle it is possible to continuously adjust the plane of polarization of the emergent beam.) In order to minimize dichroism introduced by this method, a polarization scrambler was inserted into the optical path just prior to the entrance slit of the spectrometer. This effectively made the spectrometer insensitive to the plane of polarization. (It has been reported that the scrambler may not be 100% effective due to the small diameter of the scattered light beam.[271])

The beam splitter in the microscope was another source of dichroism. Here it was necessary to use a standard (toluene) to correct the spectra for dichroic effects. The beam splitter is more efficient at reflecting light if the incident electric vector is parallel to the plane of the beam splitter. Because of this effect, the incident power at the sample was ≈2.1X greater when "perpendicular" spectra were recorded. In addition to this power effect, another complication arose because the Raman scattered light must pass back through the beam splitter. Depending on the orientation of the electric

vector, the scattered light could be attenuated.

Due to the sensitivity of lignin to 514.5 nm radiation, the (EV) parallel and perpendicular pair of spectra used to investigate orientation could not be obtained from the same location. (The initial irradiation modified the area in such a way that lignin orientation information was lost.) To circumvent this difficulty, it became necessary to collect parallel information from the first location, perpendicular from the next location, parallel from the third, and so forth along the fiber. (A total of ten locations along the fiber were investigated; thus "parallel" information was collected at five locations and "perpendicular" information was acquired at the other five). The distance between the orientation pair, i.e., electric vector (EV) parallel and EV perpendicular, locations was approximately 2.5 microns.

In the previous cell wall organization studies using Raman spectroscopy, the O-D stretching band (2410 cm^{-1}) of D_2O was used as an internal standard.[10] (The woody tissue samples were immersed in D_2O rather than water.) It was possible to include this band in the 1098-1595 cm^{-1} window because the microprobe used in these investigations was coupled to the Ramanor scanning monochromator, and thus, the spectral region from 250 cm^{-1} to 3700 cm^{-1} could be acquired at one time. This was not possible with the nonscanning Spex system because only a 1000 cm^{-1} spectral window could be studied at one time (800-1800 cm^{-1} was used for the mapping study). This necessitated using the initial laser power level as the (external) standard. (The Spectra Physics Argon

ion laser had stabilization circuits which prevented wide exclusions in output power level.) In addition to monitoring this power level, it was necessary to focus the laser beam identically for all cell wall locations to minimize the effect of focus on Raman scattered light intensity. In this way the absolute rather than relative band heights were used in the analysis. Although the methods used to standardize the spectra were not entirely satisfactory, it was felt that any difference in results between the two standardization techniques would be minor.

During the initial few minutes of 514.5 nm irradiation of wet woody tissue, significant structural changes appear to be occurring to the lignin macromolecule (the 1595 cm^{-1} band decay). Because a method could not be found to adequately stabilize lignin to laser radiation, a methodology that minimized the bias introduced by the photomodification of lignin was followed in the mapping studies. This involved using a low laser power level (30 mW), keeping acquisition time to a minimum, and attempting to treat each acquisition location identically. Even though the power level was shown not to have a significant effect on the photomodification of lignin, a 30 mW power level was used to minimize any effect it might have had on the decay. Because of the more protracted 1595 cm^{-1} band decay in black spruce, the sections were subjected to a mild acid-chlorite (AC) treatment prior to data collection. (This treatment was shown to disrupt CE/PRRE of 1595 cm^{-1} band, but not alter the percent lignin content. In several of the AC decay studies, the initial

precipitous drop in 1595 cm^{-1} band intensity was not seen but only a gradual decline in intensity during 514.5 nm laser exposure, while in others, the AC decay curve was not significantly different from the control. (To what extent this behavior was due to structural differences in the lignin macromolecule was not known.) Thus, in an attempt to modify the initial drop, the black spruce sections were treated with acid-chlorite.) Loblolly pine was not subjected to a pretreatment because its 1595 cm^{-1} decay appeared to be almost instantaneous.

The general cell wall region used in the mapping investigation was irradiated with a very defocused laser beam for one hour prior to the start of data acquisition. This was done in an attempt to initiate the photochemical reactions and thus reduce the magnitude of the background fluorescence. Earlier experiments of this nature gave mixed results. (In some cases this pre-data-acquisition irradiation reduced the background level by more than half, while in other cases, the reduction was not as pronounced.)

INSTRUMENTATION

Raman Systems

A typical Raman spectrometer system consists of the following basic components: (1) an excitation source, usually a laser; (2) optics for sample illumination; (3) a double or triple monochromator; and (4) a signal processing system consisting of a detector, an amplifier, and an output device. The

configuration of these basic components is shown in Figure 17.

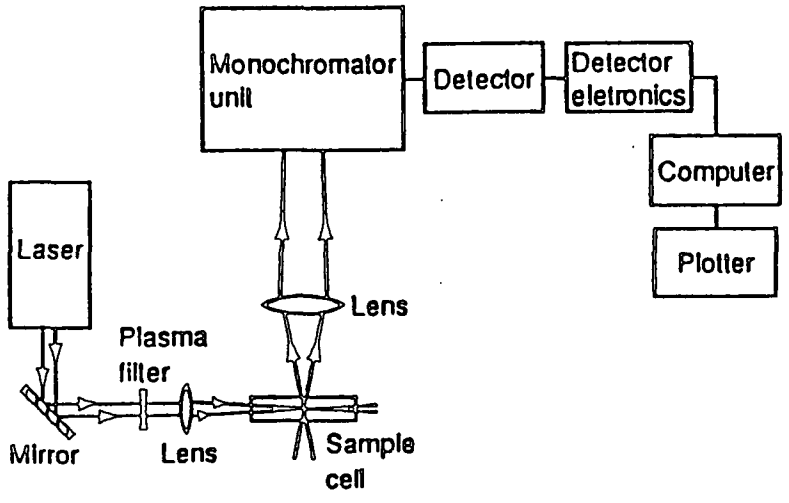

Figure 17. Schematic of a laser Raman system.

To acquire a Raman spectrum, the sample, suitably mounted, is illuminated by laser light. The collected scattered radiation is focused on the entrance slit of the monochromator whose purpose is to disperse this radiation and reject stray light. The light coming out the exit slit of the final monochromator is collected and focused on a detector which converts photons into an electrical signal after amplification. This signal (relative intensity) along with the wavelength at which the signal was produced, is stored in computer memory for signal averaging and post-acquisition processing. A typical Raman spectrum is a plot of relative intensity vs. Raman wavenumber

(wavenumber difference between the incident and scattered light).

Raman systems can be configured in two general ways depending upon the nature of the information desired. The classification is based upon the size of the data acquisition region, either macro or micro. The cutoff between the two is somewhere arbitrary, but typically micro-Raman instruments employ a microscope to deliver the incident radiation and collect the scattered light while macro-Raman instruments do not.

Information from the two types of instruments is identical in the case of homogeneous samples, but it is different with heterogeneous ones. In the latter case, macro-Raman instruments provide information which represents an average over all morphological features; the individual features which make up this average are studied with micro-Raman systems.

Macro Studies

System

The macromode spectra in this investigation were acquired with an Instruments SA Jobin Yvon Ramanor HG2S spectrometer system equipped with a thermoelectronically cooled photomultiplier tube detector (PMT). A Tracor Northern TN1500 data analyzer was coupled to the spectrometer to accumulate spectral data and was used for post-acquisition processing.

Sample excitation was done using either the 514.5 nm line of a Spectra

Physics argon ion laser (though occasionally the 457.9 and 488 nm lines were used) or the 647.1 nm line of a Spectra Physics krypton ion laser. Laser power levels varied depending on the sample and excitation wavelength, but were typically between 100 and 200 mW after the plasma line rejection filter. A 90-degree scattering geometry was employed, i.e., the incident laser beam and the axis of the collection lens were 90 degrees to each other.

The entrance slits of the double monochromator were set at 400 (or 800) microns which corresponded to a resolution of approximately 4 (or 8) cm^{-1}. Spectra were scanned at a rate of 60 wavenumbers/minute and the dwell time was 1 second. The reported spectra are averages of two to twelve scans. The spectral region between 250 cm^{-1} to 3700 cm^{-1} was studied.

High Pressure Sample Chamber

Laser-induced fluorescence from lignin-containing samples is a major hindrance to obtaining good quality spectra. Two techniques have proven effective in reducing this fluorescence. Water immersion was principally used with the Raman microprobe studies of lignocellulosics while oxygen flushing was used to study these samples using conventional (macromode) Raman spectroscopy.[244]

For the macromode investigations, 30-micron radial sections of woody tissue (air-dried) were mounted on a circular microscope coverslip by gluing the four corners of the section. The sample was inserted into a specially

constructed chamber designed to allow both gaseous flushing of oxygen and pressurization to 50 psi (Figure 18). Windows in the chamber permitted the focused incident laser beam to strike the sample and the scattered radiation to enter the monochromator. Typically a sample would be flushed with molecular oxygen for approximately 10 minutes to purge the chamber of nitrogen. Subsequently, the chamber would be pressurized to 50 psi oxygen and the irradiated sample left in this environment for 1 hour prior to data acquisition. This technique reduced the background fluorescence level dramatically and permitted the acquisition of high quality Raman spectra of woody tissue.[244] The spectra typically represent an average over 2-3 growth rings. (Lignin decay was not a problem. It has only been observed when the sample was wet. In the dry state, sample burning was prevented by reducing the incident power level and defocusing the incident beam. Care must be taken when exposing organic compounds to focused laser radiation under high pressure oxygen as rapid oxidation can lead to an explosion.)

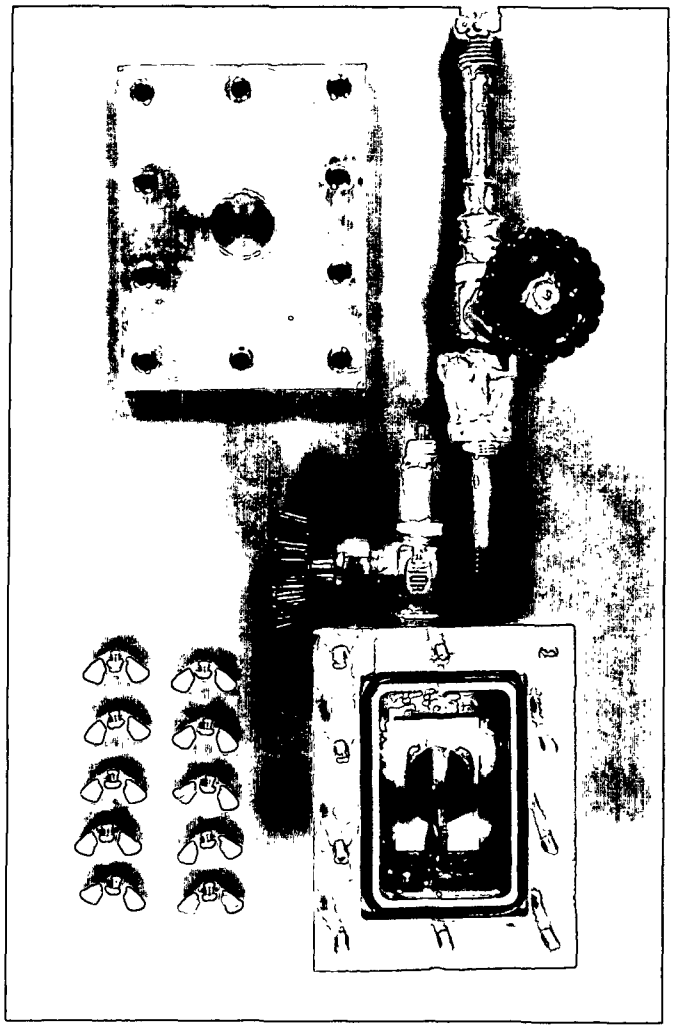

Figure 18. High pressure sample chamber.

Micro Studies

System

A recent innovation in Raman spectroscopy was the development of the Raman microprobe. It is a combination of an optical microscope and a conventional Raman spectrometer. The microscope system performs several key functions. The first is to focus the laser beam down to a spot as small as

one micron in diameter. A second function is to gather the scattered light and direct it onto the entrance slit of the spectrometer. In addition, it allows sample illumination with white light for viewing.

The Raman microprobe used in this investigation consisted of three basic components: a Spex Triplemate 1877B spectrometer, a modified Zeiss WL research-grade microscope coupled to the spectrometer, and a Tracor Northern TN6500 Optical Multichannel Spectroscopy System. The TN6500 system, in turn, consisted of a computer, detector interface, and a 1024 element intensified silicon diode array detector. (Spectrometers based on multichannel detection such as this are at least an order of magnitude faster than scanning systems using photomultiplier tube detectors.)

Both the 514.5 nm line from a Spectra Physics argon ion laser and the 647.1 nm line from a Spectra Physics krypton ion laser were used for sample excitation. Typically laser power levels were 100 mW after filter which translated to approximately 5-10 mW at the sample.

Spectra were recorded using a Zeiss 100X oil-immersion objective with a numerical aperture of 1.3 which gave a focused spot of approximately 1.5 microns in diameter. (Raman information is primarily being collected from this 1.5 micron region, although a small but unknown amount also comes from the area immediately surrounding the focused laser spot.) Spectral resolution was set to approximately 8 cm^{-1}. The reported spectra were signal averaged;

usually 100 scans were needed to obtain an acceptable signal-to-noise ratio. (Due to sensitivity of lignin to laser radiation, only 30 scans were signal averaged for the mapping spectra. These 30 scans coupled with a 3-second dwell time gave a total irradiation time of 90 seconds per spot. As a consequence of this, the mapping spectra were noisy and required post-acquisition processing to yield acceptable spectra. For a complete discussion of the post-acquisition processing, see EXPERIMENTAL MATERIAL AND METHODS - SPECTRAL ENHANCEMENT.) A 1200 grooves/mm grating was used in the spectrometer stage. With this grating, the spectral region from 800 to 1800 cm^{-1} could be displayed at one time.

Selection Of Microscope Objective

The proper choice of microscope objectives is an important consideration in microprobe investigations. Most of our previous efforts have been done with incorrect objectives; specifically, we used an oil immersion objective requiring a coverslip in an aqueous environment with no coverslip. As a result of this, resolution and light collecting efficiency suffered. Experiments were conducted to determine the magnitude of this problem.

A water-immersed, 30 micron thick radial section from black spruce wood was photographed using: (1) a Leitz 100X water immersion objective, 1.2 numerical aperture (NA), and (2) a Zeiss 100X oil immersion objective, 1.2 NA, coverslip required. In addition, Raman spectra were collected from three

different areas in the secondary cell wall using these objectives.

The visible light micrographs revealed little difference in resolution between the objectives. One reason for this was that both of these objectives were designed for use with a coverslip and no coverslip was in the optical path. When objectives are used in this manner, their image quality is apt to suffer as a result of spherical aberration.[226]

While no difference in resolution was apparent between the two objectives, the (scattered) light gathering efficiency of the water immersion objective was substantially greater. Figure 19 shows the Raman spectra from three different areas in the radial (secondary) cell wall. The water immersion objective was used for areas 1 and 3, while the spectrum from area 2 was collected using the oil immersion objective. The spectra from areas 1 and 3 almost coincide, whereas the area 2 spectrum was approximately 36% lower in intensity. A reason for this difference may be due to the objective's ability to capture the highly scattered light rays from the sample. The objective engineered for water immersion is better able to collect these highly divergent rays (the angular aperture of the front element is larger and the light gathering ability of a lens is related to its diameter).[211,212]

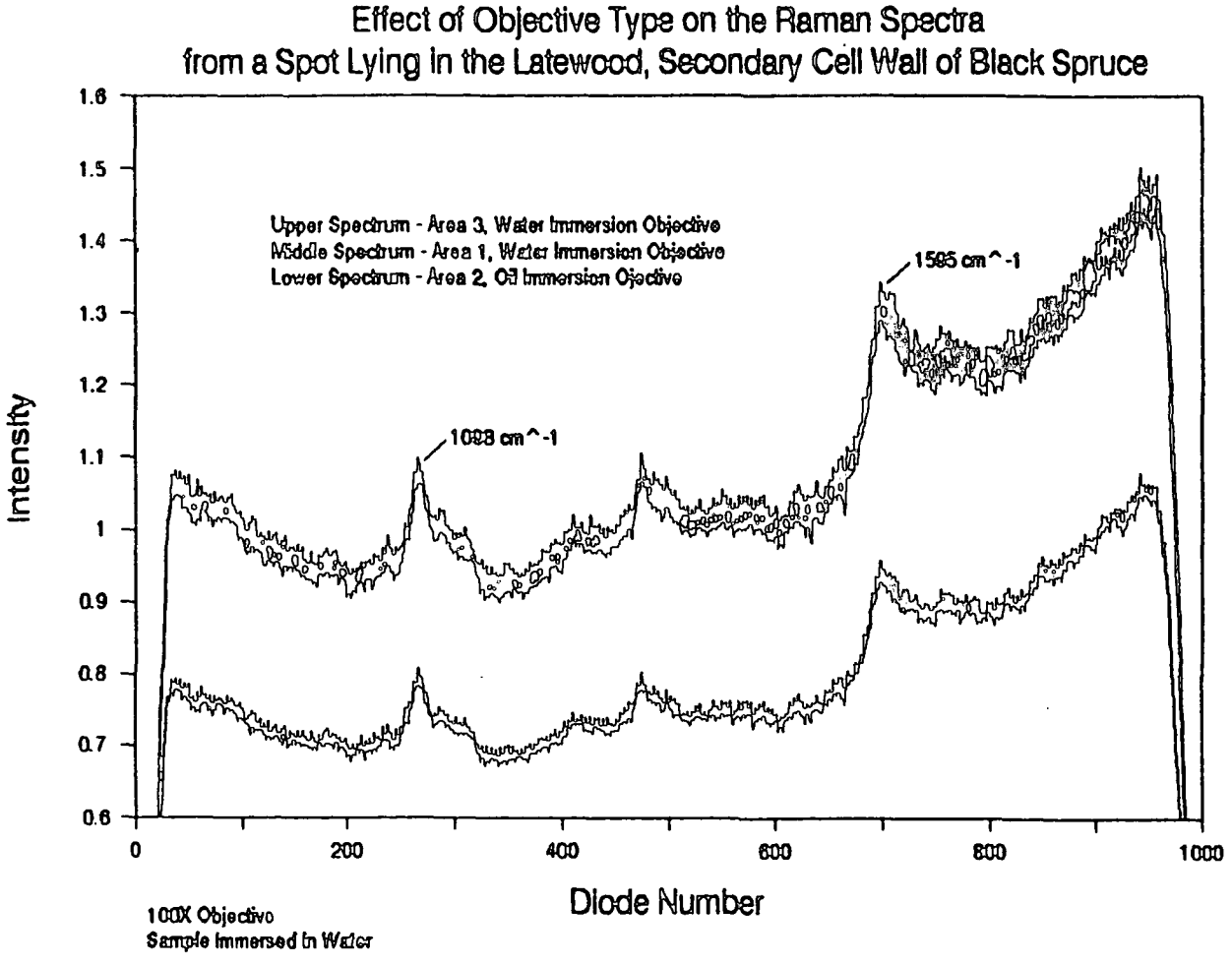

Figure 19. Raman spectra from a radial wood section of black spruce showing differences in light gathering efficiencies between 100X oil and water immersion objectives.

It has been said that an inexpensive objective used properly has the ability to outperform a well-engineered, expensive objective used improperly.[213] It was unfortunate that a 100X water immersion, without coverslip

objective was not made by any of the leading manufacturers. The Leitz objective, although engineered for water immersion, did require the use of a coverslip and was quite expensive. The Zeiss objective, although used in the wrong environment with a coverslip, performed adequately. After a long search, an obsolete Zeiss 100X objective (1.3 NA) which did not require a coverslip but which was engineered for oil immersion, was located. Its resolution matched or exceeded the Leitz objective and its light gathering efficiency was only slightly less. This was the objective used in the present study.

Motorized Stage

Mapping of the cell wall components requires a well-engineered stage that is capable of making accurate, reproducible steps (xy) as small as one micron. In addition, rotation (θ) capabilities are needed for orientation studies. At the beginning of this thesis, a manual x,y,θ stage was used in the laboratory. While this stage was marginally adequate for studying isolated areas in the cell wall, in-depth, systematic mapping was not feasible due to the difficulty in accurately positioning the sample relative to the optical axis (the one-micron probe area).

In order to overcome this problem, a custom modified motorized stage was ordered from Ludl Electronic Product (LEP). A high quality Zeiss rotary stage was used as the platform for xy motorization. Stepper motors were added to this stage. These motors are micropositioning devices that drive a precision

lead screw to generate linear motion. They were interfaced to a LEP MAC 1000 microcomputer positioning and control system. This controller allowed the user to program scanning speed and step size (one micron was the minimum step size). In addition, a proportional xy joy stick was provided which allowed quick scanning of the sample.

Sample Holder

Water immersion has been found to minimize laser-induced fluorescence from lignocellulosic samples.[214] Traditionally, this was accomplished by using a specially constructed cell and sandwiching the wet wood section between a glass microscope slide affixed to the bottom of the chamber and a coverslip with a hole in its center. A peripheral layer of silicon grease held the coverslip, and thus the section, immobile.

The procedure provided a heat sink to dissipate energy absorbed by the sample and resulted in high quality spectra due to the quenching of fluorescence. Unfortunately, the method used to immobilize the sample (silicon grease) made it cumbersome to reuse the sample chamber, usually resulted in broken drilled coverslips, and sometimes made it difficult to salvage the sample.

Because of these shortcomings, a new sample chamber was designed. As before, a flat-bottomed Pyrex beaker was glued to a microscope slide in a manner that allowed transmitted light to pass through. On the inside bottom

surface of the beaker, a circular glass slide (cut for a snug fit) was placed. The wet sample was sandwiched between a circular coverslip, through which a 4 mm hole had been drilled, and the circular glass slide. Water was added into the beaker until complete immersion of the sample took place. Instead of using silicon grease to hold the coverslip stationary, a Teflon washer and retaining ring were used. The washer's dimensions were such that it would just fit inside the beaker and would also overlie the outer margin of the coverslip, thus keeping the sample flat and holding both the sample and coverslip stationary. To prevent the coverslip from sliding under the washer, a retaining ring was used. It was made from a 1.5 cm high Teflon tube which, upon compression (of a longitudinal cut), would just fit inside the beaker. After the region of interest was centered in the coverslip's hole, the ring was pushed against the washer thus locking the coverslip and sample in position. The use of the Teflon inserts allowed the chamber and drilled coverslip to be reused with very little effort. In addition, the sample could be repositioned if necessary and easily removed for future use or micrographs.

Video Enhanced Microscopy[215]

To aid in the cell wall architecture investigations, the microprobe was equipped with video enhanced microscopy (VEM) capabilities. In principle, a video microscope is nothing more than a television camera and a video monitor coupled to a light microscope. Enhancement of the image is made possible with a digital image processor. The digitized video image can be manipulated to

enhance image attributes such as contrast, signal-to-noise ratio, high or low spatial frequencies, edge features, and shadow and highlight detail. Using VEM makes it possible to bring out cell wall details which are difficult to detect visually, and thus aid in the correlation of the Raman mapping data with morphological features under study.

Components

Figure 20 shows the components of an idealized image processing system. With our system, the signal from a Javelin JE2362 monochrome camera coupled to the Zeiss microscope could be routed to either a Sony Trinitron color monitor for direct viewing or an Imaging Technology PCVision plus frame-grabber for digitization and further processing. The host computer was an IBM-compatible Dell 386/20 MHZ machine. The images were stored on floppy disks and output to a Mitsubishi P61U video copy processor. A For•a crossline generator completed the system. Its purpose was to superimpose a crossline on the video image. This was useful for both aligning the laser beam relative to the Raman system and locating particular cell wall features.

Software

Image processing hardware requires the existence of suitable applications programs to transform the image processor from a special purpose computer into a research tool. Image Pro II software from Media Cybernetics was used in conjunction with the frame-grabber. Image Pro II operations could be accessed

by easy-to-use menus incorporating hierarchical commands and interactive windows, and they were mouse selectable.

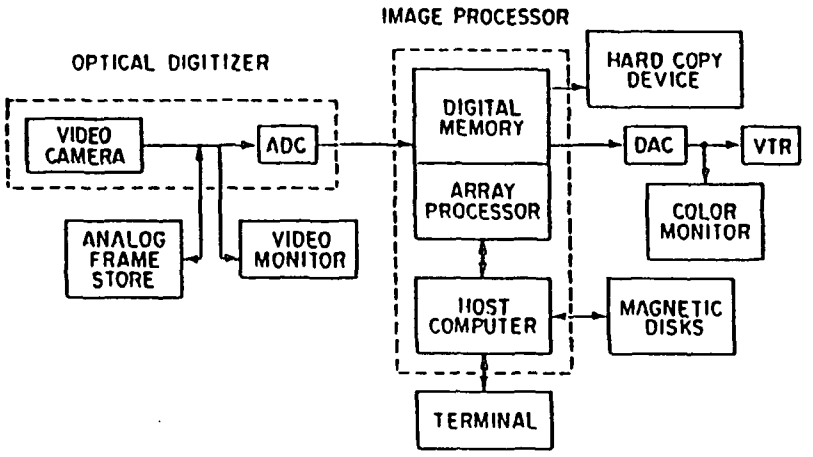

Figure 20. Block diagram of an idealized image processing system. ADC: analog-to-digital convertor; DAC: digital-to-analog convertor.[215]

An example of the capabilities of this system is shown in Figure 21. It shows a microscopic image of the earlywood-latewood transition in a radial section of black spruce. After contrast adjustment, a horizontal edge enhancement filter was applied to the image. Following this, the image was pseudo-colored to bring out intensity differences. (It is important to remember that the colors are not indicative of height differences, but are the result of assigning specific colors to intensity ranges. Notice that the

compound middle lamella region (braided appearance) and the striation-like marking in the secondary wall are very apparent. The circular features at the bottom of the image are earlywood bordered pits.

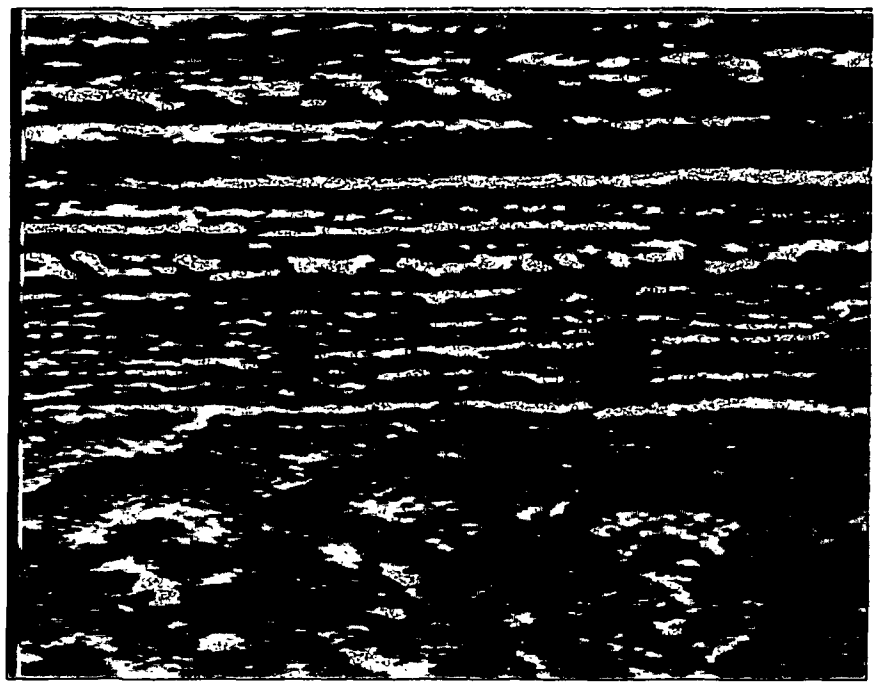

Figure 21. Enhanced video image of the earlywood-latewood transition in a radial black spruce thin section.

Sample Movement

A serious problem which had plagued this study from the onset was sample instability. In order to map the cell wall components at a micron level, it was absolutely essential that the sample not move during the acquisition period. During the initial stages of the thesis, the sample would drift in the microscope's field-of-view by as much as 10 microns during a 15-minute period.

Various simple methods were tried at first to alleviate this movement, but met with little success.

Following this, more drastic steps were taken. The spectrometer coupling and support stand for the microprobe were redesigned by the manufacturer, Spex Industries. This helped the problem slightly. Additional supports for the microprobe were tried, as well as isolating the system via a vibration isolation table (Technical Manufacturing Corporation's micro-g series optical table). These measures further reduced the movement, but did not stop it entirely. The cause of the residual movement was finally tracked down to the constrained expansion of the microscope stand caused by its heating when the illuminator was turned on for short periods of time. The tungsten lamp assembly was replaced by a fiber optic (cold light) illumination system. This last corrective measure finally stopped the unwanted sample movement. This information has been forwarded to Spex Industries to benefit other Spex microprobe users.

Assembled System Photograph

To conclude this section on microstudies, Figure 22 is included. It shows the complete microprobe system. The laser, microscope, spectrometer, and detector are shown in the upper part of Figure 22, while the lower photograph includes the TN6500 spectral analysis system, motorized stage controller, and the video-enhanced microscopy components.

Figure 22. Microprobe System.
(Upper) Laser, microscope, spectrometer, and detector;
(Lower) TN6500 spectral analysis system, motorized stage controller, and video enhanced microscopy components.

SPECIES SELECTION

Black spruce (Picea mariana (Mill.) B.S.P.) has traditionally been used in our laboratory for the in situ Raman microprobe studies of plant cell walls.[10] Due to its rather narrow (longitudinal) latewood single wall thickness (2-4 microns) it was decided to choose another species with a larger wall thickness to use in addition to black spruce in the mapping studies.

Loblolly pine (Pinus taeda L.) was chosen for a number of reasons. It was anatomically optimum, i.e., its fibers have thick latewood secondary walls (7-9 microns)[216] and few pits are present.[4] In addition, it has been thoroughly researched with regard to anatomy, deposition of the various components, etc.[216,217]

Most of the results reported for black spruce were from samples taken from the main stem of a 57-year-old tree which measured 19 cm D.B.H. and that was grown in northern Wisconsin. The results reported for loblolly pine were from samples taken from the main stem of a 60-year-old tree grown in South Carolina. (In both instances, the samples were representative of normal wood.)

SAMPLE PREPARATION

Radial sections were obtained from the green, i.e., never-dried, woody samples and were prepared by microtoming the water-saturated wood. (The

sections encompassed growth rings 40-45 for black spruce and approximately 48-51 for loblolly pine.) The sections were typically 30 microns in thickness. After sectioning, the samples were solvent exchanged into absolute ethanol (or methanol) and stored in a cool, dark location prior to use. The alcohol prevented microbial attack while dark storage minimized light-induced changes in the constituents. (Although the alcohol dehydrated the samples, it was the opinion of the author that the effects of dehydration on native-state cell wall organization would be minimal.)

All woody sections were extracted prior to acquiring Raman spectra. One reason for this was to minimize any contribution extractives might make to the interfering background fluorescence level.[284] Using a standard procedure[218] the sections were extracted in an ethanol/toluene mixture (1:2 v/v) at 25°C. Extraction times ranged from 15 to 150 hours. After extraction, the samples were again stored in absolute ethanol.

SPECTRAL ENHANCEMENT

Post-acquisition processing of the Raman data is sometimes necessary to aid both in the analysis and presentation of the spectra. The macromode spectra were typically left in their raw state, although occasionally if warranted, a Savitsky-Golay smoothing algorithm[285] was applied to them to reduce noise. This smoothing method uses a convolution approach which performs a least squares fit to a specified window of data points. The "non-

mapping" microprobe spectra were also left in an unaltered state, but did have the background (dark noise) subtracted from them.

The spectra used for the mapping studies were subjected to a high degree of post-acquisition processing. Because of lignin's sensitivity to laser light, the irradiation time for a given location was kept to a minimum, which resulted in very noisy spectra. In order to interpret these spectra, they were:

1. Background subtracted to remove the dark current contribution.
2. Smoothed using a fast Fourier transform algorithm. This technique smooths the spectrum by Fourier transforming the data, applying a filter function, and then performing a reverse Fourier transform. This method does not truncate the end data points as occurs with Savitsky-Golay smoothing.
3. Baseline corrected using multiple points. This was necessary for accurately determining peak heights.
4. Converted from diode number to wavenumber for presentation. This was accomplished by performing a least squares fit to a known diode-wavenumber relationship (toluene) and applying this derived relationship to the spectra's abscissa (diode number) values.

To further improve the spectra, a maximum likelihood restoration technique[219,220] was tried. This technique involves solving a set of N non-linear equations, where N is the number of data points and gives you the most

probable sample spectrum. The method preserves peak area, but not peak height, which turned out to be a problem. In the Raman spectra of wood, cellulose's 1098 cm^{-1} peak is not sufficiently isolated from the 1139 cm^{-1} lignin peak. (The 1139 cm^{-1} band has been assigned to aromatic C-H in-plane deformation vibrational modes[221,222].) If an area determination was used for the 1098 cm^{-1} peak, the results could be biased. The 1139 cm^{-1} lignin band decreases in intensity during laser irradiation. Because of close proximity of the two peaks, the 1098 cm^{-1} peak area also appears to decline and, contrary to this, it has been observed that cellulose is not affected by 514.5 nm laser radiation. Because of this problem, the spectral restoration technique was not applied to the mapping spectra.

The post-acquisition processing of the microprobe data was accomplished with the use of Spectra Calc software manufactured by Galactic Industries Corporation, Salem, New Hampshire. Computer programs were written as needed using the Array Basic language within the Spectra Calc Shell. Maximum likelihood spectral restoration was an applications program used in conjunction with Spectra Calc.

LIGNIN MODEL COMPOUNDS

Several lignin model compounds were used in this investigation. They are shown in Figure 23. Model compounds I and IV were synthesized by Robert Barkhau during the course of his Ph.D. thesis at the Institute and were kindly

donated to the author. Model compound III was prepared at the U.S.D.A. Forest Product Laboratory in Madison, Wisconsin. Compounds II, V, and VI were commercial samples; II came from Fluka Chemical, while compounds V and VI were purchased from Aldrich Chemical.

Spectra were acquired from both the pure compounds and 0.1M solutions in methanol. In addition, spectra were collected from compounds I-IV treated with: (1) acid chlorite (10% molar excess ClO_2^-) and (2) sodium borohydride (50% molar excess). They were sampled in glass capillary tubes which were mounted in the macrochamber of the Instruments SA Jobin Yvon Ramanor spectrometer system described previously.

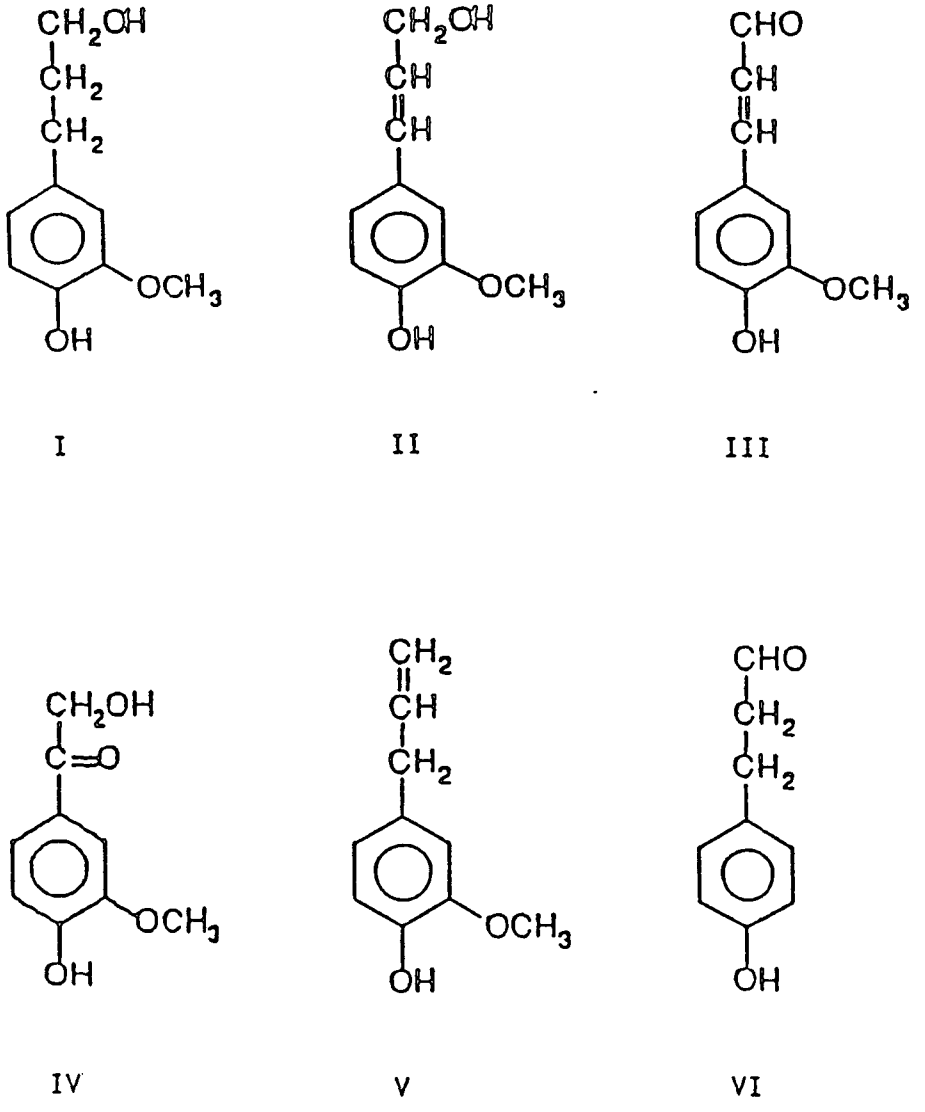

Figure 23. Lignin model compounds.

I. Guaiacyl propanol, 3-(3'-methoxy-4'-hydroxyphenyl)propan-1-ol
II. Coniferyl alcohol, 4-hydroxy-3-methoxy-cinnamyl alcohol
III. Coniferaldehyde, 3-(3'-methoxy-4'hydroxyphenyl)-2-propenal
IV. α,4-dihydroxy-3-methoxyacetophenone
V. Eugenol, 4-allyl-2-methoxyphenol
VI. Hydrocinnamaldehyde, 3-phenyl-propionaldehyde

RESULTS AND DISCUSSION

The Results and Discussion section is divided into two major parts: PHOTOCHEMICAL EFFECTS IN WOODY TISSUE and SPECTRAL MAPPING STUDIES. The results of the investigation into understanding the photodecay of the 1595 cm^{-1} aromatic ring-breathing band of lignin are presented in the first part. In the second part of this section, the results of the spectral mapping of the organization of cellulose and lignin in the secondary cell walls of black spruce and loblolly pine are presented.

PHOTOCHEMICAL EFFECTS IN WOODY TISSUE

This section is divided into three main subsections: Cell Wall Feature, Conjugation and Preresonance Raman Enhancement, and Photostabilization of Lignin. The first subsection presents the results of the investigation of the feature which developed at the location on the cell wall where the laser beam was focused while acquiring the Raman spectrum. The results of the study of Raman band intensity enhancement mechanisms using lignin model compounds and native woody tissue are detailed in the second subsection. The subsection titled Photostabilization of Lignin reports on the results of experiments to determine the causes of the photo-induced changes that occurred in the lignin macromolecule during laser irradiation and attempts to achieve photostabilization.

Woody Tissue Spectral Changes

Certain bands in the Raman spectrum of wet woody tissue have been observed to decrease during exposure to 514.5 nm laser irradiation. Figure 24 shows the Raman spectra of a spot lying in the secondary, latewood cell wall of a radial section of black spruce. The section had been extracted prior to use and was immersed in H_2O. The spectral range shown is from approximately 800 to 1800 cm^{-1}. The upper trace is the signal-averaged spectrum collected during the initial 500 seconds of 514.5 nm irradiation, while the lower spectrum is from the same spot after a 13.75-hour exposure.

The 1098 cm^{-1} band which has been identified with one of the polarization- and orientation-sensitive skeletal modes of the cellulose chain[10] does not undergo an intensity, i.e., band height, change during irradiation. In contrast to this, the bands at 1595, 1620 (shoulder) and 1654 cm^{-1} have essentially vanished. (The residual 1595 cm^{-1} peak is partly due to water's H-O-H bending vibration.) These bands arise from the lignin macromolecule and have been assigned as follows: 1595 cm^{-1} - one of the aromatic ring stretching vibrations; 1620 cm^{-1} - ring-conjugated C=C stretching vibration; and 1654 cm^{-1} - ring-conjugated C=C and C=O(?) stretching vibrations.[10,221,222]

Figures 25 and 26 show additional spectral ranges acquired from neighboring spots. The cellulose bands[126] at 330, 380, and 448 cm^{-1} again do not show significant changes in intensity after 83 minutes irradiation (Figure 25),

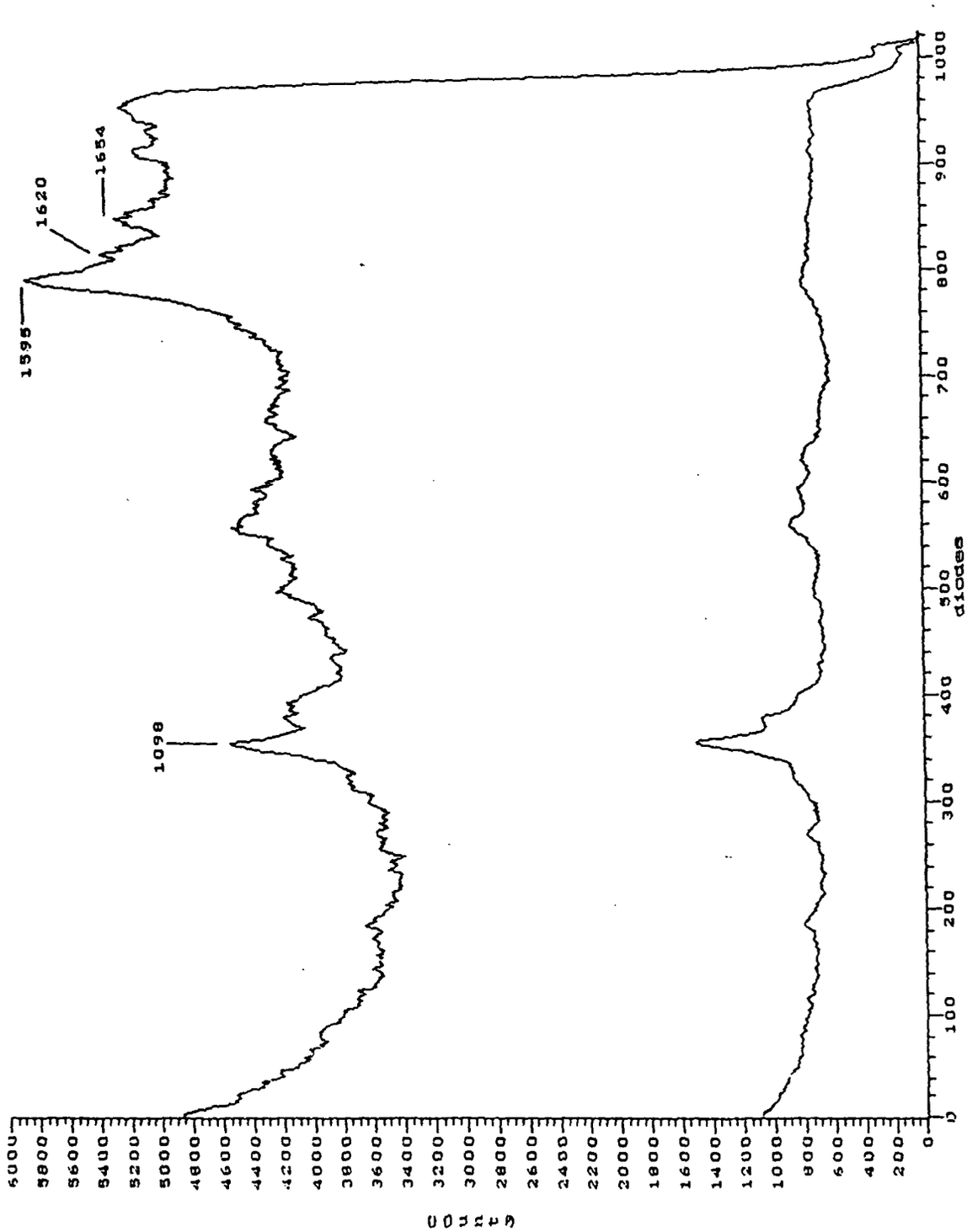

Figure 24. Raman spectra collected from a single location in the latewood, secondary cell wall of black spruce. The spectral range extends from 800 to 1800 cm^{-1}.

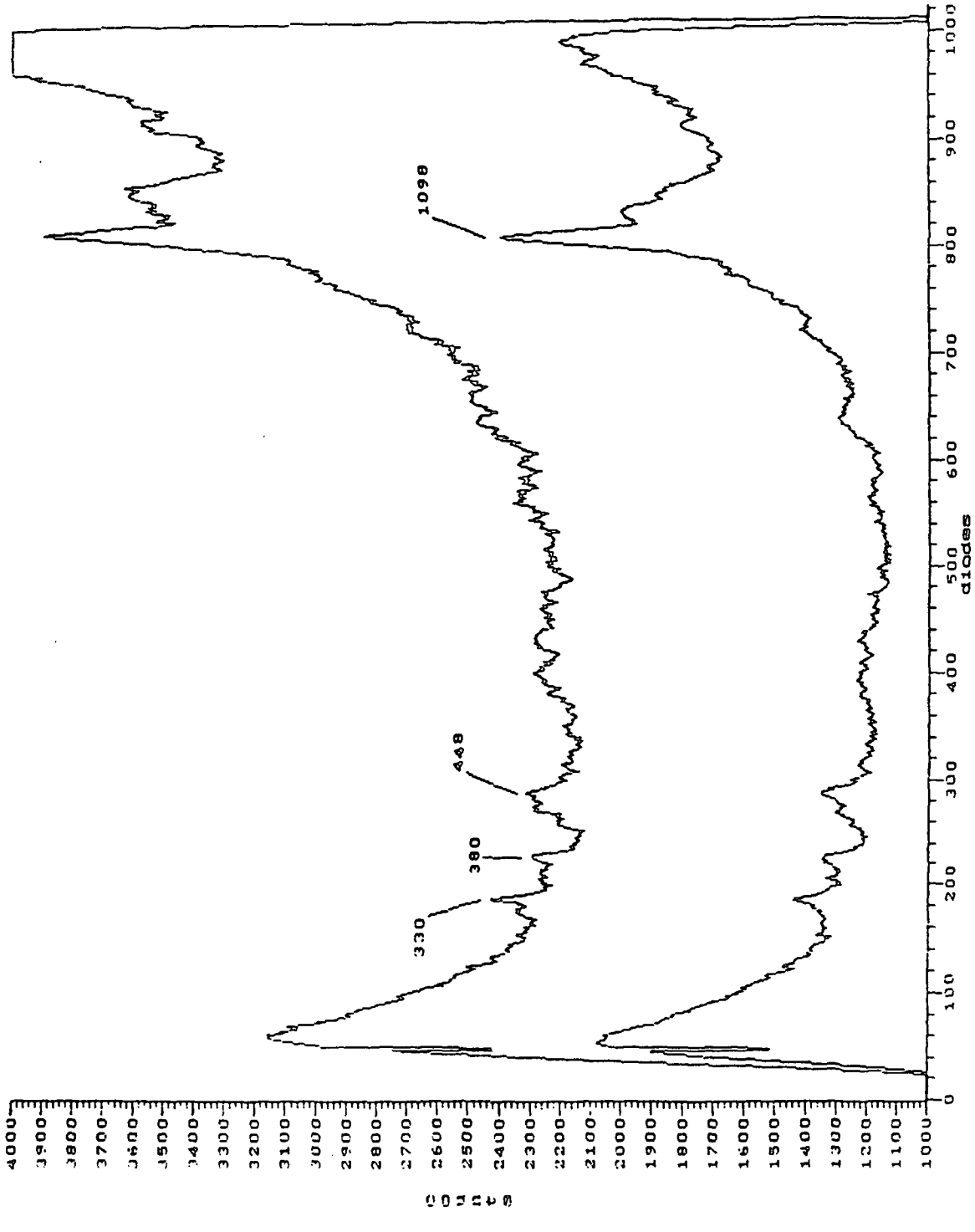

Figure 25. Raman spectra collected from a neighboring spot of that shown in Figure 24. Cellulose's 330, 380, 448, and 1098 cm^{-1} bands are shown. The lower spectrum was collected after 83 minutes of 514.5 nm irradiation. (The cause of the spectral feature at approximately 880 cm^{-1} is unknown. It does not appear in Figure 24 and, therefore, probably is an artifact.)

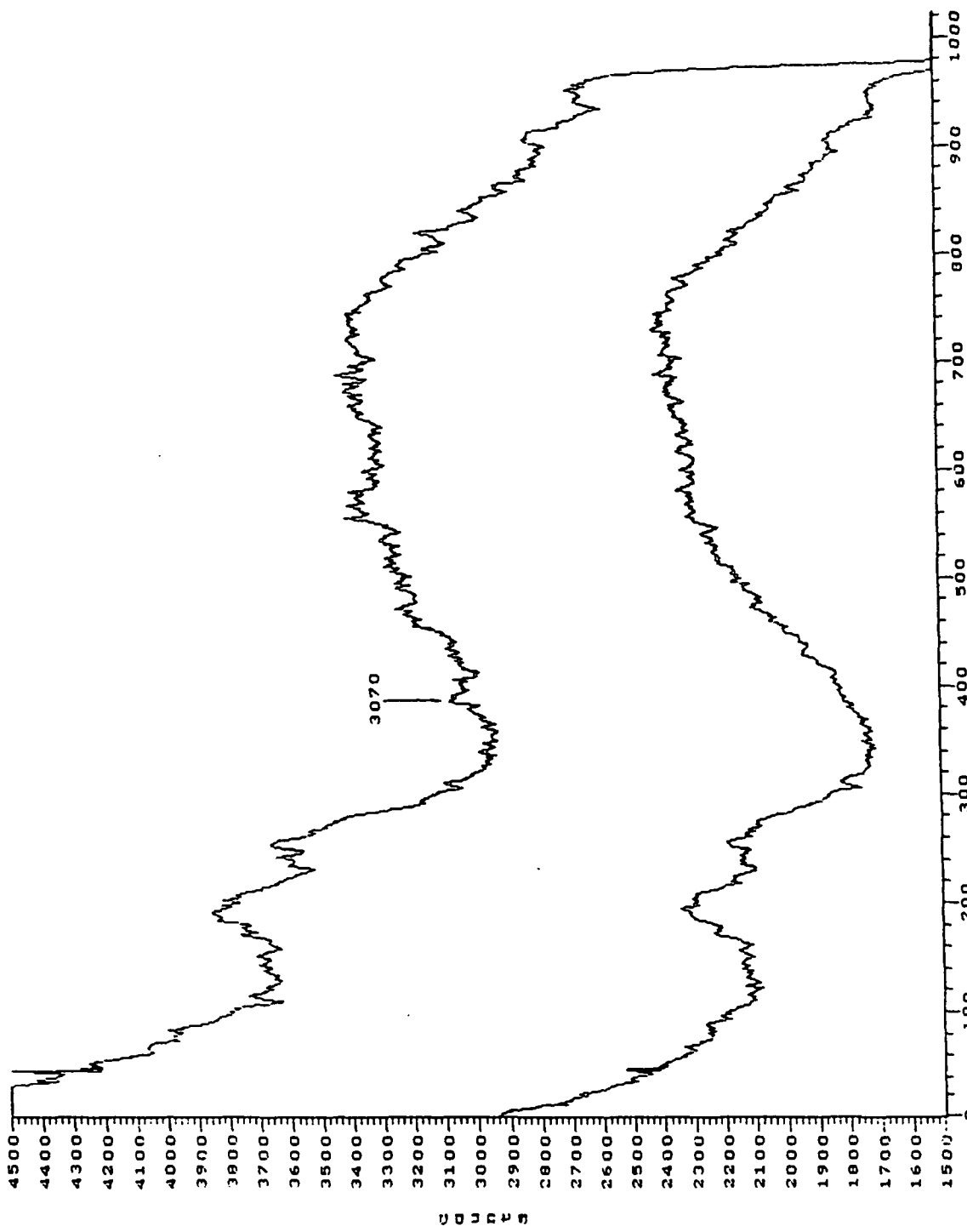

Figure 26. Raman spectra collected from a neighboring spot of that shown in Figure 24. Lignin's 3070 cm^{-1} band occurs at diode 385. The lower spectrum was collected after 83 minutes of 514.5 nm irradiation.

whereas the 3070 cm^{-1} lignin band is substantially reduced during the same period of time (Figure 26). This band has been assigned to the aromatic C-H stretching vibration.[10,221,222]

These data suggest that something is happening to the lignin macromolecule during 514.5 nm laser irradiation of wet woody tissue. (This behavior has been seen in all of the woody species investigated in our laboratory.) The almost complete disappearance of the lignin bands after a long exposure time points to a modification in the macromolecule's structure. This modification could result in a change in the Raman scattering cross-section of lignin and may involve the disruption of the aromatic ring. Whatever the mechanism is that causes this behavior in lignin, it apparently does not affect cellulose because its bands are unaltered.

In addition to the decline in lignin band intensities during irradiation, a concurrent effect is the decay of the background level. This decay, as well as the behavior of both the 1098 and 1595 cm^{-1} bands are shown in Figure 27. The spectra are from a single location in the secondary cell wall of black spruce. (The initial and final spectra were shown in Figure 24.) Approximately 17 minutes elapsed between the spectral acquisitions, and the total exposure was just under 14 hours. As can be seen from this figure, the background decayed in an exponential-like fashion and at the end of the irradiation period, the level had declined approximately 5-fold.

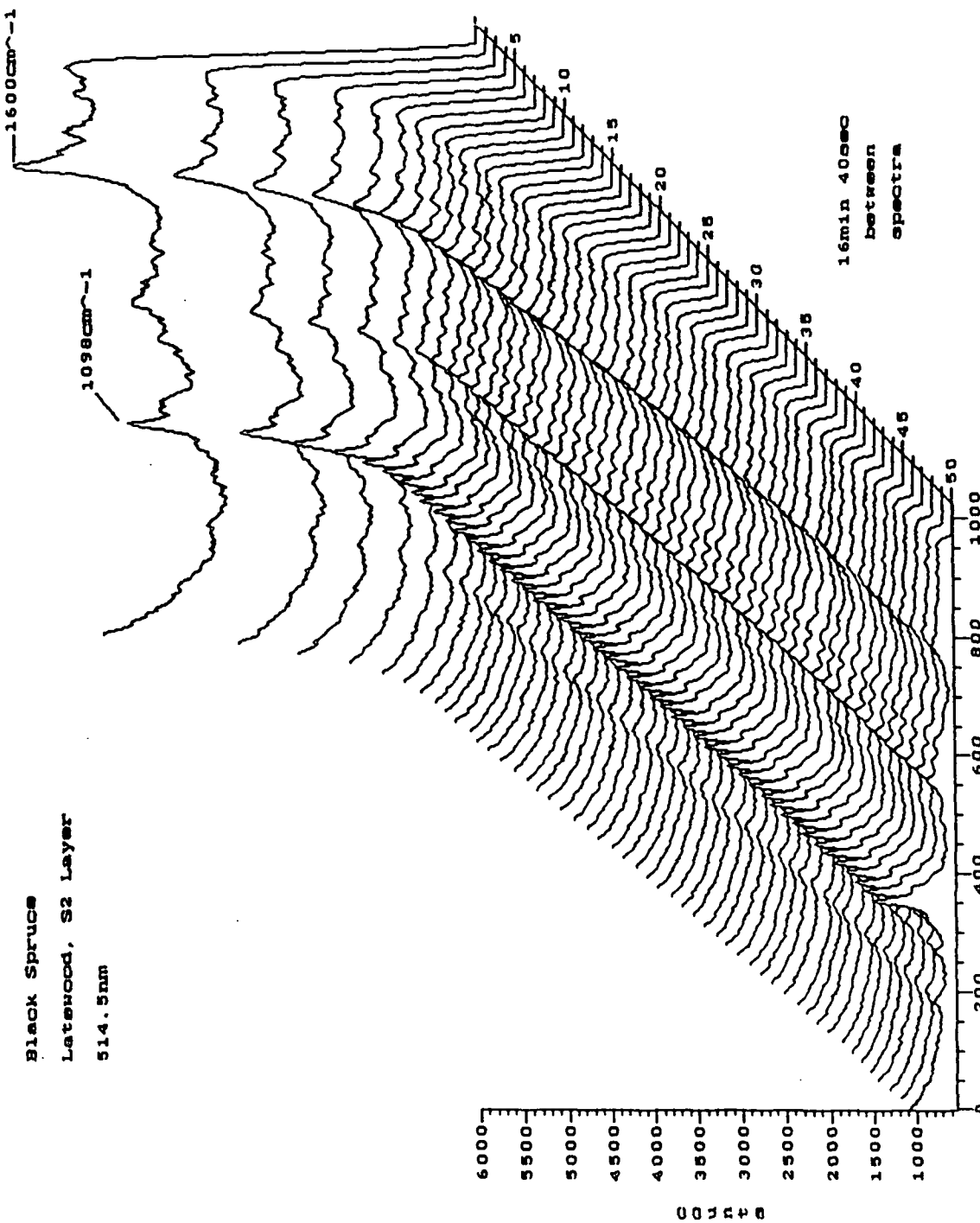

Figure 27. Sequential spectra from a single spot lying in the latewood, secondary cell wall of black spruce. The numbers on the z-axis (0-50) refer to the spectral subfile and are indicative of irradiation time. Subfile 0 was the first spectrum collected (t=8.3 min), while subfile 50 was the last (t=13.75 hrs).

The behavior of both the background level and lignin's 1595 cm^{-1} band (as well as other lignin bands) during irradiation thus appears parallel, although to what extent lignin contributes to the background level is unknown. It has been observed that the background level recovers to nearly its original level after the wet sample had been stored in the dark for 8-12 hours. In contrast to this, the 1595 cm^{-1} band does not show any sign of recovery. This may indicate that the chemical species responsible for the fluorescent background are able to reform after the initial photofragmentation reaction (drench-quench mechanism) and that these reformed species, if they are aromatic in nature, do not significantly contribute to the 1595 cm^{-1} band (their aromatic band may not be enhanced through conjugation/preresonance Raman effect). It is also conceivable that the chemical species that were initially responsible for the background are not the same ones (and/or in the same configuration, i.e., no enhancement occurring) as those that gave rise to the recovered, post-irradiation background and thus, the initial background could very well have been due to structures in the lignin macromolecule. This would explain why both show similar decay trends.

Cell Wall Feature

Concurrently with the intensity decline of the lignin bands, a mark occurred on the cell wall where the laser beam was focused. This section presents the results of the investigation into understanding the cause of the laser irradiation-induced feature.

Light Micrographs

After 514.5 nm laser irradiation of the cell wall, it was observed that marks were apparent in the irradiated regions. Depending upon the focus, these marks appeared as either dark (Figure 28a) or bright (Figure 28b) areas. (This alteration to the cell wall is seen in the middle of the micrographs.) At higher magnifications, the lamellae could be seen to be distorted in the vicinity of these areas.

Polarized light micrographs of these features did not reveal any major changes occurring in the surrounding tissue, which suggested that the disturbance is very localized and probably superficial.

Post-Irradiation Chromophore

Color micrographs of the same region shown in Figure 28 (a and b) that were taken after the section was stored in methanol and subsequently critical-point dried, reveal that a discoloration had occurred in the vicinity of the irradiated areas. As shown in Figure 29, a yellowish area can be seen surrounding the irradiated regions and extending a distance beyond them. The color is most intense in the immediate vicinity and gradually diminishes away from the irradiated region.

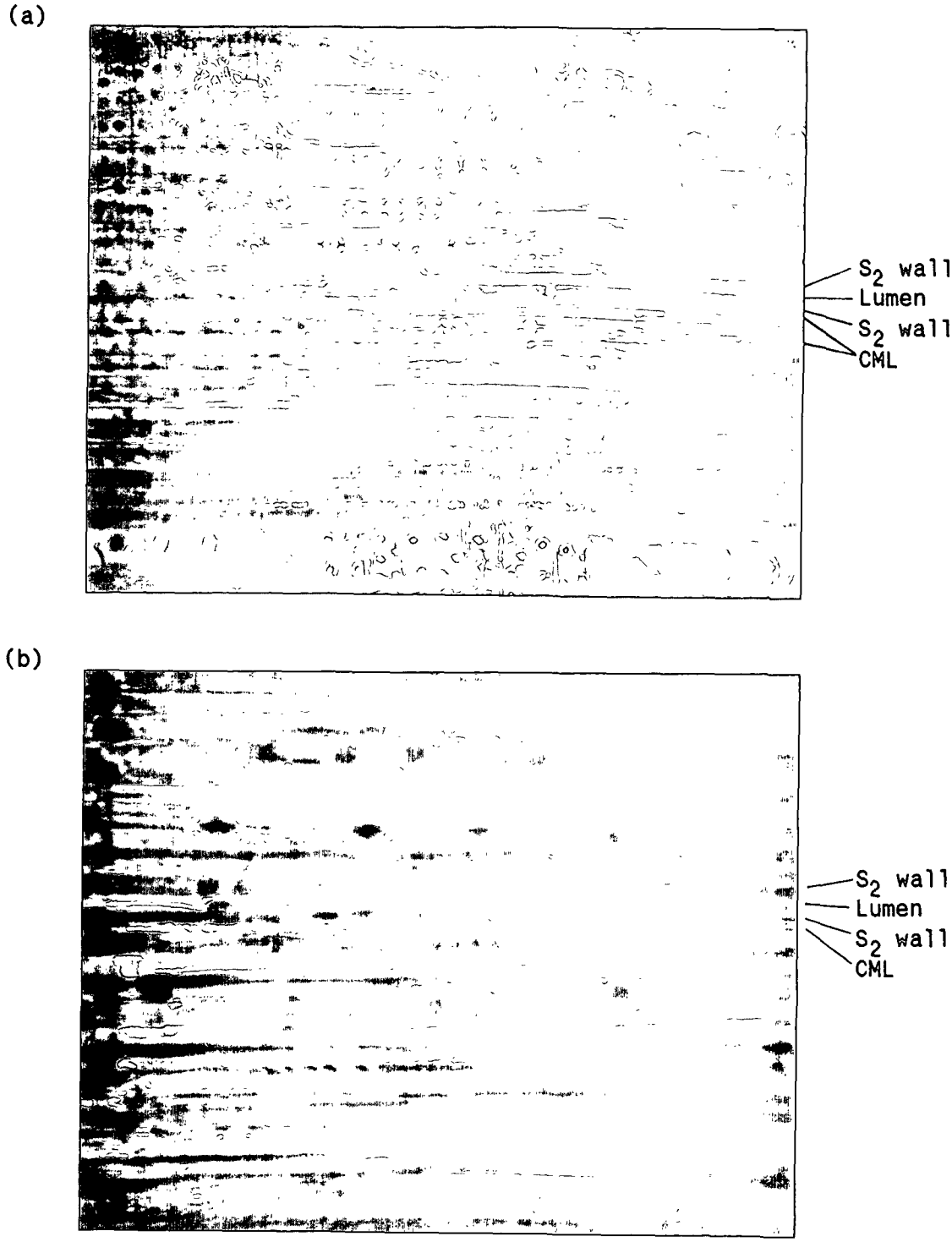

Figure 28. Light micrographs of a radial wood section from black spruce showing laser damage to the tracheid wall. (a) and (b) differ in focus and magnification; (a) 300X, (b) 600X. Sample immersed in water. Laser marks are located in the center of the micrographs.

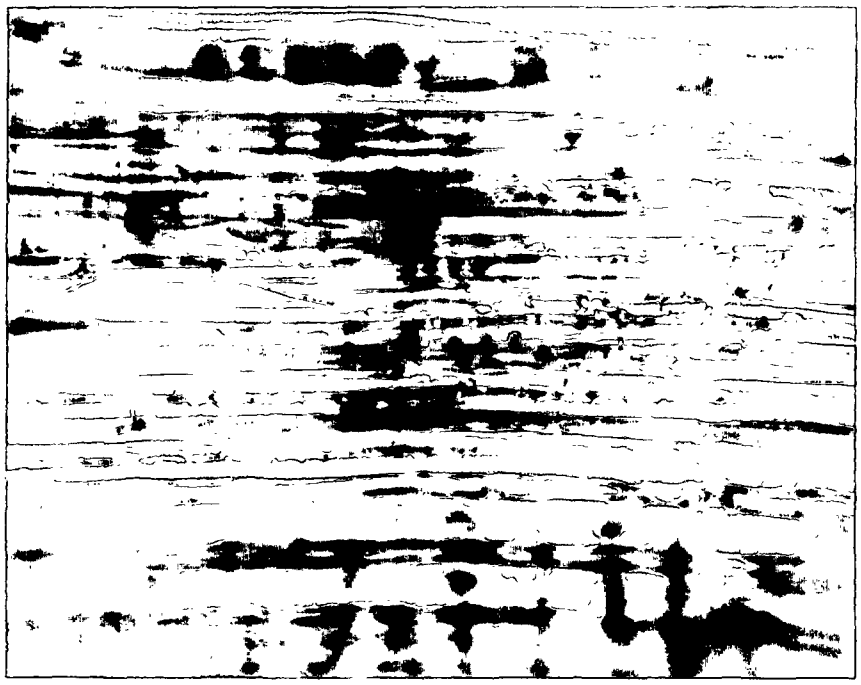

Figure 29. Light micrograph of the same region of the cell wall shown in Figure 28 after storage in methanol and critical-point dried. Magnification 600X. Laser marks are located in the center of the micrograph.

It seems likely that in addition to the physical modification of the S_2 cell wall layer, one or more chromophores have been created. The yellowish color suggests that the chromophore absorbs in the short wavelength region of the electromagnetic spectrum. It will be recalled that several researchers have proposed that the final step in photochemical oxidation of lignin is the reaction between phenoxy radicals and ground-state oxygen to form yellowish degradation products, particularly quinone-type structures.[45,52,55-57]

Given this information, it is reasonable to suggest photochemical oxidative reactions are occurring in the irradiated areas, and that the yellowish

color is due to the formation of quinonoid-type structures (and possibly other chromophoric species). The extent of the discoloration is probably due to the diffusion of the chromophore(s) which occurred during storage of the sections in methanol. (Some of the discoloration may have developed while the section was stored in methanol and, conceivably, during drying. It is not known if there was enough dissolved oxygen in the immersion water to react completely with the photo-products, i.e., radicals. The discoloration only became readily apparent after critical-point drying.) It also seems likely that the decay seen in the lignin bands during laser irradiation is intimately associated with these photochemical reactions.

Scanning Electron Micrographs

Scanning electron micrographs were taken of these same features. The irradiated regions were located with the aid of the light micrographs. It was found that tilting the sample approximately 60° gave the best relief for finding the altered regions.

Figures 30-33 clearly show the modified areas. Before discussing these areas, two curious features apparent in all of the figures need to be addressed. The first of these is that the compound middle lamella region is separated from the secondary walls. If a drying stress separation occurred, I would not have expected it to happen in the middle lamella due to its higher lignin content. It very well may be that there is a weakness in the transi-

tion region between the primary and secondary cell walls where the cellulose microfibrils change from random to a more ordered orientation. During sectioning, the forces were apparently great enough to cause this separation. (Shrinkage of the secondary wall during drying may have contributed to the separation but probably is not the major cause. If it had been, it is unlikely that the cell wall features would have kept their circular appearance after drying.) The other related feature is "pulling out" of the middle lamella material. (This "pulling out" is very apparent in Figure 32 just above the markings on the cell wall.) This most likely is due to the mechanical action of the microtome knife, although the breakup of this region remains a mystery. It may be that the 30-micron section thickness is playing a role in that this dimension roughly corresponds to the thickness of the black spruce tracheid.

Figure 30 shows approximately the same area as that seen in the light micrographs, although at slightly higher magnification, while Figures 31 and 32 are close-ups of the individual features. Figure 31 (feature no. 5) shows an area on the secondary wall that was irradiated for 500 seconds (514.5 nm, 100 mW). As can be seen from this figure, the feature is roughly circular in shape with a concentric ring-like appearance. Its diameter is approximately four times larger than the focused (central maximum) laser beam (3.8 microns _vs_. 1-1.5 microns) and encompasses the entire width of the secondary wall. The pattern can also be seen extending down the tangential face of the secondary wall. This observation lends support to the idea that the middle lamella

region was disrupted during sectioning, and that the tangential face of the S_2 layer was exposed during irradiation.

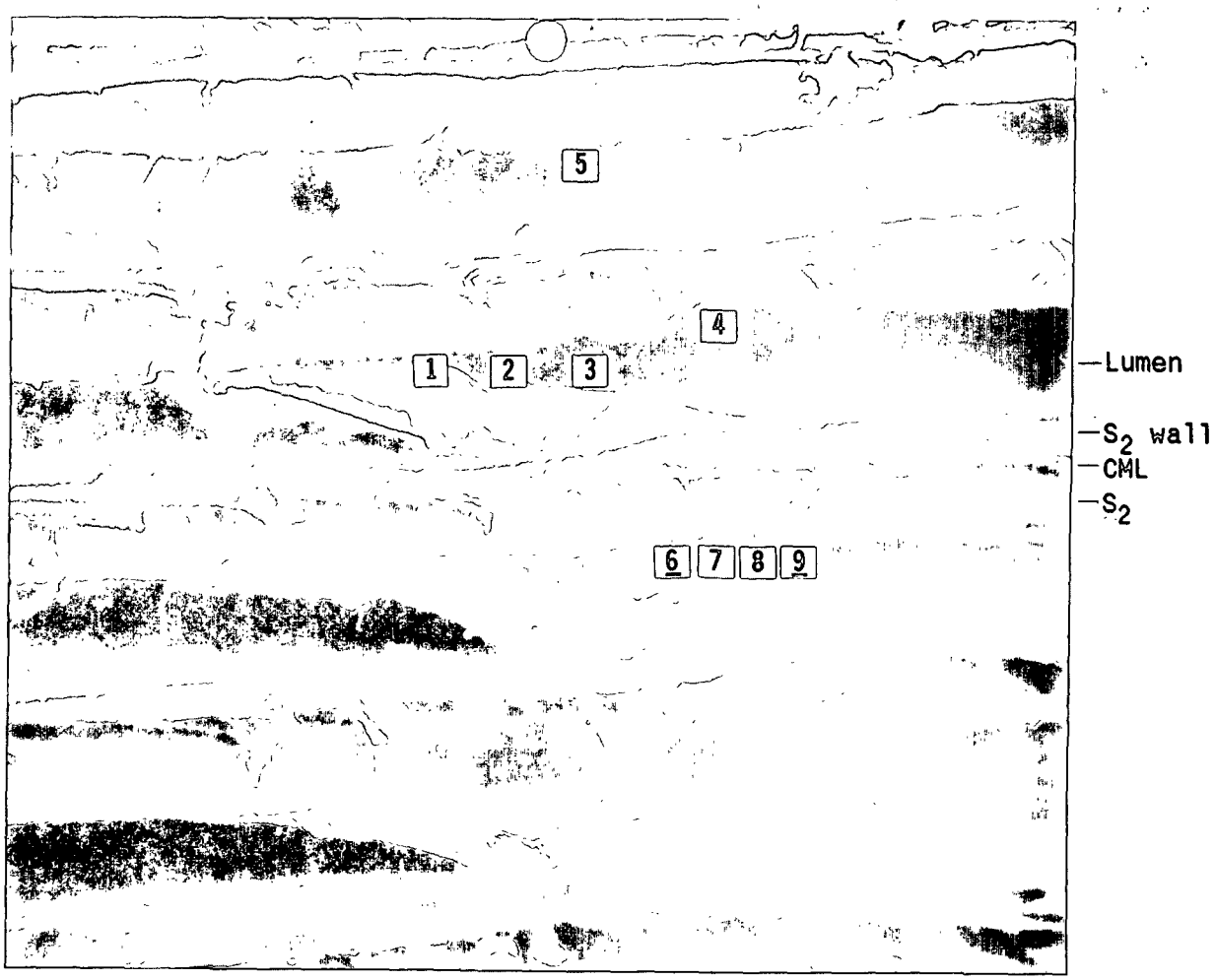

Figure 30. SEM micrograph of the black spruce radial wood section shown in Figures 28 and 29. The numbers refer to the photomodified areas on the secondary cell wall. Sample tilted 60°.

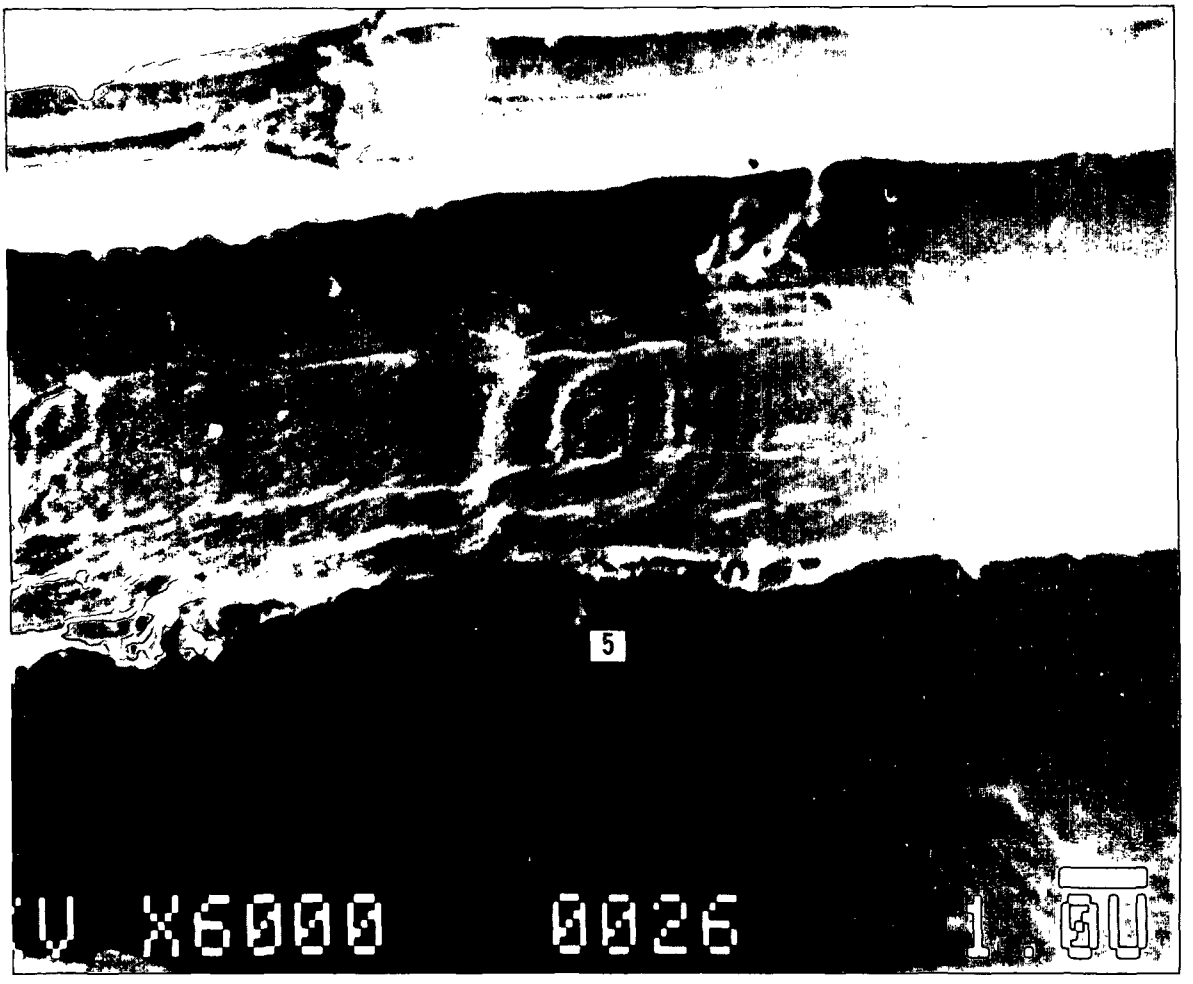

Figure 31. Close-up of a feature on the S_2 cell wall shown in Figure 30. Note the concentric ring-like appearance. The globular features near the top of the micrograph are bacteria. Sample titled 60°.

The ringed appearance of the feature suggests that its cause is probably photochemical in nature rather than thermally induced. Had thermal energy been the sole cause, it is doubtful that the ring-like features would have occurred, or if they had, that they would have quickly lost definition due to the conduction of the thermal energy.

Figure 32 shows four additional marks (features 6-9). (The exposure time, as well as excitation wavelength and power are approximately the same as for feature no. 5.) They closely resemble feature no. 5, although the normally circular rings are distorted. This is especially apparent in feature no. 6. The cause is most likely due to stresses created during critical point drying of the sample.

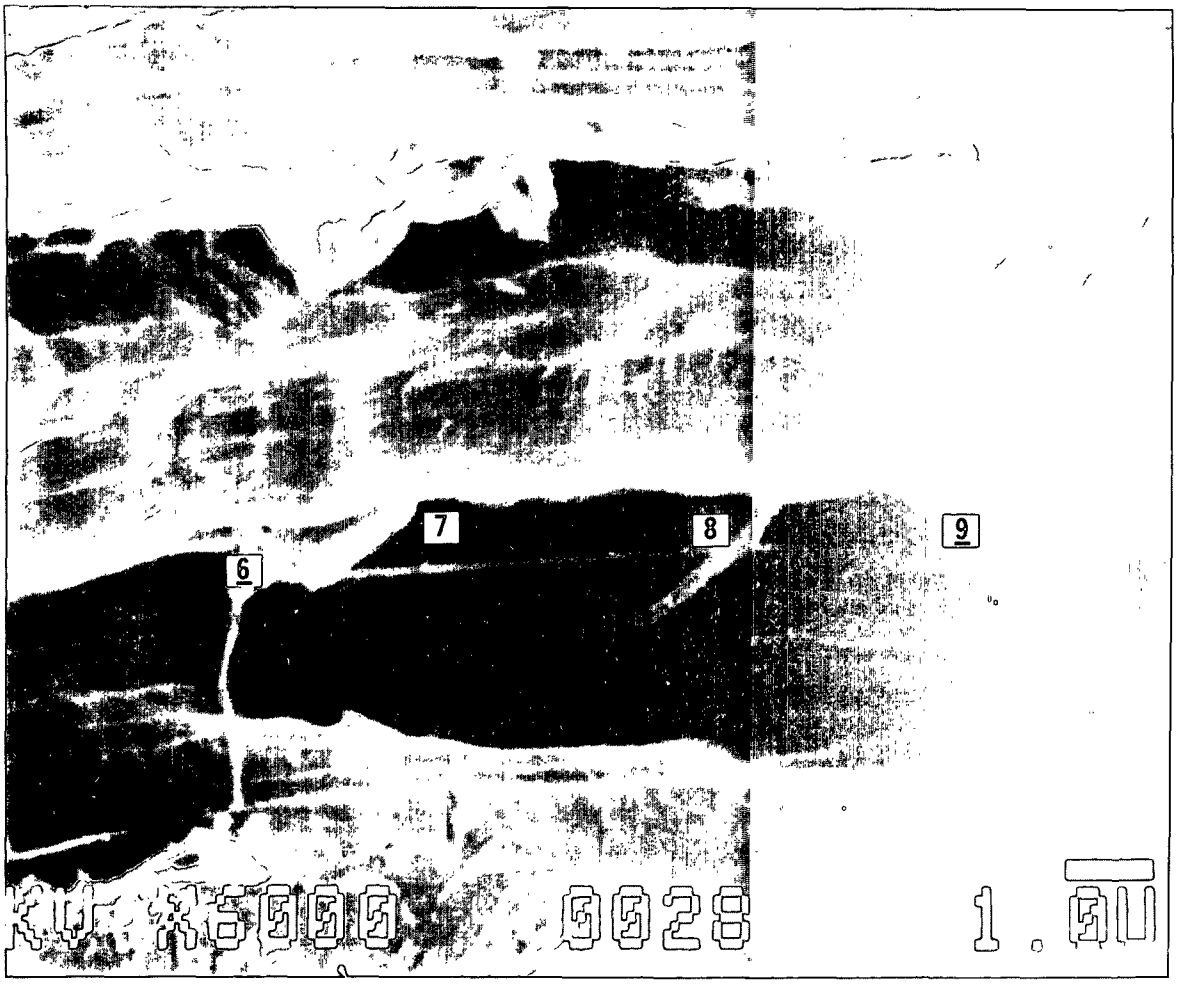

Figure 32. Close-up of features shown in Figure 30. Note the distortion of the normally circular rings in feature no. 6. Sample tilted 60°.

Effect Of Laser Power And Exposure Duration

A close-up of features 1-4 (Figure 30) is shown in Figure 33. The difference between features 1-3 is due to the incident power level. All spots were irradiated with a wavelength of 514.5 nm for 500 seconds, but a 25 mW power level was used for spot no. 1, 100 mW for spot no. 2, and 300 mW for spot no. 3. As can be seen from this micrograph, the lateral extent, number of rings, and relief of the feature is related to incident power level. The 25 mW feature is smaller, shows fewer rings, and has less of an imprint than for either the 100 or 300 mW features. Feature no. 4 shows the effect of exposure. This area was irradiated for approximately 17 hours using a 100 mW laser power level. The topography is striking. It appears that a substantial portion of the cell wall is missing. The depth of the feature at its deepest part is roughly 3 microns and its lateral extent is 8 to 10 microns. The ring-like appearance seen in the other marks is not readily apparent in this feature, although a dark circular spot can be seen in the center of the feature. This spot coincides with the spot where the laser beam was focused.

It thus appears that the lateral extent and relief of these features directly correlate to laser power and exposure. The higher the incident power level and/or the longer the irradiation time, the greater the feature's size (both in depth and diameter). In addition, the degree of yellowish coloration after the section was critical point dried follows these same trends, i.e., the extent of the discoloration as well as its intensity is greater for those

spots with the higher power levels and/or longer exposure. (Figure 29 - one inch from the top of the micrograph shows this region.)

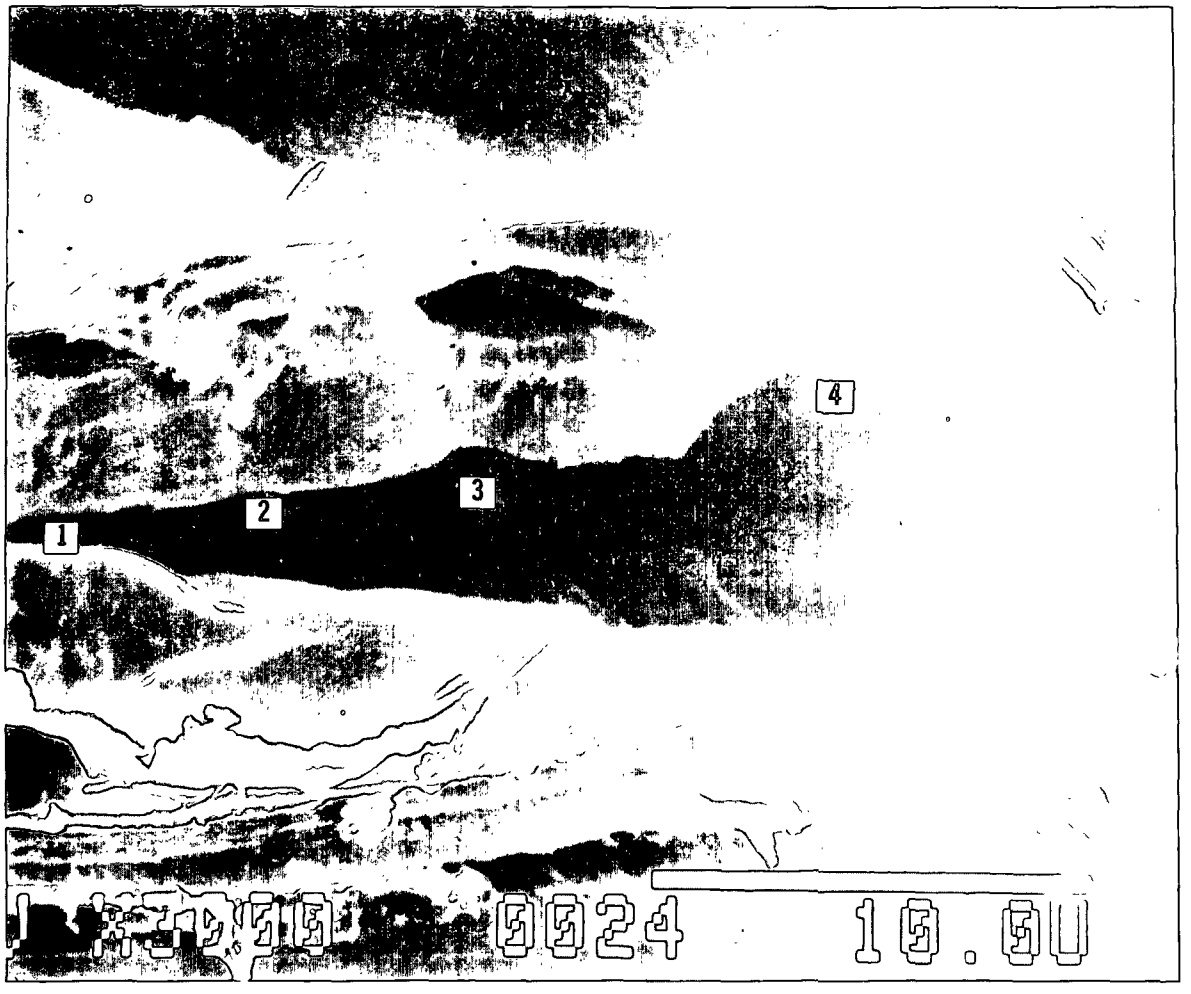

Figure 33. Close-up of features shown in Figure 30. Areas 1, 2, and 3 show the effects of laser power (25, 100, 300 mW respectively, 500 sec. irradiation time). Area 4 shows the effect of long exposure time (100 mW, 17 hour irradiation time). Sample tilted 60°.

Relationship To Incident Radiation Intensity Distribution

The ringed appearance of the features may be a photochemical manifestation of the diffraction pattern formed by a circular aperture(s) in the microscope objective. Figure 34 shows the point spread function (PSF) of an achromat objective. The PSF is the intensity pattern that results from imaging a point source. In geometrical optics, the PSF of an aberration-free system is a point. In physical optics where diffraction is considered, it is the Airy pattern, i.e., Fraunhofer diffraction at a circular aperture.[223,224]

The Airy diffraction pattern does resemble the laser markings. (Refer to feature 5 - Figure 31.) It appears that the depth of a given ring in a feature is related to the intensity of light that fell on that area - the higher the intensity, the deeper the "impression," although the magnitude of the central maximum is not apparent in topography. Table 3 shows the (ideal) relative intensity and energy distribution in the diffraction pattern of a circular aperture. The central maximum (Airy disc) contains about 98% of the total light intensity and 83.8% of the energy. Obviously, either the relief in the feature does not (linearly) correspond to light intensity, or the intensity pattern with our objective does not look like Figure 34.

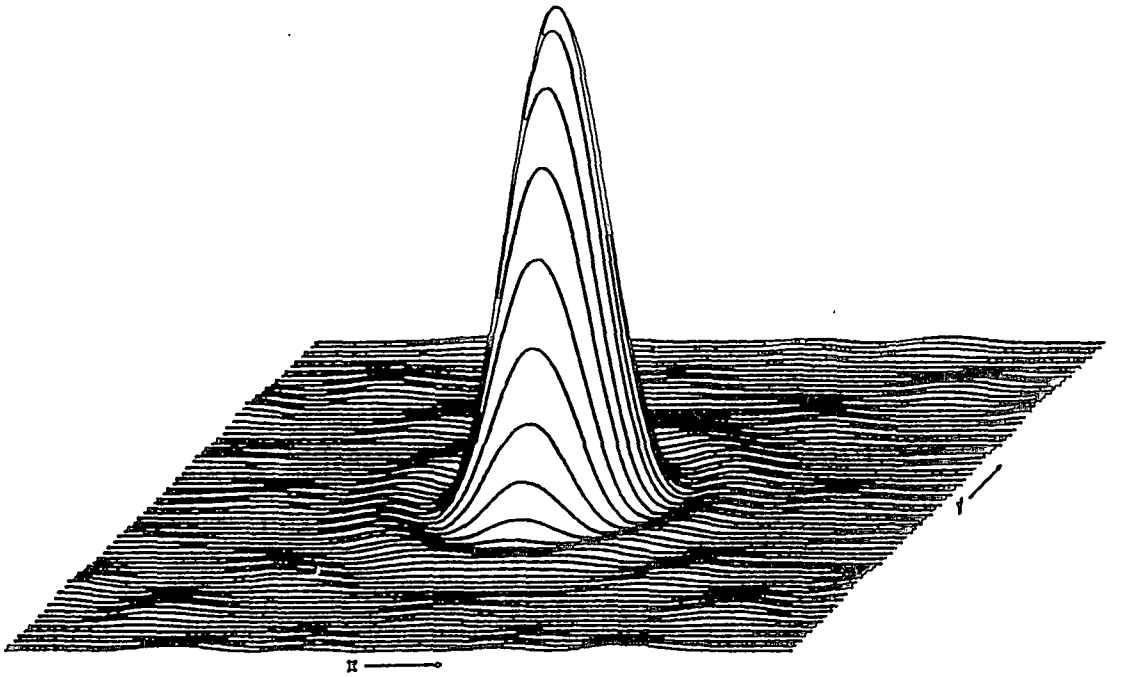

Figure 34. Point spread function of a real achromat by mercury green light.[225]

Table 3. Relative Intensity and Energy Distribution in Diffraction Pattern Produced by a Circular Aperture.[225]

	Circular Aperture		
Ring or Band	Position (x)	Relative Intensity (I_x/I_0)	Energy in Ring (%)
Central Maximum	0.0	1.0	83.8
First Dark	1.22π	0.0	
First Bright	1.64π	0.0175	7.2
Second Dark	2.23π	0.0	
Second Bright	2.68π	0.0042	2.8
Third Dark	3.24π	0.0	
Third Bright	3.70π	0.0016	1.5
Fourth Dark	4.24π	0.0	
Fourth Bright	4.71π	0.0008	1.0
Fifth Dark	5.24π	0.0	

Figure 35 is a photograph of the diffraction pattern produced by the microprobe's objective. It was taken with the aid of a front surface mirror. The excitation wavelength used was 647.1 nm. Comparing this pattern to either Figure 34 or Table 3, it can be seen that the intensity distribution differs substantially from that produced by either the (particular) achromat-type objective or circular aperture (ideal). It does however, more closely match the cell wall pattern. Note especially that there are some maxima and minima that are broader than others. This is echoed in the feature's topography.

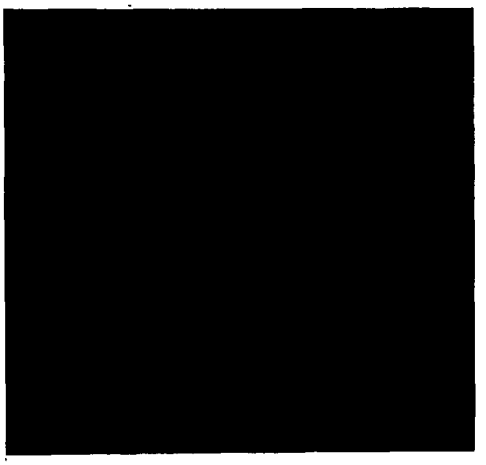

Figure 35. Diffraction pattern produced by our microprobe system using a 647.1 nm wavelength.

The reason for the different intensity distribution with our system was determined to be due to the presence of primary spherical aberration. Spherical aberration occurs when light rays passing through the central and outer

portions of a lens are not brought to focus at the same distance from the lens.[211] Figure 36 shows the diffraction pattern produced in the presence of primary spherical aberration. The resemblance to Figure 35 is remarkable.

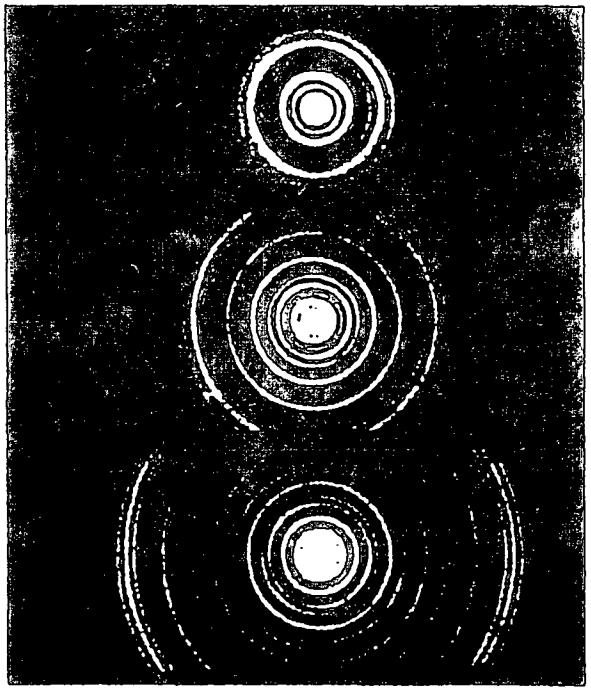

Figure 36. Fraunhofer diffraction pattern in presence of primary spherical aberration.[224]

Profile

Stereomicrographs were taken of the region shown in Figure 30 to get a qualitative feel for the topography. The sample was tilted 53° and 60° for the stereopairs. Figure 37 shows one of the stereomicrographs. In the upper center section of the picture, the irradiated areas can be seen. The progression left-to-right is 25 mW power level/500 seconds exposure, 100 mW/500

seconds, 300 mW/500 seconds, and 100 mW/17 hours. The depth to which the modification occurred is very apparent. While the 25 mW/500 seconds feature (no. 1) is very superficial, the 300 mW/500 seconds feature (no. 3) has substantial depth and the 100 mW/17 hour mark looks like a crater.

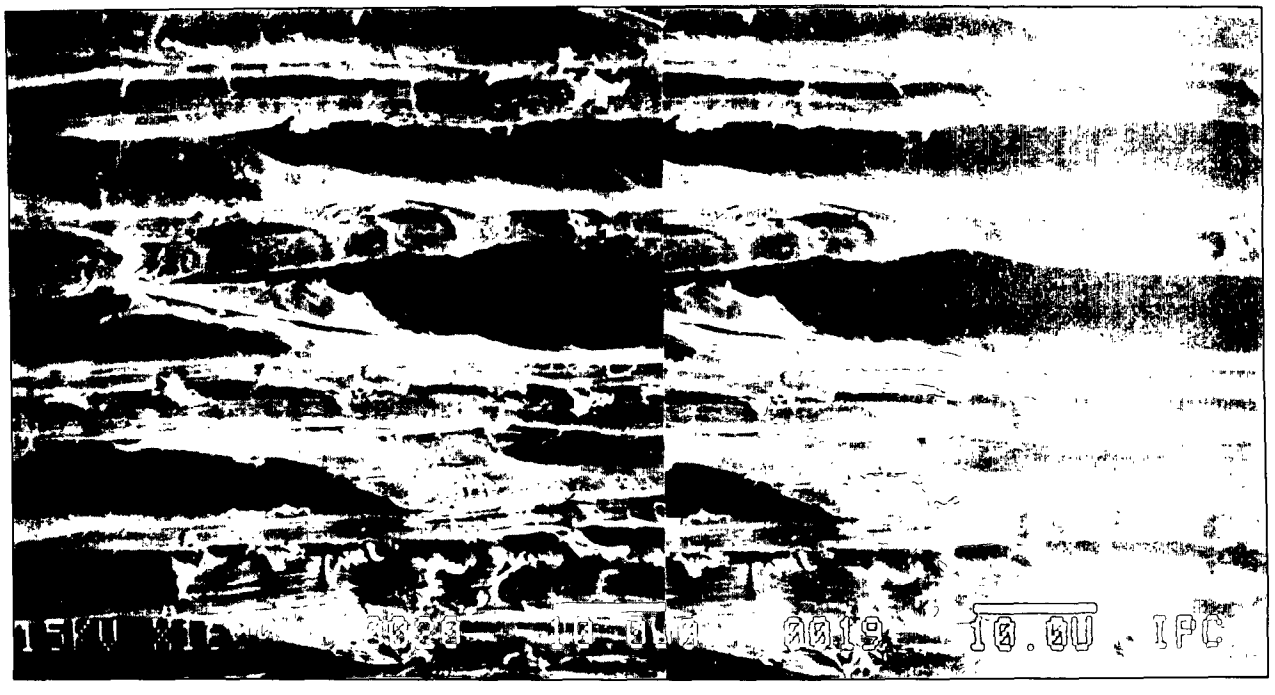

Figure 37. Stereomicrograph of a radial wood section from black spruce. Sample tilted 53° (R) and 60° (L). The irradiated region is denoted by "I".

A Tracor Northern TN8500 Image Analyzer, together with stereopair analysis software, were used to quantify the changes in topography caused by laser radiation. Using this program, feature heights at arbitrary locations could be measured.

Figure 38 presents the results for feature no. 3 (300 mW/500 seconds). Data points 2 and 3 (L to R on profile; points 0 and 1 almost coincide on the micrograph) define the surface of the S_2 layer (+0.23 microns relative to a reference point). Point 4 is located on the outer edge of the feature (+.18 microns), while points 5-12 are located in the feature's interior. Locations 6 and 7 are in the wide depression (-0.48 microns, average), while point 8 gives an indication of the depth of the feature's center (-.44 microns, it was actually located on the inner edge of the prominent ring). Point 11 is on the top of the broad ring (-0.11 microns). As a check, the depth of a location in a fissure was measured (no. 15). These data show that the central depression was in the neighborhood of 0.8 microns in depth, while the prominent ring was about 0.3 microns below the surface for this particular feature.

These data (3D stereomicrographs and the profile measurements) support the idea that cell wall material is missing from the irradiated locations. The evidence strongly suggests that lignin is the (predominant) missing material in that concurrently with the formation of these features, the Raman bands of lignin declined while those due to cellulose remained unaltered. In other words, lignin underwent a photochemically-induced solubilization.

STEREO PAIR ANALYSIS PROGRAM

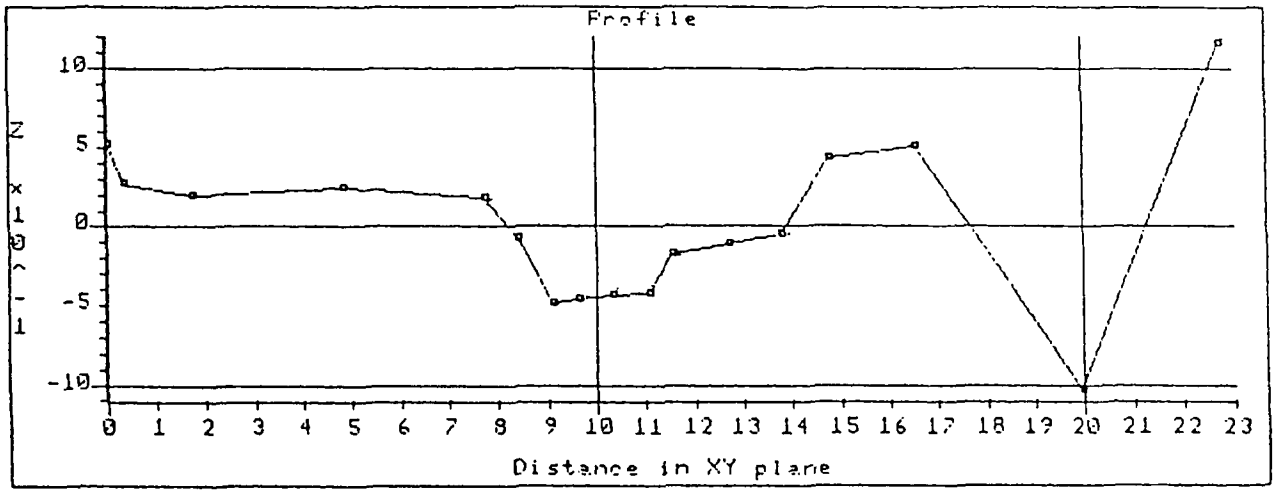

Axis	:	256			
Base	:	0.33	Mode	:	TILTED
Shift	:	0	Units	:	um

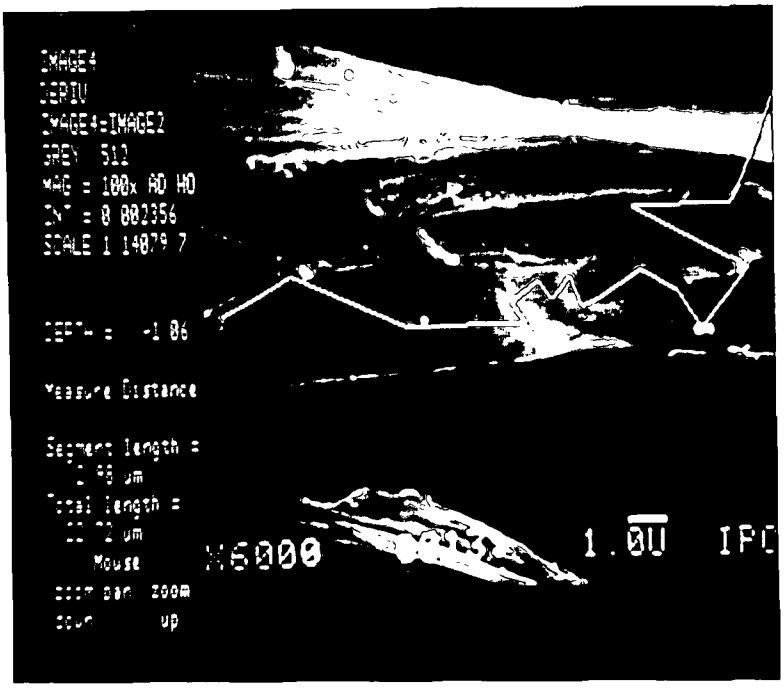

#	X	Y	Delta Z	Distance
0	23	245	0.52	.0.00
1	35	240	0.27	0.36
2	80	214	0.20	1.76
3	182	256	0.25	4.81
4	287	254	0.18	7.73
5	273	235	-0.07	8.38
6	294	218	-0.49	9.12
7	306	234	-0.47	9.65
8	322	214	-0.44	10.34
9	333	239	-0.42	11.07
10	349	234	-0.17	11.51
11	386	209	-0.11	12.72
12	420	228	-0.05	13.77
13	442	257	0.44	14.76
14	484	207	0.51	16.55
15	372	157	-1.03	19.94
16	472	155	1.17	22.72

Figure 38. Depth profile of feature no. 3 shown in Figures 30 and 33.

Environmental Scanning Electron Micrographs

As was mentioned above, the cellulose bands do not change during irradiation, while those due to lignin show a decline in intensity. The lack of change in the cellulose peaks suggests that cellulose is not being physically altered during irradiation.

In order for the features seen in the SEM micrographs to show a contoured topography, the cellulose fibrils had to have been altered spatially. It is conceivable that after lignin became solubilized and diffused away from the area, the cellulose fibrils had the freedom to collapse upon themselves. This could have occurred either during irradiation or when the sample was critical-point dried. (As mentioned above, cellulose band intensities did not change during irradiation which suggests that the topography developed during drying. Although it is not known with certainty if a small, i.e., few micron, change in position of the fibrils would be manifested in band intensity, it is likely that an intensity change would have been seen had they collapsed during irradiation, judging by the gradual decline in lignin band intensities after their initial precipitous drop.) Possibly the fibrils aggregated due to the strong cohesive interaction between cellulose chains when the lignin surrounding them was removed. Some support for this comes from an article dealing with structural changes in the cell wall during delignification.[227] In this article, the author proposes that cell wall dimensional changes during kraft delignification might be caused by just such a mechanism.

In order to investigate the effect of dehydration on the feature's topography (i.e., had the feature developed its terraced, crater-like shape prior to or after critical-point drying) micrographs were taken of an irradiated black spruce radial thin-section (wet) using the newly developed environmental scanning electron microscope (ESEM).

Basically, an ESEM is a SEM with a continuously variable specimen environment. This instrument allows direct observation of samples in their natural states, either wet or dry with no need for a conductive coating. By varying the pressure in the sample chamber, it is possible to witness dynamic processes, such as wetting and drying.

The irradiated sample was kept fully hydrated up until visualization. Micrographs were then taken as the sample dried using an ElectroScan ESEM. Figures 39 and 40 show the irradiated region (black spruce - latewood, secondary cell wall). Figure 39 was taken at 10 torr, while Figure 40 shows the irradiated area at a higher magnification with a 2.7 torr chamber pressure. The donut-like features at the bottom of Figure 39 are earlywood pits.

Irradiation features are readily apparent in both figures. As before, they appear crater-like but in contrast to the SEM micrographs, show little definition. (Internal structure can be seen in some of the features shown in Figure 40, but outgassing from the sample, as well as poor resolution, confuse the situation.)

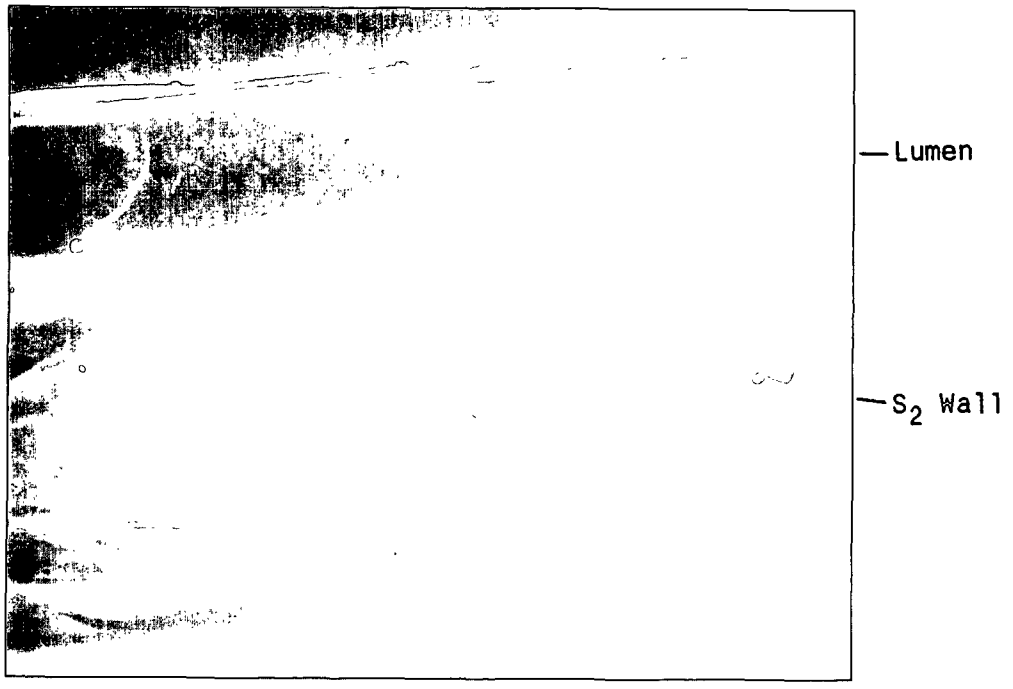

Figure 39. ESEM micrograph of laser irradiated black spruce secondary wall (latewood, radial section). The irradiation marks can be seen in the center of the micrograph just to the left of the very bright spot. 10 torr chamber pressure, 840X.

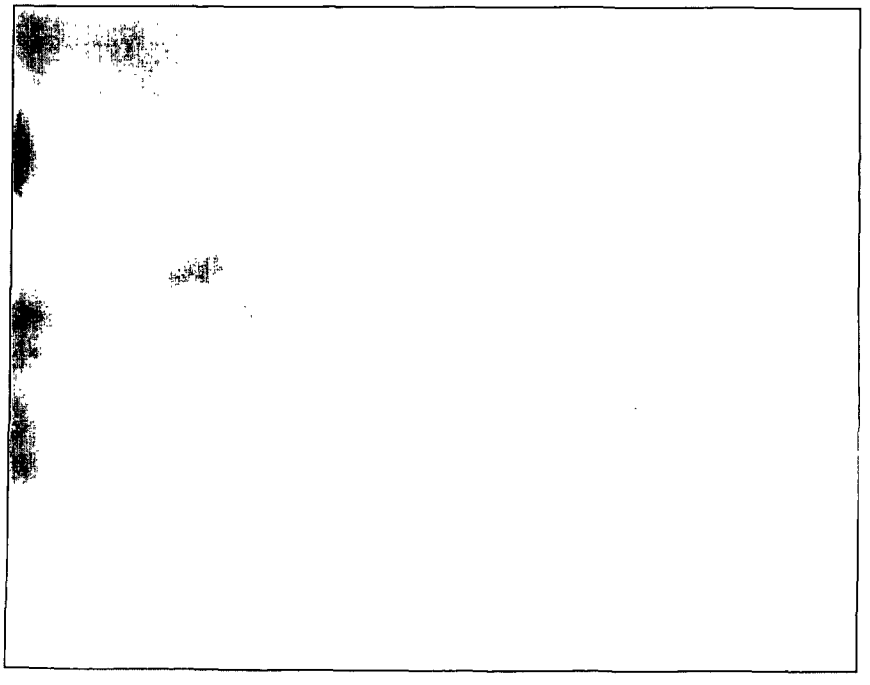

Figure 40. Close-up of irradiated area shown in Figure 39. 2.7 torr chamber pressure, 4800X.

The cellulose fibrils appear to have been spatially altered prior to the 10 torr micrograph. Assuming a 25°C temperature, the relative humidity in the chamber was approximately 55%, which gives a 10% moisture content (MC) for the section.[4] This MC is roughly that of wood during midwinter and far removed from a saturated condition (fiber saturation occurs at 25-30% MC). Attempts to photograph the sample at higher chamber pressures met with little success. (A chamber pressure of 23.8 torr is needed for the imaging of liquid water at 25°C - the saturation pressure of water vapor at that temperature.) It is thus difficult to determine from these data if the feature acquired its sunken topography while it was immersed in water or if it developed during drying. It can only be stated that the feature's crater-like topography (fibril collapse ?) had occurred prior to a moisture content of 8%.

It seems likely the event occurred during dehydration. In the wet state, water probably binds (hydrogen bonds) with the hydroxyl groups of cellulose as lignin is being solubilized. During dehydration, as the water is removed, these hydroxyl groups ultimately link together also by means of hydrogen bonds. Assuming that there are regions in the fibril's structure where cellulose is less ordered (imperfections in the crystal), it is conceivable that these regions would yield (deform) to the force developed during hydrogen bonding and thus allow the fibrils to collapse upon the underlying topography. Some support for this comes from the light micrographs. Prior to drying, the features could be seen as bright areas in the micrographs. Regard-

less of the focus, these bright areas could not be discerned in the critical-point dried sections; only the dark blotches were apparent. The light areas could be a manifestation of the open, noncollapsed nature of the region, while the dark blotches occur because the region is more closed due to the collapse of the fibrils.

Thermal vs. Photochemical Processes

The features' structure suggests that the primary mechanism in their formation was photochemical rather than thermal. If thermal energy were the sole cause, the ring-like nature of the features would most likely be quickly lost due to conduction of the energy.

When using the microprobe, the radiant flux (radiant power/unit area) at the point of focus is very high ($\approx$ 1300 MW/m^2, assuming 10mW at the sample and a one micron beam diameter). If dry wood sections are used, this irradiance level quickly causes them to burn. Immersion of the section in water allows the majority of this energy to be dissipated before damage can take place.

In order to rule out thermal effects, the approximate local temperature at the sample during irradiation was determined using Equation 11, which was developed in the theory section of this thesis.

$$T(K) = \frac{hc\nu_1}{k}\left[\ln\left(\frac{I_S}{I_{AS}}\right)-3\ln\left(\frac{\nu_0-\nu_1}{\nu_0+\nu_1}\right)\right]^{-1} \qquad [11]$$

Due to the nature of the Raman scattering process, only those bands close to the excitation frequency could be used in the determination . (The antiStokes bands are very low in intensity and quickly lost in the background.) Unfortunately, this necessitated using only cellulose bands in the temperature calculation.

The sample was a black spruce radial section, 30 microns in thickness. The area examined was located in a latewood, secondary cell wall. The excitation wavelength was 514.5 nm and the power level was 200 mW. The 330 and 380 cm^{-1} cellulose bands were investigated.

Table 4 presents the results. The values in the parentheses reflect a different baseline used in the intensity measurements. The difference between the 330 cm^{-1} and 380 cm^{-1} temperature values is probably due to the uncertainty in determining the 380 cm^{-1} antiStokes band height, which was quite weak. These temperatures (41-87.5°C) are well below those that could cause thermal damage to the cell wall. In most cases, 100 mW is used rather than 200 mW, which would lower the calculated temperature. These data are for cellulose; lignin which has been shown to absorb 514.5 nm radiation could conceivably experience a higher temperature. If this was the case, however, the cellulose data would most likely be affected.

There could be a possible problem with these data. In order to measure the antiStokes bands, the sample had to be irradiated to lower the background.

When the spectrum was collected, lignin had already undergone photomodification. This means that the temperature could be higher, but how much higher depends upon the amount of absorbed energy that is thermalized in lignin. It is known that bubbles did not form during irradiation, which indicates that the local water temperature probably did not exceed 100°C.

Table 4. Determination of the local sample temperature.

Band Position (cm^{-1})	Average S/AS Ratio	Temperature (°C)
330	3.37 (3.70)	87.5 (63.6)
380	4.33 (5.07)	72.3 (41.0)

(A sample of the spectra used in these determinations is located in Appendix 1.)

While thermal energy cannot be ruled out as a contributor to the formation of the features, it seems unlikely that the local temperatures were high enough to cause damage to the polymer(s). Thermal energy (temperature) may be important in an indirect manner. Photophysical processes, which occur in a polymer matrix, depend on the glass transition temperature (T_g). Below T_g, matrix limitations of translation and rotation possibilities will be most pronounced.[48] It has been reported that T_g for lignin under water-soaked conditions ranges from 80 to 100°C depending on the frequency of measurement.[228-231] This temperature could have been reached during irradiation. Thus it is conceivable that temperature may play a role in the formation of the feature by allowing the thermal softening of lignin.

These data then support the idea that the mechanism which gave rise to the feature was primarily photochemical in nature.

The feature's topography and behavior to laser radiation can adequately be explained on the basis of photochemistry. Areas on the cell wall which received higher intensity and/or longer exposure would have experienced a larger number of light-induced reactions (initiated by the absorption of 514.5 nm photons) with the concurrent generation of (phenoxy) radicals. These primary and secondary reactions probably resulted in the fragmentation and dissolution of lignin. This solubilization would have been greater in those areas where more photochemical reactions occurred, i.e., the areas of higher intensity and/or longer exposure. These areas, due to more lignin being removed, would be expected to show greater relief upon sample dehydration and collapse of the cellulose fibrils. This would explain the imprint of intensity distribution of the incident laser beam on the cell wall, as well as the effect of incident power level on feature depth and lateral extent (Figure 33, nos. 1-3). (The higher the power level, the greater the intensity in the central and subsidiary maxima [rings] and thus the greater likelihood of photochemical reactions.) The reason for the disappearance of the rings in the feature that was irradiated for 17 hours (Figure 33, no. 4) might be attributed to diffusion of the photoexcited entities into these areas and the subsequent dissolution of lignin or, more probably, by slight sample movement during irradiation.

Lignin Dissolution

Gas Chromatography/Mass Spectrometry Study

The data point to the dissolution of lignin during laser irradiation. The evidence is, for the most part, indirect. (The observation that concurrent with the decline of lignin bands during irradiation, a feature developed on the cell wall which, in SEM/ESEM micrographs, appeared to show that cell wall material was missing.) In an attempt to substantiate lignin's dissolution, the water in which an irradiated section was immersed was analyzed using gas chromatography/mass spectrometry (GC/MS).

Rough calculations indicated that the concentration of solubilized lignin would be in the parts-per-billion range for a 4x4x1 micron feature (100 mW, 500 second) using 10 mL of water and assuming the density of lignin to be approximately 1.3 g/cm.[3,4] To increase the probability of detecting lignin fragments, 16 areas on a latewood, secondary cell wall of black spruce were irradiated. The excitation wavelength was 514.5 nm with a power level of 300 mW. The exposure duration for each location was in the neighborhood of ten minutes. A SEM micrograph of the irradiated region is shown in Figure 41. The magnitude of the disturbance is readily apparent. (The fissures are the result of electron beam damage by the SEM.)

In addition to the immersion water, two controls were also investigated. One control (10 mL of water in which an identical section was immersed for the

same period of time) was used to determine whether there are soluble materials in the (nonirradiated) wood section. The second control (10 mL of water that was in the sample container for the same time period) served to determine if the epoxy cement used in the sample container was soluble in water.

Figure 41. SEM micrograph of the black spruce section used in the GC/MS investigation showing three irradiation marks.

Prior to analysis, the samples were evaporated to a 1 mL volume and silated Following this, they were analyzed by Leroy Borchardt at the Institute of Paper Chemistry using a Hewlett-Packard 5985 GC/MS instrument with an OV-17 column.

The data were difficult to interpret. Initially the samples were run in the standard manner (total ion). The only readily apparent features in this

spectrum were identified as belonging to water and/or epoxy cement. Due to the very low concentration of the postulated lignin fragments, it became necessary to search for specific ions using selective ion monitoring (enhanced sensitivity).

Various authors have proposed that quinone-type structures are major degradation products in the photooxidation of lignin.[45,52,55,58] Based on this, the ions chosen were quinonoid lignin structures. These ions, along with their mass-to-charge ratios (m/e), are depicted in Figure 42.

m/e 107 m/e 121

m/e 123 m/e 138

Figure 42. Ions searched for in the GC/MS investigation for solubilized lignin.

The results were open to question. If the peaks due to the controls were accounted for, there remain several relatively weak features which may be due

to the selected ions. The peaks (retention time) are listed in Table 5 and the spectra will be found in Appendix 2. As indicated in the table, the only relatively strong features were seen in the m/e 123/138 spectra.

Table 5. GC/MS (SIMS) Analysis for Solubilized Lignin.

m/e	Sample Peak (Retention Time, min.)	
	1.4X	
123,138	1.5(W)	
123,138	2.2(VW)	
	2.4-2.5X	
	2.8X	
123	3.2(W)	X - peak occurred in controls
	4.1-4.2X	
	4.7-4.8 X	VW - very weak
	5.6-5.7X	
	5.8X	W - weak
	6.1-6.2X	
	6.8X	M - medium
121	7.2(VW)	
107	7.8(M)	S - strong
138	8.0(S)	
	8.1X	
	8.3X	
	9.8X	
123	10.0(S)	
	10.2X	
121	10.5(M)	
	12.8X	
	13.2X	
	13.3X	
	13.6X	
	14.2X	

These results indicated that something was present in the irradiated sample water, but a trace amount of a contaminant could negate the results at

these concentrations. However, given what is known about the photooxidative degradation of lignin, it is possible that the unaccounted for peaks in the spectra are due to p-quinonoid structures.

Lignin Diffusion

The evidence suggests that lignin undergoes photooxidative degradation which results in the fragmentation of the macromolecule and subsequent solubilization. (It is not known whether partial or total solubilization of lignin would occur, but it is felt that partial solubilization would be more probable because of complexity of the lignin macromolecule.) In order for this to be plausible, the lignin fragments must be able to diffuse away from the irradiated region very rapidly to account for the observation that the features are readily apparent within a minute of irradiation.

The average distance through which a material has diffused in a certain time is given by:

$$X^2 = 2Dt \qquad [12]$$

where X equals the distance the particle diffuses, t is the migration time, and D is the diffusion coefficient.[232] The diffusion coefficient for free diffusion of lignin macromolecules in water has been determined to be 10^{-6}-10^{-7} cm^2/s.[233-235] Substituting these values into equation 12 and

assuming a one-second migration time gives a 4.5 - 14.1 micron diffusion distance. This distance is more than adequate to explain the observation that the features are apparent within 60 seconds of irradiation.

These diffusion distance values are probably too large. It is unlikely that the lignin fragments would be entirely unencumbered as they were diffusing away from the region, but would be constrained by cellulose microfibrils and hemicelluloses. This could substantially retard their diffusion rate.

Recent studies concerning the leaching of lignin from pulp fibers suspended in water show that the average diffusion coefficient is several orders of magnitude smaller than that expected for free diffusion of lignin macromolecules in water.[236-237] The value given is 3×10^{-14} cm^2/s. In addition, it has been observed that the rate of lignin leaching increases dramatically above 70°C. (Goring[237] postulated that this effect may be due to physical changes in the structure of the fiber associated with the thermal softening of the hemicelluloses in the fiber wall - $T_g \approx 55°C$ for hemicelluloses saturated with water[238].)

Calculations showed that the local sample temperature during laser irradiation was in the neighborhood of 80°C. At this temperature, it is likely that hemicelluloses (and lignin) have experienced thermal softening. If adjustments are made for the effect of temperature on lignin's diffusion coefficient (Figure 43), then a distance of ≈0.5 microns in 60 seconds is

obtained. Thus it is plausible that lignin fragments could diffuse far enough away from the irradiated region to account for the formation of the feature within a 60-second time period.

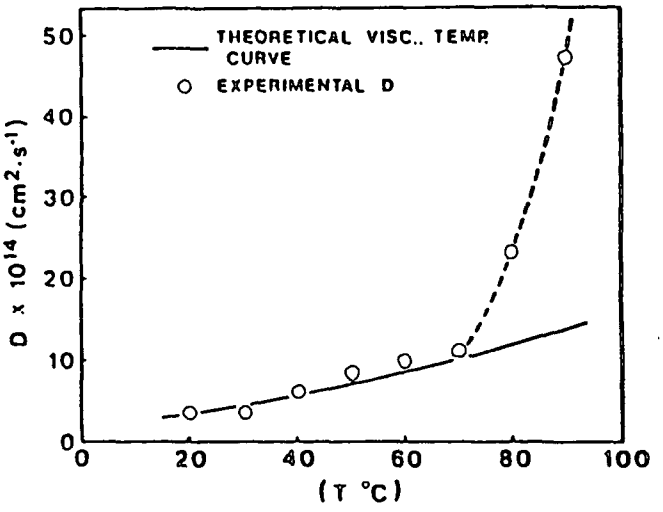

Figure 43. Plot of the intrafiber diffusion coefficient (D) vs. the temperature (T). The solid line corresponds to the increase with temperatures of D expected from the Stokes-Einstein equation.[237]

Summary

This section has presented the results of the investigation of the feature which developed at the location on the cell wall where the laser beam was focused while acquiring the Raman spectrum. The major conclusions are:

1. Wet woody tissue underwent a complex series of photochemical reactions which were initiated by the absorption of 514.5 nm photons.
2. These reactions resulted in an imprinting of the incident intensity

distribution on the secondary cell wall layer that became readily apparent during SEM visualization.

3. This imprinting was most likely the result of the photochemically induced (partial) solubilization of lignin.
4. These reactions also resulted in the formation of a yellowish-colored chromophore(s). GC/MS analysis suggested that these degradation products included quinone structures.

Conjugation And Preresonance Raman Enhancement

The following section reports on the study of Raman band enhancement mechanisms using lignin model compounds and native woody tissue. This study was an outgrowth of the investigation into understanding the factors which contributed to the photomodification of lignin.

General Discussion

During the early stages of this investigation, an experiment was undertaken to determine the relationship between lignin content and lignin's 1595 cm^{-1} band intensity for loblolly pine groundwood. (The paper which resulted from this investigation is located in Appendix 3.) The approach was based on recording the Raman spectra of groundwood before and after successive acid-chlorite delignification treatments and correlating the observed 1595 cm^{-1} band intensity to the Klason and total lignin content of the wood.

The results of this experiment are shown in Figure 44. It can be seen that the 1595 cm^{-1} band height exhibited a rapid decline followed by a gradual linear trend. These results were interpreted to indicate that during the initial stages of delignification, a particularly sensitive aromatic ring substituent was preferentially attacked, which resulted in a decrease of the scattering coefficient associated with the 1595 cm^{-1} band.

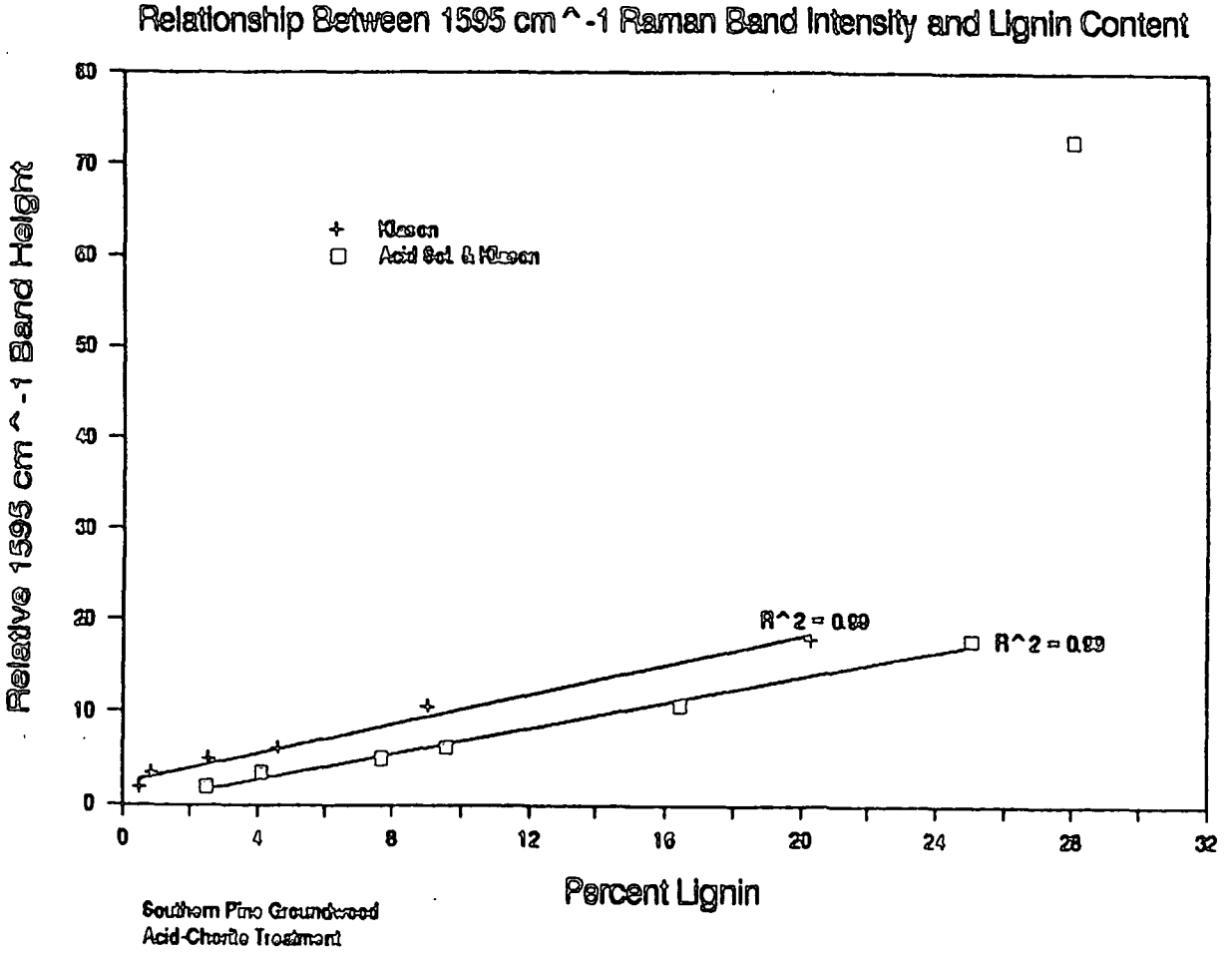

Figure 44. Variation of the intensity of the 1595 cm^{-1} band with lignin content.

The trend observed in the intensity of the 1595 cm^{-1} band during delignification is similar to the decline seen during irradiation of untreated wood, i.e., an initial rapid drop followed by a more gradual decline (Figure 45, cellulose's 1098 cm^{-1} band was used as an internal standard and the incident electric vector was parallel to the long axis of the cell wall). Taken together, these data suggest that the initial rapid drop is (primarily) due to a change in the scattering cross-section, while the subsequent decline most likely reflects the loss of aromaticity/solubilization of the ring. This change in the scattering coefficient could be brought about by the disruption of the bonding pattern of specific, substituted phenylpropane units which contribute disproportionally to the intensity of the 1595 cm^{-1} band, i.e., their scattering coefficient is enhanced.

It has been known for some time that the Raman intensities of certain bands are sensitive to both excitation wavelength and conjugation.[203-205,207] The first effect is termed resonance Raman enhancement (RRE), while the latter is referred to as conjugation enhancement (CE). (If the excitation wavelength falls near but not within the electronic absorption band, the first effect is commonly referred to as preresonance Raman enhancement (PRRE).) Experiments were undertaken to assess the contribution of these enhancing mechanisms to the intensity of lignin's 1595 cm^{-1} aromatic ring breathing band. Both lignin models and wood samples were used in this assessment.

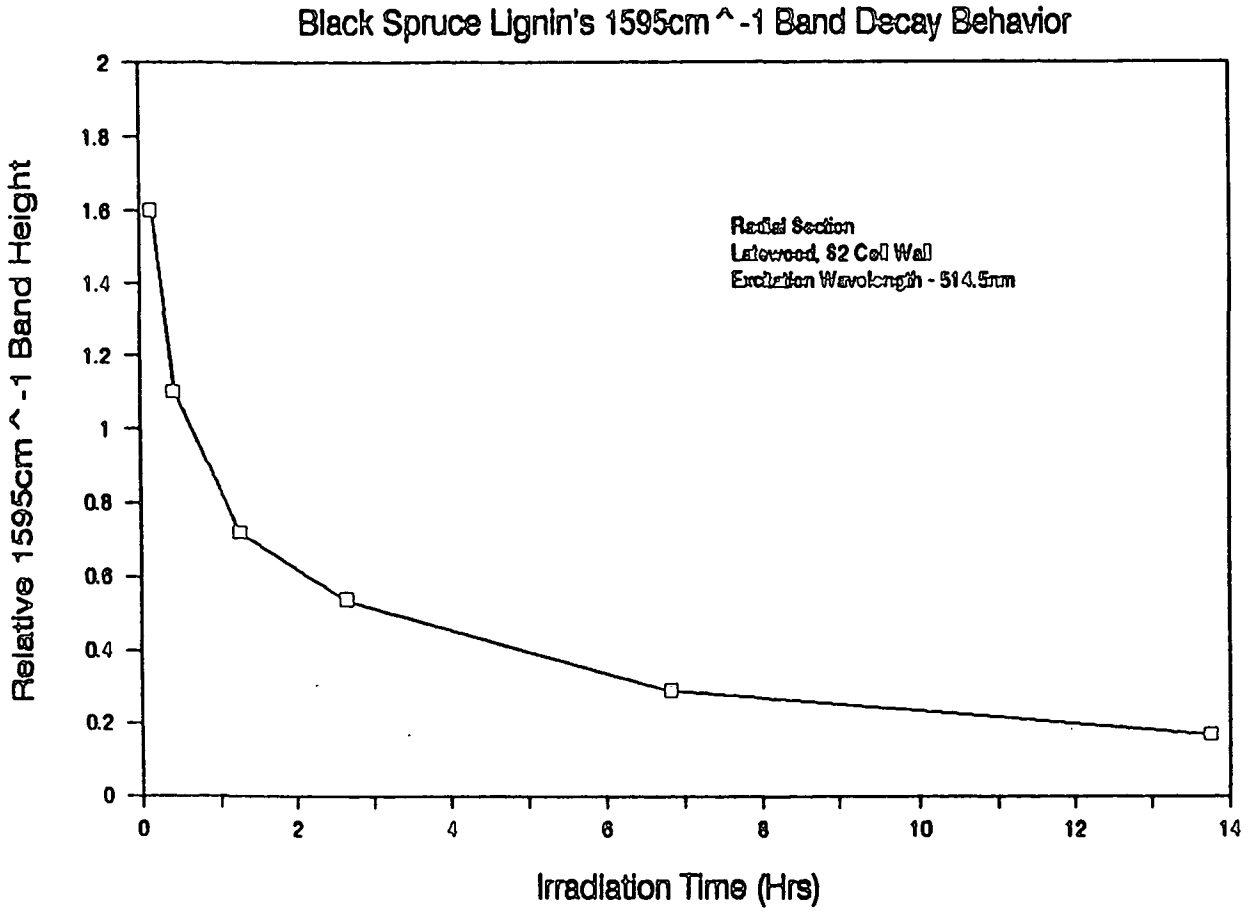

Figure 45. Effect of 514.5 nm laser radiation on black spruce lignin's 1595 cm^{-1} band.

Instrument Response To Excitation Wavelength

The excitation wavelength is varied to assess the preresonance Raman enhancement (PRRE) contribution to a particular band. The intensity of those bands associated with the absorbing species dramatically increases as the

frequency of light approaches the electronic absorption band. The spectrometer system's response to wavelength is not uniform over the frequency range needed to investigate these effects. The primary cause of this nonuniform response is usually due to the spectrometer's gratings, although the detector may also make a significant contribution.[239,240] Before the effect of excitation wavelength on 1595 cm^{-1} band intensity could be determined, a correction had to be made to the data to account for the system's nonuniform response.

The method chosen for this correction involved recording the spectrum of toluene using the various excitation wavelengths. (The excitation wavelengths chosen for this study included the 457.9, 488.0, and 514.5 nm lines from an Argon ion laser, the 647.1 nm line from a Krypton ion laser, and the 1064 nm line from a Nd:YAG laser. The Nd:YAG laser was part of a Spex Industries' FT-Raman system.) For each excitation wavelength, the intensity of the symmetric ring breathing band (1004 cm^{-1}) was used to normalize the other band intensities. This was needed to correct for differences in incident power levels, as well as the reciprocal fourth power dependence on wavelength of Raman scattering. Eleven toluene bands were used which covered the spectral range from 292 to 3038 cm^{-1} (macro system). Following this, the relative band intensities were normalized to the 514.5 nm response. This involved dividing the relative height (intensity) for a given 514.5 nm band by the respective relative band height for the other excitation wavelengths.

The outcome of this procedure was a series of eleven numbers for each

excitation wavelength (Table 6). These numbers were the correction factors (multipliers) to be applied to the (PRRE) data. In order to correct band intensities which did not coincide with one of the toluene bands, either linear interpolation or a curve fitting routine was used. (The results were similar.) The response correction curve when using an excitation wavelength of 647.1 nm is shown in Figure 46a for the macro (Ramanor) system, and Figure 46b for the microprobe. In the latter case, only six toluene bands were used. In both instances, the data have been fitted with an equation of the form $y=A+Bx+Cx^2$.

Table 6. Excitation Wavelength Correction Factors for the Jobin Yvon Ramanor HG2S Spectrometer System. Based on Toluene and Referenced to the 514.5 nm Argon Ion Laser Line.

Raman Band (cm^{-1})	Excitation Wavelength (nm)				
	457.9	488.0	514.5	647.1	1064
292	1.28	1.02	1(1.00)(1)	0.684(0.866)(1)	--
498	1.32	1.05	1(1.11)	0.758(0.855)	1.72
606	1.08	0.968	1(1.05)	0.898(1.04)	1.56
784	1.17	1.05	1(1.06)	0.880(0.922)	0.714
1004	1	1	1(1)	1 (1)	1
1029	1.06	1.04	1(1.15)	1.29 (1.41)	1.17
1198	0.903	0.943	1(1.12)	1.65 (1.80)	0.880
1370	0.829	0.928	1(1.12)	1.94 (2.14)	0.756
1594	0.851	0.888	1(1.12)	2.44 (2.52)	0.701
2898	0.594	0.836	1(1.15)	6.08 (9.89)	0.535
3038	0.598	0.854	1(1.09)	6.81 (11.1)	0.433

(1) The PMT power supply had to be replaced. This necessitated optimizing the tube voltage which changed the response. The values enclosed in parentheses reflect this change.

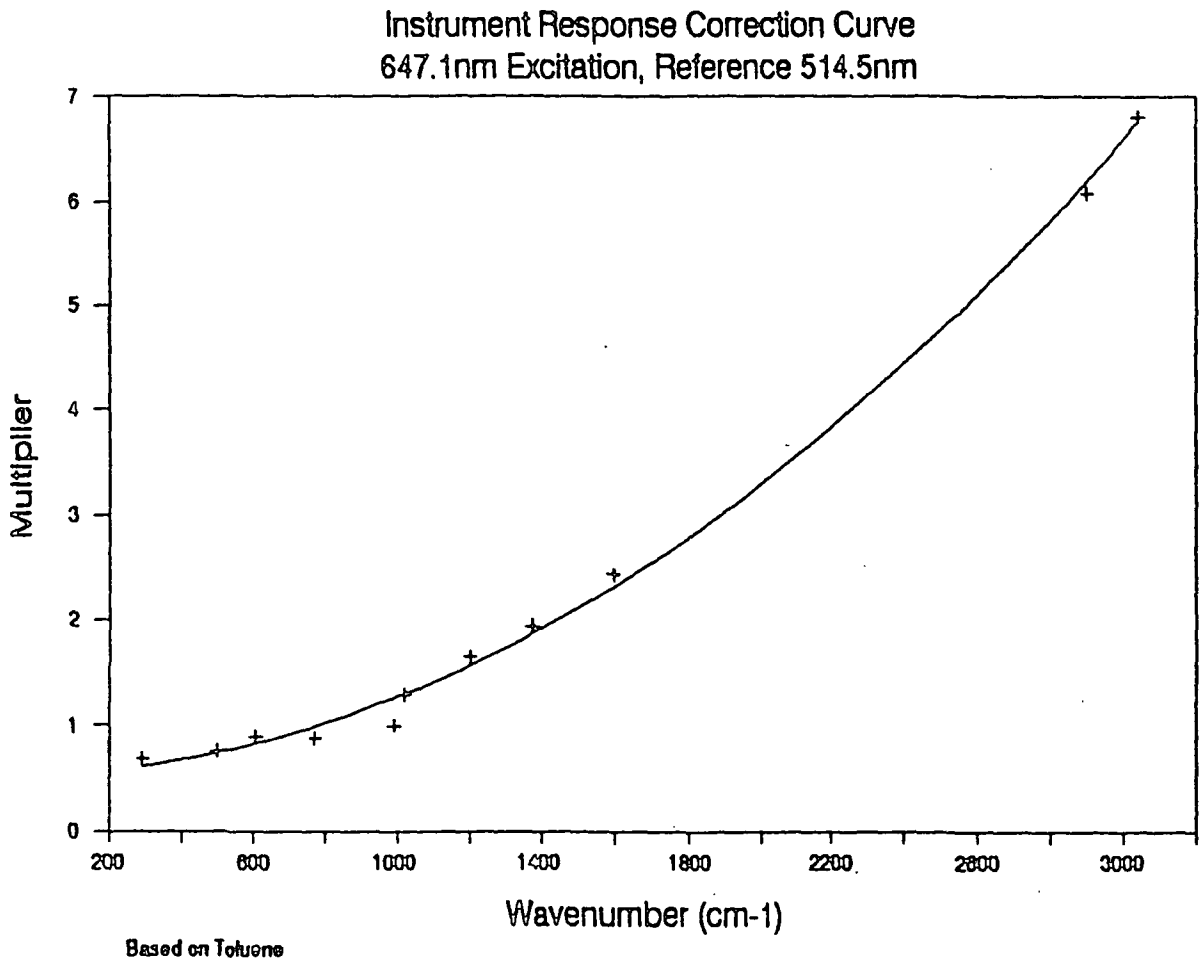

Figure 46a. Ramanor system instrument response correction factors when using a 647.1nm excitation wavelength.

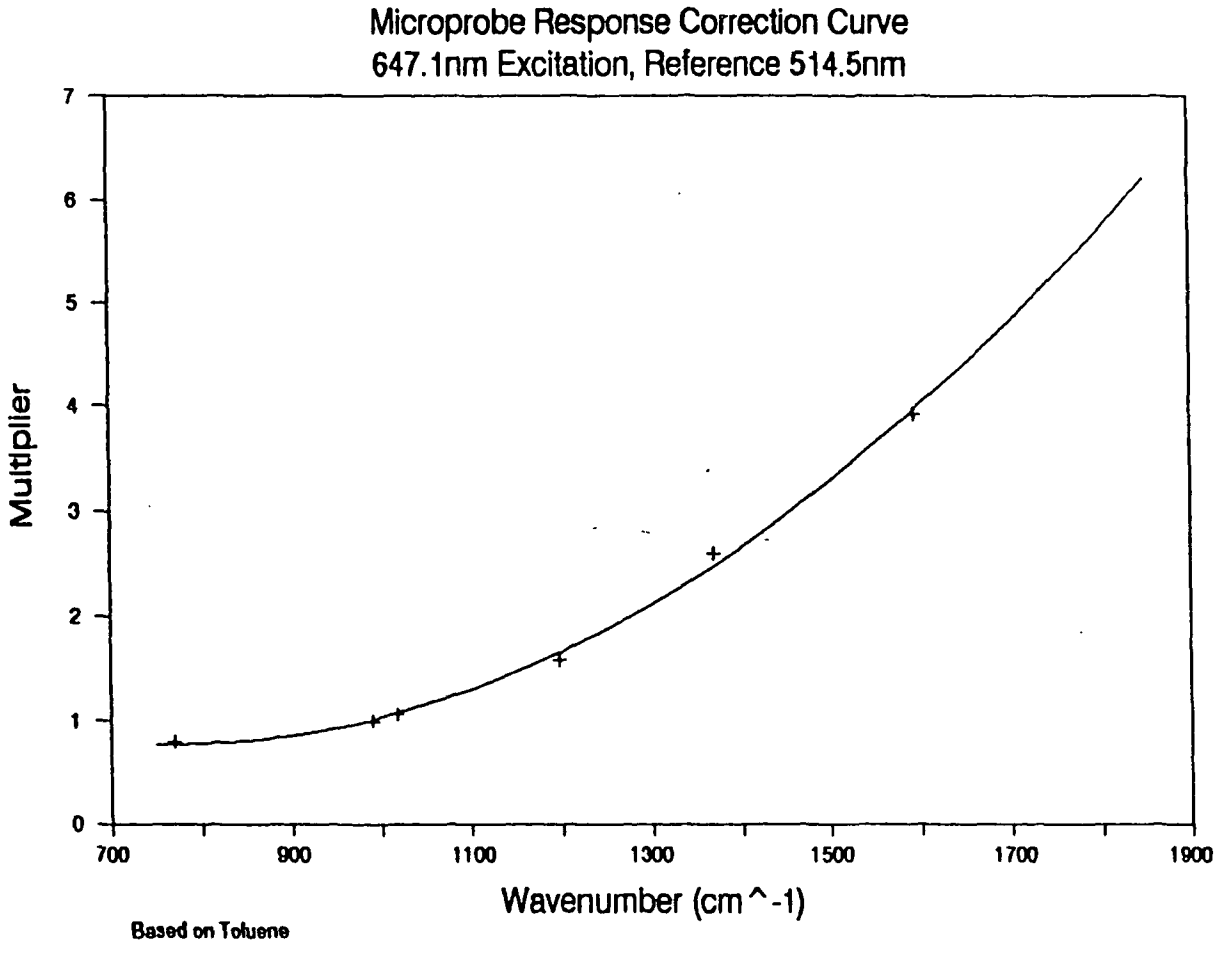

Figure 46b. Microprobe system instrument response correction factors when using a 647.1nm excitation wavelength.

Model Compound Study

Schmid et al. have reported that the intensity of the ≈1600 cm^{-1} band of benzene derivatives is dependent on the substituents.[100] In the case of double bond conjugated substituent groups, the band intensity was found to depend on the degree of pi-electron conjugation between the ring and the substituent. Native lignin contains both α-carbonyls and double bonds in its propyl side chain, both of which can enter into conjugation with the aromatic ring.

The model compounds (I-IV) depicted in Figure 23 were used to investigate the effect of conjugation on the intensity of the ≈1600 cm^{-1} aromatic ring breathing band. All are monolignols based on guaiacyl phenyl propane, differing only in the occurrence and location of the double bonds. (An exception was α,4-dihydroxy-3-methoxyacetophenone (IV) which only had a two-carbon side chain.) Their 0.1M solutions in methanol were studied using the macro-Raman system. The intensity of methanol's 1450 cm^{-1} CH_2 bending vibration served as a reference. To rule out the possibility of preresonance Raman enhancement occurring with 514.5 nm excitation wavelength, Raman spectra were also obtained using 647.1 and 1064 nm wavelengths.

Table 7 presents the results of this investigation. All data have been corrected for instrument response. Three of the monolignols showed a preresonance Raman enhancement of their ≈1600 cm^{-1} bands. Coniferaldehyde's 1595 cm^{-1}

band showed the largest effect; 68% of its 514.5 nm intensity was due to PRRE. The percentages for α,4-dihydroxy-3-methoxyacetophenone and coniferyl alcohol were 37% and 30%, respectively. In contrast to these, guaiacyl propanol showed little or no PRRE of its 1610 cm^{-1} band. (These percentages were obtained by subtracting the PRRE-free relative intensity [1064 nm value] from the 514.5 nm relative intensity [which had contributions from PRRE, CE, and nonenhanced scattering], dividing the result by the 514.5 nm relative intensity, and multiplying by 100.)

It will be recalled that preresonance Raman enhancement arises when the energy of the incident photons is close to an electronic excitation level of a molecule, i.e., an absorption band. Apparently, a wavelength of 514.5 nm was sufficiently close to the absorption bands for three of the monolignols to bring about PRRE of their ≈1600 cm^{-1} bands. These monolignols all contain ring conjugated double bonds; both coniferyl alcohol and α,4-dihydroxy-3-methoxyacetophenone have one, while coniferaldehyde has two.

It is known that as the extent of conjugation increases, the excited electronic transition frequency decreases, i.e., the wavelength of maximum absorption is shifted to longer wavelengths.[210] As a consequence of this bathochromic shift, the preresonance Raman enhancement effect would increasingly be felt as conjugation increased (wavelength of maximum absorption shifted closer to the excitation frequency). This could explain why coniferaldehyde, being a more conjugated system, had a larger PRRE contribution to

Table 7. Effect of Excitation Wavelength and Conjugation on the Relative ≈1600 cm^{-1} Ring Breathing Band Intensity.

Model Compound	Relative ≈1600 cm^{-1} Band Intensity $I_{\approx1600}$ (Model)/I_{1450} (MeOH) (Excitation Wavelength, nm) 514.5	647.1	1064[1]	Conjugation Enhancement Factor (Based on Guaiacyl Propanol)
Guaiacyl Propanol	0.039	0.030 (0.036)[2]	0.041	1
Coniferyl Alcohol	0.403	0.273 (0.284)	0.294	7.9
α,4-Dihydroxy-3-Methoxy-Acetophenone	0.462	0.294 (0.291)	0.288	8.1
Coniferaldehyde	5.56	3.21	1.76	48.9[3]

(1) An assumption which has been made throughout these studies is that PRRE does not contribute significantly to band intensity when using a 1064 nm excitation wavelength.

(2) For the first three model compounds, the 647.1 nm and 1064 nm intensity values did not differ significantly from each other and were averaged for the analysis. (The expected trend of decreasing intensity with longer excitation wavelengths is actually reversed for both guaiacyl propanol and coniferyl alcohol which suggests that the slight difference in relative intensities between the these two excitation wavelengths is probably due to experimental error.)

(3) This value could be inflated because the 1064 nm value may not be entirely free of PRRE.

its 1595 cm^{-1} band than any of the other, less conjugated monolignols. The effect appears to be additive, at least in this limited study. Having zero (guaiacyl propanol), one (coniferyl alcohol/α,4-dihydroxy-3-methoxyacetophenone), or two (coniferaldehyde) ring conjugated double bonds in the propyl side chain resulted in an 8%, 30/37%, or 68% contribution to the intensity of the ≈1600 cm^{-1} band, respectively.

In order to substantiate the effect of conjugation on the maximum absorption wavelength (and hence the PRRE contribution to ≈1600 cm^{-1} band intensities) UV-Visible absorption spectra were obtained for the monolignols using a Hewlitt-Packard 8452A diode array spectrometer. The solvent used was methanol (or a methanol/water mixture; water did not effect the absorption spectra). The concentration for each monolignol was adjusted so that its absorbance would fall within the range of 0.2 to 1.0 AU.

Figure 47 shows the absorption spectra. (The nomenclature used to discuss the spectra is that adopted by Polcin and Rapson[241] and Doub and Vanderbelt[242,243] and is based on benzene. Only the behavior of the K- [secondary] band and the B- [second primary] band will be discussed.)

Guaiacyl propanol had the typical B-band maximum of an oxy-substituted benzene ring at 280 nm and another maximum close to 255 nm (K-band) due to the double bonds in the benzene ring.[241] Introduction of a conjugated double bond either in the C_α=C_β (coniferyl alcohol) or C_α=O (α,4-dihydroxy-3-methoxy-

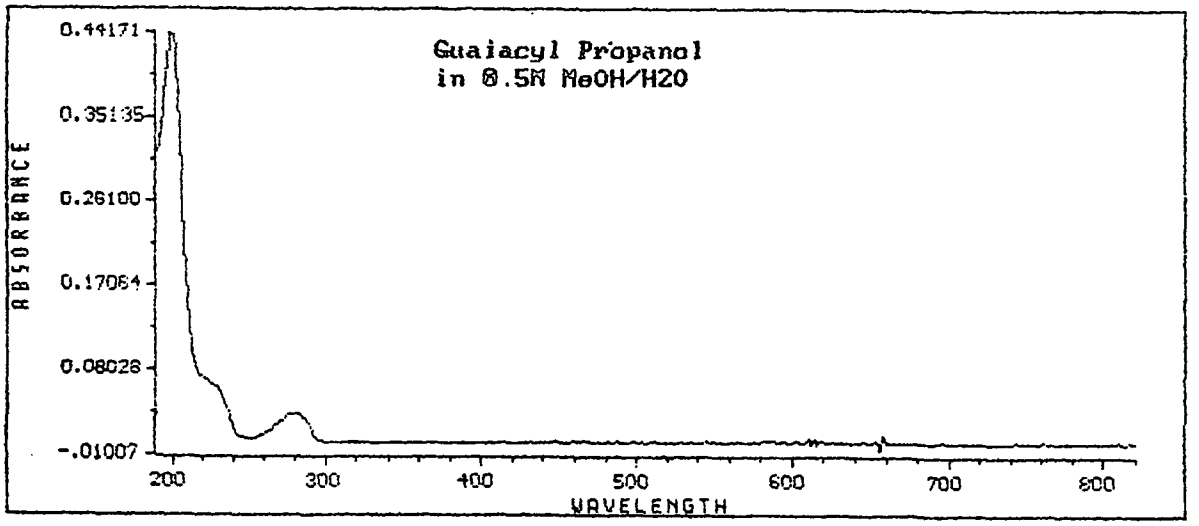

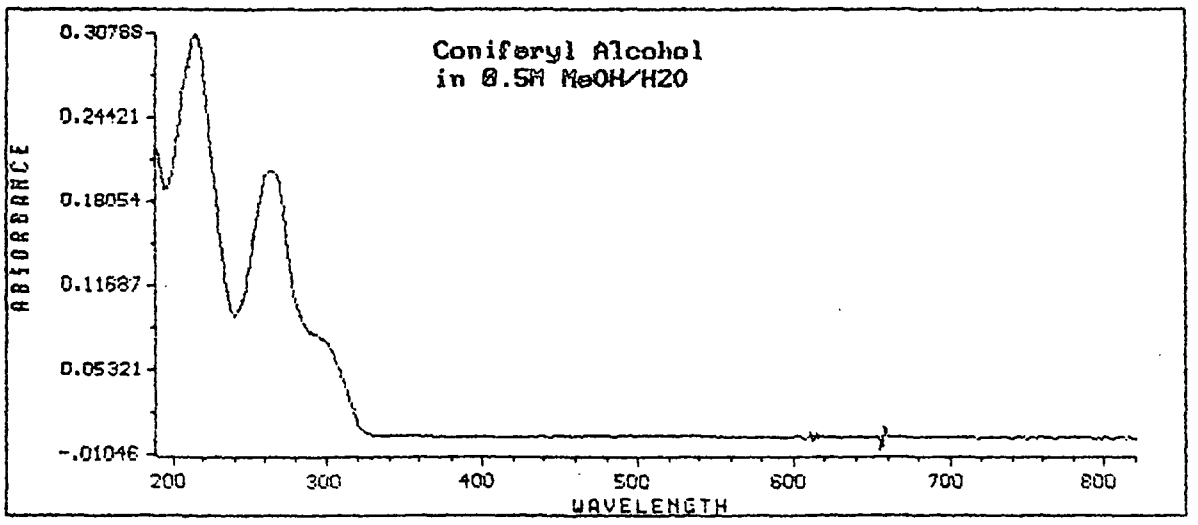

Figure 47. Absorption spectra of the monolignols.

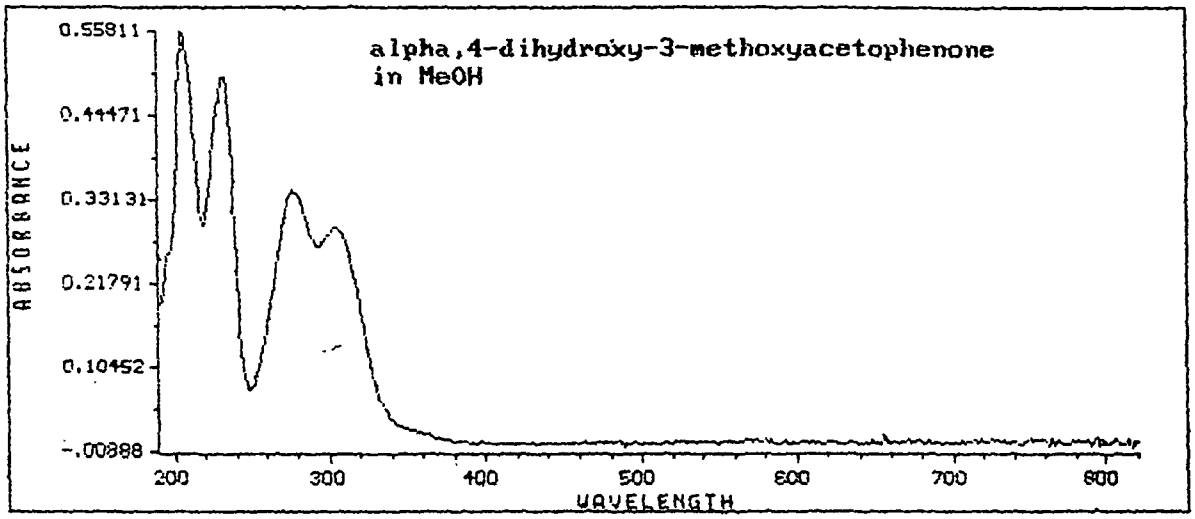

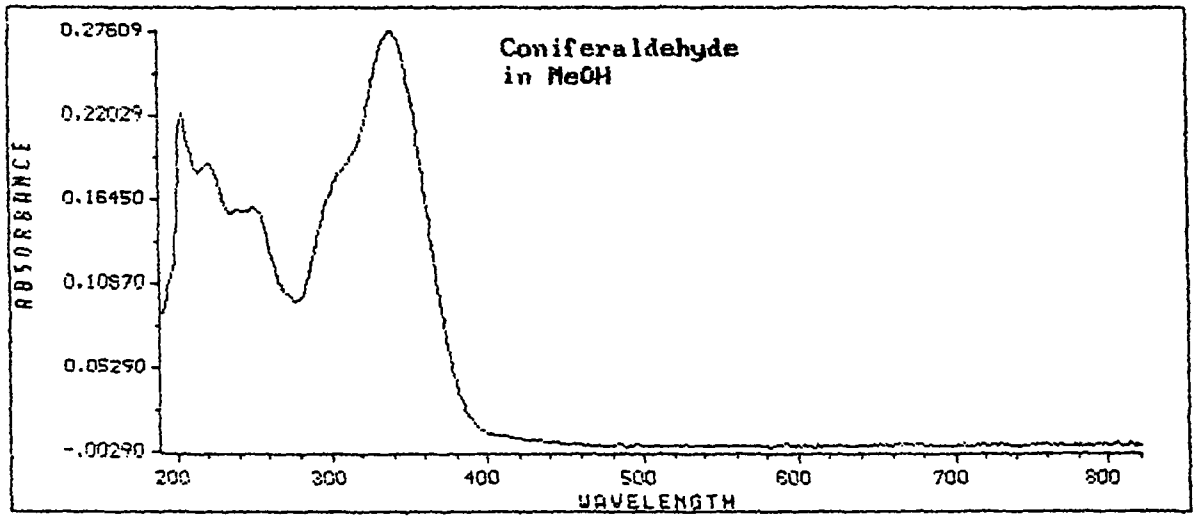

Figure 47 contd. Absorption spectra of the monolignols.

acetophenone) position resulted in a shift of both K- and B-bands to longer wavelengths, as well as their intensification. (K/B: 265/300 nm for coniferyl alcohol, 275/305 nm for α,4-dihydroxy-3-methoxyacetophenone). The combination of both a carbonyl group and conjugated double bond in the side chain (coniferaldehyde) resulted in a further shift of the maxima into longer wavelengths (K/B: 305/340 nm) and a strong intensification of the B-band.

These absorption data demonstrate that as the extent of conjugation increased, the absorption maxima were shifted to longer wavelengths. This would explain the order observed in the PRRE contribution to the ≈1600 cm^{-1} on band intensities for the monolignols. The PRRE contribution was a function of the wavelength of maximum absorption which, in turn, was a function of the extent of conjugation. The more conjugated the system, the larger the bathochromic shift of the absorption band(s) towards 514.5 nm and, hence, the greater the PRRE contribution. It is not known if the additive nature of the extent of conjugation on the PRRE contribution was specific to these monolignols or, given the limited data, even real.

A surprising aspect of these experiments was the sensitivity of the PRRE contribution to the wavelength of maximum absorption. Coniferaldehyde's B-band was located at 340 nm, which was 174 nm removed from the excitation wavelength and yet 68% of its 1595 cm^{-1} band intensity was due to PRRE. (This absorption band was fairly broad with a tail that extended to approximately 460 nm. Thus the difference between the excitation wavelength and the wave-

length of maximum absorption was probably closer to 50 to 100 nm, although the absorption at these longer wavelengths was very low.)

In order to determine the effect of conjugation on the intensity of the ≈1600 cm^{-1} band, the relative band intensities when using 1064 nm excitation (assumed to be free of PRRE) were analyzed. (Conjugation enhancement does not depend on the excitation wavelength.) As can be seen from Table 7, the α-carbonyl in α,4-dihydroxy-3-methoxyacetophenone resulted in a 8.1 fold enhancement, the α-β double bond in coniferyl alcohol gave a 7.9 fold enhancement, and the combination of both these substituents (conjugated α-β double bond and γ-carbonyl) in coniferaldehyde resulted in an enhancement factor of 48.9. These factors are relative to guaiacyl propanol which does not have any conjugated substituents. (It is conceivable that for coniferaldehyde the relative intensity when using 1064 nm excitation was not entirely free of PRRE and thus that the 48.9 CE factor was [slightly] inflated.)

These studies revealed that both intensity enhancing mechanisms, namely preresonance Raman and conjugation, contribute to the monolignol's ≈1600 cm^{-1} band intensity. Figure 48 summarizes the contribution of each effect to the relative intensity of this band when using 514.5 nm excitation. (The nonenhanced contribution was based on guaiacyl propanol.) It can be seen that the PRRE contribution was dominant in the more conjugated system (coniferaldehyde: 68% PRRE, 31% CE, 1% nonenhanced; α,4-dihydroxy-3-methoxyacetophenone: 37,55,8%; coniferyl alcohol: 30,61,9%; guaiacyl propanol 8,0,92%). (The

percentages were obtained from the data in Table 7 by dividing the relative intensity contribution for each mechanism [PRRE+CE+nonenhanced (NE): 514.5 nm value; CE+NE: 1064 nm value; NE: guaiacyl propanol value] by the 514.5 nm relative intensity and multiplying by 100.)

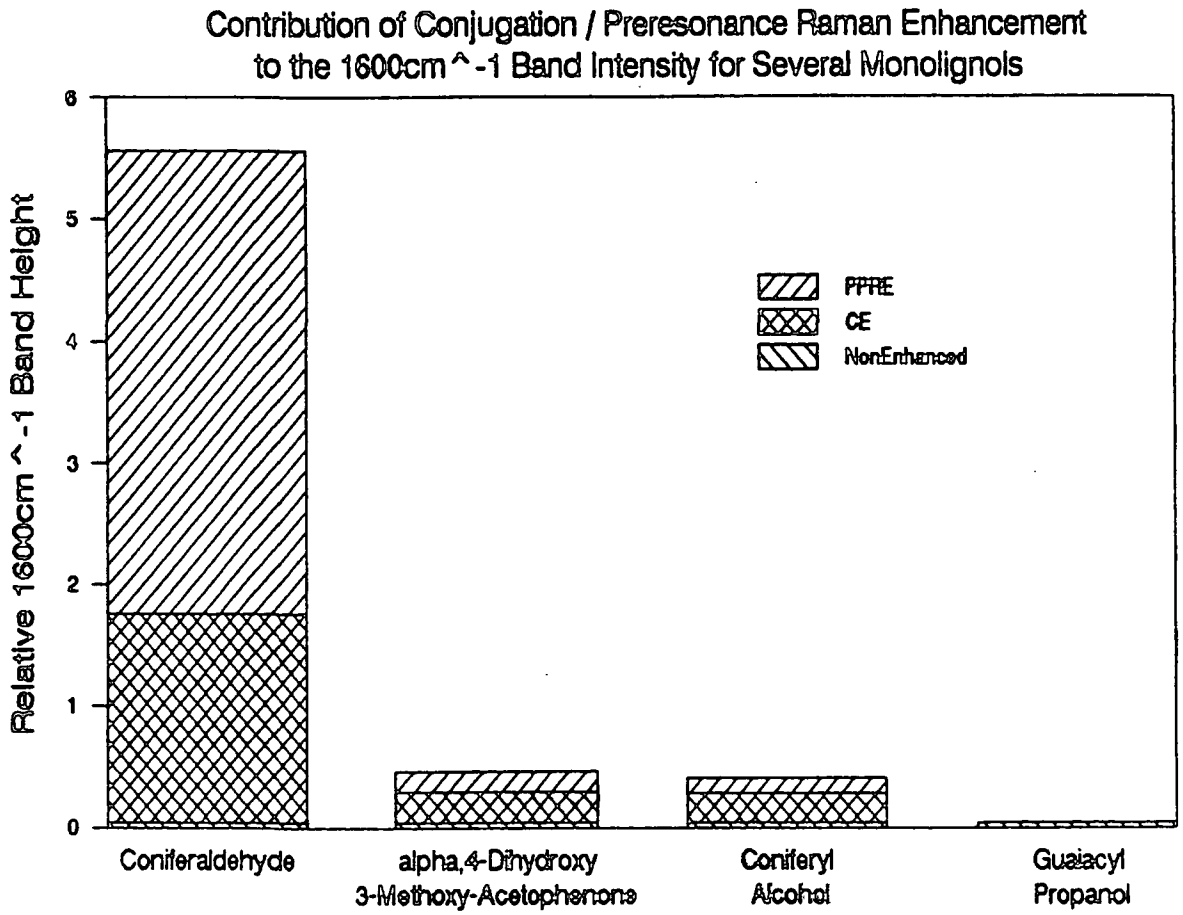

Figure 48: Contribution of conjugation/preresonance Raman enhancement to the ≈1600 cm^{-1} band intensities for several monolignols. Referenced to 514.5 nm excitation.

In addition to the 1595 cm^{-1} aromatic ring breathing band, two other bands in coniferaldehyde were analyzed. These were the 1615 cm^{-1} (conjugated $C_\alpha=C_\beta$ stretching vibration) and the 1660 cm^{-1} (conjugated $C_\gamma=O$ stretching vibration) bands. The literature suggests that all vibrational bands involved in conjugation should be subject to enhancement.[94-100,102,106]

The results (corrected for instrument response) are tabulated in Table 8 and shown in Figure 49. As before, the band intensities using 1064 nm excitation were used to assess conjugation effects. For all bands, the mechanism which dominated was PRRE (1595 cm^{-1}: 68% PRRE, 31% CE, 1% nonenhanced (NE)*; 1615 cm^{-1}: 64, 33, 3%; 1660 cm^{-1}: 60, 39, 1%). These data suggest that the PRRE contribution was uniform, i.e., the vibrations depended on the same absorption frequency.

Schmid et al. findings using diphenylpolyenes paralleled these results.[102,106] These authors found uniform PRRE of both the ≈1600 cm^{-1} ring and C=C stretching vibrations. In contrast to this, the ≈3000 cm^{-1} aromatic CH valence vibration did not exhibit any PRRE or CE. They interpreted this latter result by making the assumption that the Raman scattering tensor was composed of two parts [$\alpha=\alpha(\pi)+\alpha(\sigma)$], associated with a contribution by π and σ

*The nonenhanced contribution was based on guaiacyl propanol for the 1595 cm^{-1} band, eugenol (4-allyl-2-methoxyphenol, unconjugated $C_\beta=C_\gamma$ double bond) for the 1615 cm^{-1} band, and hydrocinnamaldehyde (3-phenyl-propionaldehyde, unconjugated $C_\gamma=O$ double bond) for the 1660 cm^{-1} band.

Table 8. Effect of Excitation Wavelength on the Intensity of Coniferaldehyde's 1595 cm^{-1}, 1615 cm^{-1}, and 1660 cm^{-1} Bands.

Raman Band (cm^{-1})	Relative Band Intensity I_{Band}/I_{1450} (MeOH) (Excitation Wavelength, nm) 514.5	1064
1595	5.46	1.76
1615	3.54	1.26
1660	1.48	0.592

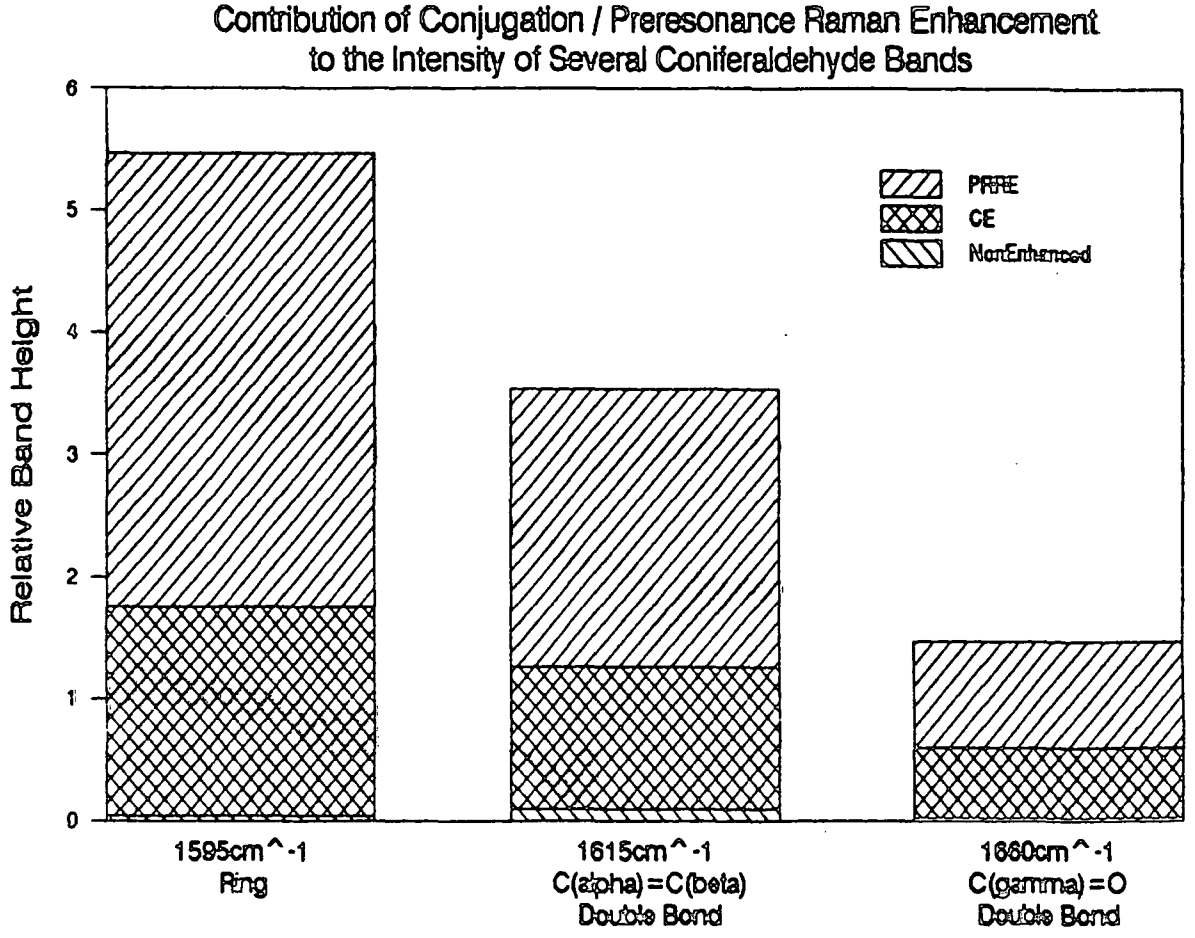

Figure 49. Contribution of conjugation and preresonance Raman enhancement to the intensity of several coniferaldehyde bands. Referenced to 514.5 nm excitation.

electrons, respectively, to the derived polarizability, and assumed that the intensity of the aromatic CH vibration essentially only depended on $\alpha(\sigma)$.

In summary, the model compound studies revealed the ≈1600 cm^{-1} aromatic ring breathing vibration was subject to both conjugation and preresonance Raman enhancement. For both effects, the enhancement factor and the contribution to the band intensity were found to depend on the conjugation, i.e., as the system became more conjugated, the extent of enhancement increased dramatically and the contribution to total band intensity increased for PRRE and decreased for CE. (Apparently PRRE increased faster than CE as the extent of conjugation became greater.) In the more conjugated system (coniferaldehyde) the dominant band-enhancing mechanism was PRRE.

In addition, these studies revealed that the contribution of CE and PRRE to the intensity of other bands involved in conjugation (e.g., coniferaldehyde's 1615 cm^{-1} - $C_\alpha=C_\beta$ and 1660 cm^{-1} - $C_\gamma=O$) was similar to that observed for the ≈1600 cm^{-1} band. This implied that these Raman bands showed the same dependence on absorption frequency (excitation wavelength).

Two of the most surprising aspects of these results were:

1. All of the conjugated double bond-containing monolignols were capable of absorbing 514.5 nm photons (PRRE) even though their wavelength of maximum absorption was substantially displaced from this excitation wavelength.

2. The magnitude of band enhancement in the most conjugated system (coniferaldehyde).

Woody Tissue

Black spruce and loblolly pine were used to assess the contribution of CE and PRRE to native-state lignin's 1595 cm^{-1} band intensity. The samples were run in the dry state using the high pressure oxygen macromode cell.

Table 9 shows the changes in intensity of the 1595 cm^{-1} band when the excitation wavelength was varied. All values have been corrected for instrument response. These data, along with their regression curves, have been plotted in Figure 50. (The regression equation used to fit these data was of the form $y=1/(A*(x+B)^2+C)$.)

Table 9. Effect of Excitation Wavelength on Lignin's 1595 cm^{-1} Band Intensity.

Excitation Wavelength (nm)	Relative 1595 cm^{-1} Band Intensity (I1595/I1098 + I1595/I2900)/2	
	Black Spruce	Loblolly Pine
457.9	4.45	4.41
488.0	2.70	3.30
514.5	2.50	2.98
647.1	1.77	1.88
1064.0	1.53	1.36

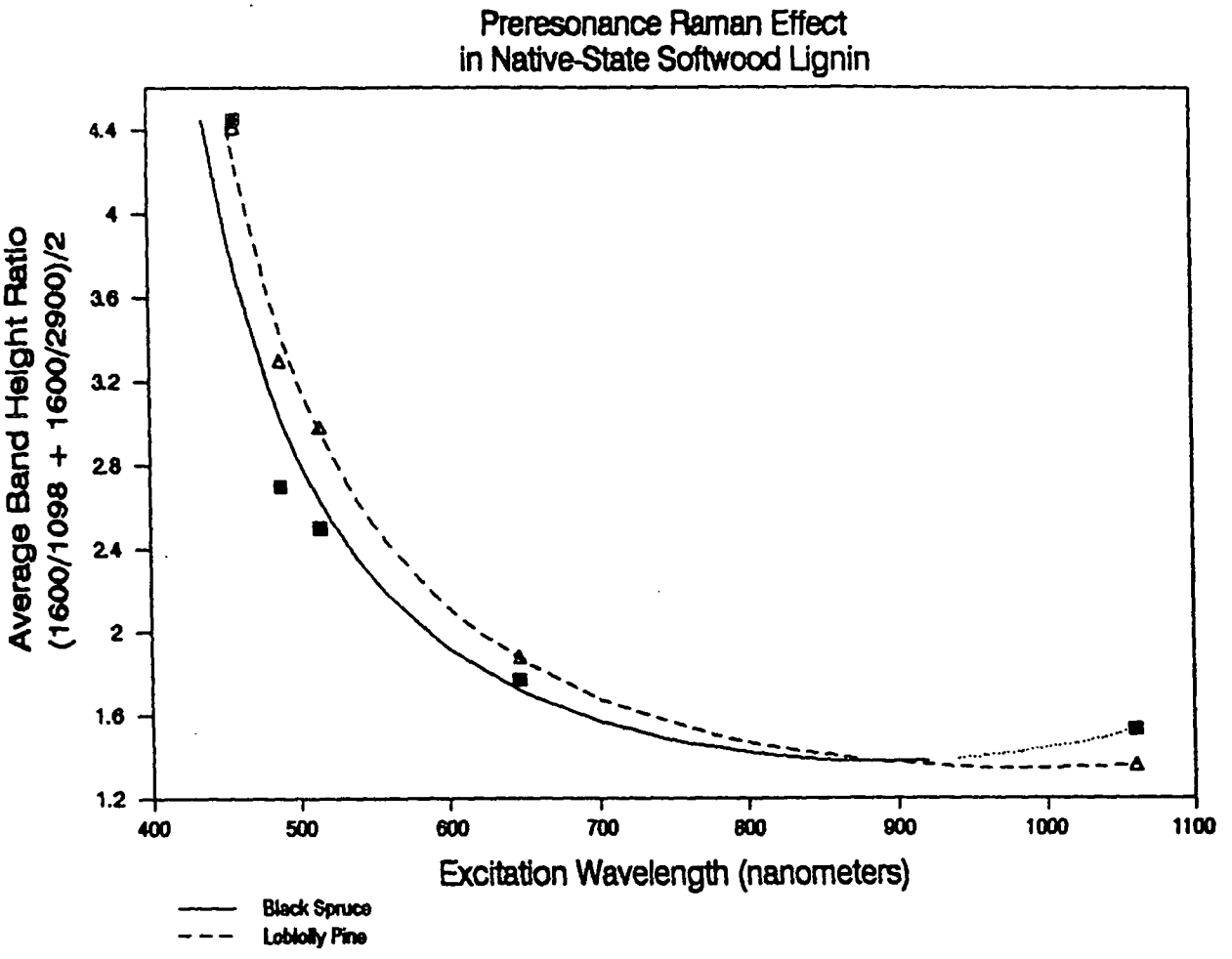

Figure 50. Preresonance Raman effect in native-state lignin.

The data reveal that the 1595 cm^{-1} band of lignin was subject to preresonance Raman enhancement. For PRRE to occur, structural units in the lignin macromolecule (chromophores) must be absorbing the incident radiation. (Evidence for this absorption can be seen in Figure 51 where black spruce's absorption spectrum is shown together with the PRRE behavior of lignin's 1595 cm^{-1} band.)

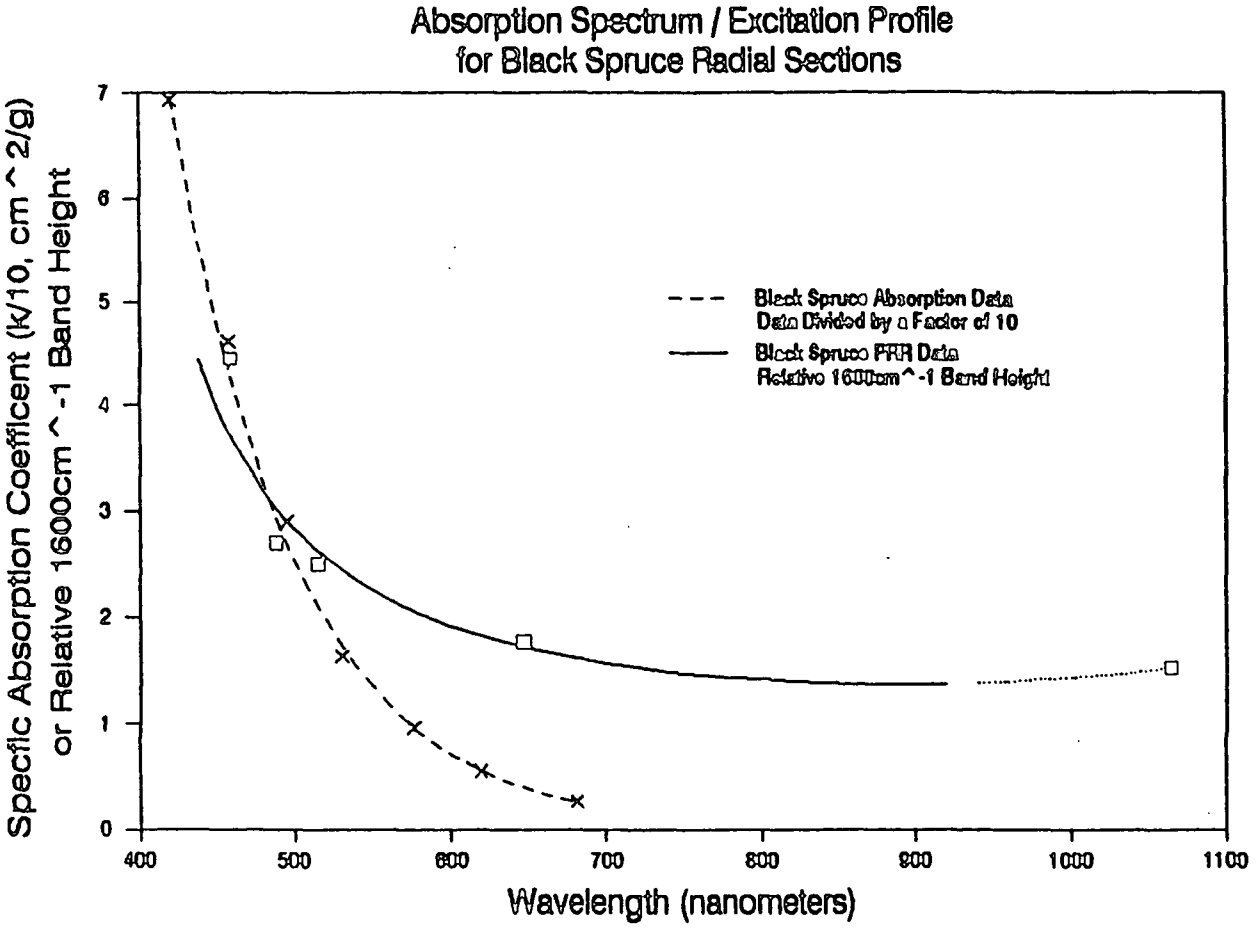

Figure 51. Absorption spectra and excitation profile for black spruce.

Units in lignin which have been shown to absorb (near-UV and) visible radiation include:

1. Coniferyl alcohol-type units, 6% of the C-9 units[154,245],
2. α-carbonyls, 6% of the C-9 units[154,245],
3. Coniferaldehyde-type units, 2-4% of the C-9 units[27-29],

4. Quinonemethide units, 3% of the C-9 units[37,38].

In addition, other quinonoid structures[38] and (phenoxy) radicals[42] which may be present in native wood are capable of absorbing these wavelengths. As was demonstrated in the previous model compound study, PRRE of the ≈1600 cm^{-1} band did occur with coniferyl alcohol, coniferaldehyde, and the α-carbonyl containing α,4-dihydroxy-3-methoxyacetophenone. (It should be noted that the same units which are responsible for PRRE would also contribute to CE.)

The regression curves for both wood species (Figure 50) are approximately parallel which indicates that even if differences in lignin makeup exist between the two species, the structural unit's (chromophore's) response to excitation wavelength is approximately the same.

In order to determine the contribution of CE to the 1595 cm^{-1} band intensity (514.5 nm excitation), the PRRE-free 1064 nm (1595/1098) values were analyzed. (The regression curves shown in Figure 50 indicate that PRRE does not significantly contribute to the relative 1595 cm^{-1} band intensity at excitation wavelengths greater than 900 nm.) Both conjugation enhancement and nonenhanced Raman scattering contribute to this intensity.

Raman spectra were collected from both guaiacyl propanol and cellobiose (0.1M solutions in 0.5M methanol/water) to assess the nonenhanced contribution to the relative 1595 cm^{-1} band intensity. (Guaiacyl propanol was used as the lignin model because its Raman bands did not show enhancement. Cellobiose was

chosen as the model for cellulose because it was readily available and dissolved completely.) The results of these experiments indicated that at equal concentrations, the intensity of lignin's 1595 cm^{-1} band should equal the intensity of cellulose's 1098 cm^{-1} band, i.e., the scattering coefficients are approximately the same. According to Isenberg[217] the concentration of cellulose is roughly 2 to 2.5X that of lignin in black spruce and loblolly pine wood. These data taken together indicate that, on the average, the nonenhanced (NE) relative 1595 cm^{-1} band intensity should be approximately 0.4. (Orientation effects on intensity are not considered in this analysis.) If this analysis is reasonably correct, then CE contributes significantly to (514.5 nm) 1595 cm^{-1} band intensity as Table 10 shows. (This is not surprising in light of the fact that the structural units in lignin which give rise to PRRE would also contribute to CE.)

From these studies, it is clear that both conjugation and preresonance Raman effects can contribute to enhancement of the 1595 cm^{-1} band of lignin in native woody tissue. Figure 52 summarizes these findings. The individual relative contributions to band intensity from each mechanism (referenced to 514.5 nm excitation) were: black spruce - 37% PRRE, 49% CE, 14% NE; loblolly pine - 56% PRRE, 33% CE, 11% NE. (These percentages were obtained from the data in Table 10 by dividing the relative intensity contribution for each mechanism by the 514.5 nm relative intensity (PRRE+CE+NE contributions) and multiplying by 100. These values are probably specific to the particular thin

section and could change depending on the location from which the section was taken.) The difference in the PRRE and CE contributions between the two species (and also within a single species - see footnote #3 from Table 10) may reflect structure differences in lignin such as the type of units and their number.

Table 10. Preresonance Raman and Conjugation Effects on the Relative 1595 cm^{-1} Band Intensity.

	Relative 1595 cm^{-1} Band Intensity I_{1595}/I_{1098}		
	(Excitation Wavelength, nm)		
Woody Species	514.5 (PRRE+CE+NE)[1]	1064 (CE+NE)[2]	(NE)
Black Spruce	2.80[3]	1.78	0.4
Loblolly Pine	3.78	1.64	0.4

(1) Contributions from preresonance Raman enhancement (PRRE) conjugation enhancement (CE), and nonenhanced scattering (NE).

(2) Data have been corrected for instrument response.

(3) This value which is the average intensity for three closely spaced regions on the woody section, was found to be location specific. A thin section from a different block of black spruce wood gave a value of 3.44. This may indicate that the average structure of lignin varies over relatively closely spaced regions in the tree.

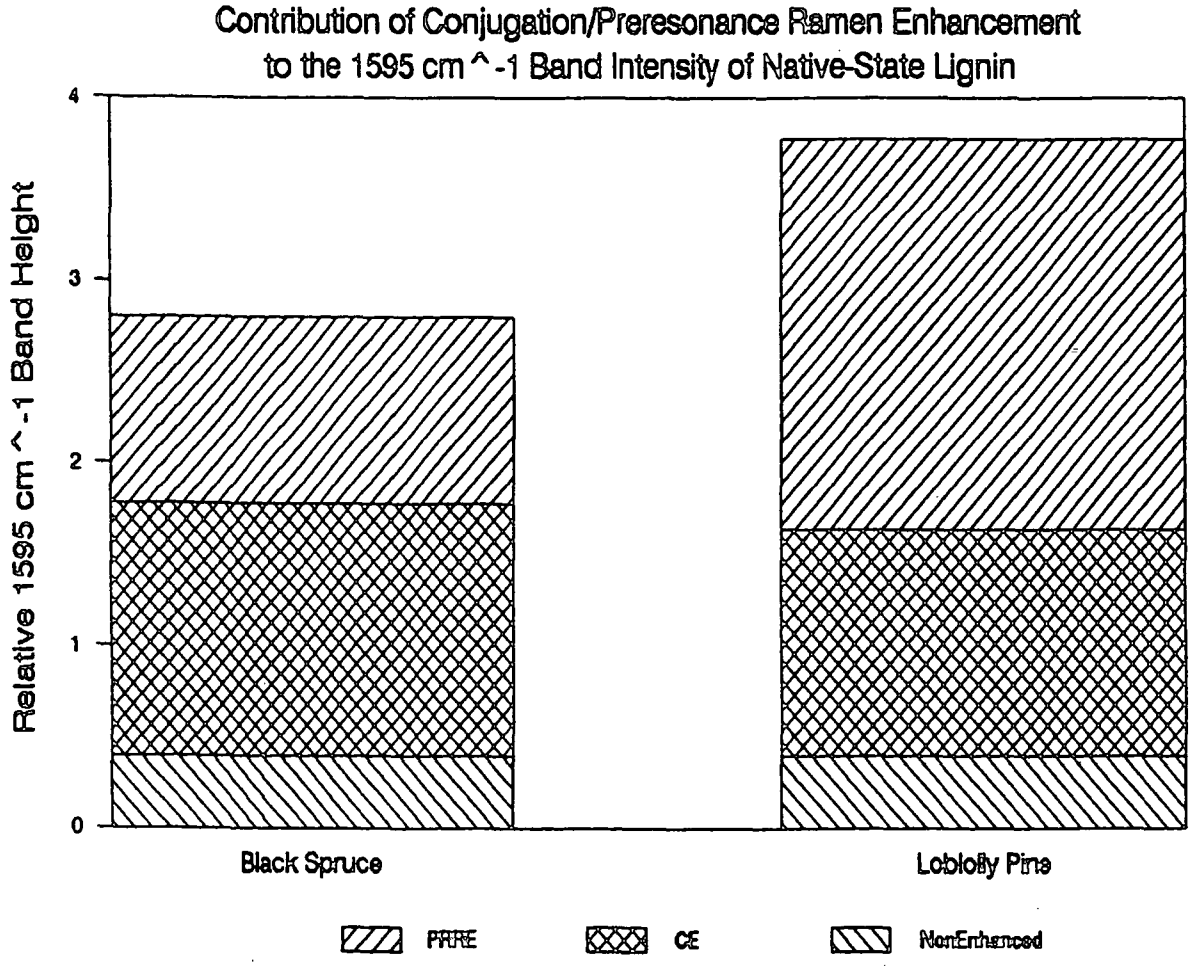

Figure 52. Contribution of conjugation/preresonance Raman enhancement to the 1595 cm^{-1} band intensity of native-state lignin. Referenced to 514.5 nm excitation.

This idea finds support in the model compound study. This study revealed that the more conjugated the system became, the greater the enhancement factor (CE and PRRE) and the larger the contribution of PRRE to total band intensity. These results suggest that loblolly pine with its greater

1595 cm^{-1} band intensity (both black spruce and loblolly pine have similar lignin concentrations) and larger PRRE contribution may have a higher degree of conjugation in its lignin macromolecule. For example, this would be possible if loblolly pine lignin contained more coniferaldehyde type units than did black spruce lignin. (It could be argued that the difference in the relative 1595 cm^{-1} band intensity between the two species is not so much due to species differences in lignin makeup but is simply a manifestation of spot-to-spot variation within a species. This may be partly the cause of the difference but, I believe, the suggestion of species differences in lignin makeup is valid for the following reason: Even though the relative 1595 cm^{-1} band intensity of black spruce lignin was found to be section specific, the largest value encountered for black spruce [3.44] did not exceed the relative 1595 cm^{-1} band intensity values for loblolly pine lignin [values ranged from 3.65 to 3.92] and, in the majority of cases, the relative intensities were much less than 3.44.)

Photostabilization Of Lignin

Prior to mapping the organization and compositional variability of lignin in plant cell walls using micro-Raman spectroscopy, it became necessary to stabilize the macromolecule to laser radiation. This section reports on the results of experiments to determine the causes of the photo-induced changes that occurred in the lignin macromolecule during laser irradiation and attempts to achieve photostabilization.

Possible Causes Of Photodegradation

It is generally accepted that the principal reactions in the light-induced degradation of wood are photooxidative in nature.[35,44-46] The initial steps in the photooxidation degradation involve the absorption of the incident photons by chromophoric groups (in the lignin macromolecule) followed by free radical formation.[48]

Chromophoric Groups

The potential chromophores/chromophoric groups include transition metal complexes (with lignin ?), α-carbonyls, conjugated double bonds (both coniferyl alcohol- and coniferaldehyde-type structures), quinonoid structures (quinone- and quinonemethide-type structures), and phenolic hydroxyls.[43]

Charge-Transfer Complexes

Charge-transfer complexes (CTC) are molecular complexes formed by the weak interaction of electron donors and electron acceptors. In general, the absorption spectrum of a CTC retains the individual absorption bands of its donor and acceptor components, but an additional band(s) due to the complex as a whole is observed. The general shape of these bands is asymmetric, being broader on the high frequency side.[249]

An additional chromophoric system which may contribute to visible light absorption was discovered during the PRRE/UV-Visible absorption studies. What

appeared to be a charge-transfer band was observed in the absorption spectrum of an approximately equimolar mixture of cellobiose and coniferyl alcohol in methanol/water (Figure 53). The band centered at 520 nm was not seen in either one of the individual absorption spectra.

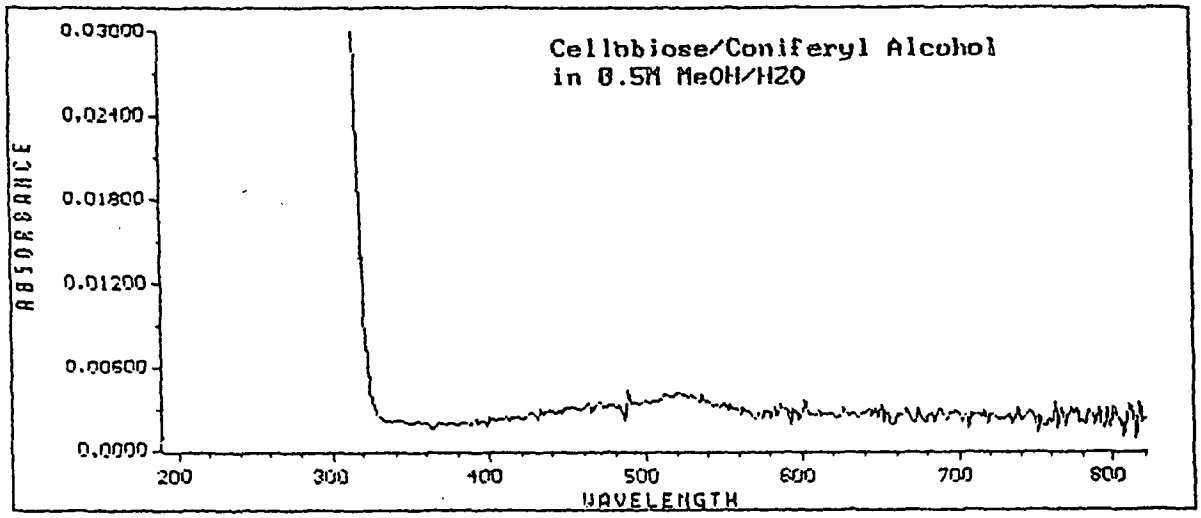

Figure 53. UV-Visible absorption spectrum of a mixture of cellobiose and coniferyl alcohol in 0.5M methanol/water. (Compare to the absorption spectrum of coniferyl alcohol shown in Figure 47.)

The occurrence of this new band, together with its general charge-transfer like shape, suggests that this feature may be due to a charge-transfer interaction between cellobiose (σ-orbital type or n [lone electron pair] type donor ?) and coniferyl alcohol (π-orbital type acceptor ?). (It is known that some type of interaction occurs because the normally water-insoluble coniferyl alcohol dissolves in a cellobiose/water solution.)

The intensity of the 520 nm band is very low (approximately 0.002 AU). Using the Bouguer/Lambert-Beer Law[11,12] gave a molar absorptivity of 20 l/mol·cm. It thus appears that the magnitude of any charge-transfer interaction between these species is small.

Raman experiments were conducted to ascertain if cellobiose altered coniferyl alcohol's 1610 cm^{-1} band intensity. As can be seen from Table 11, the relative 1610 cm^{-1} band intensity was significantly affected in the presence of cellobiose. The band intensity increased by 56% and 39% using 514.5 nm and 647.1 nm excitation wavelengths, respectively.

Table 11. Effect of Cellobiose on Coniferyl Alcohol's 1610 cm^{-1} Relative Band Intensity.

	Relative 1610 cm^{-1} Intensity(2) I_{1610} (coniferyl alcohol)/I_{1450} (MeOH)	
	(Excitation Wavelength)	
Chemical Species(1)	514.5	647.1
D-Cellobiose (CB)	-	-
Coniferyl Alcohol (CA)	4.1	3.45
CB + CA	6.4	4.8

(1) 0.1M D-cellobiose in 0.5M MeOH/water,
0.1M coniferyl alcohol in 0.5M MeOH/water,
0.05M D-cellobiose + 0.05M coniferyl alcohol in 0.5M MeOH/water.

(2) Data have been corrected for instrument response and concentration differences.

The data show that enhancement of coniferyl alcohol's 1610 cm^{-1} band occurred in the presence of cellobiose and that the magnitude of the enhancement was wavelength dependent. This latter point, which is indicative of PRRE, points to the formation of a species capable of absorbing incident radiation, i.e., a chromophore. This chromophore could be responsible for the 520 nm band seen in the UV-Visible absorption spectrum of cellobiose/coniferyl alcohol and conceivably could be a CTC between these chemical species.

Whether these results are directly applicable to native wood is not known. Cellulose and lignin may not behave in the manner observed in this model system. (It is also conceivable that a charge-transfer interaction could develop between hemicelluloses and lignin. This possibility was not investigated.)

The Role Of Free Radicals

Free radicals are important intermediates in the photooxidative degradation reactions of wood (lignin).[33,43,54-58] After the absorption of light by chromophores present in wood, electronically excited molecules are generated. These excited molecules (lignin units) subsequently lead to the formation of various free radicals by dissociation or by reaction with other molecules. These free radicals could include lignin polymer alkyl (P·, e.g., benzyl alcohol type), lignin polymer alkylperoxy (POO·), and lignin polymer alkyloxy (PO·, e.g., phenoxy type) radicals as well as low molecular weight radicals such as R·, ROO·, RO·, HO·, etc.

Electron Spin Resonance Study

Experiments were undertaken to assess the population of free radicals in black spruce thin sections prior to laser exposure. Hon found no evidence for intrinsic free radicals in wood and suggested that the customary observed "intrinsic" free radicals may well be an artifact created during mechanical preparations and/or created by exposure to (fluorescent) light.[41] It has also been reported that phenoxy radicals are present in lignin preparations and absorb in the 500-600 nm region of the electromagnetic spectrum.[42] If free radicals are present prior to laser irradiation, they could contribute to the absorption of 514.5 nm photons. This, in turn, would generate additional free radicals, which could absorb 514.5 nm photons, etc. (Generally, free radicals are very reactive and are encountered only as intermediates in chemical reactions. Lignin-based radicals [phenoxy] are exceptionally stable because they can form resonance structures with the aromatic ring.[48])

Electron spin resonance (ESR; also known as electron paramagnetic resonance, EPR) is a very powerful and sensitive method for detecting and quantifying free radicals. For the reader interested in learning about the theory and practice of this technique, see references 250-254.

ESR spectra are characterized by four parameters: g-value, hyperfine splittings, line widths, and intensity. Only two of these, g-value and intensity, are important to this study. The g-value is the absolute magnetic field

position of the line of an ESR spectrum and has some value in characterizing the type of radical being observed. The intensity of the spectral signal (integrated area) is directly proportional to the number of free radicals in the sample.

This study was undertaken to look at the effect of mechanical action, gaseous atmosphere, and fluorescent light on radical generation in air-dried black spruce wood and was carried out at the University of Wisconsin-Milwaukee's Biomedical Research Center using their Varian E109 spectrometer. The results are shown in Figure 54. In this figure, the code at the bottom is (A,B/C,D), where the letters refer to:

A. Extent of mechanical action during sample preparation - large (lg) or fine matchstick. (The fine matchstick received a greater degree of mechanical [cutting] action than did the large matchstick.)

B. Sectioned in darkness (dk) or light (lt).

C. Sectioned and stored in air or nitrogen (N2).

D. Exposed to light (lt) or kept in darkness (dk) after sectioning.

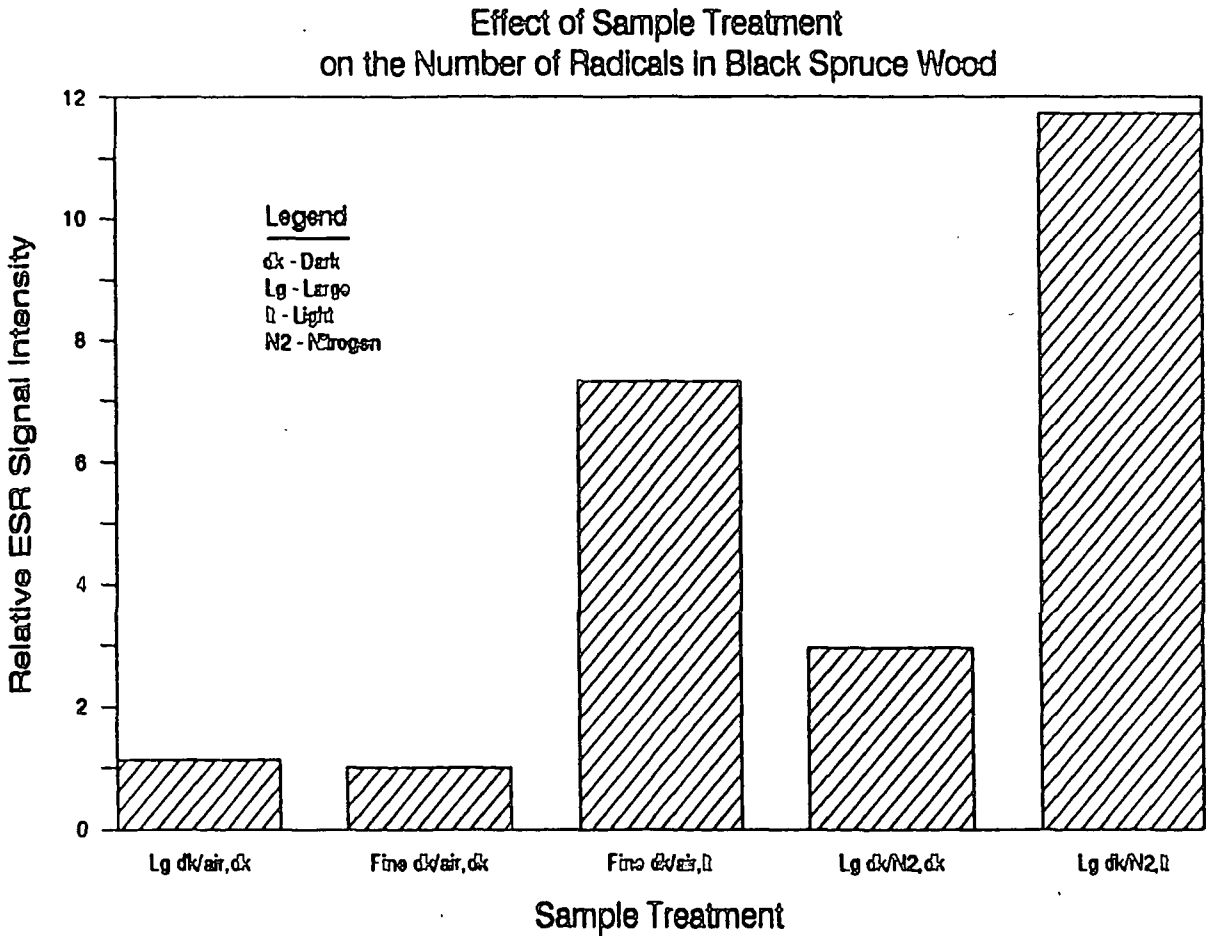

Figure 54. Effect of sample treatment on the number of radicals in black spruce wood.

The major conclusions drawn from this study were:

1. Free radicals are produced as a result of mild mechanical action (Lg dk/N_2,dk), but their number was not sensitive to the different degrees of mechanical treatment used in this study (Lg dk/air,dk vs. Fine dk/air,dk).

2. Black spruce wood readily interacts with fluorescent light to produce radicals. Irradiation with fluorescent lights (40 hours) resulted in a 7-fold (air) and 4-fold (N_2) increase in the number of radicals, (Fine dk/air,dk vs. Fine dk/air,lt; Lg dk/N_2,dk vs. Lg dk/N_2,lt).
3. Oxygen (air) did not appear to be essential for radical formation (Lg dk/N_2,dk or Lg dk/N_2,lt); but
4. Oxygen (air) can participate and appears to act as a radical quencher (Lg dk/air,dk vs. Lg dk/N_2,dk or Lg dk/N_2,dk vs. Lg dk/N_2,lt).
5. The g-values which did not differ significantly (They ranged from 2.0021 to 2.0023.) and the Gaussian line shapes of the ESR curves suggest that a number of closely related (phenoxy-type) radicals were being produced during these treatments.

These findings are similar to what other researchers have observed using loblolly pine[41] and yellow poplar.[53]

The implication of these results is that free radicals (produced during sample preparation) may be present in the woody sections prior to laser irradiation and may therefore participate in the laser light-induced photooxidative degradation reactions of lignin. (See the next section for a continuation of this discussion.)

The Role Of Water

Immersion of the sample in water has traditionally been used in our

laboratory both to minimize thermal degradation and to reduce the level of background fluorescence in the Raman spectra of wood.[214] When using this technique, the intensity of certain lignin bands decayed with time. In contrast, these same bands did not show decay when the sample was dry. (This stability was observed regardless of the gaseous environment surrounding the sample. It has been seen with nitrogen, air, and fluorescence-reducing oxygen.) These observations strongly suggest that water is involved in the decay process. It may be an active participant by entering into the degradation reactions or its role may be more passive, e.g., it may swell the fiber and/or provide a medium for diffusion of the lignin fragments.

Hon and Feist[255] have observed that the concentration of photo-induced free radicals in wood was a function of moisture content. When the moisture content in wood increased from zero to 6.3%$_{OD}$, an enhancement of free radical formation was observed, but beyond this stage, the rate of radical decay increased. They speculated that water facilitated light penetration into the accessible regions of the cell wall and served to "swell up the nonaccessible regions." They reasoned that by opening up these less accessible regions of the wall (for light penetration), new surfaces were provided where free radicals could be generated. Beyond a moisture content of 6.3%, an excess amount of water was thought to exist. The authors suggested that the excess water could then have served as a radical acceptor to trap free radicals thereby reducing the ESR intensity, i.e., the rate of generation was exceeded by the

rate of trapping. They hypothesized that the trapping reaction could involve the establishment of an equilibrium between water molecules and phenoxy radicals to form phenoxy radical-water complexes. (Whether their results can be extended to water-immersed fibers is unknown. If these findings are applicable, the presence of radicals in the immersed woody thin section prior to laser exposure is in doubt and thus their contribution to the initial absorption of 514.5 nm photons is unknown.)

The above study suggests that water may act as a radical scavenger as well as assume a more passive role. It has also been speculated that water is able to quench excited states by intermolecular collisions or long-range dipole-dipole resonance interactions.[256] Both radical scavenging and excited state quenching are photostabilizing mechanisms and therefore would be expected to protect the wood (lignin) against photooxidative degradation, not foster it. It is conceivable that hydroxy and hydroperoxy radicals, as well as hydrogen peroxide are formed during irradiation via secondary reactions and it is these species which contribute to the decay.

Water's specific function(s) in the decay process remain unknown. All that can be said with certainty is that water must be present for the decay reactions to occur.

Photostabilization Studies

Photostabilization involves the retardation or elimination of unfavorable

light-induced degradative pathways. Chemical modification of the reactive centers or the addition of compounds capable of deactivating the photoexcited species and/or preventing radical formation are two approaches commonly used. Figure 55 summarizes the various photostabilization methods used to protect wood against photodegradation.

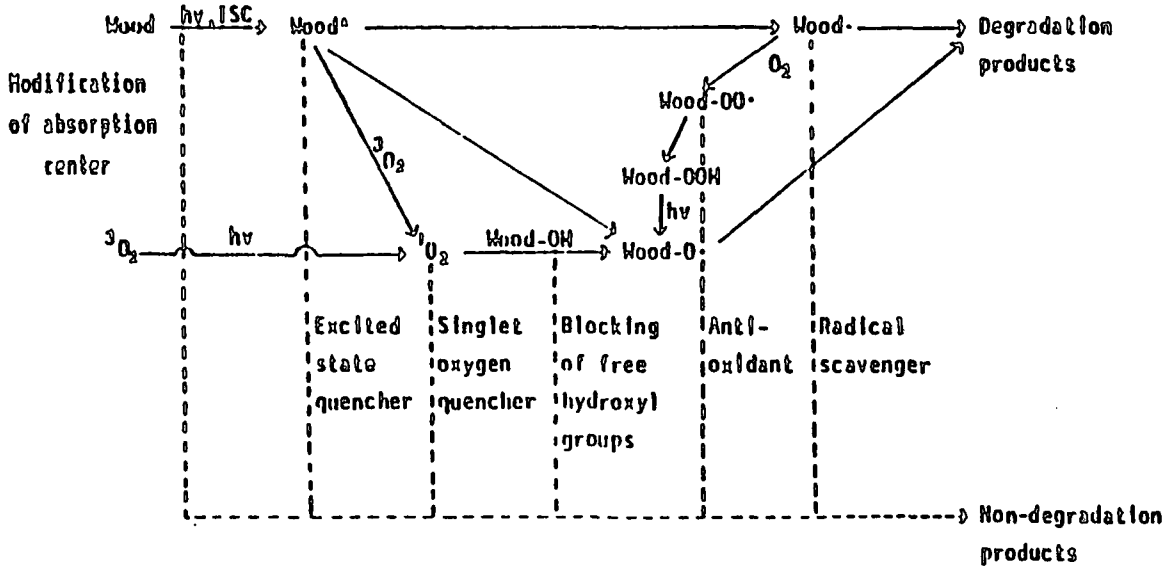

Figure 55. Schematic representation of degradation in wood and methods used to retard or eliminate the unfavorable pathways.[47] (ISC: intersystem crossing).

In the following two sections, Model Compound Study and Woody Tissue, the results of experiments designed to photostabilize lignin to laser radiation will be presented. The techniques used and degradation pathways blocked are shown in Table 12. (The specifics for each treatment are given in Appendix 4.)

Table 12. Photostabilization Treatments.

Treatment	Purpose
DTPA	Modification of absorption center - transition metal complexes
Acid-Chlorite	Modification of absorption center - probably $C_\alpha=C_\beta$ and ring conjugated carbonyls
Sodium Borohydride	Modification of absorption center - ring conjugated carbonyls and quinonoid structures
Trimethylphosphite	Modification of absorption center - quinonoid structures
Methylation	Blocking of free phenolic hydroxyl groups
Copper II Chloride	Excited state quencher/(radical scavenger ?)
Potassium Iodide	Excited state quencher/radical scavenger
Oxygen	Excited state quencher
Glycerol	Nonaqueous immersion medium - eliminate water's contribution to the decay process

Model Compound Study

Lignin model compound studies were undertaken to clarify the changes observed in the Raman spectra when chemically modifying woody tissue in an attempt to achieve photostabilization.

1600 cm^{-1} Region Band Assignments

The first part of this study was directed towards clarifying the 1600 cm^{-1} region band assignments for native lignin. Previous work in our laboratory

has shown that the 1595 cm^{-1}, 1620 cm^{-1} (shoulder), and 1654 cm^{-1} bands in the Raman spectra of woody tissue are due to lignin.[222] The 1595 cm^{-1} band has been ascribed to aromatic ring breathing modes.[221] The 1620 cm^{-1} band is thought to be due to $C_\alpha=C_\beta$ stretching vibrations while the 1654 cm^{-1} band may have contributions from both $C_\alpha=C_\beta$ and conjugated C=O stretching vibrations.

Raman spectra were obtained from model compounds I-IV using 514 nm excitation to help clarify the 1620 cm^{-1} and 1654 cm^{-1} band assignments. Table 13 summarizes the results. The pair of bands centered on 1600 cm^{-1} are due to symmetric (larger wavenumber band) and asymmetric planar ring vibrations of the aromatic ring.[257] The effect of conjugation on the position of the $C_\alpha=C_\beta$ band can be seen in the table. This band was shifted to a lower frequency as the degree of conjugation increased; band position shifted from 1655 cm^{-1} (0.1M coniferyl alcohol) to 1615 cm^{-1} (0.1M coniferaldehyde). (Part of this shifting is the result of increased conjugation and part is caused by vibrational coupling.)

The results of this study support the assignment of lignin's 1620 cm^{-1} band to $C_\alpha=C_\beta$ stretching vibrations. The cause of the 1654 cm^{-1} band is not as clear. Native lignin contains approximately 6% coniferyl alcohol-type structures, 6% α-carbonyl containing units and from 2-4% coniferaldehyde-type units.[27-29,154,245] The presence of these structures in lignin suggest that $C_\alpha=C_\beta$ and $C_\gamma=O$ contribute to the 1654 cm^{-1} band. Furthermore, it is conceivable that the $C_\alpha=O$ band in native lignin is conjugation shifted to the

1660 cm^{-1} region.

Table 13. Lignin's 1600 cm^{-1} Region Band Assignments.(1)

	Band Positions (cm^{-1})			
Model Compound	Aromatic Ring Stretching	$C_\alpha=C_\beta$ Stretching	$C_\alpha=O$ Stretching	$C_\gamma=O$ Stretching
α,4-Dihydroxy-3-Methoxyacetophenone	1590/1600(2) 1590	--	1680 1670	--
Coniferaldehyde	1590/1605 1595	1625 1615	--	1660 1660
Coniferyl Alcohol	1605 1610	1660 1655	--	--
Guaiacyl Propanol	1600/1610(sh)(3) 1610	--	--	--

(1) The spectra can be found in Appendix 5.

(2) Upper values - pure compounds, lower - 0.1M in methanol.

(3) sh - shoulder.

Chemical Modification

The next part of the model compound study was directed towards understanding the spectral changes that occurred when lignin's structure was chemically modified with acid-chlorite and sodium borohydride.

Acid-Chlorite Treatment

Acid-chlorite chemistry is complex because of the multitude of species

involved. In an acid-chlorite solution, a mobile equilibrium exists between chlorine dioxide, chlorous acid, hypochlorous acid and elemental chlorine. All of these species are capable of entering into reactions with lignin.[259]

Results from phenolic lignin model compound studies suggest at least two separate reaction paths are involved in the chlorine dioxide/acidified chlorite oxidation of these monolignols.[260-265] One reaction path leads to formation of muconic acid derivatives from a ring-opening reaction and the second path yields substituted para-quinones. Lindgren[265] has proposed the following general mechanism for the formation of these reaction products (Figure 56).

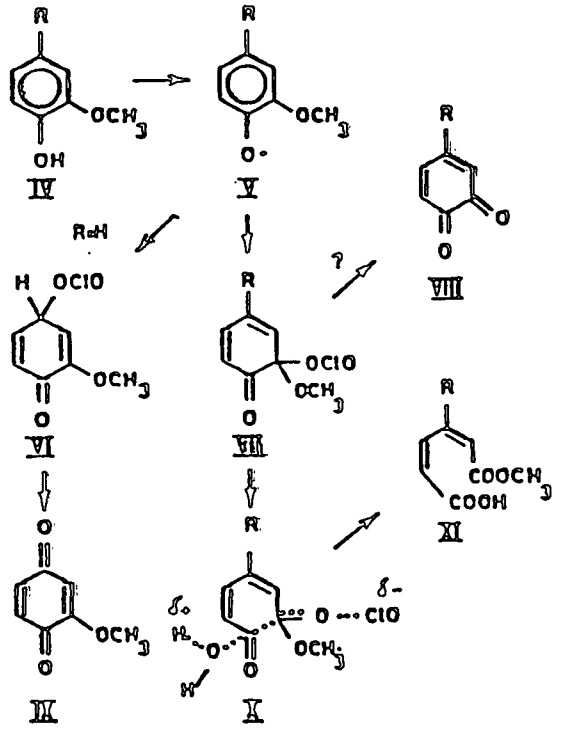

Figure 56. Chlorine dioxide oxidation of guaiacyl derivatives.[266]

It has been reported that the oxidation of monolignols containing conjugated double bonds exhibited a different pattern.[266,267] In this case the preferential site of initial attack was the double bond rather than the free phenolic hydroxyl.

Raman spectra were collected from guaiacyl propanol, α,4-dihydroxy-3-methoxyacetophenone, coniferyl alcohol, and coniferaldehyde treated with acid-chlorite (10% molar excess ClO_2^-). Upon the addition of the monolignol to the acid-chlorite solution, an intense color developed for both α-4-dihydroxy-3-methoxyacetophenone and coniferaldehyde. It ranged from amber (α-4-dihydroxy-3-methoxyacetophenone) to deep amber (coniferaldehyde). In spite of this apparent reaction, these monolignols were not completely solubilized after 6 hours. (The undissolved material was removed prior to acquiring the Raman spectra. Raman analysis of this material showed it to be the unreacted monolignol.) Guaiacyl propanol and coniferyl alcohol, in contrast to this, did not show a color change but did dissolve completely in the acid-chlorite solution within this time period. (It is felt that the initial solubility of a particular monolignol in the acid-chlorite solution was determined more by solvent [water] interactions rather than ClO_2^- chemical reactions.) Water's 3400 cm^{-1} OH stretching band was used for normalization. (The assumption was made that the OH stretch from water was the principal contribution to this band and the "concentration" of water was the same for the monolignol/acid-chlorite solutions.) The results are shown in Table 14 and the spectra can be

found in Appendix 6.

Table 14. Effect of Acid-Chlorite (AC) Treatment on the 1600 cm^{-1} Region Monolignol Bands.

Model Compound[1]	Band Position (cm^{-1}) AC	Control[2]	≈1600[3] / 3400	1655[3] / 1610
α,4-Dihydroxy-3-Methoxyacetophenone	1575[4] 1640 1720(?)	1590 1670	--	n/a[5]
Coniferaldehyde	1570(6) 1600(sh) 1625(w) 1660(vw)	1595 1615 1660	--	n/a
Coniferyl Alcohol	1590 1660	1610 1655	0.34(0.26)	0.32(0.14)
Guaiacyl Propanol	1610	1610	0.056(0.053)	n/a

(1) 0.075M monolignol, 0.083M $NaClO_2$.

(2) 0.1M in methanol.

(3) Values in parentheses are the ratio after sample was stored under nitrogen at 4°C for 16 days (coniferyl alcohol), 26 days (guaiacyl propanol).

(4) Bands obscured by fluorescence background.

(5) Not applicable.

(6) sh-shoulder, s-strong, w-weak, vw-very weak.

The interpretation of these results, made somewhat difficult by the complex chemistry occurring in an acid-chlorite system, is as follows:

1. α,4-dihydroxy-3-methoxyacetophenone - The immediate color change that occurred upon introducing the monolignol into the acid-chlorite solution points to a fairly rapid chemical reaction and the formation of colored degradation products. (The absence of both 1590 cm^{-1} [ring] and 1670 cm^{-1} (C_{α}=O) Raman bands supports this.) It is likely that the degradation products included quinone- and muconic acid(?)-type structures as evidenced by the Raman bands. Quinones have strong Raman bands at 1565-1585 cm^{-1} and 1660-1675 cm^{-1}.[268] (It is believed that these bands are due to C=C and C=O stretching vibrations, respectively. The ≈1575 cm^{-1} band is stronger with o-quinonoid structures while the ≈1665 cm^{-1} band is more intense with p-quinonoid structures.[268]) The presence of the 1575 cm^{-1} band suggests the formation of o-quinone type structures. The 1640 cm^{-1} and 1720 cm^{-1} bands could be due to the C=O stretch in -COOH, and $-COOCH_3$ groups, respectively[257], but it is difficult to say with certainty. Referring to Figure 56, it may be that the reaction pathway leading to o-quinonoid formation is favored over the other pathways and the limited amount of reagent prevented the formation of the other end products (?).

The interpretation was hindered by the very high level of background fluorescence. The Raman bands were little more than "bumps" on the fluorescence curve. The origin of this fluorescence is unknown, but it must be related to the specific degradation products.

2. Coniferaldehyde - As was the case for α,4-dihydroxy-3-methoxyacetophenone, the acid-chlorite solution became colored upon the addition of coniferaldehyde. This again is indicative of a fairly rapid chemical reaction and formation of colored products. The very strong feature at 1570 cm^{-1}, together with the deep amber color of the solution point to quinonoid degradation products, probably o-quinone type species.

   The fluorescence background was very high and obscured much of the details. Besides the (enhanced ?) 1570 cm^{-1}, the only other features in the 1600 cm^{-1} region were very weak bands at 1600 cm^{-1}, 1625 cm^{-1} and 1660 cm^{-1}. These bands are most likely due to unreacted monolignol (the reagent was limiting).

3. Coniferyl alcohol - Coniferyl alcohol appeared to react substantially slower than either of the carbonyl-containing monolignols. The aromatic ring breathing (shifted to ≈1590 cm^{-1}) and $C_\alpha=C_\beta$ (≈1655 cm^{-1}) stretching bands, while affected, were readily apparent after treatment. Both of these bands declined in intensity. Using the 0.1M in methanol data (10.3X Raman conjugation and preresonance enhancement of the 1610 cm^{-1} band relative to guaiacyl propanol, 1655 cm^{-1} band ≈2.3X 1610 cm^{-1} band intensity) and assuming the aromatic ring was not affected (see guaiacyl propanol no. 4, below), the 1590 cm^{-1} and 1660 cm^{-1} bands declined 45% and 77%, respectively, after 6 hours and 58% and 90% after 16 days. The 1660 cm^{-1} band behavior points to the disruption of the conjugated

ethylenic bond. It is believed that the decline of the 1590 cm^{-1} band is primarily due to the loss of CE/PRRE brought about by an attack on the C_α=C_β bond rather than modification of the aromatic ring. (The spectra do not show any evidence of either quinone- or muconic acid-type structures - see next paragraph.)

The lack of color change and absence of bands in the 1570 cm^{-1} and 1670 cm^{-1} regions suggest that quinones were not formed (under these reaction conditions). It seems likely that the limited reagent precluded the further reaction of the modified coniferyl alcohol. Apparently the chemistry favored the attack on the conjugated ethylenic bonds over further reactions with the modified coniferyl alcohol to form quinone- and/or muconic acid-type structures.

4. Guaiacyl propanol - It is unlikely that a reaction occurred between guaiacyl propanol and acid-chlorite (under these particular reaction conditions). Guaiacyl propanol's 1610 cm^{-1} aromatic ring breathing band was the only feature (other than water's 1630 cm^{-1} H-O-H bending band) to occur in the 1600 cm^{-1} spectral region. Had degradative reactions taken place, it is likely that strong features would have been seen in the 1570 cm^{-1} and/or 1670 cm^{-1} regions. Even after 26 days (under nitrogen at 4°C) the relative band height decreased by only 5% and it is unknown if this decrease was real or simply due to experimental error.

In summary, conjugated carbonyl-containing structures (α,4-dihydroxy-3-methoxyacetophenone and coniferaldehyde) were particularly sensitive to acidified chlorite oxidation. The color change as well as the appearance of the ≈1570 cm^{-1} Raman band strongly suggested the formation of o-quinone type reaction products. The reason for this sensitivity may be related to oxygen's lone pair of electrons (C=O:) which could interact with acid-chlorite species. In contrast to this, coniferyl alcohol with its conjugated ethylenic bond did not react as quickly (or as completely) with acid-chlorite. The coniferyl alcohol data suggested that an attack on $C_\alpha=C_\beta$ was favored over further reactions with the ring to form colored degradation products. Apparently this selective attack only takes place when there are no additional ring conjugated groups. If these groups are present ($C_\gamma=O$ - coniferaldehyde), then further reactions (ring) leading to the formation of quinones occur. Guaiacyl propanol did not appear to react with acid-chlorite under the experimental conditions suggesting that ring conjugated groups are necessary to initiate a reaction.

Sodium Borohydride Treatment

Sodium borohydride is an effective reducing reagent. The types of structures reduced depend on the solvent. In hydroxylic solvents, aldehyde and ketone groups are rapidly reduced at 25°C.[8]

Raman spectra were collected from model compounds I-IV treated with 50%

excess $NaBH_4$ (molar basis) using 514.5 nm excitation. All of the models were soluble in the $NaBH_4$ solution. Water's 3400 cm^{-1} OH stretching band was used for normalization. The results are shown in Table 15. The spectra are located in Appendix 7.

Table 15. Effect of Sodium Borohydride Treatment on the 1600cm^{-1} Region Monolignol Bands.

Model Compound(1)	Band Position (cm^{-1}) BH	Control(2)	≈1600/3400	Enhancement(3) Factor
α,4-Dihydroxy-3-Methoxyacetophenone	1595	1590 1670	0.0789	1.05
Coniferaldehyde	1580/1595(sh) 1640	1595 1615 1660	0.714	9.5
Coniferyl Alcohol	1580/1590(sh) 1640	1610 1655	0.896	11.9
Guaiacyl Propanol	1590/1600	1610	0.0753	1.0

(1) 0.167M monolignol, 0.250M $NaBH_4$.

(2) 0.1M in methanol.

(3) Relative to guaiacyl propanol.

The interpretation of these results is as follows:

1. α,4-dihydroxy-3-methoxyacetophenone - The absence of the 1670 cm^{-1} band is indicative of the reduction of the α-carbonyl group. As is demonstrated by the last column in Table 15, the loss of this group reduced

the extent of conjugation which impacted the enhancement (both CE and PRRE) of the 1595 cm^{-1} band. This value is essentially equal to that of guaiacyl propanol which does not contain any conjugated substituents.

2. Coniferaldehyde - After treatment with $NaBH_4$, the model acquired a coniferyl alcohol-type structure with the reduction of its γ-carbonyl group (loss of 1660 cm^{-1} band). As a result of the decrease in conjugation brought about by the loss of this group, the C_α=C_β 1615 cm^{-1} band was shifted to a higher frequency (1640 cm^{-1} - same position as C_α=C_β band in $NaBH_4$ treated coniferyl alcohol) and the ≈1590 cm^{-1} band enhancement (CE and PRRE) was decreased to the approximate level seen in treated coniferyl alcohol. (Previously it was shown that because of its extended conjugated system [both ethylenic and carbonyl bonds can enter into conjugation with the aromatic ring], coniferaldehyde's 1595 cm^{-1} relative band intensity was approximately an order of magnitude larger than that of the coniferyl alcohol.)

3. Coniferyl alcohol - Treatment of the monolignol with $NaBH_4$ had little effect on its structure. The ≈1585 cm^{-1} band enhancement (CE and PRRE) is approximately equal to that seen with the 0.1M in methanol control (11.9 vs. 10.3). It is believed that the C_α=C_β 1655 cm^{-1} band was shifted to a lower frequency (1640 cm^{-1}) primarily because of solvent effects. (The aromatic bands were shifted an equivalent amount which supports this supposition.) The nature of this solvent interaction is not known, but

solvent effects such as this are reported in the literature.[258] (There is some evidence that minor changes occurred; the $C_{\alpha}=C_{\beta}$/ring ratio changed slightly from that seen in the control spectrum [1.5 vs. 2.3]. Whether this is also due to solvent effects is not known.)

4. Guaiacyl propanol - Guaiacyl propanol did not appear to be affected by treatment with $NaBH_4$.

To summarize, sodium borohydride treatment reduced ring conjugated carbonyls (α - 1670 cm^{-1} and γ - 1660 cm^{-1}) but did not disrupt the aromatic ring ($\approx$1600 cm^{-1}) or ring conjugated ethylenic ($C_{\alpha}=C_{\beta}$ - 1615/1655 cm^{-1}) bands.

Woody Tissue

This section will present the results of experiments directed towards stabilizing lignin to 514.5 nm radiation. Black spruce 30-micron radial sections were chiefly used to assess the effect of the photostabilization treatments. In these studies the incident electric vector was parallel to the long axis of the cell wall and cellulose's 1098 cm^{-1} band was used as an internal standard. (Previously it was shown that this band was stable to 514.5 nm laser radiation and the effect of mild acid-chlorite oxidation/sodium borohydride reduction on cellulose has been reported to be minor.[8,267]) The behavior of lignin's 1595 cm^{-1} band towards laser radiation was monitored using the sequential data acquisition capability of the Raman microprobe. A 100X objective was used and all samples were immersed in water unless otherwise noted.

Excitation Wavelength

The effect of excitation wavelength on the decay of lignin's 1595 cm^{-1} band is shown in Figure 57. As can be seen, using 647.1 nm excitation did not stop the decay although the magnitude of the disruption appeared to be less. The 514.5 nm data points lie below the 647.1 nm data points even though the PRRE contribution would be expected to be greater when using 514.5 nm excitation. In order for this to occur, lignin's structure had to have undergone a greater disruption when using 514.5 nm excitation.

In order to get an estimate of the initial (t=0) 1595 cm^{-1} band intensities, Raman spectra were collected from a sequential section using the high pressure oxygen cell. The relative intensities were found to be 3.44 and 2.80 for 514.5 nm and 647.1 nm excitation, respectively. (These relative intensities were assumed to be of the same order of magnitude as the S_2 1595 cm^{-1} band intensities would have been if 1595 cm^{-1} band decay had not occurred. This assumption may not be entirely valid but is useful as a first approximation. The problems with this assumption are: (1) The 1098 cm^{-1} and 1595 cm^{-1} band intensities obtained with the macromode Raman system include contributions from areas other than the secondary wall. Thus, these average intensities may not be representative of the individual (S_2) ones. (2) It has been observed that the Raman intensity of cellulose's 1098 cm^{-1} band (internal standard) is somewhat lower when the sample is dry rather than wet. It is believed that this effect is due to a partial scrambling of the electric

vector in the dry woody sample. This would have the effect of slightly inflating the relative 1595 cm^{-1} intensity.)

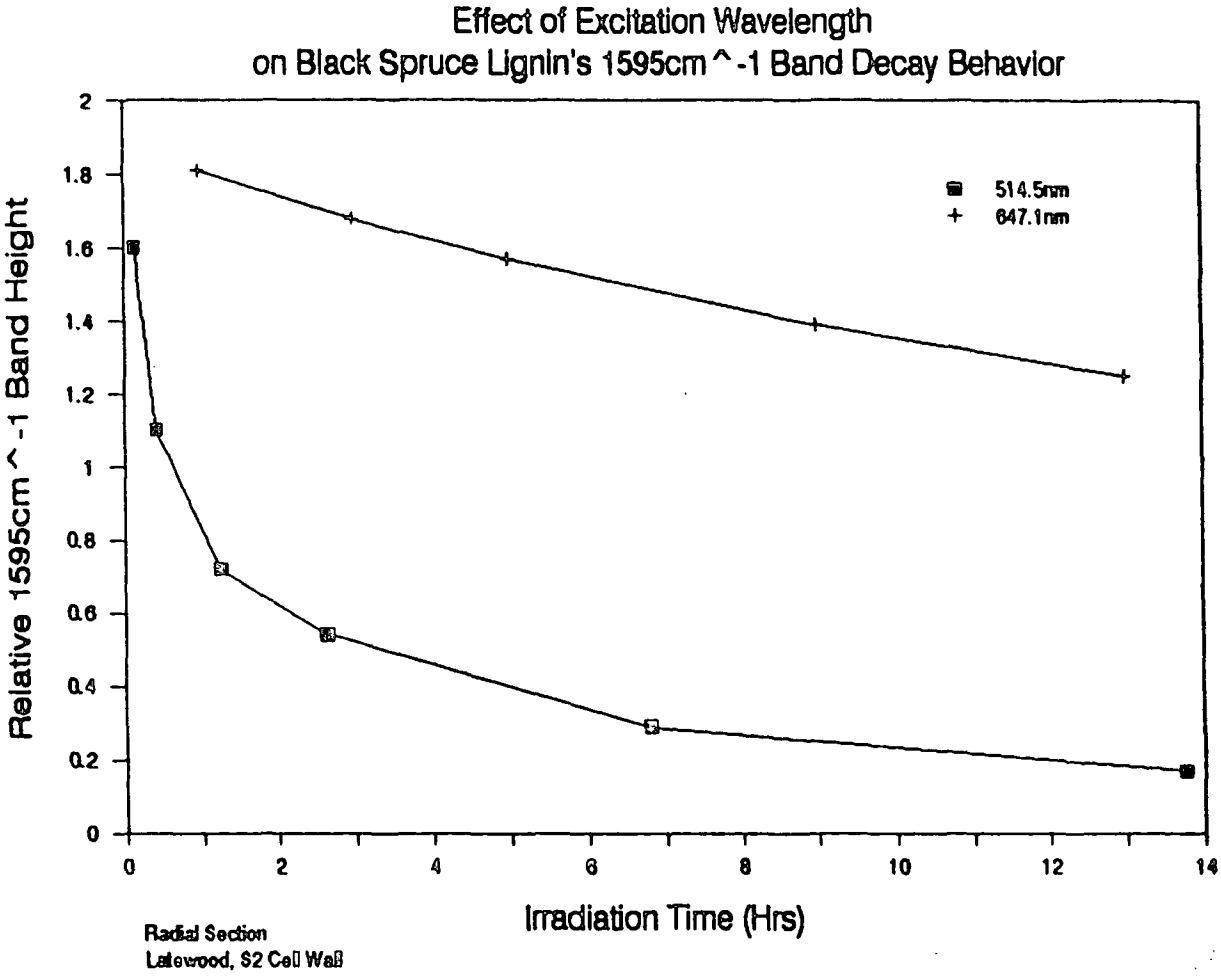

Figure 57. Effect of excitation wavelength on black spruce lignin's 1595 cm^{-1} band decay behavior.

The 1595 cm^{-1} relative intensities (3.44 - 514.5 nm excitation and 2.80 - 647.1 nm excitation) show the expected effect of PRRE; using an excitation

wavelength closer to the absorption band(s) resulted in a greater intensity. If these numbers are reasonably correct, then both curves show an initial precipitous drop (disruption of enhancement mechanisms) followed by a slowing of the decay rate. The drop is more pronounced when using 514.5 nm excitation. This may be partly due to the greater PRRE contribution but most likely is also due to the greater disruption of the lignin macromolecule as indicated above. The gradual decline seen in both curves may be indicative of the loss of aromaticity/destruction of the ring. (Earlier experiments revealed that the unenhanced relative 1595 cm^{-1} band intensity would be approximately 0.4. [Orientation effects on intensity were not considered in the analysis.] Black spruce's 1595 cm^{-1} band intensity falls below this level, which may possibly indicate that either the aromatic ring was disrupted or "lignin" became solubilized and diffused away from the area.)

Chemical Modification

Acid-Chlorite/Sodium Borohydride Treatment

Before investigating the decay behavior of acid-chlorite and sodium borohydride treated wood, macromode (O_2) spectra were acquired to observe the changes which had occurred to the 1600 cm^{-1} region bands. The sections were treated with: (1) acid-chlorite (AC), (2) sodium borohydride (BH), (3) AC followed by BH, and (4) BH followed by AC. After treatment, they were dried under nitrogen prior to Raman collection. In these studies (both macro and

micro) sequential sections were used to minimize location differences. (The treatment specifics are located in Appendix 4 and the spectra can be found in Appendix 8.)

Table 16 and Figure 58 show the effect of these treatments on black spruce's 1600 cm^{-1} region band intensities. It can be seen that the treatments disrupted CE/PRRE to varying degrees. The most severe disruption occurred with the acid-chlorite (AC)/sodium borohydride (BH) treatment while AC alone only had a slight effect on the band intensities. These data suggest that the sodium borohydride treatment was more severe than acid-chlorite. (Acid-chlorite was shown to be very reactive towards carbonyl-containing structures and yet the BH treatment which attacks carbonyl groups had the greater effect on the band intensities, i.e., the degree of CE/PRRE disruption was greater when using BH.) The extent of the acid-chlorite treatment used here (30 min. at 25°C) has been shown not to alter the lignin content (Klason and Klason + acid-soluble) of southern pine groundwood.[269]

The extent of the disruption of CE/PRRE can be seen by comparing the 514.5 and 647.1 nm 1595 cm^{-1} relative intensities. The AC values which are approximately equal to the control values indicate only a very minor disruption occurred to the lignin macromolecule during treatment. In contrast to this, both BH/AC and AC/BH essentially showed no difference between the two intensities. This suggests that these treatments altered the lignin molecule in such a way as to make this band insensitive to wavelength (647.1 nm) but at

the same time keeping some degree of CE enhancement. (The nonenhanced 1595 cm^{-1} band intensity is approximately 0.4.)

Table 16. Effect of Chemical Pretreatment on the 1600 cm^{-1} Region Bands of Black Spruce[1].

Treatment	1595/1098	1620/1098	1654/1098	1620/1595	1654/1595
Control	3.4 (2.8)[2]	1.8	0.44	0.52	0.13
Acid-Chlorite	3.3 (2.7)	1.6	0.39	0.49	0.11
Sodium Borohydride	2.3 (1.7)	1.2	0.27	0.53	0.12
BH/AC	1.7 (1.7)	0.77	0.15	0.51	0.07
AC/BH	1.5 (1.5)	0.78	0.11	0.45	0.09

(1) 514.5 nm excitation, high pressure O_2 cell.

(2) Values in parentheses were obtained using 647.1 nm excitation; corrected for instrument response.

One very curious observation is that the bands do not significantly change relative to each other in any of the treatments. (The 1620/1595 and 1654/1595 ratios are approximately the same with the possible exceptions of AC/BH - both, and BH/AC - 1654/1595). The previous model compound studies revealed that acid-chlorite treatment affected the ring conjugated carbonyl and C_α=C_β Raman bands, while sodium borohydride treatment was shown to only effect ring conjugated carbonyl bands. Thus both the 1620 cm^{-1} (C_α=C_β) and 1654 cm^{-1} (C_α=C_β and ring conjugated carbonyls) bands should be affected.

(All bands would be affected due to loss of enhancement, but their heights would be expected to change relative to each other as was seen in the model compound studies.)

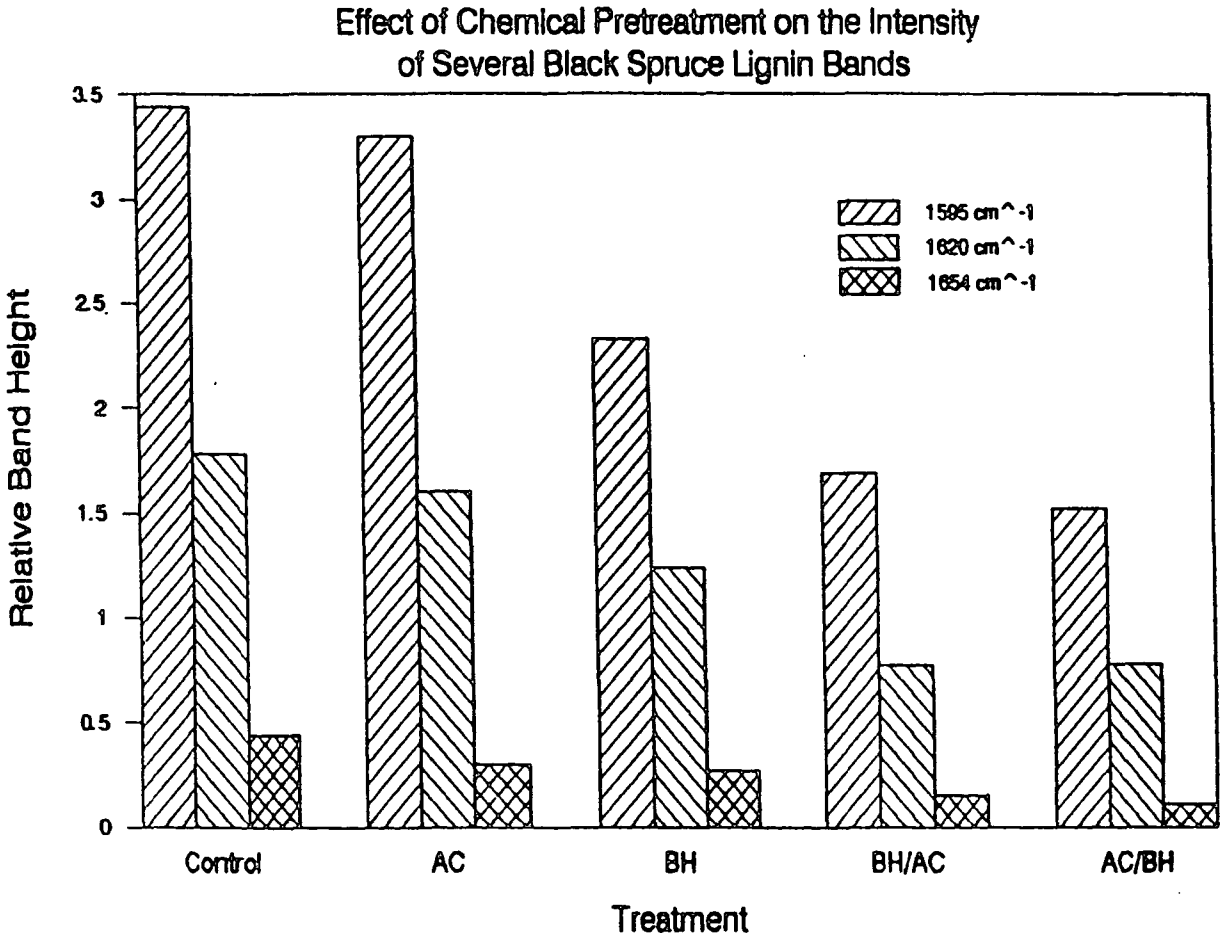

Figure 58. Effect of chemical pretreatment on black spruce lignin's 1600 cm^{-1} region band intensities.

These findings suggest that:

1. The treatments were fairly mild.

2. The Raman bands probably have contributions from multiple lignin units/groups, some of which may not be affected during treatment.
3. The fact that band enhancement was significantly altered for most of the treatments suggests that specific groups (or structural units containing these groups) which contribute disproportionally to the band intensities are particularly sensitive to chemical modification.

Figure 59 (a) and (b) show the 1595 cm^{-1} band decay behavior from locations in the secondary cell wall layers of black spruce thin sections. The initial values (t=0, macro-O_2) are included for comparison. (These initial values are only approximate and may be too large for the reason given in the preceding section.) These treatments did not significantly alter the decay behavior. All the spectra show an initial precipitous drop followed by a lessening of the slope. The general shapes of the curves are similar, but the specific values differ. Part of the reason for this difference is due to the disruption of CE/PRRE but part may also be due to location differences. The acid-chlorite and sodium borohydride curves can be seen crossing above the control curve (very early in the irradiation period in the case of acid-chlorite, later for sodium borohydride). Whether this is due to spot-to-spot variation or represents different kinetics is not known. It is possible that both treatments altered the chemistry that led to the disruption of the aromatic ring. (All curves fall below the nonenhanced value of ≈0.4 which may be indicative of aromatic ring disruption/destruction.)

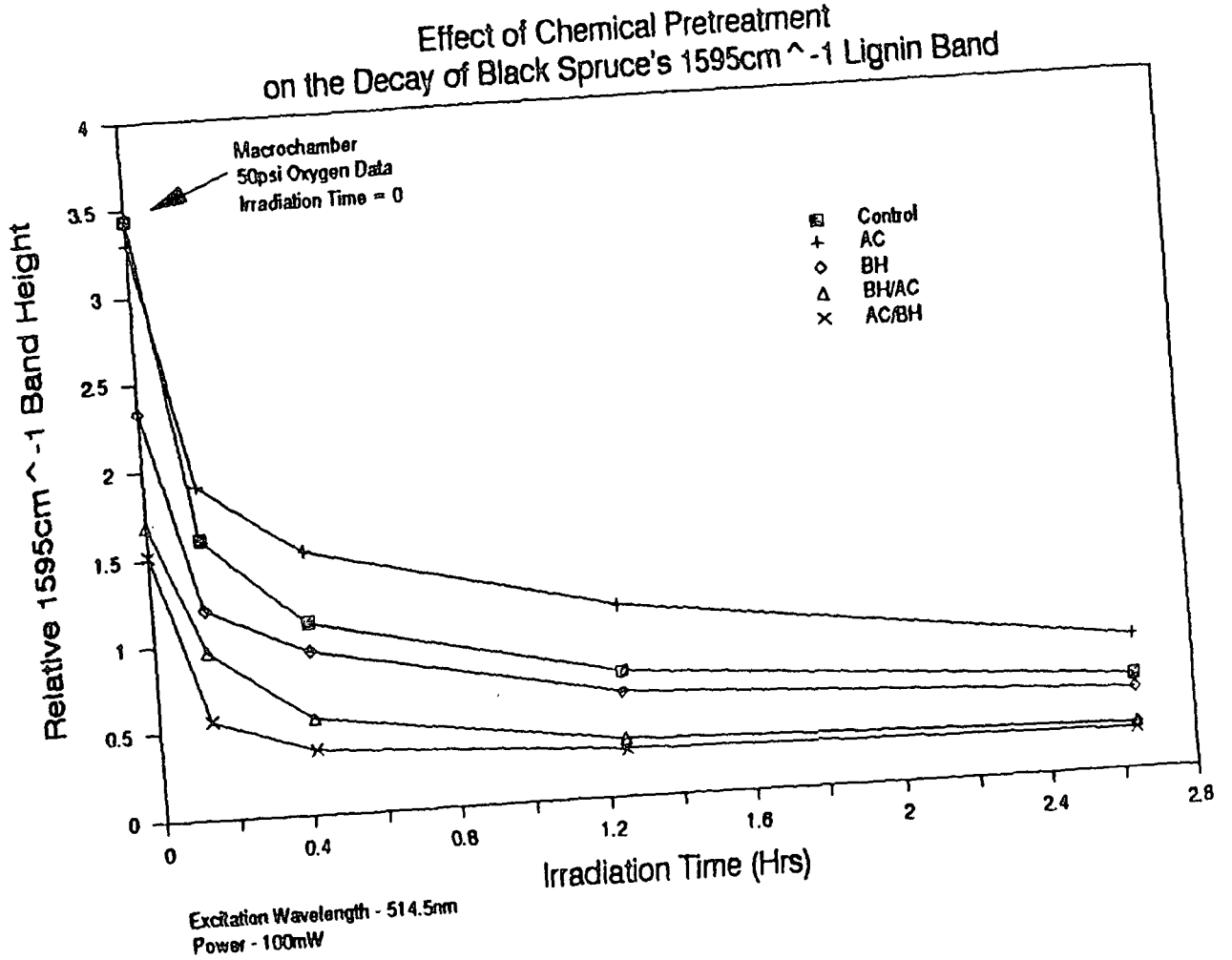

Figure 59a. Effect of chemical pretreatment on the decay of black spruce lignin's 1595 cm^{-1} band. Short irradiation times.

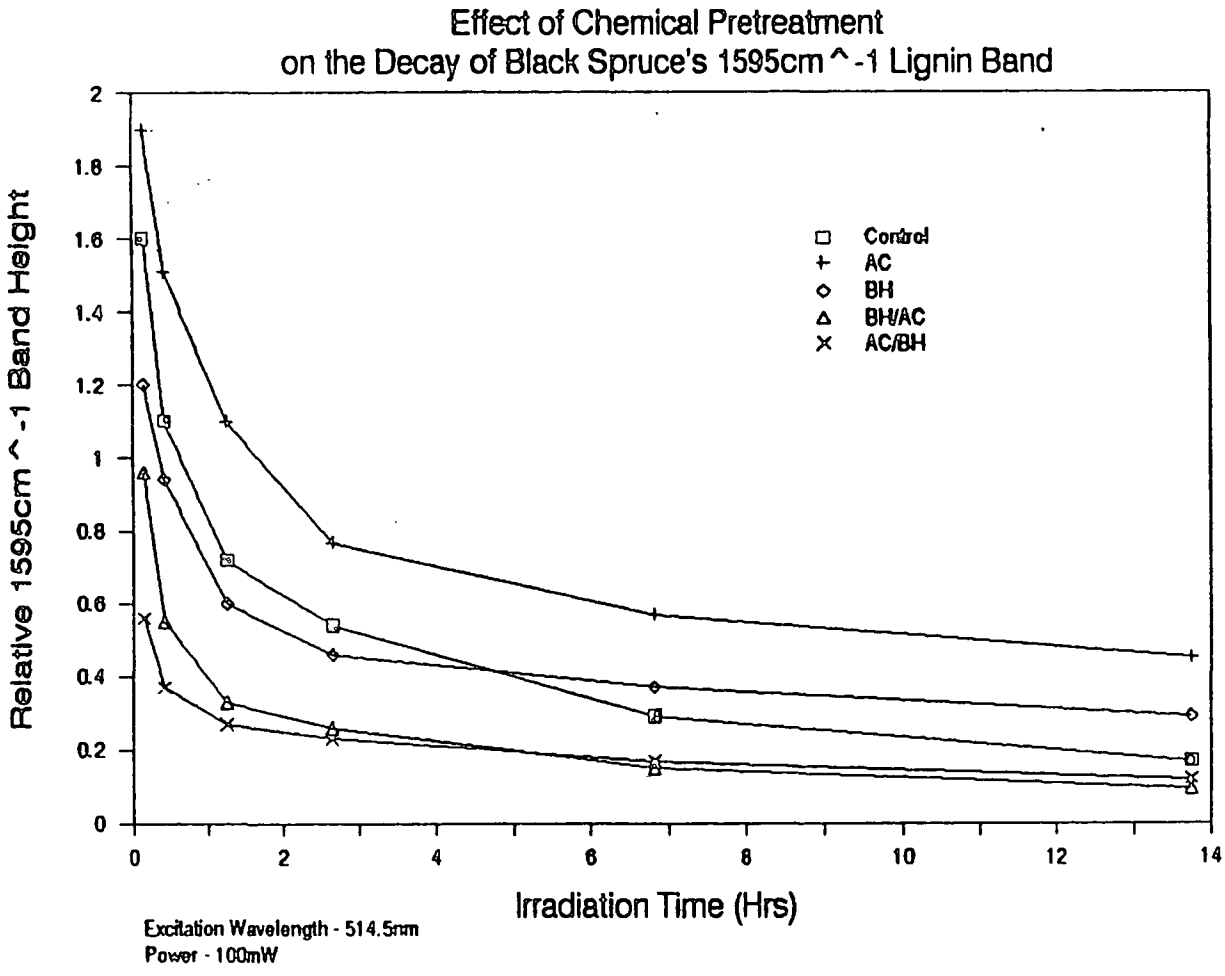

Figure 59b. Effect of chemical pretreatment on the decay of black spruce lignin's 1595 cm^{-1} band. Long irradiation times.

Table 17 presents the relative percent loss of the initial (8.3 min.) 1595 cm^{-1} values together with the relative 1595, 1620, and 1654 cm^{-1} band intensities. As can be seen, the 1595 cm^{-1} band showed a significant decline after ≈14 hours of 514.5 nm irradiation regardless of the treatment. The percent decay was slightly less for acid-chlorite (AC), sodium borohydride (BH), and AC/BH treated sections. Whether this is due to a modification of lignin's structure brought about by these treatments is not known. It could also be due to structural differences in lignin, i.e., spot-to-spot variations in the sensitivity to chemical modification.

Table 17. Effect of Chemical Pretreatment on Black Spruce Lignin's 1600 cm^{-1} Region Bands - Microprobe, S_2 Cell Wall Layer.[1]

	Initial Ratios (8.3 min. Irradiation)			
Treatment	$\frac{1595}{1098}$	$\frac{1620}{1098}$[2]	$\frac{1654}{1098}$	% 1595 cm^{-1} Band Decay after 13.75 hrs Irradiation (Relative to 8.3 min Value)
Control	2.2	0.16	0.34	89
AC	2.1	0.12	0.20	76
BH	1.6	0.09	0.27	76
BH/AC	1.0	0.10	0.18	91
AC/BH	0.52	0.04	0.04	79

(1) 514.5 nm excitation.

(2) These data are questionable due to low band intensities.

The order of the 1620 and 1654 cm^{-1} band intensities parallels the 1595 cm^{-1} intensity. (The order is most likely a manifestation of the loss of band enhancement brought about by the treatments as shown by the O_2 data.) The only obvious exception is the AC and BH order for the 1654 cm^{-1} band. It may be that either the AC value is too low or the BH value is too large. This was not seen in the macrochamber O_2 data which suggests that the AC and BH order was probably the result of spot-to-spot variations.

It is apparent that none of the treatments was able to stop lignin's 1595 cm^{-1} band decay. In spite of the disruption of CE/PRRE, decay still occurred. These results support the idea that the initial rapid part of the decay is primarily due to the loss of CE/PRRE. The subsequent gradual decline is most likely due to the loss of aromaticity/dissolution of lignin brought about by secondary photochemical reactions. The reason that the treated sections still underwent lignin decay in spite of the loss of band enhancement may be due to other structures in lignin which were not affected by these treatments (or the treatments were not 100 percent effective).

Trimethylphosphite Treatment

Trimethylphosphite (TMP) has been shown to react with quinones to effectively block the quinone's oxygens from participating in reactions[270] (Figure 60). In an attempt to determine if quinones (which are speculated to be present in native wood) contribute to the absorption of 514.5 nm photons,

black spruce sections were treated with TMP. Because of unwanted reactions which could possibly occur in water (and perhaps oxygen), the sections were first run dry under nitrogen then subsequently under oxygen in the macromode high pressure cell. Figure 61 shows the Raman spectrum obtained in an oxygen environment. (The relative 1595 cm^{-1} band intensity was essentially the same in both gaseous environments. The only obvious difference in the spectra was that the background was substantially lower in the oxygen environment.) The width of the 1595 cm^{-1} band appears to be greater in the treated section. (Oxygen's 1550 cm^{-1} peak, which is readily apparent in untreated wood spectra [O_2 environment], is hidden by the 1595 cm^{-1} band.) This may be indicative of a reaction between TMP and lignin. In addition, the 2900/1098 cm^{-1} ratio is larger in the treated wood which most likely reflects the C-H contribution from TMP (1.5 vs. 1.1). If quinones were responsible for absorption/PRRE (and TMP reacted with them) then the relative 1595 cm^{-1} and 1654 cm^{-1} band intensities would be expected to be lower in TMP-treated wood. This is not what is observed. Both bands are more intense in the TMP-treated wood (1595 cm^{-1} band: 3.6 vs. 2.4, 1654 cm^{-1}: 2.4 vs. 2.1). It may be that the absorption band(s) of the adduct are in the visible region and therefore the lignin bands are subject to PRRE(?). These data do not refute the suggestion that quinones are present in native-wood and therefore can contribute to absorption of 514.5 nm photons. The TMP reaction may indicate their presence, but their contribution to absorption/PRRE/decay is not known.

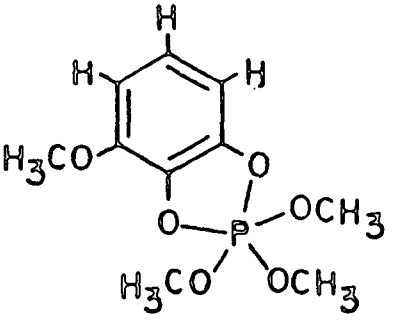

Figure 60. Product of the reaction between trimethylphosphite and 3-methoxy-1,2-benzoquinone.[270]

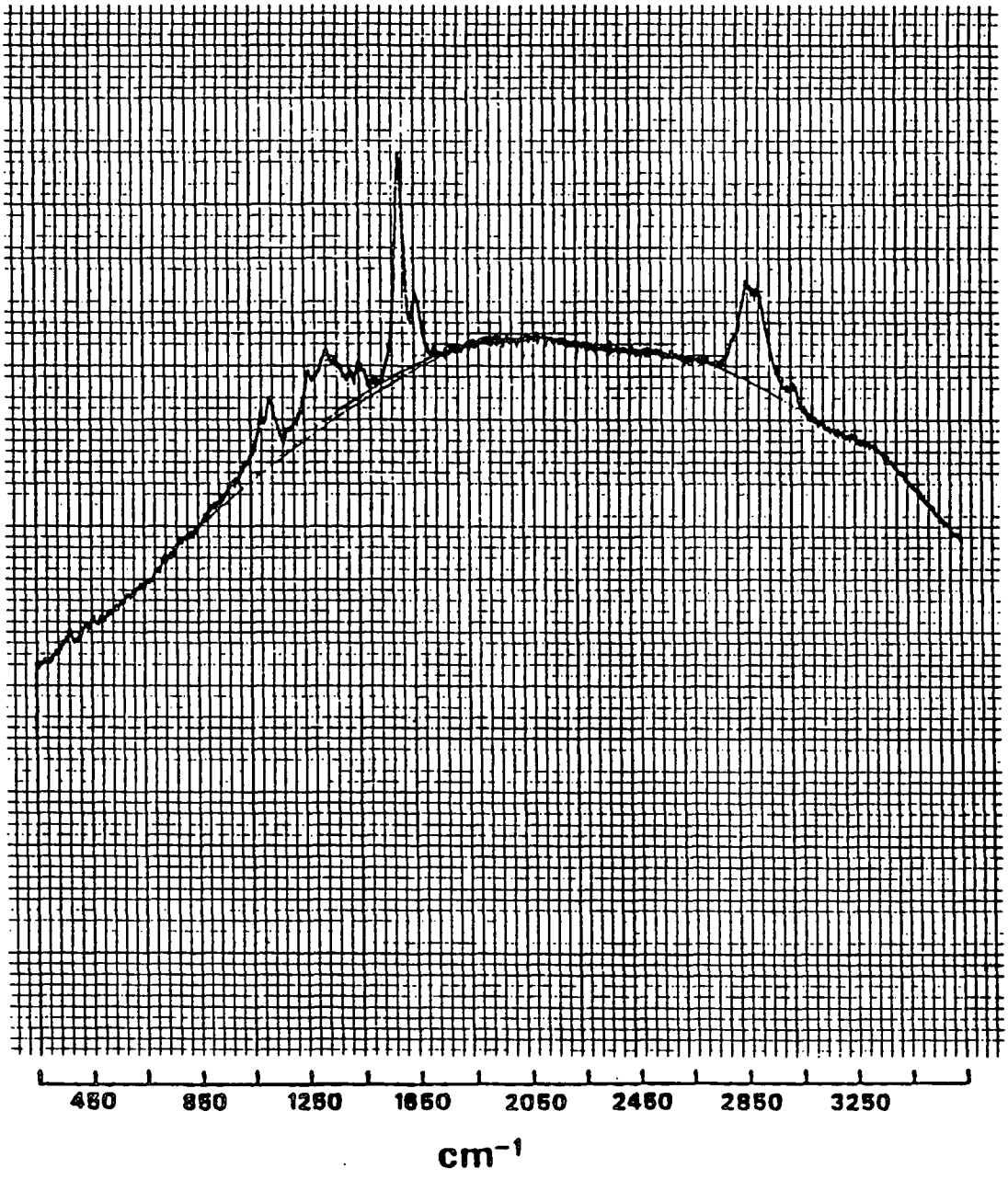

Figure 61. Raman spectrum of a black spruce thin section treated with trimethylphosphite.

Methylation And Chelation

The effects of methylation and chelation on the 1595 cm^{-1} band decay are shown in Figure 62. Treatment of the extracted black spruce section with an acetone wash followed by DTPA did little to alter the decay. (The slight difference is most likely a location variation.) In contrast to this, methylation appeared to alter the initial precipitous drop. It is likely that blocking the phenolic OH groups minimized the disruption of the conjugated structures present in lignin, e.g., coniferaldehyde-type structures. Previous studies revealed the methylation slowed photoyellowing reactions but did not entirely stop them.[62-65] The gradual decline is still seen with this treatment, supporting the idea that the initial drop is primarily due to the loss of band enhancement while the more gradual decline is a manifestation of ring destruction. It is likely that either residual phenolic hydroxyl-containing structures or other lignin structural elements were present after treatment to initiate the (primary) photochemical reactions. These reactions probably produced chemical species (phenoxy radicals ?) which attacked the aromatic ring. (The methylation data, which were obtained from Umesh Agarwal [USDA, Forest Products Laboratory], are from a cross-section of black spruce rather than a radial section. As a result of this, the relative 1595 cm^{-1} band intensity is slightly inflated because cellulose's 1098 cm^{-1} band [internal standard] is less intense in a cross-section due to orientational effects.)

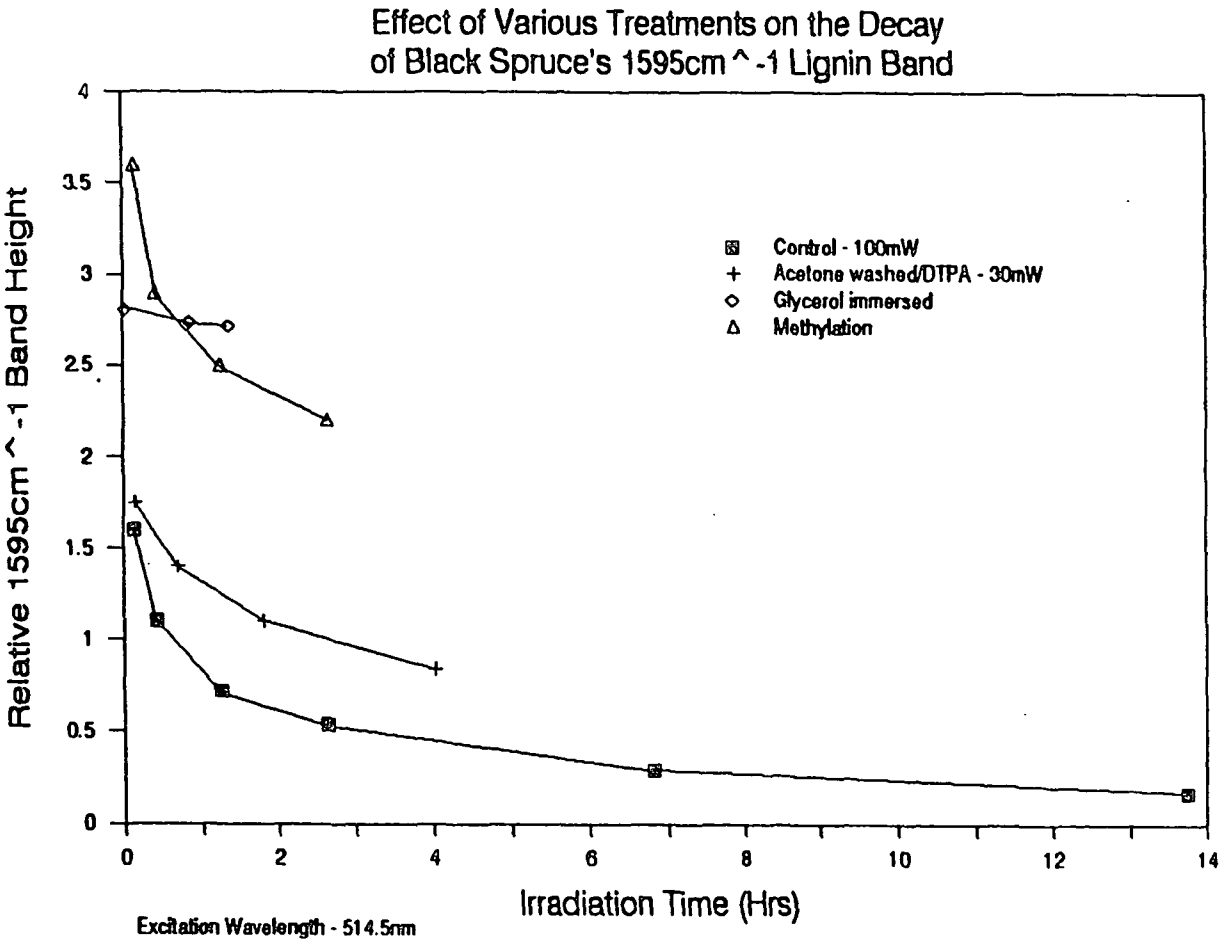

Figure 62. Effects of various treatments on the decay of black spruce's 1595 cm^{-1} lignin band.

Quenching Agents

In order to investigate the effect of excited state quenchers/radical scavengers on 1595 cm^{-1} band decay, black spruce sections were immersed in 0.1M solutions of potassium iodide (KI) and copper (II) chloride ($ClCu_2$)

during 514.5 nm laser exposure. Figure 63 presents the result of these investigations. As can be seen, potassium iodide did little to alter the decay behavior whereas copper (II) chloride had a significant effect on decay. This treatment minimized the loss of CE/PRRE 1595 cm^{-1} band enhancement. The gradual decline can still be seen which suggests that CuII ions did little to alter this aspect of the decay (destruction of the ring).

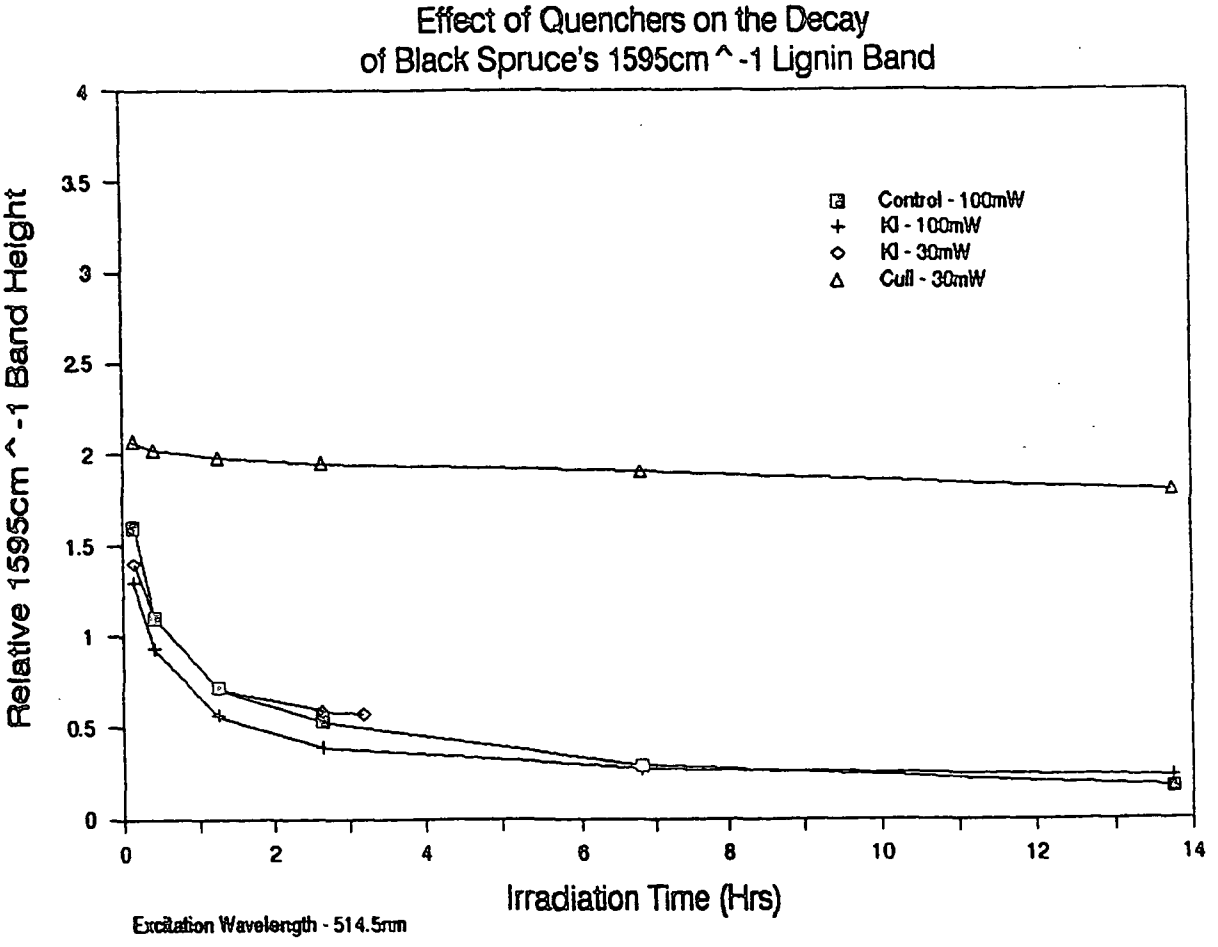

Figure 63. Effect of quenchers of the decay of black spruce lignin's 1595 cm^{-1} band.

It is conceivable the CuII ions deactivated some of the photoexcited chromophores before conjugation-destroying reactions occurred (which would have reduced the extent of PRRE). If (phenoxy) radicals are the cause of the gradual decline, CuII ions did not prevent their formation nor did they act as a radical scavenger.

It might have been possible to alter the CuII ion concentration to maximize the photostabilizing effect had not an interfering chemical reaction occurred. The brass in the microscope objective reacted with the solution and CuCl precipitated as the following chemistry shows:

Scheme 7.

$$CuCl_2 \longleftrightarrow Cu^{2+} + 2Cl^-$$

$$Cu^{2+} + Cu^0 \longleftrightarrow 2Cu^+$$

$$\downarrow$$

objective

$$Cu^+ + Cl^- \longleftrightarrow CuCl\ (ppt)$$

$$Zn^0 + Cu^{2+} \longleftrightarrow Zn^{2+} + Cu^0$$

$$\downarrow \qquad\qquad \downarrow \quad \downarrow$$

objective solution plated on objective

The CuCl interfered with data collection after a short period of time. Figure 64 shows the interfering crystals of copper (I) chloride which grew during laser exposure.

The effect of laser power level on lignin decay can also be seen in this figure. The 30 mW and 100mW KI curves are not significantly different from

each other. These data suggest that laser power does not have a significant effect on decay.

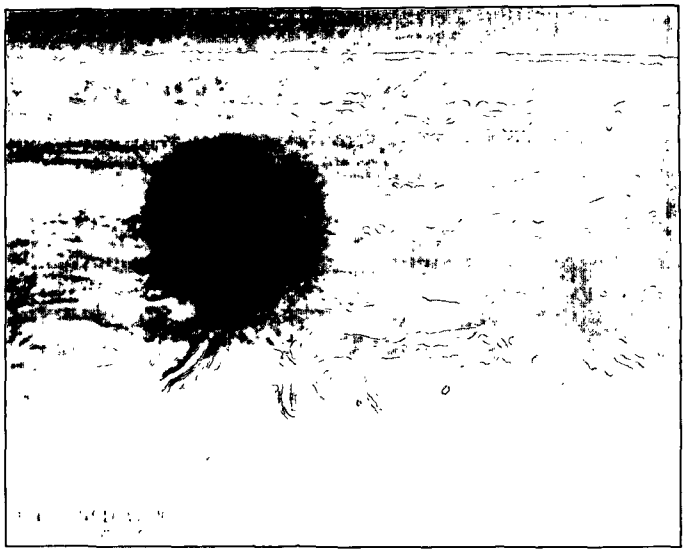

Figure 64. Video image of the interfering CuCl crystals which developed during 514.5 nm exposure when the black spruce sample was immersed in $CuCl_2$.

Oxygen has proven to be an effective fluorescence background quencher when using the macromode high pressure cell. A special oxygen flow-through cell was constructed to determine if dry wood sections could be used with the microprobe. (Usually when using 514.5 nm radiation with the microprobe, the Raman signal is overwhelmed by the fluorescence and the dry sample quickly burns.) The cell consisted of a microscope slide on which the top of a

poly(ethylene) container (trademark) was cemented. The top and bottom of this container had holes cut into them. One accommodated the objective (bottom of container) while the other allowed the wood section to be taped on the microscope slide. A section of a surgical rubber glove (three attached fingers) served to seal the container and the microscope objective (center finger) and permitted the flow of oxygen through the cell (the two outside fingers).

While oxygen quenching is a viable technique for the macromode system, it did not work with the microprobe. Rather than decreasing, the relative 1595 cm^{-1} band increased in intensity after exposure to 514.5 nm radiation. The initial value was 2.6 after 8.3 minutes of laser exposure; it increased to 5.3 after approximately 7 hours and by the end of 12 hours, the relative height was ≈7. The background level behaved similarly; at the end of approximately 12 hours of 514.5 nm exposure, the level had increased about 6 times. (Cellulose's 1098 cm^{-1} band was almost lost in this background level.) Apparently the higher power density altered the chemistry/kinetics. It is probable that the lignin macromolecule was modified in such a way as to increase the 1595 cm^{-1} band enhancement.

Nonaqueous Immersion Medium

A black spruce section was immersed in glycerol to both investigate water's role in the 1595 cm^{-1} band decay and to determine if immersion in another medium would be a viable alternative technique. (Water has tradition-

ally been used because it minimizes thermal damage and quenches the interfering background fluorescence.) Glycerol did not prove to be satisfactory as an immersion medium. After a short period of irradiation time (≈9 min. @ 100 mW, ≈82 min. @ 30 mW) a modification took place. Only two bands were readily apparent after this time, one at 1325 cm^{-1} and another at 1600 cm^{-1}. The 1098 cm^{-1} band was not seen even though the background level fell during irradiation. Apparently lignin was photomodified and the modified material masked the cellulose features. (Water's thermal conductivity is two times greater than glycerol's (0.001429 vs. 0.000703 cal/sec.·cm^2·cm·°C), so it is probable that thermal energy played a role. The time it took the sample to become photomodified when using different laser power levels (30 and 100 mW) supports this idea. It took approximately 9 times longer for photomodification to occur when using a lower incident power level, i.e., a smaller energy input.)

Up until the modification took place, the relative 1595 cm^{-1} intensity decreased only slightly (≈8%) - see Figure 62. In addition, the reduction in background level was not as pronounced as that seen when the sample was immersed in water. Thus, water appears to be intimately involved both in lignin decay and reduction of background fluorescence.

It is interesting to note that the initial relative 1595 cm^{-1} band intensities were significantly greater when the sample was dry (oxygen: macro - 3.4, 2.8; micro - 2.6) or immersed in glycerol (2.5) as compared to when the sample was immersed in water (≈1.6). These data suggest that a very

rapid modification of the lignin macromolecule occurs in an aqueous environment.

Concluding Remarks

Attempts to stabilize native-state lignin to laser radiation met with little success. Reduction, oxidation, and substitution reactions of the lignin macromolecule, as well as the use of fluorescence quenchers/radical scavengers failed to stop the decay of lignin's 1595 cm^{-1} band. The chemical treatments did, however, alter the percent contribution of CE/PRRE to the 1595 cm^{-1} band intensity. Several treatments showed promise, e.g., glycerol immersion and the use of CuII ions, but unwanted side reactions prevented their use. The decay data (as well as the extent of enhancement) were found to be very location-specific which suggests that the structure of the lignin macromolecule may vary from location to location in the secondary cell wall.

The decay of lignin has been found to be a multifaceted problem. Blocking the known reaction centers did not stop the decay which suggests that alternative pathways exist. It is possible that other species (chromophores) which are not greatly affected by these treatments are present in the wood and thus contribute to absorption/decay. It has been suggested that simple extraction does not completely remove colored wood extractives such as polyphenolic flavanoid structures because they are either covalently bonded to wood polysaccharides or lignin.[241] In addition to extractives, a CTC between

cellulose and lignin may occur in woody tissue and could contribute to absorption. It is conceivable that structures such as these initiate photochemical processes which eventually lead to the modification and destruction of the lignin macromolecule.

To conclude this section on photostabilization, the 1595 cm^{-1} decay behavior for both black spruce and loblolly pine is shown in Figure 65. The oxygen high pressure cell values are included to indicate the approximate magnitude of the initial decline in band intensity. As can be seen, loblolly pine experienced a quicker drop in 1595 cm^{-1} band intensity than did black spruce. It is possible that loblolly pine's 1595 cm^{-1} band had a higher PRRE contribution than black spruce. The model compound studies revealed that those models with the strongest absorption had the greater PRRE of their ≈1600 cm^{-1} bands (coniferaldehyde). It may be the loblolly pine has more absorption centers of this type and that these are very sensitive to photochemical modification. (An analogy can be found in the acid-chlorite studies. It was shown that in woody tissue, a substituent which contributed significantly to the 1595 cm^{-1} band intensity was very sensitive to AC treatment. Model compound studies revealed the carbonyl-containing models were extremely reactive to AC treatment. Taken together, these very sensitive species/groups could be coniferaldehyde-type structures and it is these structures in wood which contribute significantly to photochemical decay.)

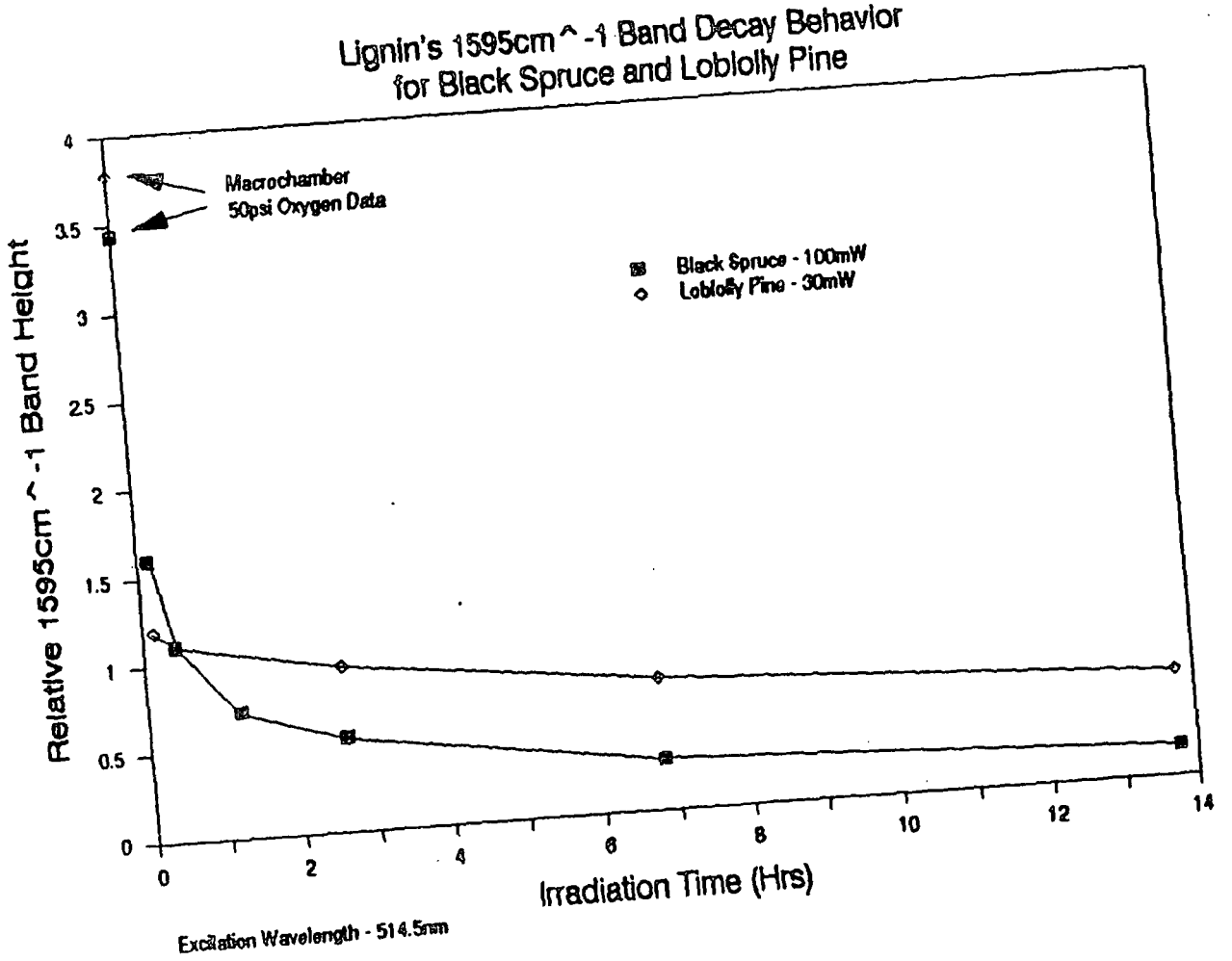

Figure 65. Lignin's 1595 cm^{-1} band decay behavior for black spruce and loblolly pine.

SPECTRAL MAPPING STUDIES

In this section, the results of the spectral mapping of the organization of cellulose and lignin in the secondary cell walls of black spruce and loblolly pine are presented.

Introduction

The results of the photostabilization treatments were disappointing in regards to the spectral mapping of the organization of lignin in secondary cell walls. None of the chemical treatments stopped the decay of the 1595 cm^{-1} lignin band during laser exposure of wet woody tissue. (The use of 647.1 nm excitation was not feasible even though the disruption to the lignin macromolecule was shown to be less, because of the protracted acquisition time needed to obtain reasonable spectra; a minimum of 50 minutes was required.) Although complete photostabilization of lignin was not achieved, a methodology that was thought to minimize the bias introduced by lignin modification was followed in these studies (see EXPERIMENTAL MATERIAL AND METHODS - EXPERIMENTAL PROGRAM).

As was previously mentioned, the rotation of the electric vector relative to morphological features, which was used to infer information about molecular orientation, was accomplished by using a laser line rotator rather than sample rotation. This was necessary because of the sensitivity of lignin to laser radiation and the difficulty in accurately positioning the sample after rotation. When using this method, it was necessary to use a standard to correct

the spectra for dichroic effects introduced by the microscope's beam splitter. (The optics in the microscope and spectrometer favor one polarization direction over another. An electric vector scrambler was used to make the spectrometer insensitive to the plane of polarization). Because of this dichroism, the incident power at the sample was ≈2.1X greater when "perpendicular" spectra were recorded. In addition to this power effect, another complication arose because the Raman-scattered light must pass back through the beam splitter. Depending on the orientation of its electric vector, the light intensity could be attenuated as shown below.

Figure 66 shows the correction factor based on toluene. (The toluene curve reflects both power and polarization effects.) The correction factor data points were calculated by dividing the "perpendicular" intensity for a given toluene band of known polarization by the "parallel" intensity for the same band. The factors range from ≈1.3 (100% polarized) to 2.1 (depolarized). (The depolarization ratio is defined as the perpendicular intensity divided by the parallel intensity for a given band and ranges from 0 to ≈0.75.) As can be seen, the effect of band polarization was to diminish the power effect (2.1X).

A second curve is included in Figure 66 to show that the toluene behavior can be adequately predicted on the basis of beam splitter effects alone (i.e., there is very little polarization leakage from the scrambler). This curve was calculated by determining the effect of a 60:40 (R/T) beam splitter on the reflected and transmitted light intensities and by using the observed

2.1X power effect.

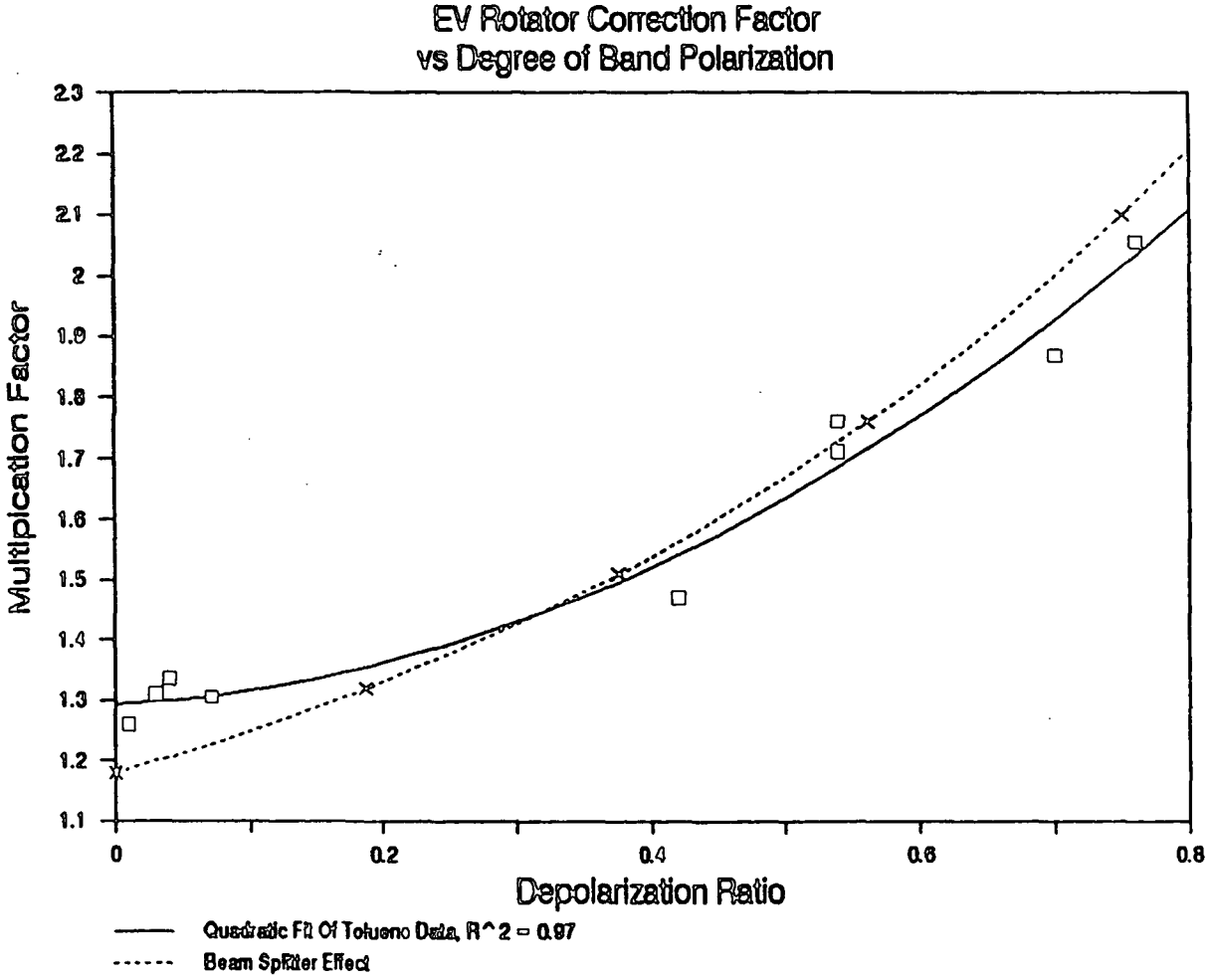

Figure 66. Correction factor for dichroic effects introduced by the microscope's beam splitter.

Because cellulose and lignin bands may vary in their degree of polarization, it became necessary to attempt to determine the correction factors for the 1098 cm^{-1} and 1595 cm^{-1} parallel/perpendicular band intensities. In order

to ascertain these values, "orientation" spectra were acquired from a single location in the S_2 wall of black spruce. The pair of spectra were both parallel, but in one the incident EV was vertical upon entering the beam steering optics and the fiber was oriented left-to-right in the microscope's field of view, while in the other the EV was horizontal and the fiber was oriented top to bottom. In this manner the only difference in band intensities between the pair of spectra would be due to dichroic effects (ignoring lignin decay). The 1098 cm^{-1} band correction factor was found to be 1.33 while the 1595 cm^{-1} band correction factor ranged from 1.6-2.1 (1.8 average). (It is conceivable that these correction factors are species/location specific. In order to correct the data, it was necessary to assume that these differences would be minor and thus the 1.33 and 1.8 factors could be used universally.)

In the mapping studies, these values (1.33 and 1.8) were used to correct the data for beam splitter dichroic effects. The "perpendicular" intensities were divided by 1.33 (cellulose) or 1.8 (lignin) for black spruce and the parallel intensities were multiplied by these same values for loblolly pine. (It made little difference which method was used, although correcting the parallel data resulted in inflating the 1595/1098 cm^{-1} ratios by approximately 35% relative to the alternative method.)

In order to map cellulose and lignin organization in the cell walls of black spruce and loblolly pine, several assumptions had to be made. The lack

of an internal standard necessitated using the initial laser power level and microscope focus to standardize the spectra. (This meant that absolute rather than relative band intensities were used in the analysis.) It was assumed that any difference in results between the two standardization techniques (internal vs. external) would be minor. The loss of lignin orientation information during a second acquisition from the same location precluded obtaining parallel and perpendicular data from a single location. The parallel and perpendicular orientation "pair" had to be collected from neighboring spots ≈2.5 microns apart. It was assumed that linear interpolation could be used to estimate the "missing" orientation value at each location. The sum of the EV parallel and EV perpendicular intensities for a particular component at each cell wall location was assumed to be representative of the component's concentration at that location. The use of the electric vector rotator necessitated introducing correction factors for the band intensities, which, although they might vary from location to location because of polarization effects, were assumed to be unchanging.

Woody Tissue

Black Spruce

Figure 67 shows the cell wall region used for the mapping studies before (a) and after (b) irradiation. The darker regions above and below the irradiation marks are fiber lumens. The extent of cell wall disruption is readily

apparent after the 90-second irradiation period. The marks can be seen to vary in intensity and size. Part of this is due to focus, and part may be caused by a variation in the structure of the lignin macromolecule. (These video prints have been enhanced to bring out details which were otherwise not as apparent.)

(a)

Figure 67. Video enhanced prints showing the area used in the mapping studies of black spruce before (a) and after (b) irradiation. The grid pattern is depicted in (c). Locations are numbered 1-10 (L to R). Radial section.

(b)

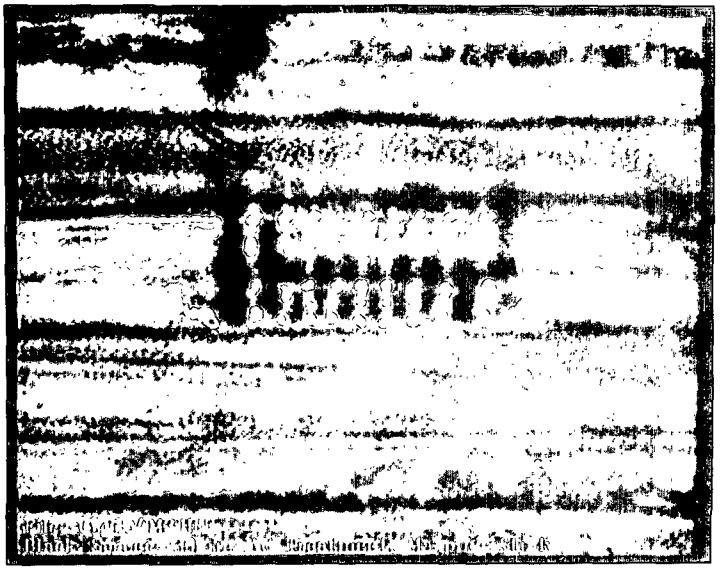

(c)

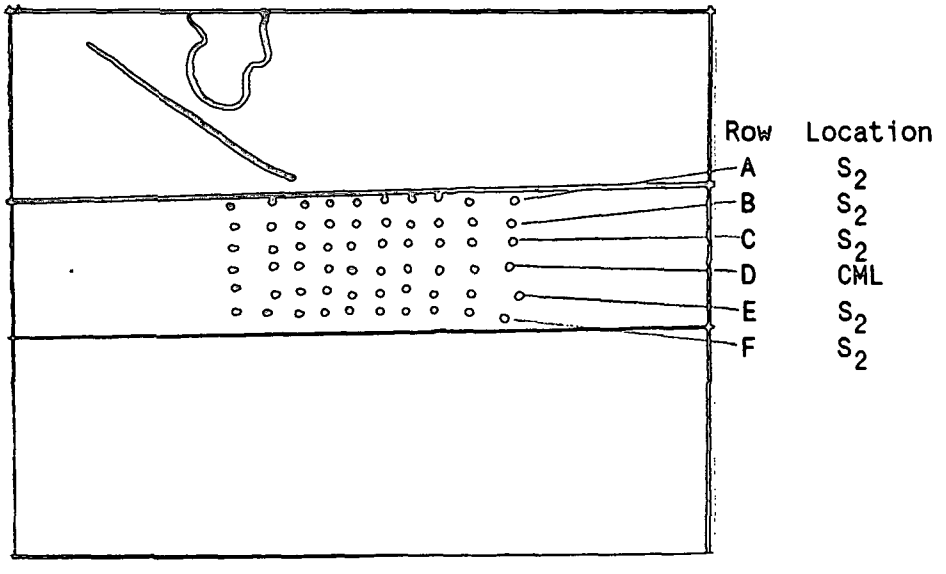

Figure 67 contd. Video enhanced prints showing the area used in the mapping studies of black spruce before (a) and after (b) irradiation. The grid pattern is depicted in (c). Locations are numbered 1-10 (L to R). Radial section.

Figures 67c and 68 show the approximate locations of data points. The sampling grid was 10 (along the longitudinal axes of the fibers) by 6 (perpendicular to the longitudinal axes of the fibers). This grid area included three distinct morphological regions: the S_2 cell wall layer from one fiber (rows A-C), the compound middle lamella between (row D), and the S_2 layer of the adjoining fiber (rows E and F). Thus, a total of 60 data points was used in the analysis.

The position and spacing of the analysis points shown in Figure 68 and used in the following topographic plots were determined from Figure 67b with the aid of Image-Pro II image processing software. The row F, spot 1 (bottom row, first spot on the left) analysis point served as the origin. The irregular spacing of the data points was due to the difficulty in accurately positioning the cell wall in relationship to the probe beam of the laser.

Figures 69-76 show the topographic plots of Raman band intensity vs. cell wall location. Because of the various assumptions, which were mentioned above, these plots should be considered zero order approximations and are meant to show trends and not absolute values.

As was previously mentioned, the (EV) parallel and perpendicular pair of spectra which were used to investigate orientation, could not be obtained from the same location. To circumvent this difficulty, it became necessary to collect parallel information from the first location, perpendicular from the

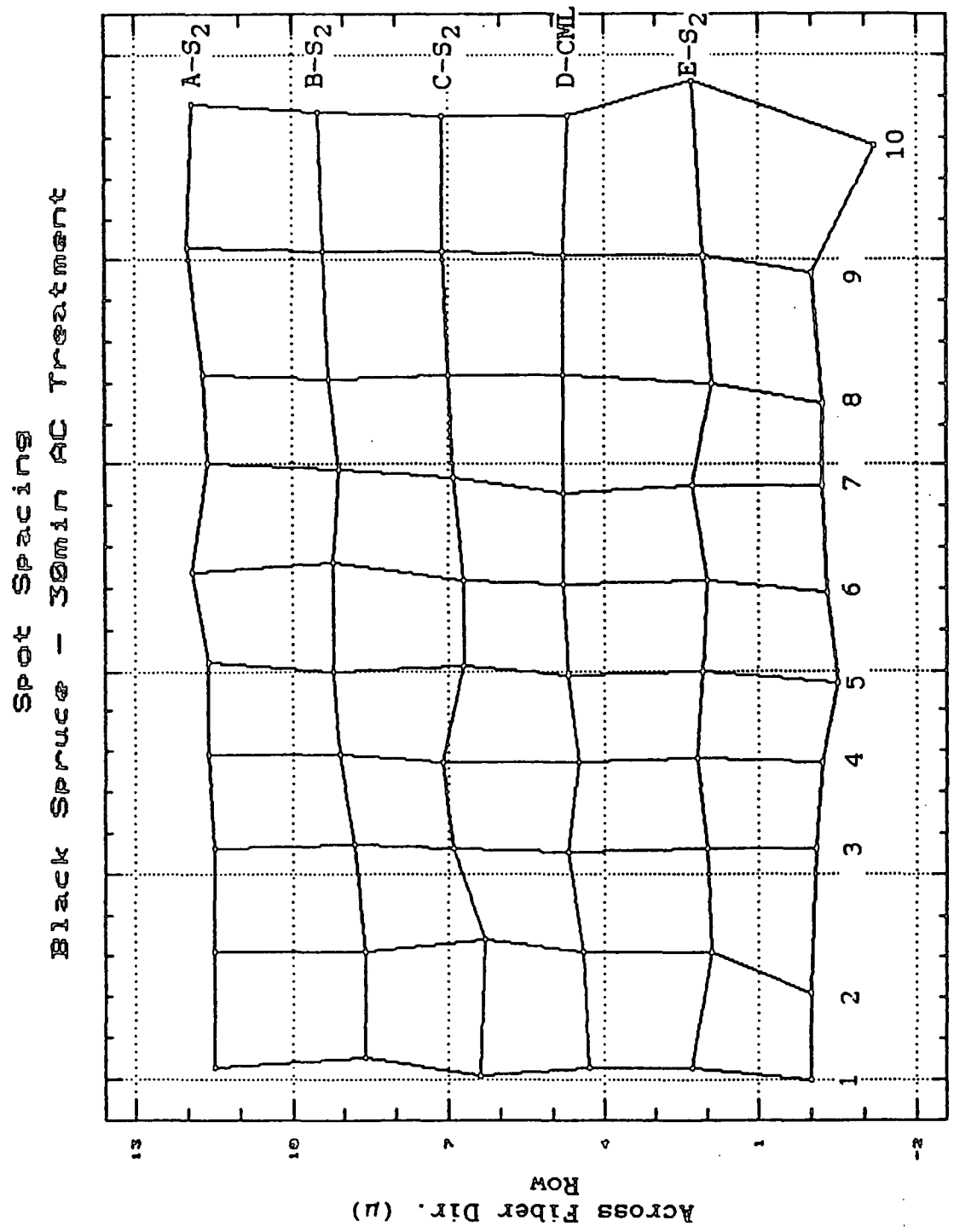

Figure 68. The position and spacing of the analysis points used in the spectral mapping study of black spruce cell wall organization. The row F, spot 1 (bottom row, first spot on the left) analysis point served as the origin.

next location, parallel from the third, and so forth along the fiber. Thus in these topographic plots, the "parallel" data were collected from row A: spots 1, 3, 5, 7, and 9; row B: spots 2, 4, 6, 8, 10; row C: spots 1, 3, etc. while the "perpendicular" data were collected from row A: spots 2, 4, 6, 8, 10; row B: spots 1, 3, 5, etc. The missing intensities were determined by linear interpolation. For those locations where interpolation was not possible (i.e., the end points), the neighboring (row) intensity value was used. Thus for the "parallel" data, the row A/spot2 intensity is an interpolated value (the intensities at spots 1 and 3 were used) while the row A/spot 10 (end point) intensity has the same value as row A/spot 9 (actual data point).

Figures 69-71 are topographic plots of cellulose's 1098 cm^{-1} band intensity vs. cell wall location: Figure 69 - EV parallel; Figure 70 - EV perpendicular; Figure 71 - EV parallel + EV perpendicular.* Comparing Figures 69 and 70, it can be seen that the general shape of the parallel and perpendicular plots is, for the most part, similar but that the parallel intensity values are greater. This latter point most likely reflects the preferential orientation of the long axis of the cellulose chains in planes parallel to the cell wall (radial section).

*Selected spectra and band height vs. location plots can be found in Appendix 9.

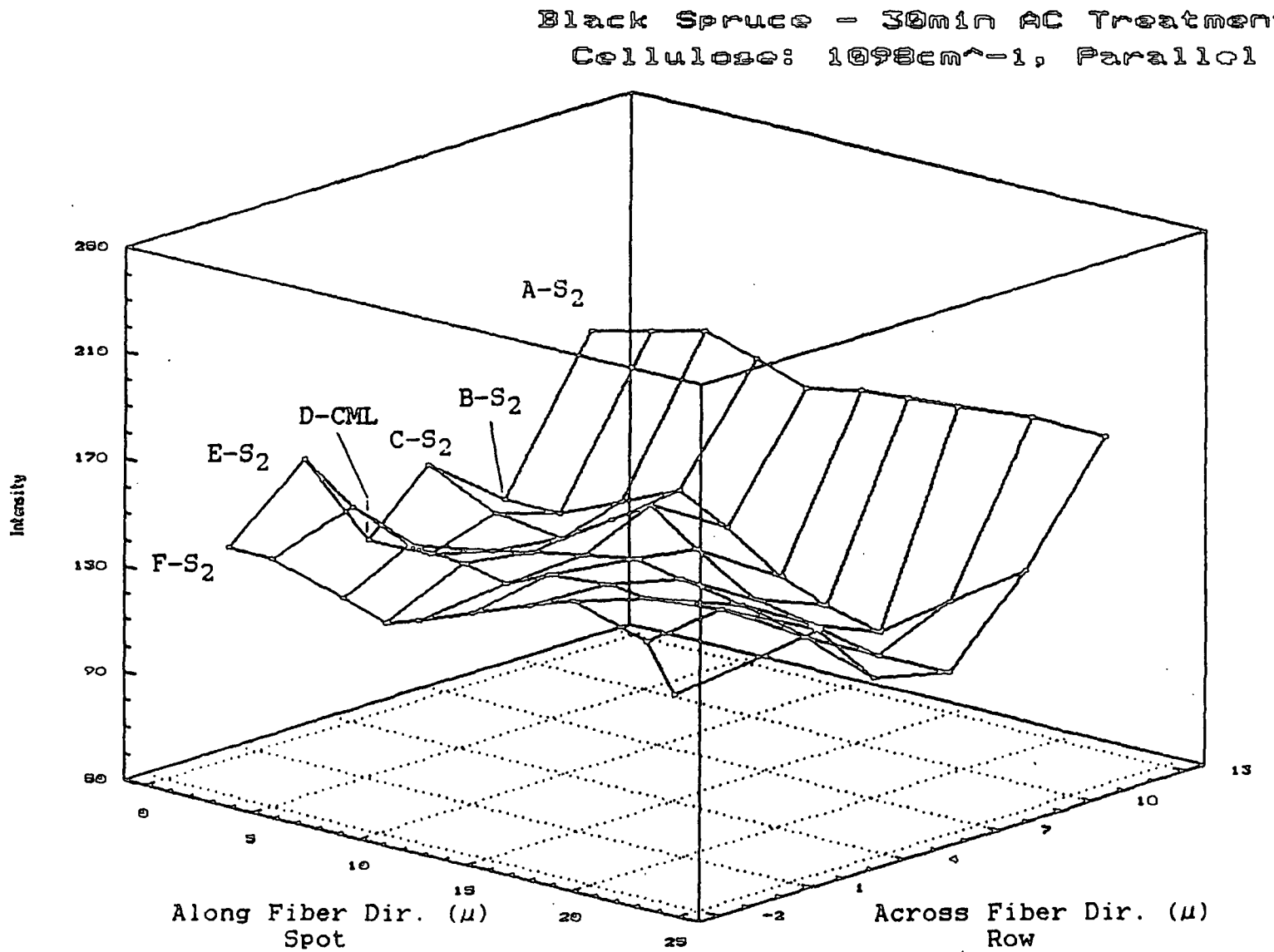

Figure 69. Topographic plot of cellulose's 1098 cm^{-1} band intensity vs. cell wall location for black spruce. EV parallel to the longitudinal axis of the fiber (radial section). The row F/spot 1 (leftmost point on the plot) analysis point served as the origin.

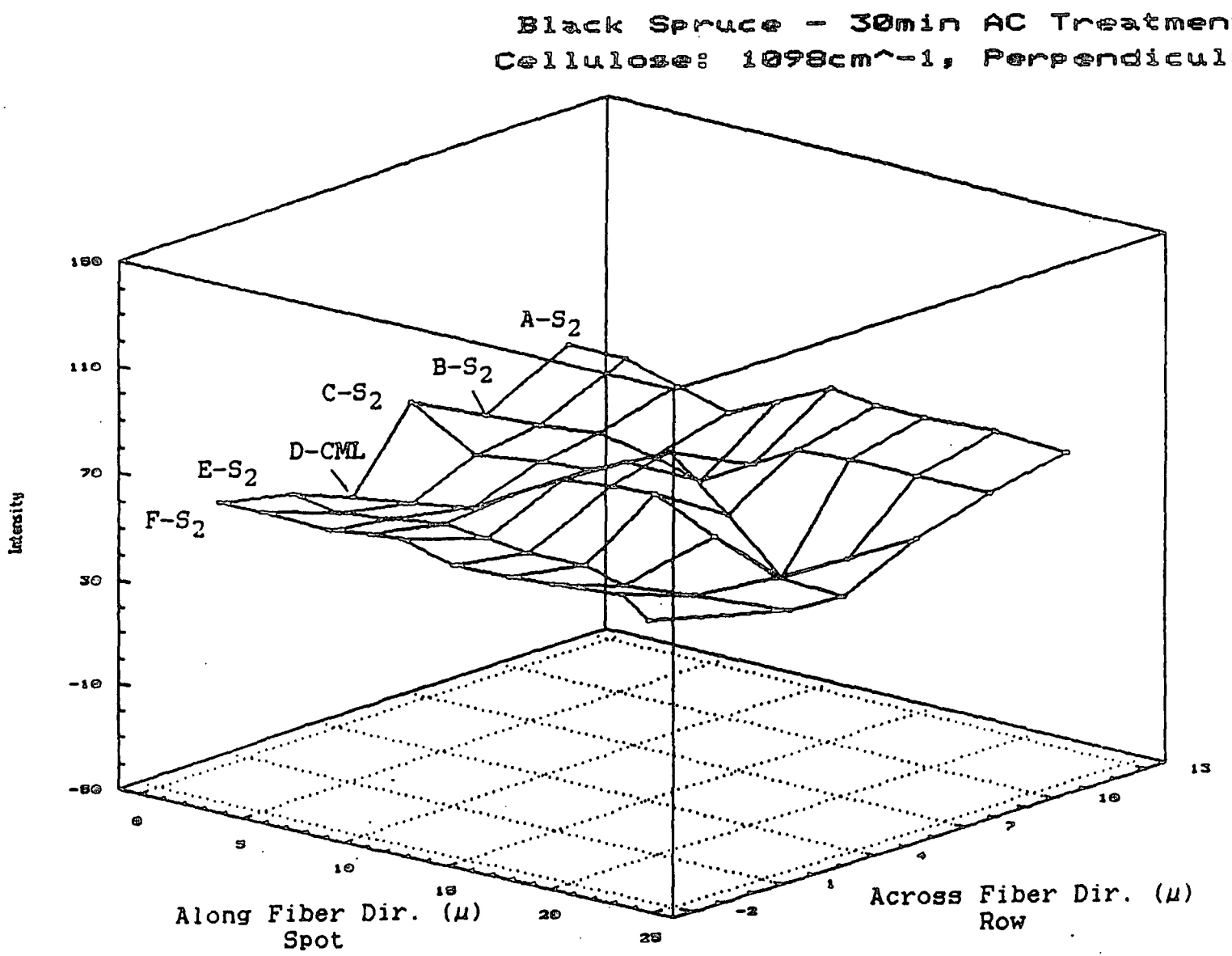

Figure 70. Topographic plot of cellulose's 1098 cm^{-1} band intensity vs. cell wall location for black spruce. EV perpendicular.

The general shape of both the parallel and perpendicular topographic plots is echoed in the concentration plot (Figure 71). Because of this, it is believed that the general shape of these plots is dictated more by concentration than orientation. Referring to this figure, it can be seen that the cellulose concentration is not uniform but varies over the different morphological cell wall regions. The concentration appears to decline across the cell wall in going from the lumen to the CML; however, this trend is not universal.. (For example, the concentration at the row C/spot 1 [S_2] location is greater than that at the neighboring S_2 and CML locations [row B/spot 1 and row D/spot 1, respectively].) This suggests that there is a variation in concentration not only between the different cell wall regions but also within a single region.*

The 1098 cm^{-1} band intensities at the row A data locations (located along the inner S_2) for both the parallel and perpendicular EV orientations were found to be consistently much higher than the 1098 cm^{-1} band intensities at the other locations (rows B-F). The reason for this behavior is not known. No

*The "row" mapping data for cellulose and lignin concentration in both of the woody species were subjected to regression analysis to determine if the trends in Raman band intensity seen along the fiber were linear. In general, the R^2 values were very low and typically did not exceed 0.3. This suggested that either the trends in the data were not highly linear or that if linearity occurred, it was on a finer scale than 25 microns.

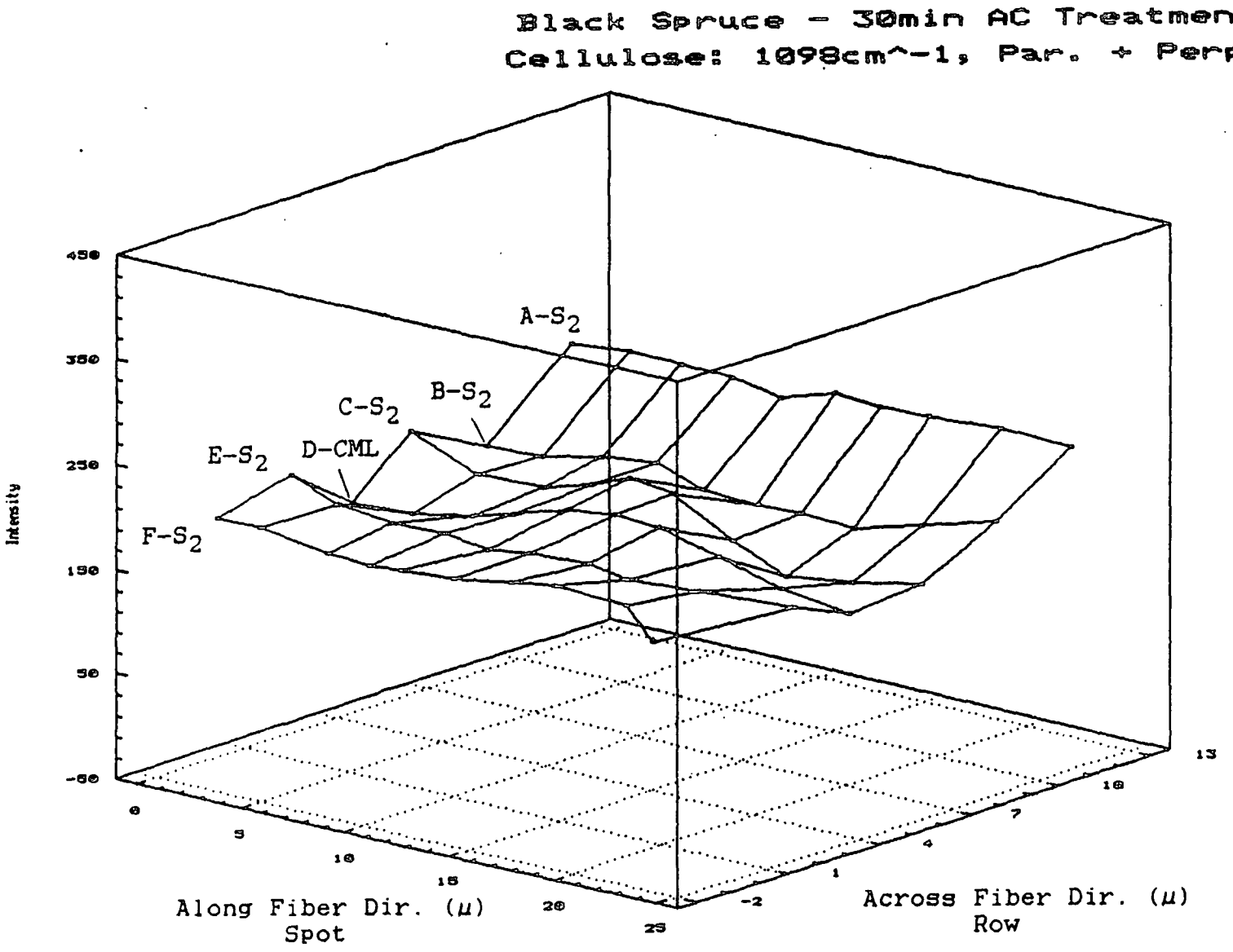

Figure 71. Topographic plot of cellulose concentration vs. cell wall location. EV parallel + perpendicular 1098 cm^{-1} band intensities.

gross differences between this row and the others were apparent in the video images. (The cellulose concentration in the neighborhood of the S_2-S_3 interface has been reported to be slightly lower than the concentration in the middle of the S_2 layer[4], not higher.)

The row averages were also analyzed to more clearly see the trends in organization between the various morphological regions. (Attempts to correlate the fine morphological features with the data were not successful. For the most part, data from regions that visually appeared different did not show significant differences. Thus only the gross morphology, i.e., inner/outer S_2 and CML, was used in the following analysis.)

Table 18 presents the row means and their standard deviation for black spruce. Each mean represents the average intensity over a ≈20 micron long by ≈1.5 micron wide region of the cell wall (five locations, ≈5 microns apart). (The interpolated orientation values, which were used in the topographic plots, were not included in this analysis.) As can be seen from this table, the standard deviation varies significantly from location to location. It is not known if this is an artifact caused by the methodology used or is indicative of variability in the biopolymers' organization from one cell wall location to another.

The cellulose data are plotted in Figure 72. This figure shows the variation in cellulose's 1098 cm^{-1} band intensity over the different cell wall

Table 18. Acid-Chlorite Treated Black Spruce Row Means and Standard Deviations.(1)

	Cellulose 1098 cm^{-1} Band Intensity						Lignin 1595 cm^{-1} Band Intensity					
	Parallel		Perpendicular		P+P		Parallel		Perpendicular		P+P	
Location	Mean	σ	Mean	σ	Mean	σ	Mean	σ	Mean	σ	Mean	σ
S_2	173.0	5.0	66.9	6.7	239.9	3.8	175.8	8.5	159.2	7.3	335.0	13.2
S_2	118.5	15.5	55.2	8.9	173.6	18.2	118.9	13.9	121.0	5.8	239.8	13.5
S_2	119.2	16.2	52.6	13.7	169.3	28.2	103.7	20.9	108.1	10.5	207.8	11.0
CML	122.1	8.8	48.5	11.5	170.5	18.2	104.9	28.3	110.0	29.4	214.8	56.9
S_2	137.8	9.0	46.2	2.3	186.9	9.3	122.4	23.3	115.9	24.7	243.5	38.1
S_2	127.9	10.9	52.0	2.5	179.1	10.2	109.2	23.7	96.6	11.3	209.2	33.6

Lignin/Cellulose 1595/1098 Ratio

	Parallel		P+P	
	Mean	σ	Mean	σ
S_2	1.02	0.04	1.40	0.08
S_2	1.02	0.18	1.39	0.14
S_2	0.87	0.17	1.25	0.23
CML	0.87	0.28	1.29	0.46
S_2	0.88	0.11	1.30	0.17
S_2	0.85	0.19	1.17	0.19

(1) Perpendicular data corrected for dichroic effects, 1098 cm^{-1} band: perp./1.33; 1595 cm^{-1} band: perp./1.8.

regions.

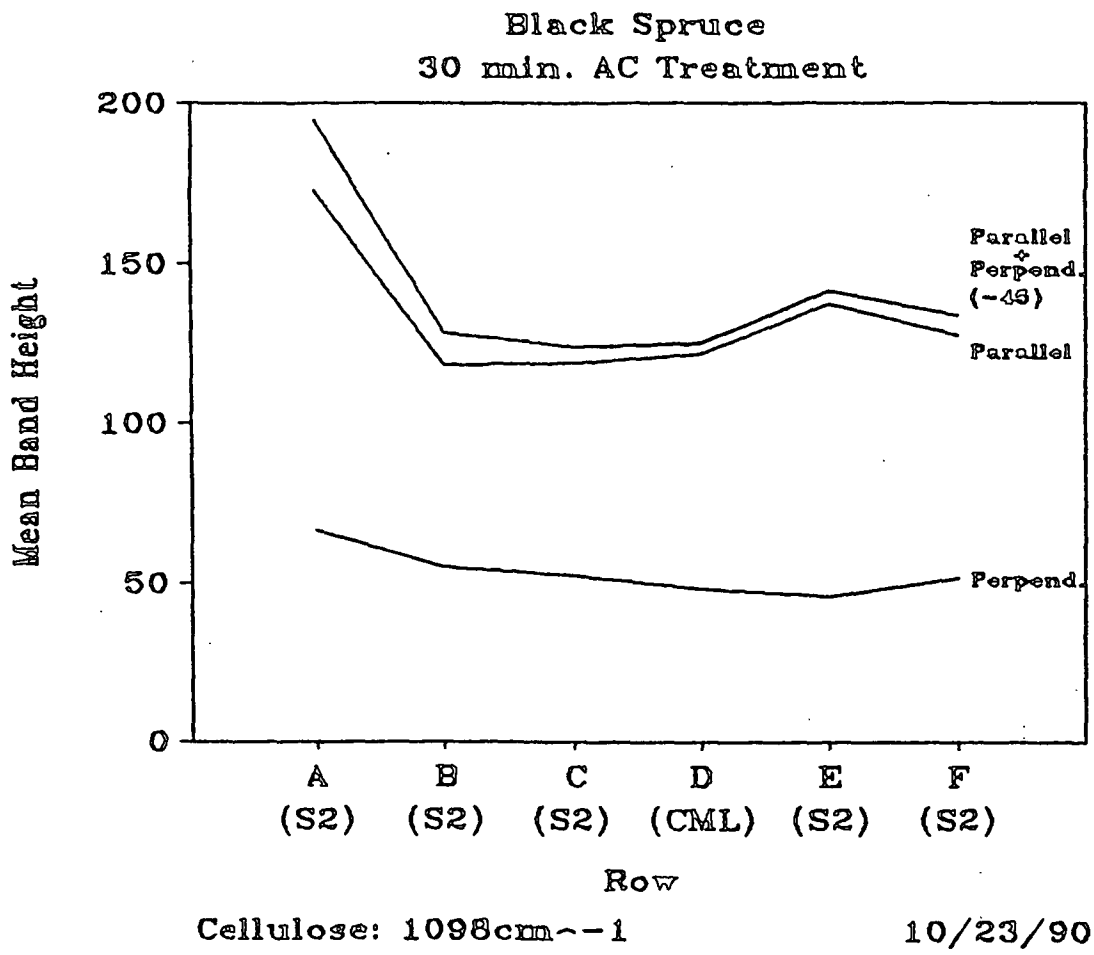

Figure 72. The variation of cellulose's 1098 cm^{-1} band intensity over different morphological regions in the latewood cell walls of acid-chlorite treated black spruce fibers.

It can be seen from Figure 72 that, on the average, the parallel intensity values are substantially greater than the perpendicular intensity values for all of the cell wall locations. This most likely reflects the preferential orientation of the chain axis of cellulose in planes parallel to the

cell wall (radial section). These data further suggest that for one of the fibers ("A-D" fiber), the chain axis of cellulose is slightly more oriented parallel to the cell wall (radial section) in the inner S_2 and this orientation becomes less pronounced closer to the CML. This preferential orientation is not as apparent for the adjoining fiber ("D-F" fiber).

Assuming that cellulose does not vary greatly in orientation over a 2.5 micron distance, the EV parallel + perpendicular data indicate that the peak cellulose concentration occurs in the inner S_2 and declines to a minimum in the outer S_2 for one fiber ("A-D" fiber). It remains at that level in the CML region between the fibers. The adjoining fiber ("D-F" fiber) shows a flatter cellulose profile. For this fiber, only a slight peak in concentration is seen to occur in the middle of the S_2 wall layer. Figure 73 shows a summation of known and inferred data for the distribution of the cell wall constituents in conifers.[4] The Raman cellulose concentration data for the "D-F" fiber parallel the average trend seen in this figure, i.e., the peak cellulose concentration occurred in the inner S_2 cell wall layer and declined to a minimum near the compound middle lamella. The "A-D" fiber does not show this same trend which is due in part to the higher "A" value.

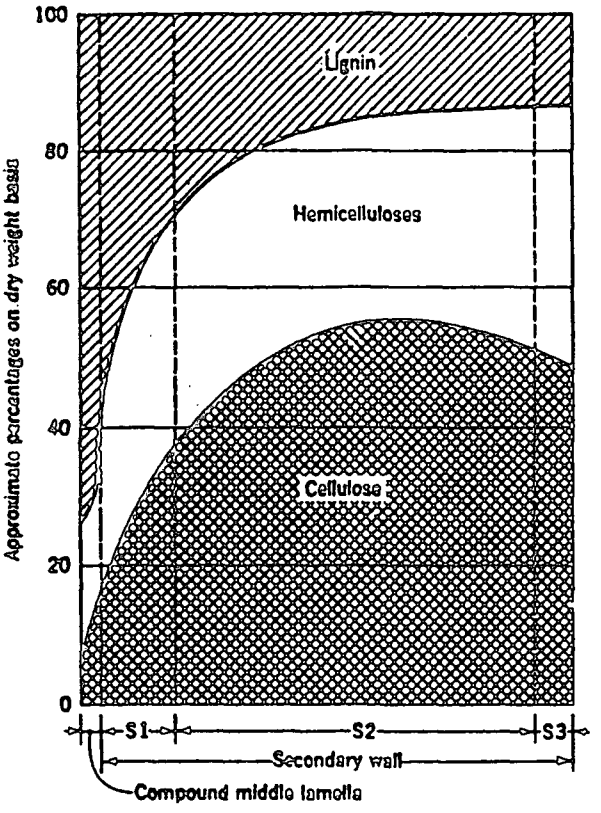

Figure 73. Distribution of the principal chemical constituents within the various layers of the cell wall in conifers.[4]

The topographic plots of lignin's 1595 cm^{-1} band intensity *vs.* cell wall location are shown in Figures 74-76: Figure 74 - EV parallel; Figure 75 - EV perpendicular; Figure 76 - EV parallel + EV perpendicular. Comparing Figures 74 and 75, it can be seen that the general shape of the plots is, for the most part, similar and that the parallel intensity values are only slightly greater than the perpendicular values. These data suggest that the aromatic rings in lignin are only slightly preferentially oriented in planes parallel

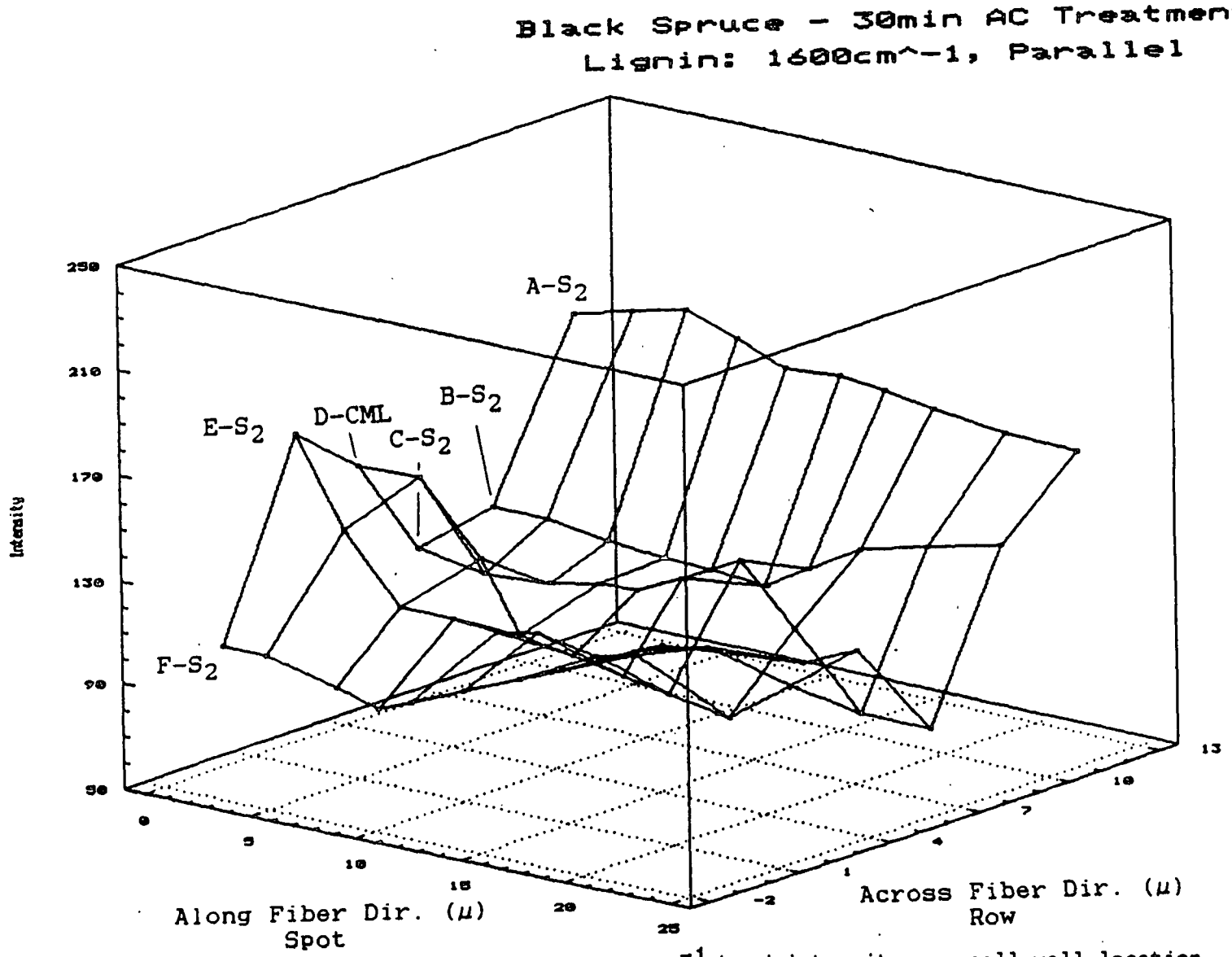

Figure 74. Topographic plot of lignin's 1595 cm^{-1} band intensity vs. cell wall location for black spruce. EV parallel to the longitudinal axis of the fiber (radial section). The row F/spot 1 (leftmost point on the plot) analysis point served as the origin.

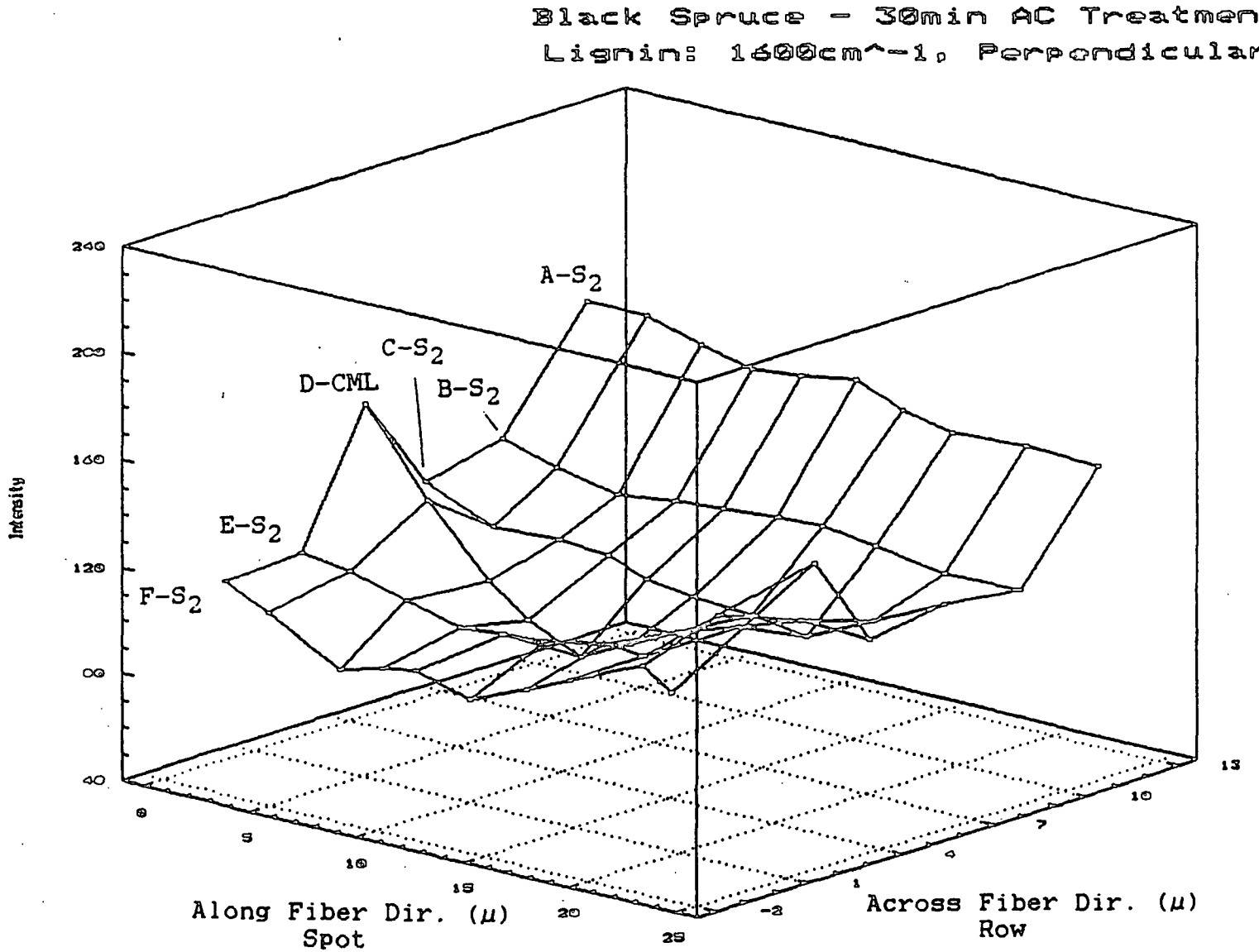

Figure 75. Topographic plot of lignin's 1595 cm^{-1} band intensity vs. cell wall location for black spruce. EV perpendicular.

to the cell wall (radial section). There also appear to be regions where this preferential orientation is not seen; this is especially apparent in the CML region. This latter observation may be indicative of the occurrence of nodes in the molecular orientation of lignin.

The general shape of the EV parallel, EV perpendicular, and concentration (EV parallel + EV perpendicular) plots (Figures 74, 75, and 76, respectively) is, for the most part, similar. Because of this similarity, it is believed that the general shape of these plots is primarily due to concentration rather than orientation. Referring to Figure 76, it can be seen that the lignin concentration is not uniform but varies over the different morphological cell wall regions. The concentration appears to decline from the lumen to CML; however, this trend is not universal. (For example, the concentration at the first few CML locations [row D, spots 1 and 2] is noticeably greater than the concentration at the surrounding S_2 wall locations [rows C and E, spots 1 and 2].) This suggests that there is a variation in concentration not only between the different cell wall regions but also within a single region. (These data probably still reflect band enhancement effects in spite of the acid-chlorite pretreatment. An outcome of this is that the observed trends are possibly the result of both concentration differences and localized variations in the structure of the lignin macromolecule. The latter would impact the degree of 1595 cm^{-1} band enhancement.)

As was the case with the cellulose data, the 1595 cm^{-1} band intensities

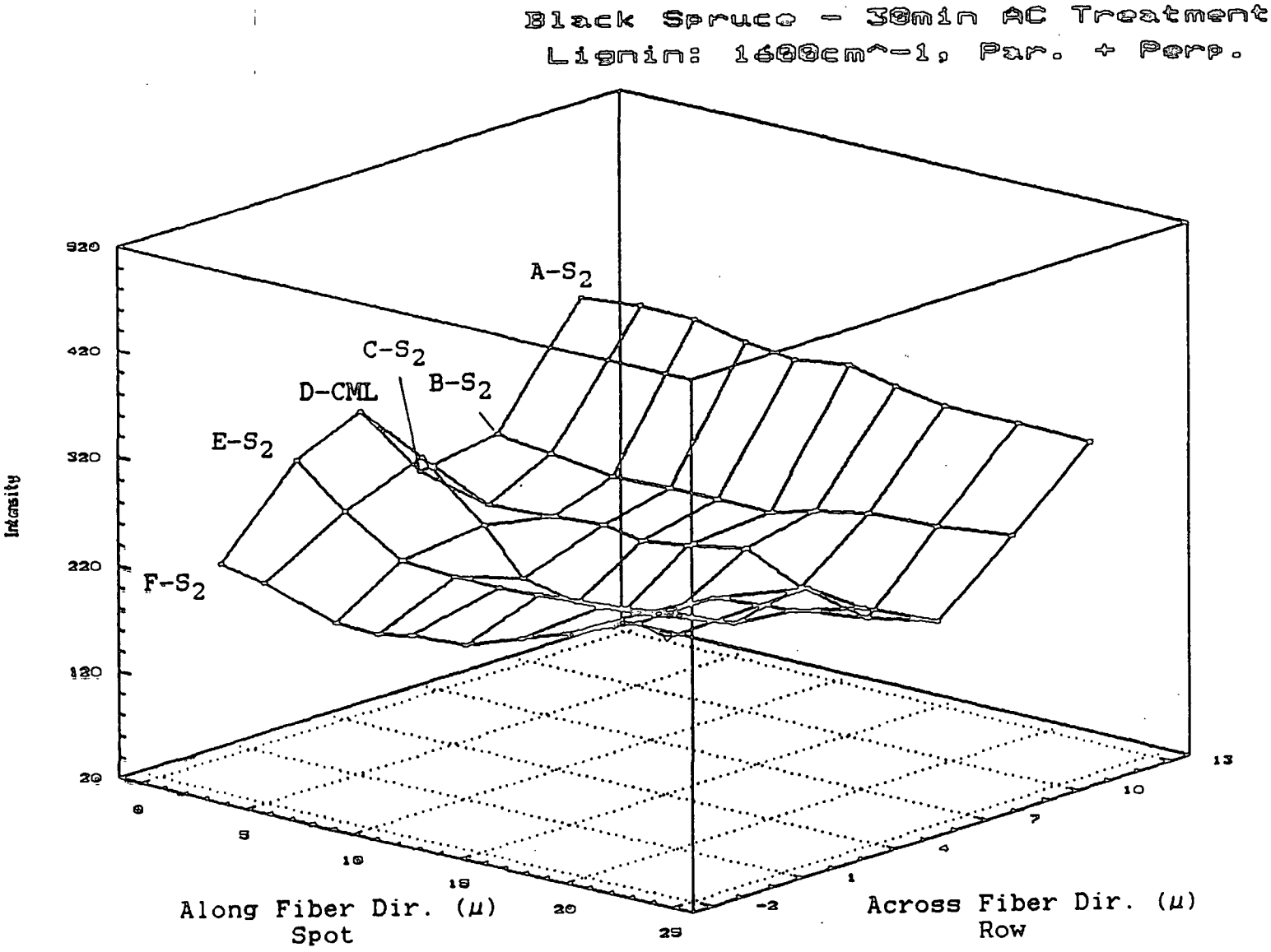

Figure 76. Topographic plot of lignin concentration vs. cell wall location. EV parallel + perpendicular 1595 cm^{-1} band intensities.

at the row A data locations for both the parallel and perpendicular EV orientations were found to be much higher than the 1595 cm^{-1} band intensities at the other locations (rows B-F). The fact that both cellulose and lignin data show this behavior suggests a common origin, but what that origin is remains unknown. (These row A data may reflect real variability within the cell wall, but further studies are needed to adequately address this issue.)

The row averages for the 1595 cm^{-1} band intensity were also analyzed to investigate the general trends in organization across the various morphological cell wall regions. These data are shown in Table 18, page 254, and plotted in Figure 77. (These values represent the average 1595 cm^{-1} intensity over a 20-micron region in the cell wall.) It can be seen from this figure that, on the average, the perpendicular intensity values are slightly greater than the parallel intensity values from the middle of the S_2 layer of one fiber though the CML region to the outer S_2 layer of the other fiber. It is not known if this reflects a preferential orientation of the aromatic rings in planes perpendicular to the cell wall (radial section) or is the result of the acid-chlorite pretreatment and/or an incorrect EV rotator band intensity correction factor.

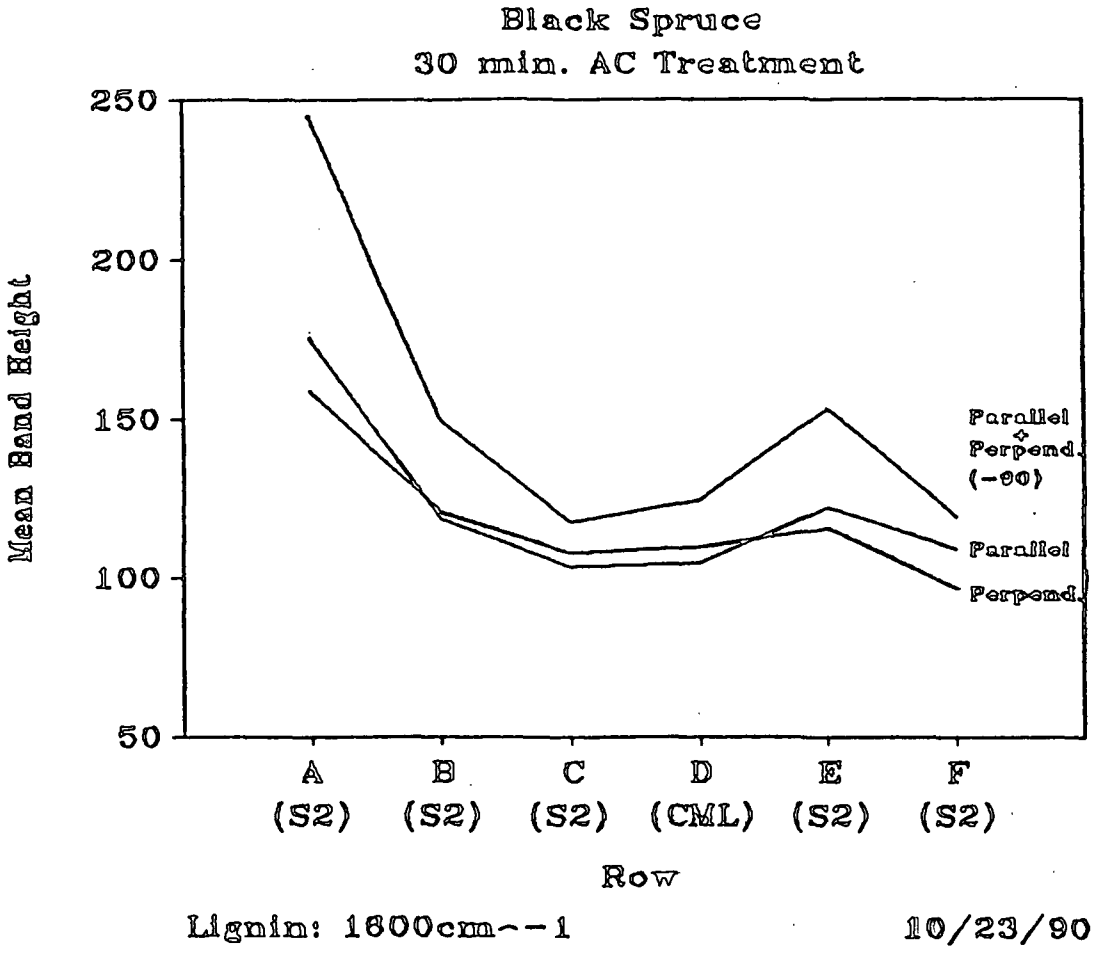

Figure 77. The variation of lignin's 1595 cm^{-1} band intensity over different morphological regions in the latewood cell walls of acid-chlorite treated black spruce fibers.

The EV parallel + perpendicular curve above, for the most part, parallels the cellulose (concentration) curve (Figure 72). The peak lignin concentration occurs in the inner S_2 (due to the high "A" value) and declines to a minimum in the outer S_2 for one fiber ("A-D" fiber). It then rises slightly in the CML region. The adjoining fiber ("D-F" fiber) shows a flatter lignin

profile. For this fiber, only a slight peak in concentration is seen to occur in the middle of the S_2 wall layer. Referring to Figure 73, the generally accepted distribution of lignin is a decrease from CML to inner S_2. These Raman data deviate from this distribution substantially. As indicated above, the CML region shows a very low lignin concentration. It is possible that the CML lignin was more sensitive to acid-chlorite treatment and consequently experienced a greater loss of band enhancement, thus impacting these "concentration" data.

The 1595/1098 cm^{-1} ratio was used to investigate the interrelationship between the macromolecular organization of cellulose and lignin. The topographic plots of this ratio vs. cell wall location are shown in Figures 78 and 79: Figure 78 - EV parallel; Figure 79 - EV parallel + EV perpendicular. The general shape of these plots is, for the most part, similar, which again suggests that orientation does not make a significant contribution to their general shape.

The 1595/1098 cm^{-1} ratio is fairly uniform over the cell wall region studied (Figure 79). This may be indicative of a uniformity in concentration of cellulose and lignin. (It may also be due, in part, to similar degrees of 1595 cm^{-1} band enhancement reflecting a uniformity in structure of the acid-chlorite treated lignin macromolecule.) An obvious exception to this uniformity occurs in the CML region, especially in the area of spots 1-3, where the ratio is substantially larger. These larger values reflect the higher

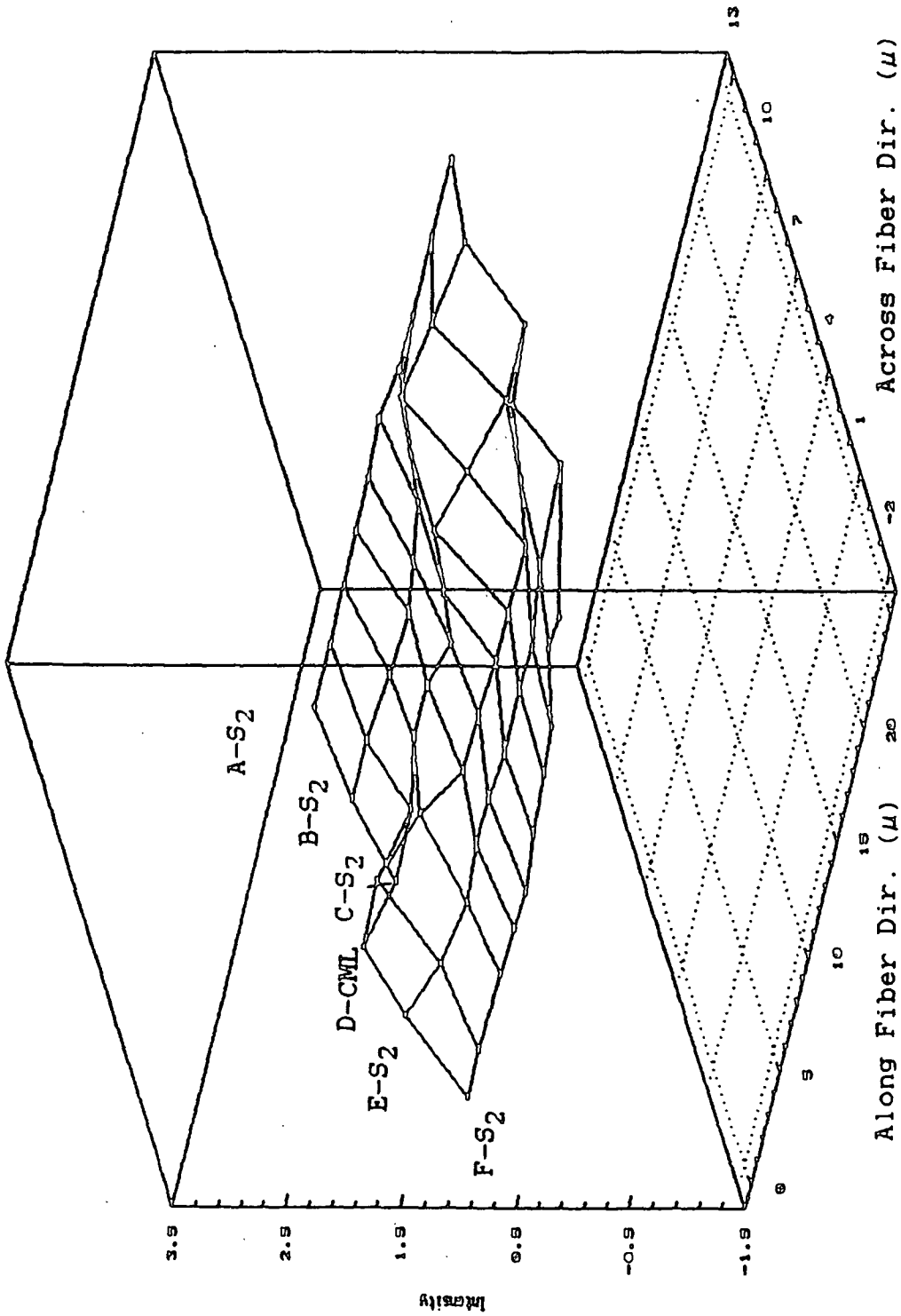

Figure 78. Topographic plot of the lignin-to-cellulose ratio (1595/1098 cm^{-1}) vs. cell wall location for black spruce. EV parallel to the longitudinal axis of the fiber (radial section). The row F/spot 1 (leftmost point on the plot) analysis point served as the origin.

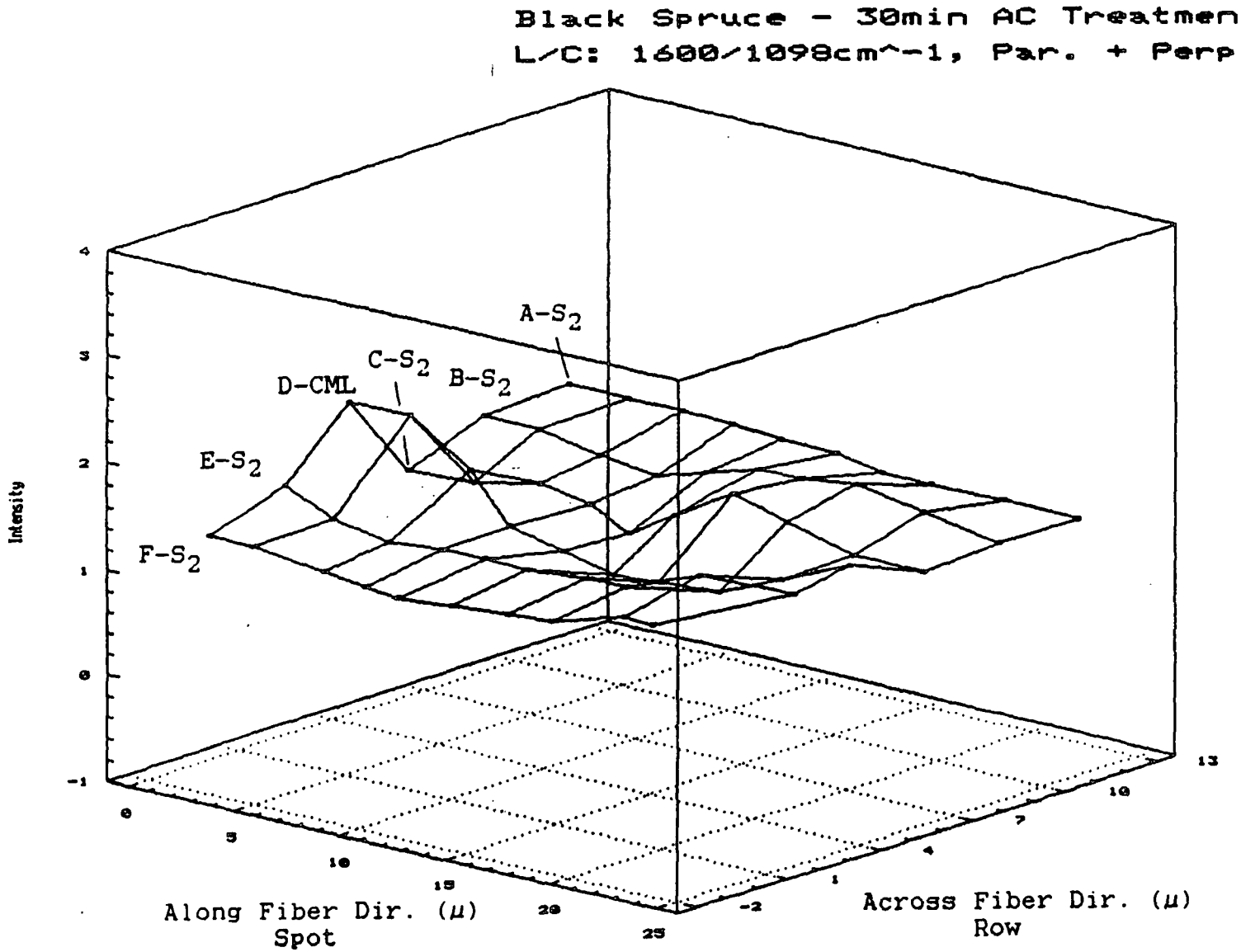

Figure 79. Topographic plot of the lignin-to-cellulose ratio (1595/1098 cm^{-1}) vs. cell wall location for black spruce. EV parallel + perpendicular.

lignin concentration and/or degree of residual 1595 cm^{-1} band enhancement in this region and are probably indicative of regional differences in the organization of lignin. (The lignin topographic plots (Figures 74-76) show this same feature.)

The variation of the average 1595/1098 cm^{-1} ratio over the different morphological regions of acid-chlorite treated black spruce is shown in Figure 79. As was seen in the 1595/1098 cm^{-1} topographic plots, the lignin-to-cellulose ratio is fairly uniform over the area investigated. For one of the fibers, the average ratio (EV parallel + perpendicular curve) decreases slightly from the inner S_2 to the outer S_2 cell wall layer, while the opposite trend is observed for the adjoining fiber. To what extent these data suggest a uniformity in the concentration of cellulose and lignin is unknown for the reason given in the preceding paragraph.

It is not known to what extent these data represent the native-state organization of cellulose and (especially) lignin in black spruce cell walls. The purpose of the acid-chlorite (AC) pretreatment was to modify the initial protracted drop in 1595 cm^{-1} band intensity during laser irradiation. It was envisioned that the AC treatment would minimize the bias introduced by the photomodification of lignin. (This treatment was shown to disrupt CE/PRRE of 1595 cm^{-1} band, but not alter the percent lignin content. In several of the acid-chlorite decay studies, the initial precipitous drop in 1595 cm^{-1} band intensity was not seen but only a gradual decline in intensity during 514.5 nm

laser exposure, while in others, the AC decay curve was not significantly different from the control.) Whether this pretreatment was successful is difficult to assess. It may have minimized the bias introduced by lignin decay but it also may have disrupted CE/PRRE of the 1595 cm^{-1} in a nonuniform manner, i.e., CML lignin appeared to be more sensitive to acid-chlorite than lignin in the S_2 cell wall layer.

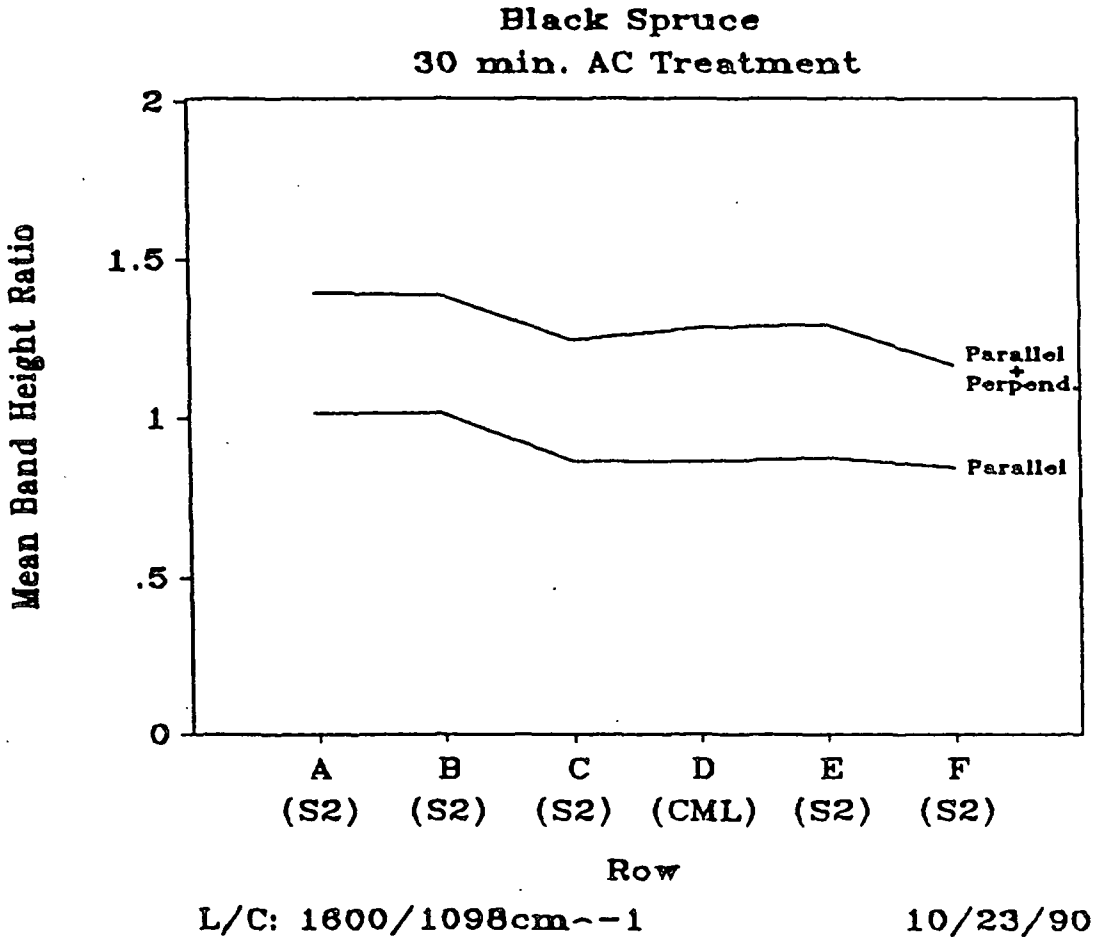

Figure 79. The variation of the 1595/1098 cm^{-1} ratio over different morphological regions in the latewood cell walls of acid-chlorite treated black spruce.

Loblolly Pine

Figure 80 shows the cell wall area used in the mapping studies of loblolly pine before (a) and after (b) 90 seconds of irradiation. The wide feature, which runs left to right just above the center of the micrograph, is a lumen. The finger-like projections which extend into the lumen are probably a sectioning artifact. As was the case for black spruce, a substantial disruption appears to have occurred during this 90-second time interval. The cell wall markings appear to vary in size and intensity. The reason for these variations is not known but conceivably could be due to microscope focus effects and/or variations in the sensitivity of lignin to 514.5 nm radiation.

(a)

Figure 80. Video enhanced prints showing the area used in the mapping studies of loblolly pine before (a) and after (b) irradiation. The grid pattern is depicted in (c). Locations are numbered 1-10 (L to R). Radial section.

(b)

(c)

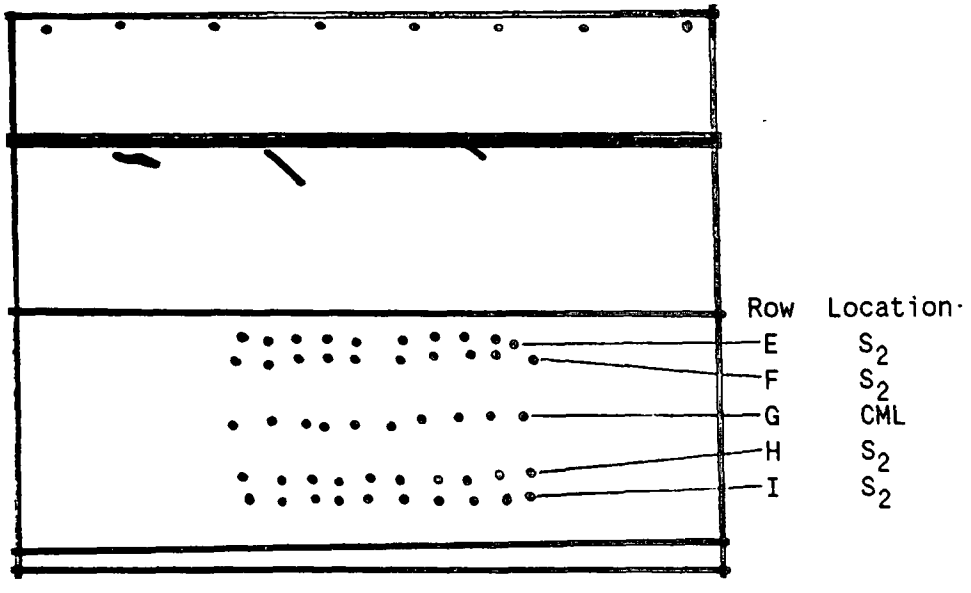

Figure 80 contd. Video enhanced prints showing the area used in the mapping studies of loblolly pine before (a) and after (b) irradiation. The grid pattern is depicted in (c). Locations are numbered 1-10 (L to R). Radial section.

Figures 80c and 81 show the approximate locations of data points. (The cell wall region investigated is where the lower irradiation marks are located. Row A, spot 1 is the upper left mark; the mark to the left of and between Rows A and B occurs at the location used to "condition" the A1 spot as described in EXPERIMENTAL MATERIAL AND METHODS - EXPERIMENTAL PROGRAM.) The sampling grid was 10 (along the longitudinal axes of the fibers) by 5 (perpendicular to the longitudinal axes of the fibers). This grid area included three distinct morphological regions: the S_2 cell wall layer from one fiber (rows E and F), the compound middle lamella between (row G), and the S_2 layer of the adjoining fiber (rows H and I). A total of 50 data points was used in the analysis.

The position and spacing of the analysis points shown in Figure 81 and used in the topographic plots were determined from Figure 80b with the aid of the Extended Analysis Module in Image-Pro II image processing software. The row I, spot 1 (bottom row, first spot on the left) analysis point served as the origin. As was the case for black spruce, the irregular spacing of points was due to the difficulty in accurately positioning the cell wall in relationship to the optical axis of the microscope/laser beam.

Figures 82-89 show the topographic plots of Raman band intensity vs. cell wall location. Because of the various assumptions which were made in order to map cellulose and lignin organization, these plots should be considered zero order approximations and are meant to show trends and not absolute values.

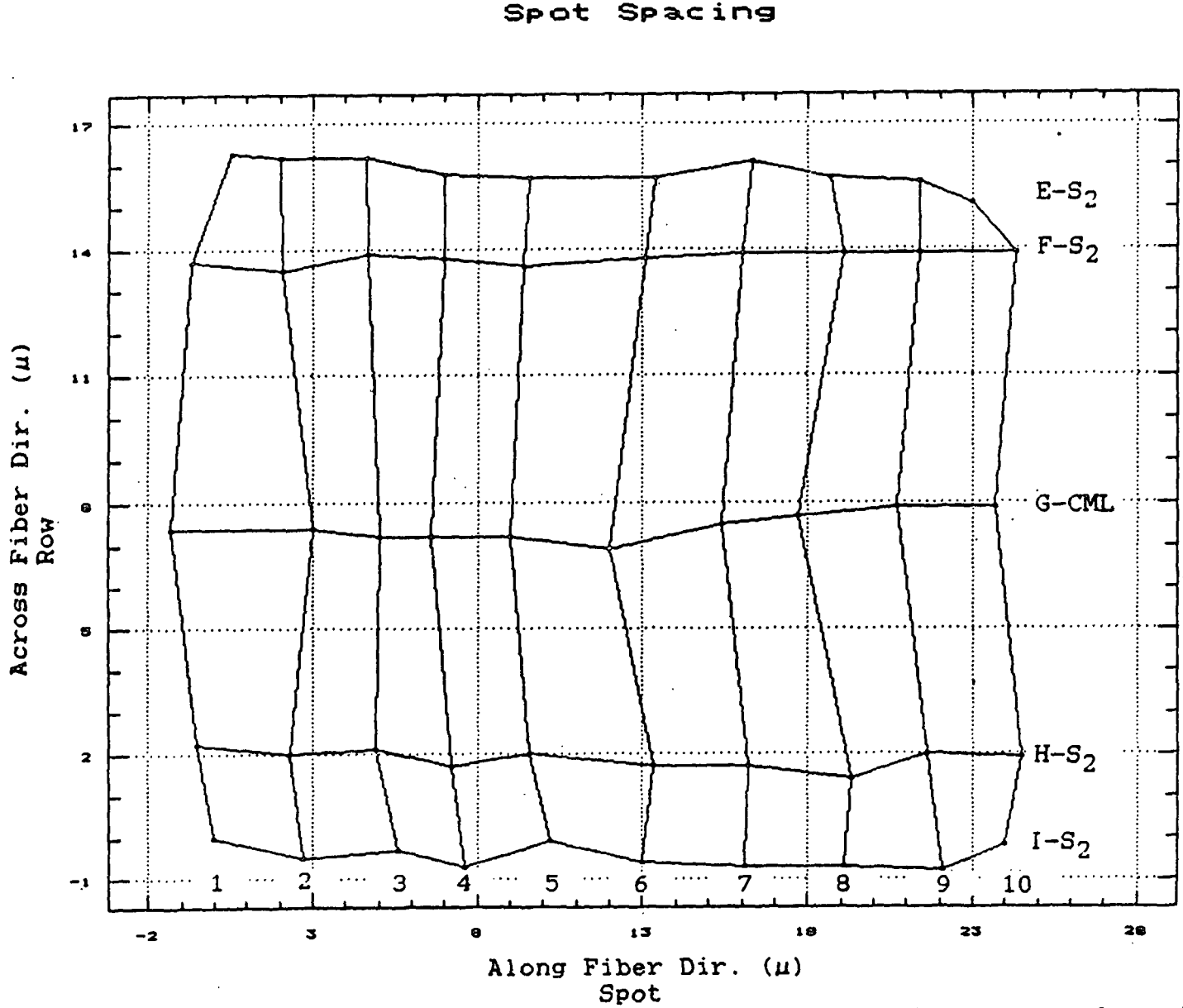

Figure 81. The position and spacing of the analysis points used in the spectral mapping study of loblolly pine cell wall organization. The row I, spot 1 (bottom row, first spot on the left) analysis point served as the origin.

The (EV) parallel and perpendicular pair of spectra could not be obtained from the same location because of lignin decay. To circumvent this difficulty, it became necessary to collect parallel information from the first location, perpendicular from the next location, parallel from the third, and so forth along the fiber. Thus in these topographic plots, the "parallel" data were collected from row E: spots 1, 3, 5, 7, and 9; row F: spots 2, 4, 6, 8, 10; row G: spots 1, 3, etc. while the "perpendicular" data were collected from row E: spots 2, 4, 6, 8, 10; row F: spots 1, 3, 5, etc. The missing intensities were determined by linear interpolation. For those locations where interpolation was not possible (i.e., the end points), the neighboring (row) intensity value was used.

Figures 82-84 are topographic plots of cellulose's 1098 cm^{-1} band intensity vs. cell wall location: Figure 82 - EV parallel; Figure 83 - EV perpendicular; Figure 84 - EV parallel + EV perpendicular.* Comparing Figures 82 and 83, it can be seen that the general shape of the parallel and perpendicular plots is somewhat similar. Both plots show a v-shape with the minimum occurring in the CML region; the v-shape is very pronounced in the parallel plot, while it is much flatter in the perpendicular plot. In general, the parallel intensity values are greater, which most likely reflects the preferential orientation of the chain axis of cellulose in planes parallel

*Selected spectra and band height vs. location plots can be found in Appendix 10.

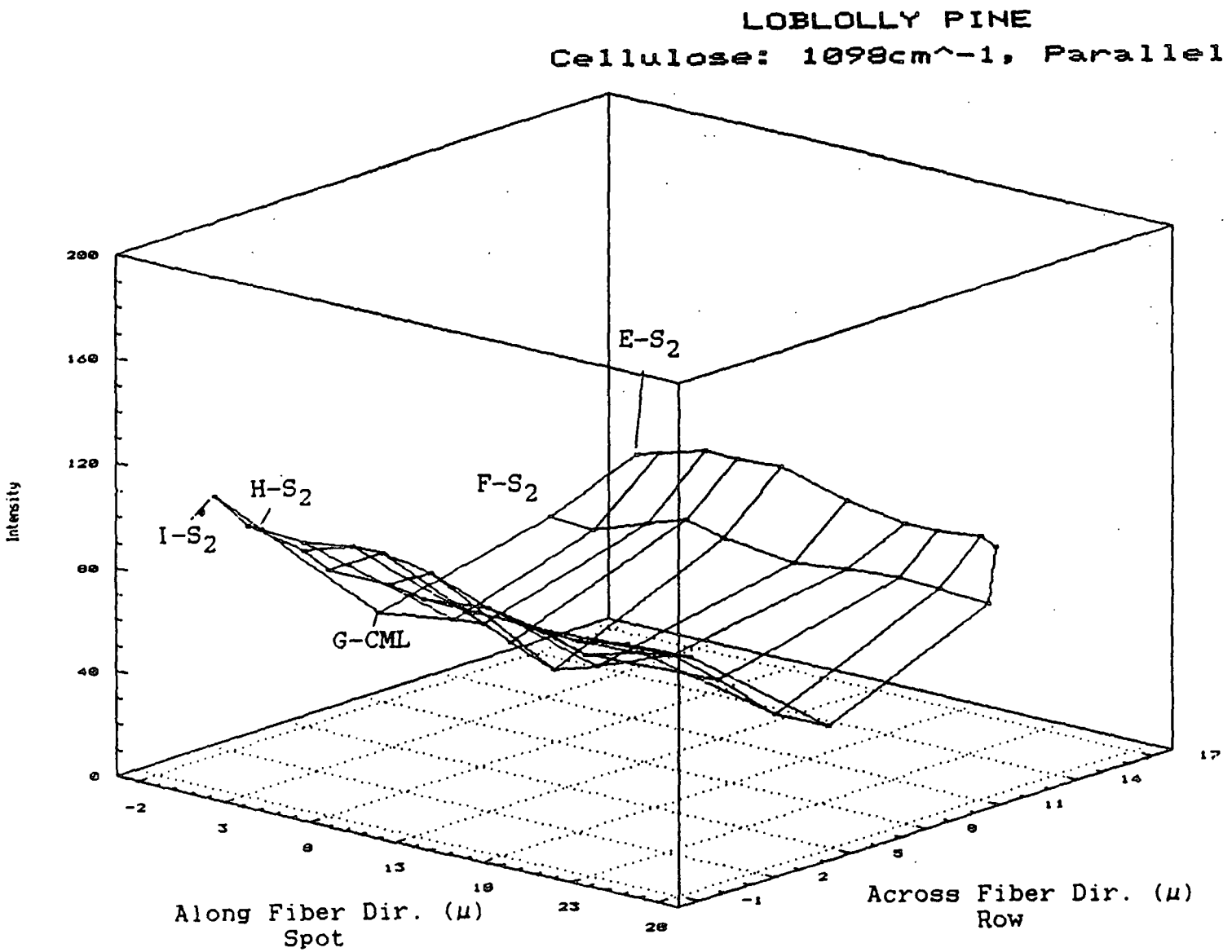

Figure 82. Topographic plot of cellulose's 1098 cm^{-1} band intensity vs. cell wall location for loblolly pine. EV parallel to the longitudinal axis of the fiber (radial section). The row I/spot 1 (leftmost point on the plot) analysis point served as the origin.

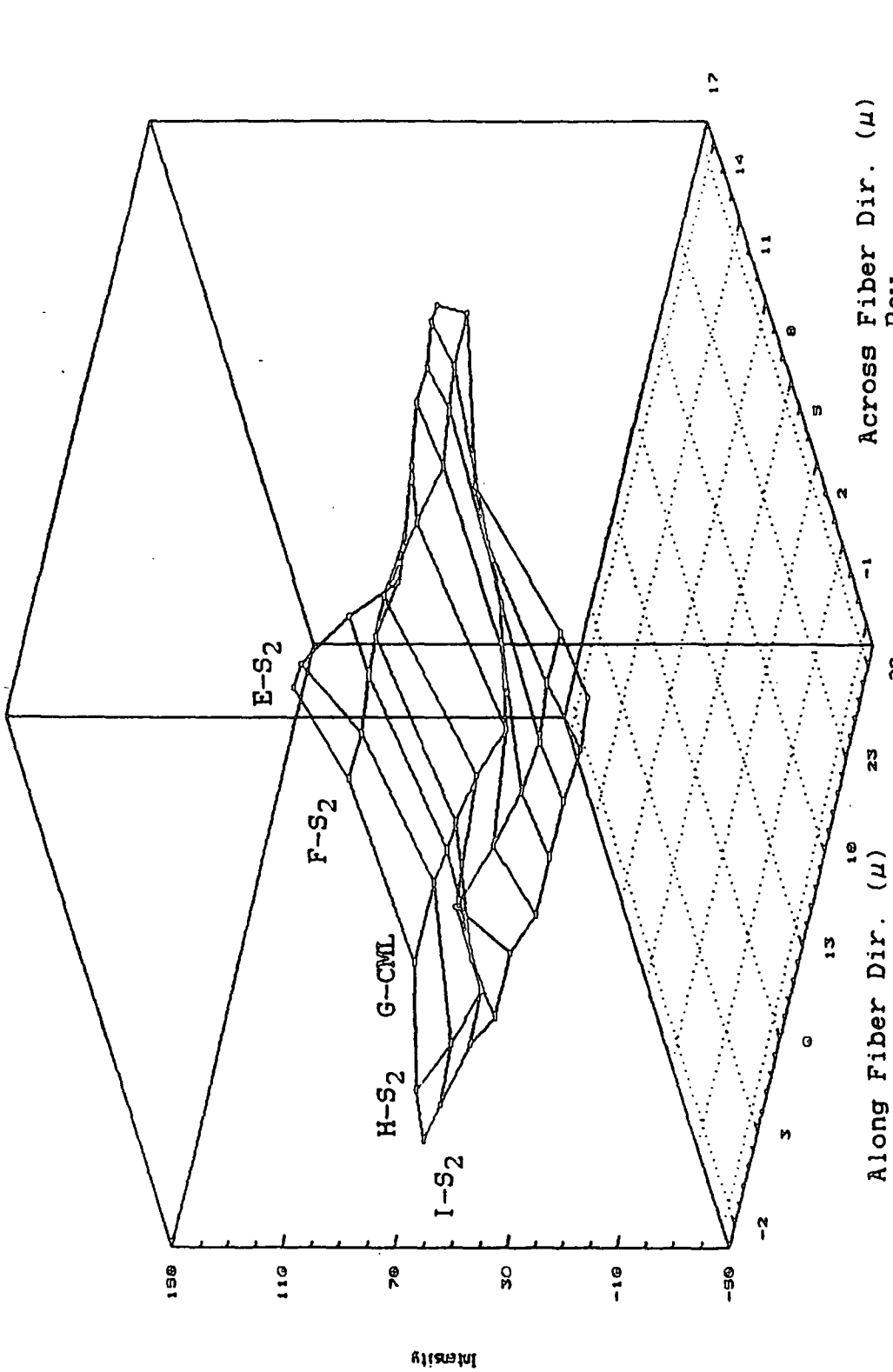

Figure 83. Topographic plot of cellulose's 1098 cm^{-1} band intensity vs. cell wall location for loblolly pine. EV perpendicular.

to the cell wall (radial section). (The localized regions of higher intensity, e.g., at locations row E/spot 2 [S_2] and row H/spot 5 [S_2], in the perpendicular plot may be indicative of the occurrence of nodes in the molecular organization of cellulose. The fact that these regions of higher intensity are not as apparent in the parallel topographic plot suggests that they are primarily caused by differences in cellulose orientation rather than concentration.)

The general shape of both the parallel and perpendicular topographic plots is mirrored in the concentration plot (Figure 84). Because of this similarity in shape, it is believed that the overall shape of these plots is dictated more by concentration than by orientation. In this figure, it can be seen that the cellulose concentration is not uniform but varies over the different morphological cell wall regions. The concentration appears to decline across the cell wall in going from the inner S_2 (row E or I) to the CML (row G). This trend is fairly universal over the region studied. There is one region (spot 5/rows I, H, and G) which obviously deviates from this trend. Here the concentration rises slightly in going from the inner S_2 (row I) to outer S_2 (row H) and then declines to a minimum in the CML region (row G). This particular trend parallels the generally accepted cellulose distribution within conifer cell walls (Figure 73). (This area also showed a higher EV perpendicular intensity, which suggests that both concentration and orientation play a part.) These data suggest that a variation in concentration occurs not only between the different cell wall regions but also within a single region.

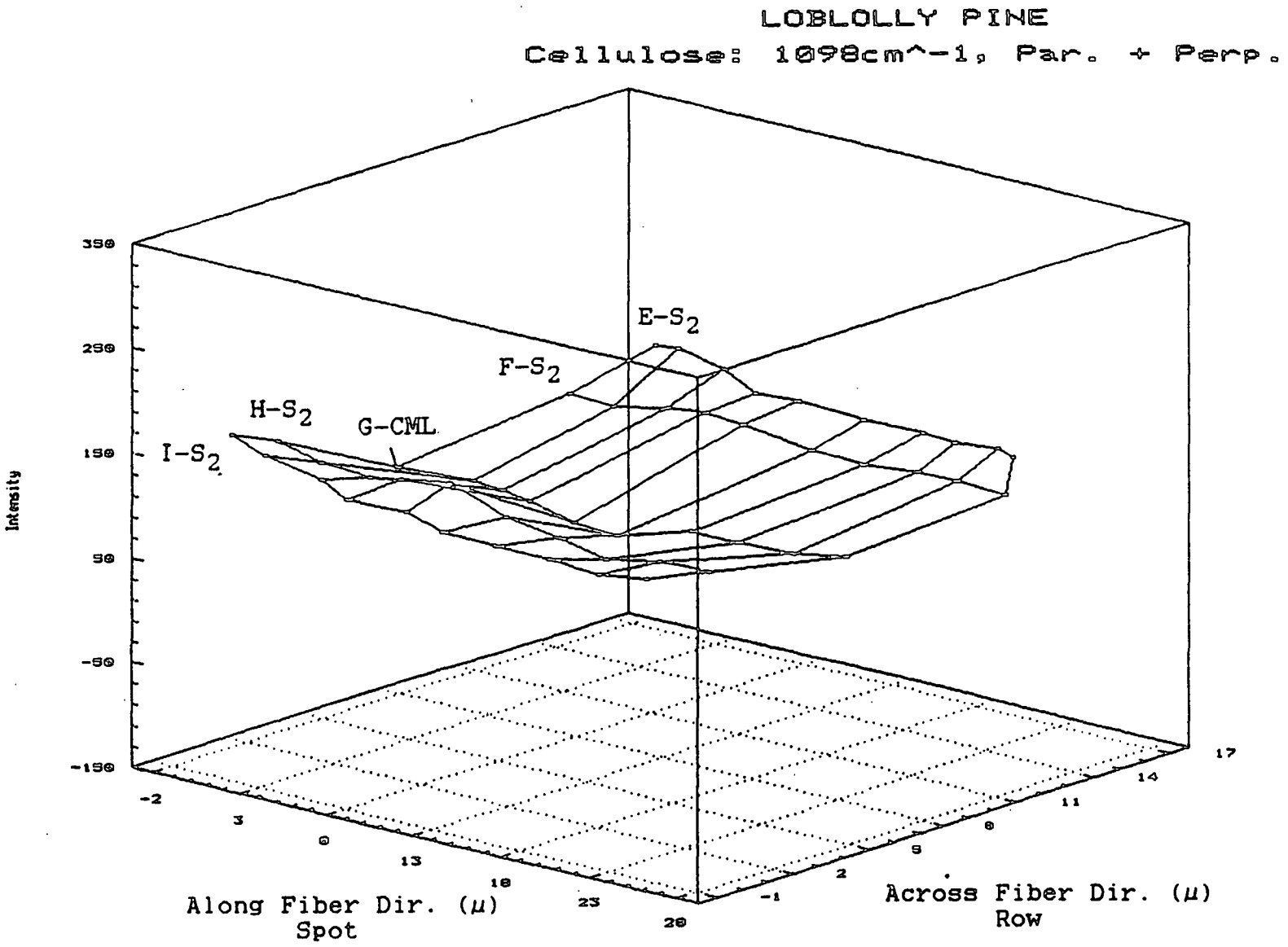

Figure 84. Topographic plot of cellulose concentration vs. cell wall location. EV parallel + perpendicular 1098 cm^{-1} band intensities.

The row averages were also analyzed to more clearly see the trends in organization between the various morphological regions. (As was the case with black spruce, there appeared to be little correlation between fine morphological features and the Raman data. For example, the cellulose concentration data from location row E/spot 6 [Figure 84] was not significantly different from the row E/spots 5 & 7 data even though the row E/spot 6 location appeared visually different, i.e., darker [Figure 80]. Thus only the gross morphology, i.e., inner/outer S_2 and CML, was used in the following analysis.)

Table 19 presents the row means along with their standard deviations for each Raman band. Each mean represents the average intensity over a ≈20 micron long by ≈1.5 micron wide region of the cell wall (five locations, ≈5 microns apart). (The interpolated orientation values, which were used in the topographic plots, were not included in the analysis.) In contrast to black spruce, the standard deviations for the parallel and perpendicular cellulose data fall into a rather narrow range (EV parallel σ: black spruce - 5.0 to 16.2; loblolly pine - 3.9 to 8.1). This may be indicative of a more uniform organization of cellulose along, i.e., parallel to, the fiber wall in loblolly pine compared to black spruce (at least for the cell wall regions investigated). The CML standard deviations for the loblolly pine lignin data are generally smaller than the neighboring S_2 values. It is conceivable that the CML lignin was more sensitive to 514.5 nm photons and thus quickly experienced a "leveling" of intensity, i.e., conjugation and preresonance Raman enhancement

Table 19. Loblolly Pine Row Means and Standard Deviations.(1)

	Cellulose 1098 cm^{-1} Band Intensity						Lignin 1595 cm^{-1} Band Intensity					
	Parallel		Perpendicular		P+P		Parallel		Perpendicular		P+P	
Location	Mean	σ	Mean	σ	Mean	σ	Mean	σ	Mean	σ	Mean	σ
S_2	77.4	5.2	42.3	9.7	119.7	7.6	316.2	30.1	273.6	36.2	589.8	56.8
S_2	60.7	3.9	42.2	4.2	102.9	5.1	253.7	19.7	229.1	17.7	482.8	35.1
CML	37.9	6.9	38.9	9.6	76.8	10.2	297.4	21.9	278.7	14.4	576.1	26.8
S_2	81.2	7.9	48.3	7.4	129.5	10.7	267.6	21.4	258.1	25.9	525.7	46.4
S_2	93.9	8.1	46.2	8.3	140.1	16.4	319.1	46.1	274.6	28.9	593.8	74.6

Lignin/Cellulose 1595/1098 Ratio

	Parallel		P+P	
	Mean	σ	Mean	σ
S_2	4.08	0.27	4.94	0.55
S_2	4.21	0.55	4.71	0.53
CML	8.00	1.12	7.62	1.08
S_2	3.31	0.28	4.07	0.29
S_2	3.39	0.29	4.24	0.31

(1) Parallel data corrected for dichroic effects, 1098 cm^{-1} band: par. x 1.33; 1595 cm^{-1} band: par. x 1.8. This method inflates L/C ratio ≈ 35%.

were very quickly disrupted.

The cellulose data are plotted in Figure 85. This figure shows the variation in intensity of cellulose's 1098 cm^{-1} band over the various morphological regions.

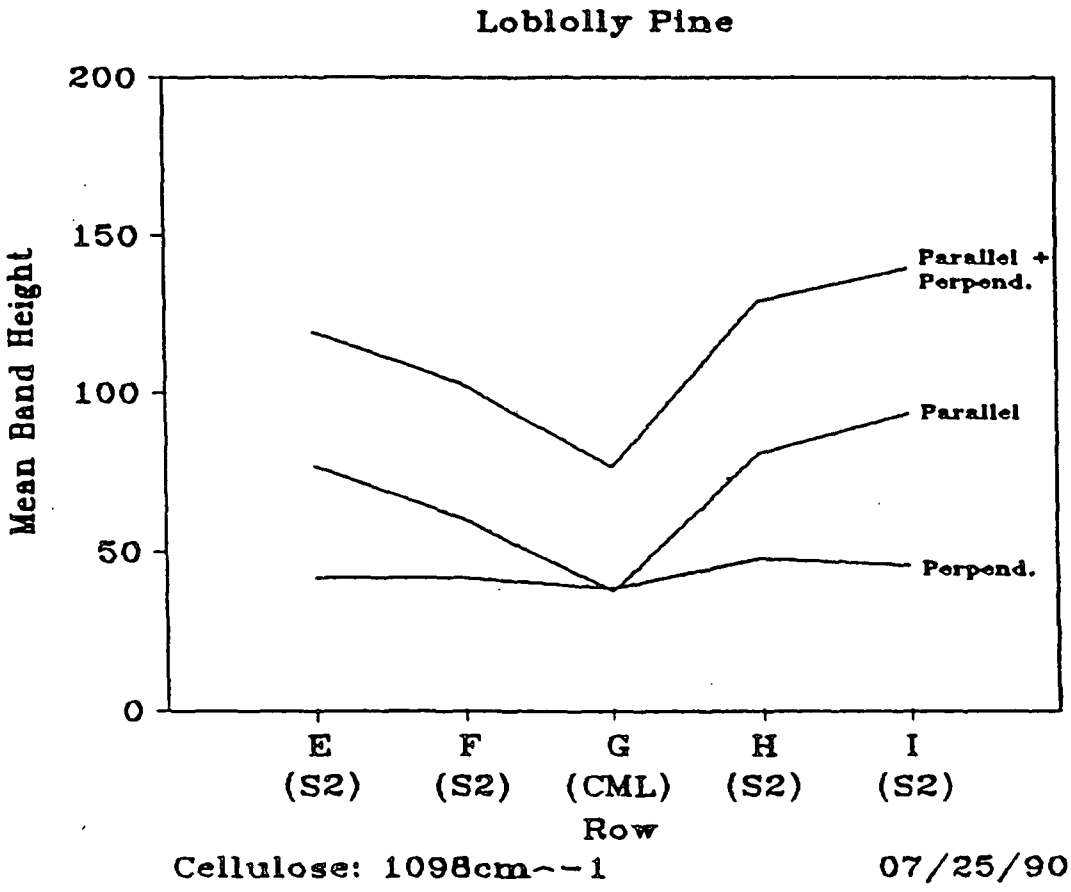

Figure 85. The variation of cellulose's 1098 cm^{-1} band intensity over different morphological regions in the latewood cell walls of loblolly pine tracheids.

It can be seen from this figure that, on the average, the parallel inten-

sity values are greater than the perpendicular intensity values for all of the secondary wall locations. This most likely reflects the preferential orientation of the chain axis of cellulose in planes parallel to the cell wall (radial section). In contrast to this, the EV parallel values and EV perpendicular values are approximately equal to each other in the CML region. It is unlikely that these data imply a slight preferential orientation of the chain axis in planes perpendicular to the cell wall. Rather, it is believed that this may be an artifact created by the use of the EV rotator intensity correction factor, i.e., the 1.33 factor for the parallel data may have been too small and thus the parallel curve should be displaced upwards. These data also suggest that, on the average, cellulose is more oriented parallel to the cell wall in the inner S_2 layer and this becomes less pronounced closer to the CML. (The distance between the EV parallel curve and the EV perpendicular curve decreases as the CML region is approached.) The reason for this orientation trend is not known.

If the assumption is made that cellulose orientation does not vary significantly over a 2.5 micron distance, then the EV parallel + perpendicular data indicate that the peak cellulose concentration occurs in the inner S_2 cell wall layer and declines to a minimum near the CML. This trend is seen for both the "E-G" fiber and the "I-G" fiber, although the peak concentration differs slightly. These data parallel the generally accepted trend for cellulose concentration in conifer cell walls (Figure 73).

The topographic plots of the 1595 cm^{-1} lignin band intensity vs. cell wall location are shown in Figures 86-88: Figure 86 - EV parallel; Figure 87 - EV perpendicular; Figure 88 - EV parallel + EV perpendicular. Comparing Figures 86 and 87, it can be seen that the general shape of the intensity plots is very similar and that the parallel intensity values are greater than the perpendicular values. This latter point may be indicative of the preferential orientation of the aromatic rings in lignin in planes parallel to the cell wall (radial section). In contrast to black spruce, there do not appear to be regions where this preferential orientation does not occur. This may indicate that the orientation of the aromatic rings in lignin is more uniform in loblolly pine compared to black spruce (at least for the areas investigated).

As was the case for cellulose, the general shape of the concentration (parallel + perpendicular) plot (Figure 88) is very similar to both the parallel and perpendicular plots (Figures 86 and 87, respectively). This suggests that their general shape is primarily dictated by concentration rather than by orientation. In Figure 88, it can be seen that the lignin concentration is not uniform but varies over the different morphological regions. The concentration appears to decline from the inner to outer S_2 and then increase in the CML region. While this trend appears to be universal, the specific location concentrations vary. This indicates that there is a variation in concentration not only between the different cell wall regions

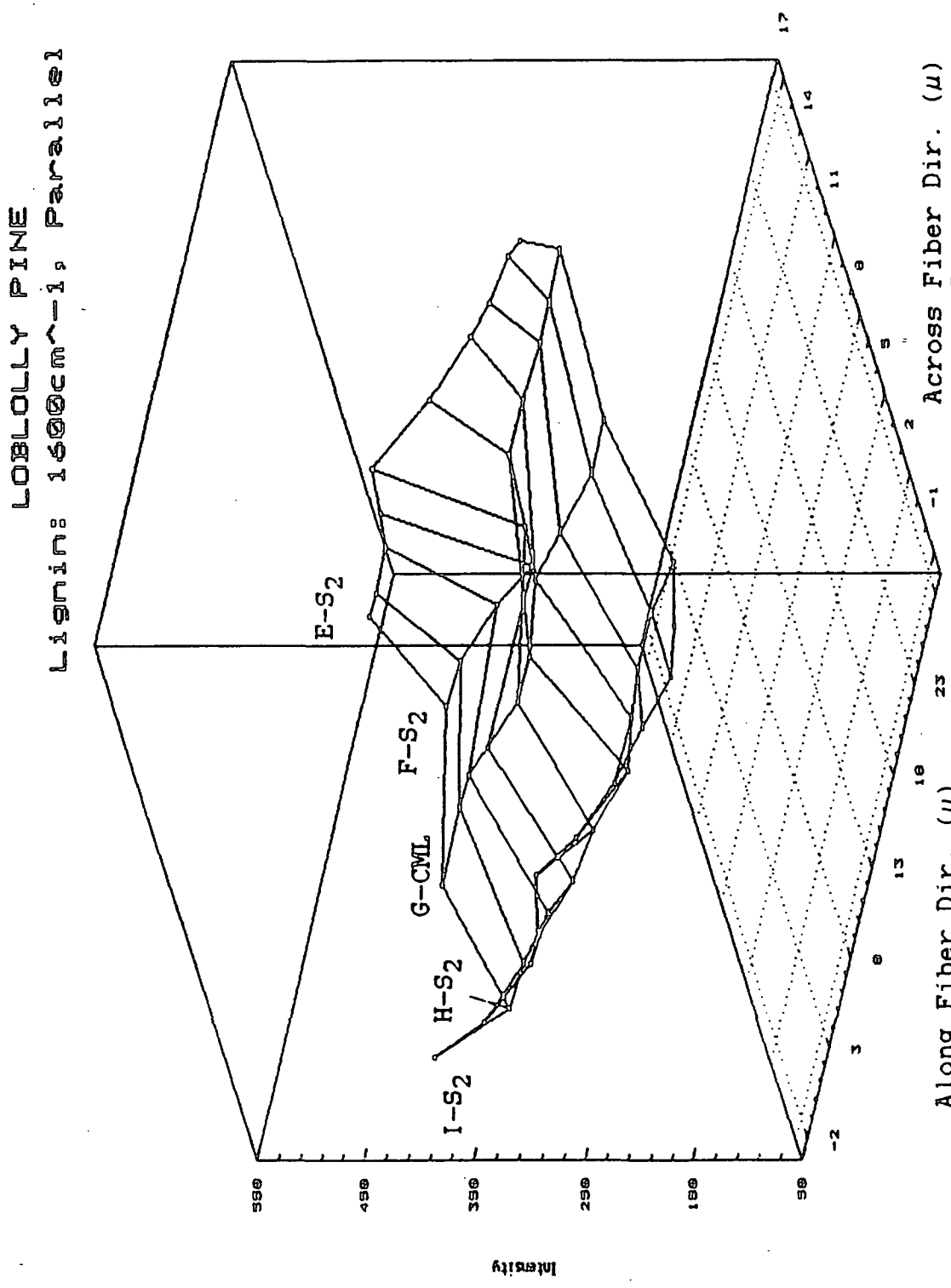

Figure 86. Topographic plot of lignin's 1595 cm^{-1} band intensity vs. cell wall location for loblolly pine. EV parallel to the longitudinal axis of the fiber (radial section). The row I/spot 1 (leftmost point on the plot) analysis point served as the origin.

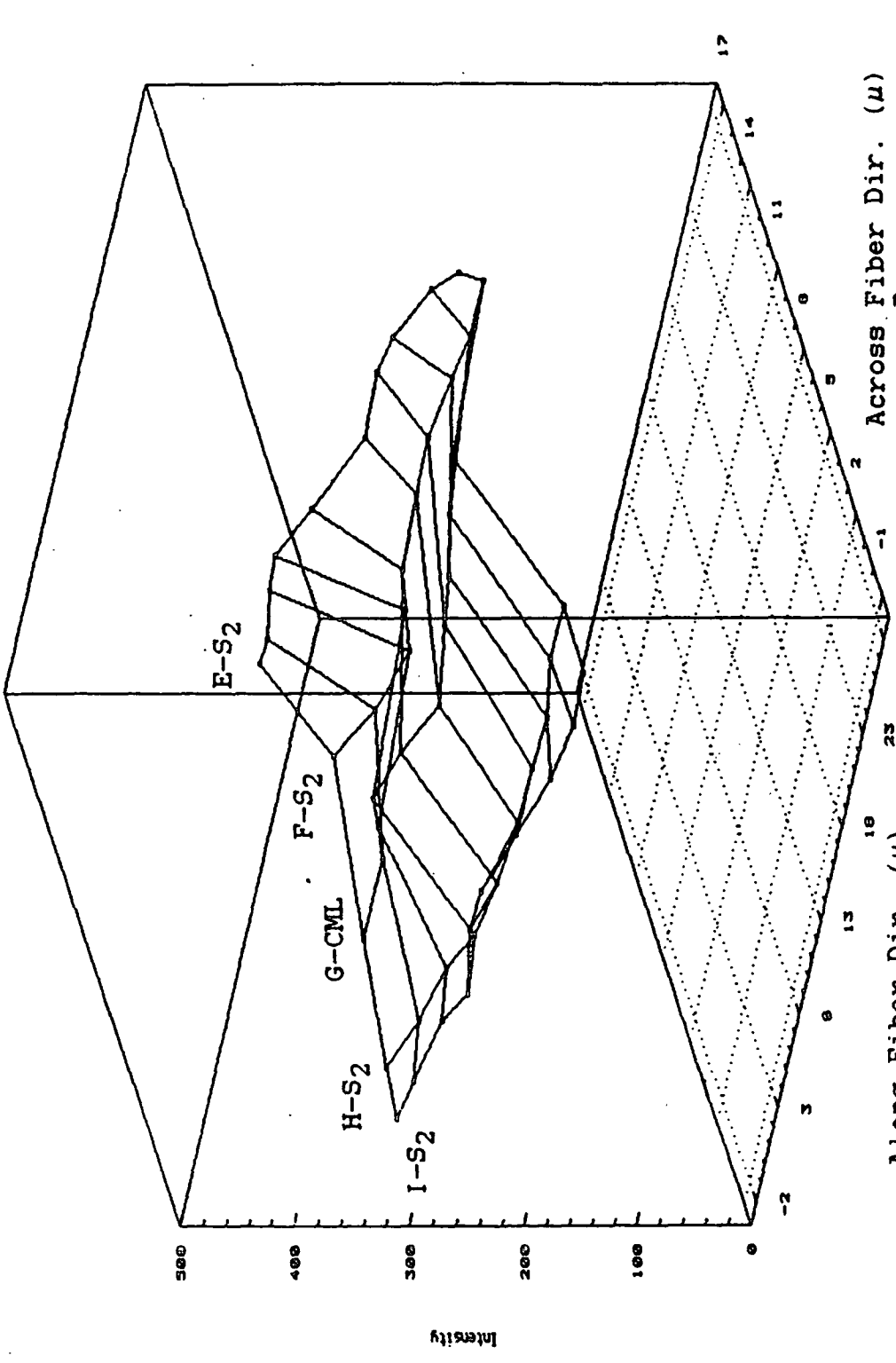

Figure 87. Topographic plot of lignin's 1595 cm^{-1} band intensity vs. cell wall location for loblolly pine. EV perpendicular.

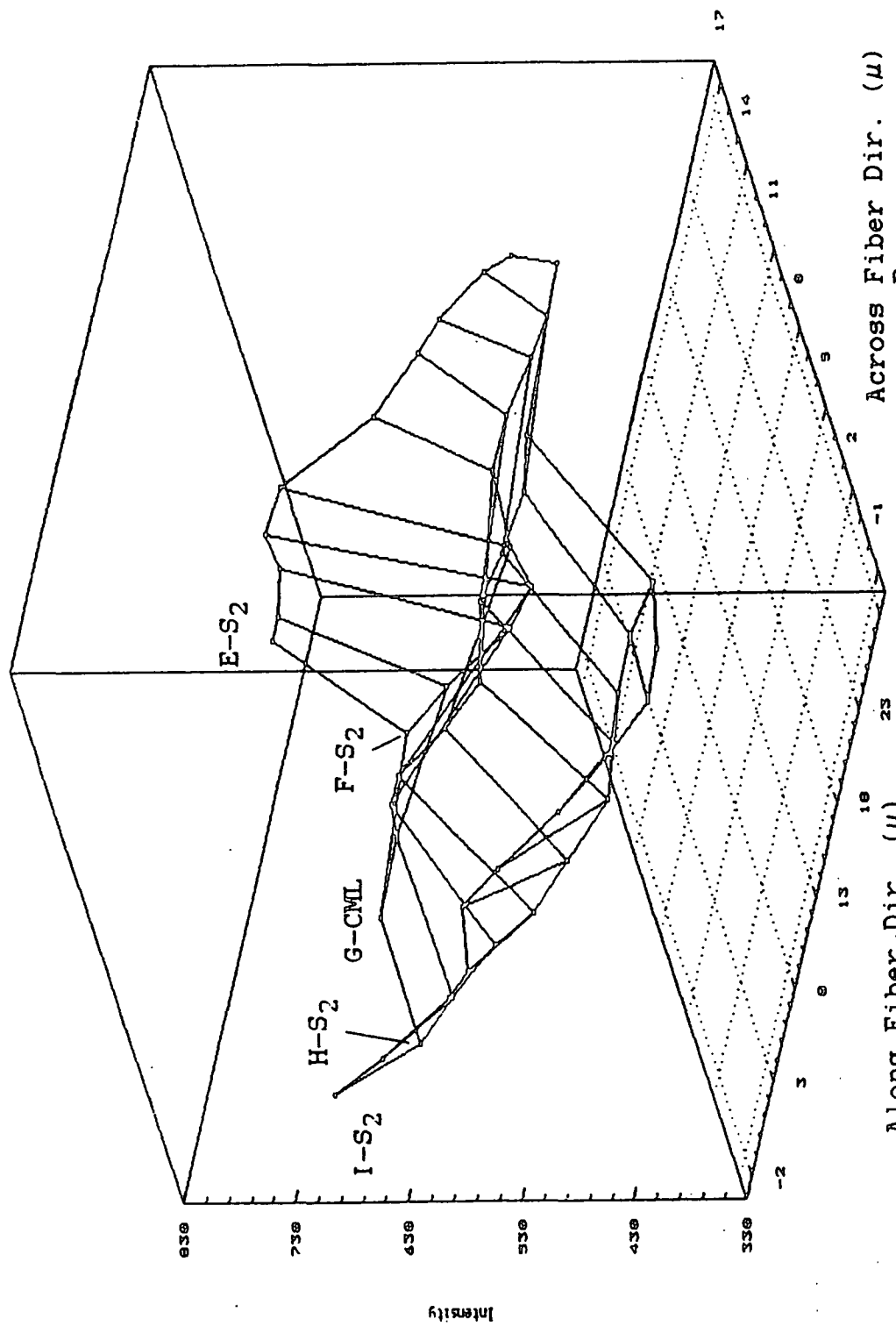

Figure 88. Topographic plot of lignin concentration vs. cell wall location for loblolly pine. EV parallel + perpendicular 1595 cm^{-1} band intensities.

but also within a single region. (To what extent the observed trends are due to concentration differences is not known. They could also be partly caused by localized variations in the structure of the lignin macromolecule which would then impact the degree of 1595 cm^{-1} band enhancement.)

The row averages for the 1595 cm^{-1} band intensity were analyzed to investigate the general trends in organization across the various morphological cell wall regions. These data are shown in Table 19, page 279, and plotted in Figure 89. It can be seen from Figure 89 that the EV parallel intensity values are consistently greater than the perpendicular values. This suggests that, on the average, the aromatic rings are preferentially oriented in planes parallel to the cell wall (radial section). These data also indicate that, in general, the aromatic rings of the phenylpropane units in lignin are slightly more oriented parallel to the cell wall in the inner S_2 region than in the outer S_2 layer. While the outer S_2 region still shows this preferential orientation, the difference between the EV parallel and EV perpendicular 1595 cm^{-1} band intensity is less. The reason for this variation in lignin orientation across the secondary wall is unknown.

The observed trends in aromatic ring orientation across the various morphological cell wall regions parallel the orientation trends observed for cellulose. This suggests that during biogenesis, cellulose may have acted as a template for lignin organization as was proposed by Atalla.[196]

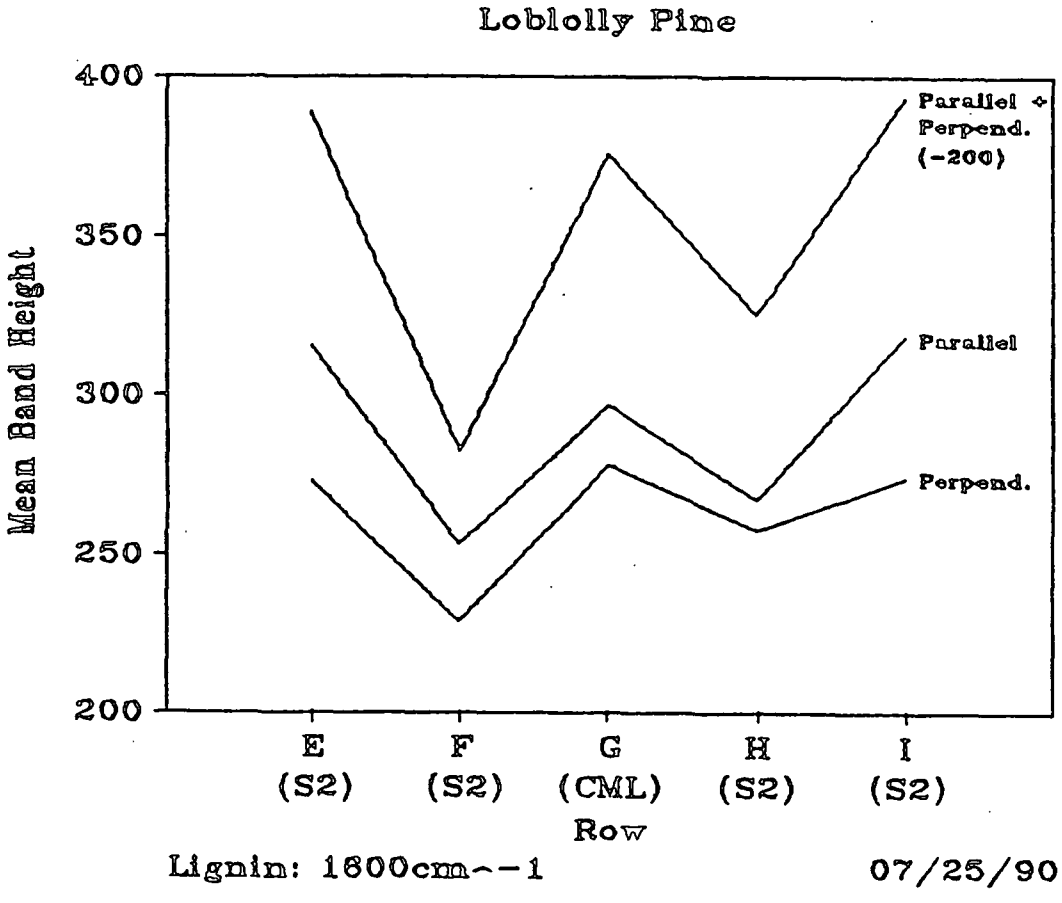

Figure 89. The variation of lignin 1595 cm^{-1} band over different morphological regions in the latewood cell walls of loblolly pine tracheids.

Assuming that the aromatic rings in lignin do not vary significantly in orientation over a distance of 2.5 microns, the EV parallel + perpendicular data indicate that the lignin concentration decreases from a high value near the lumen to a minimum in the outer S_2, and then increases in the CML region. This trend in lignin concentration parallels that found by Heazel[272] using sulfonated southern pine latewood chips and agrees with the generally accepted

lignin distribution in conifer cell walls (Figure 73).

There seems to be some disagreement in the literature regarding the distribution of lignin within the secondary cell wall. Some researchers[9,166,181,273,274] favor a uniform distribution of lignin across the S_2 layer, while others suggest that a gradient exists, i.e., there is some decline in lignin content in going from the outer to the inner S_2 as shown in Figure 73. If one assumes a uniform lignin distribution, then the gradient could be the result of structural differences in the lignin macromolecule across the secondary wall. (These localized structural differences would impact the degree of 1595 cm^{-1} lignin band enhancement.) Some support for this idea is found in the literature. There is evidence of differences in the phenolic hydroxyl content between the secondary wall and middle lamella in spruce.[275-277] It is conceivable that structural differences such as this could exist within the S_2 of loblolly pine.

The 1595/1098 cm^{-1} ratio was used to investigate the interrelationship between the macromolecular organization of cellulose and lignin. The topographic plots of this ratio vs. cell wall location are shown in Figures 90 and 91: Figure 90 - EV parallel; Figure 91 - EV parallel + EV perpendicular. (Due to the method employed to correct the data for dichroism, the L/C values are inflated by ≈35%.) The general shape of these plots is very similar, which again suggests that orientation does not make a major contribution to their general shape.

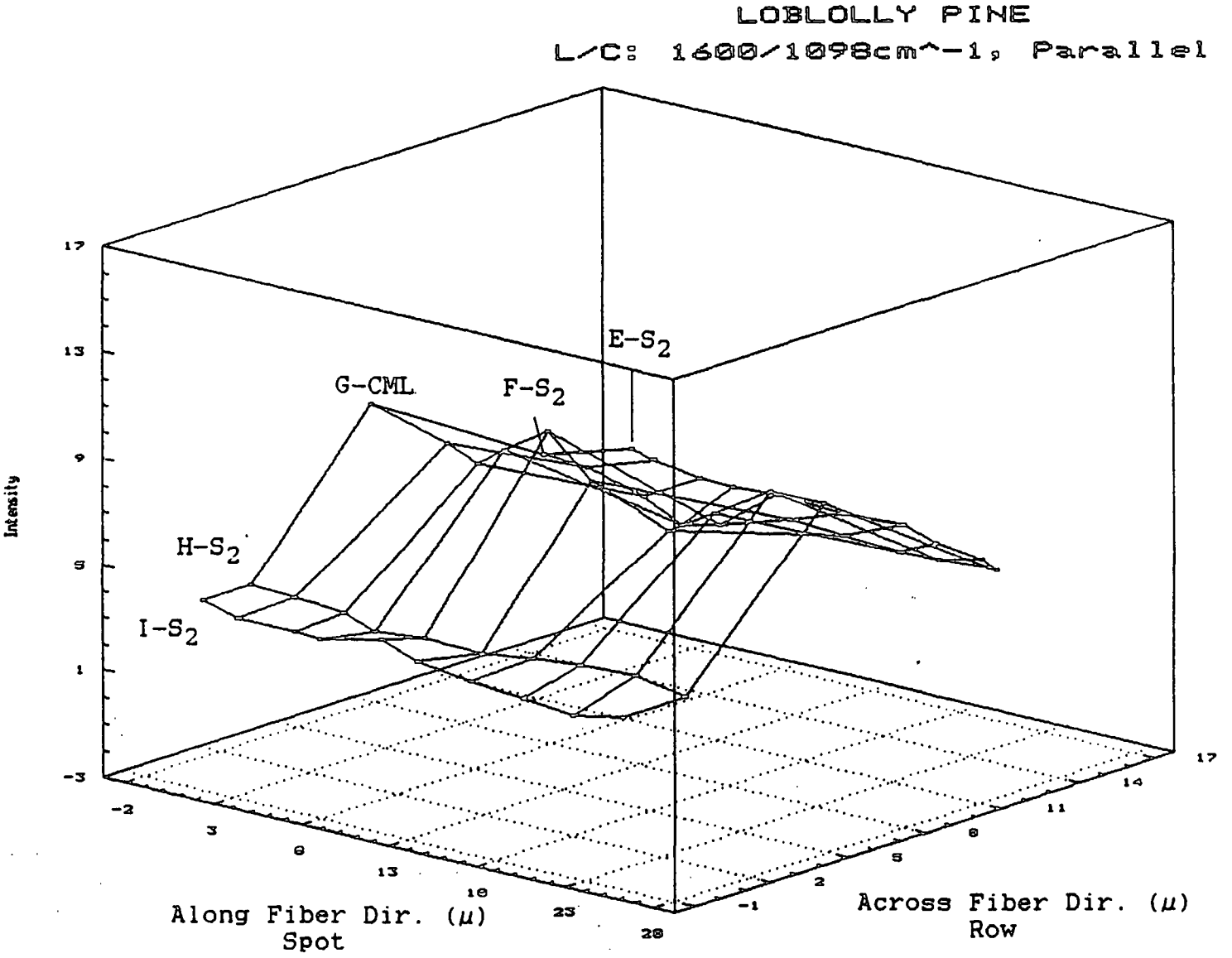

Figure 90. Topographic plot of the lignin-to-cellulose ratio (1595/1098 cm^{-1}) vs. cell wall location for loblolly pine. EV parallel to the longitudinal axis of the fiber (radial section). The row I/spot 1 (leftmost point on the plot) analysis point served as the origin.

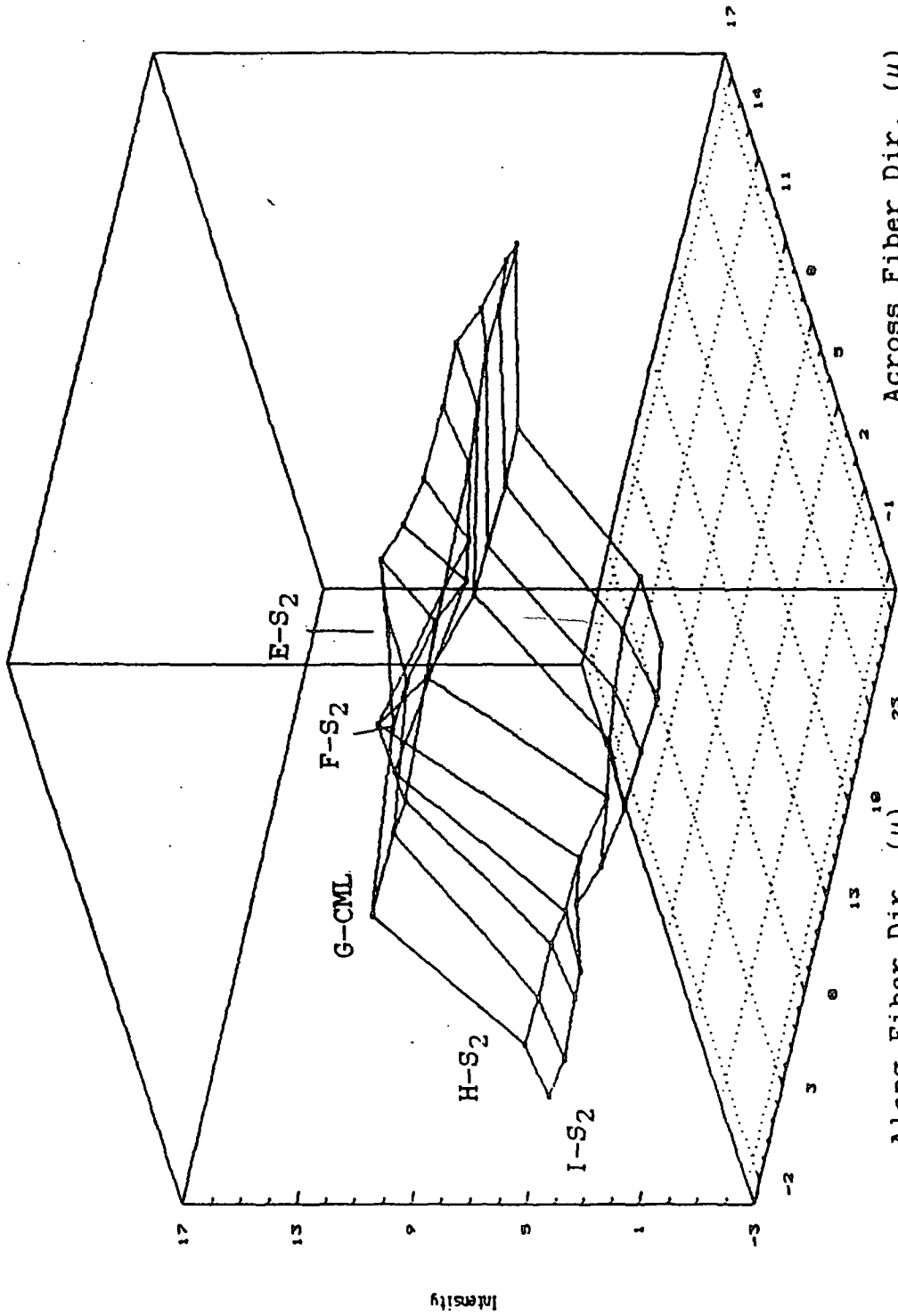

Figure 91. Topographic plot of the lignin-to-cellulose ratio (1595/1098 cm^{-1}) vs. cell wall location for loblolly pine. EV parallel + perpendicular.

As shown in Figure 91, the 1595/1098 cm^{-1} ratio is fairly uniform in an along-the-fiber direction, which may be indicative of a uniformity in concentration of cellulose and lignin in this direction. An obvious exception to this uniformity occurs in the CML region. The ratio at the row G/spot 5 location is substantially larger than the adjoining (CML) ratios. (This intensification probably reflects a regional difference in the organization of cellulose and lignin, i.e., the composition at this location changes in such a way so as to increase the lignin-to-cellulose ratio.) In contrast, the 1595/1098 cm^{-1} ratio is not uniform across these regions. It is significantly more intense along the CML region than it is along either of the S_2 regions. Whether this is due to concentration effects or reflects different degrees of 1595 cm^{-1} band enhancement brought about by localized variations in the structure of the lignin macromolecule is not known.

The variation of the average 1595/1098 cm^{-1} ratio over the different morphological regions of loblolly pine is shown in Figure 92. It can be seen from the parallel + perpendicular curve that, on the average, the lignin-to-cellulose ratio is uniform within and of the same magnitude between the S_2 cell wall regions and that the ratio is significantly larger in the CML region. The first observation suggests that the composition of the S_2 cell wall layer does not vary significantly between the two fibers studied. The latter probably reflects the lower cellulose concentration and the higher lignin concentration/degree of 1595 cm^{-1} band enhancement in the CML region.

The trend of the EV parallel + perpendicular curve very closely resembles the across fiber trends seen in the previous 1595/1098 cm^{-1} topographic plots. This similarity is believed to be a consequence of the uniformity in organization of cellulose and lignin. (It can also be seen from this figure that the EV parallel curve crosses the EV parallel + perpendicular in the CML region. It is believed that this is an artifact created by the use of the EV rotator intensity correction factors and the method used to average the data.)

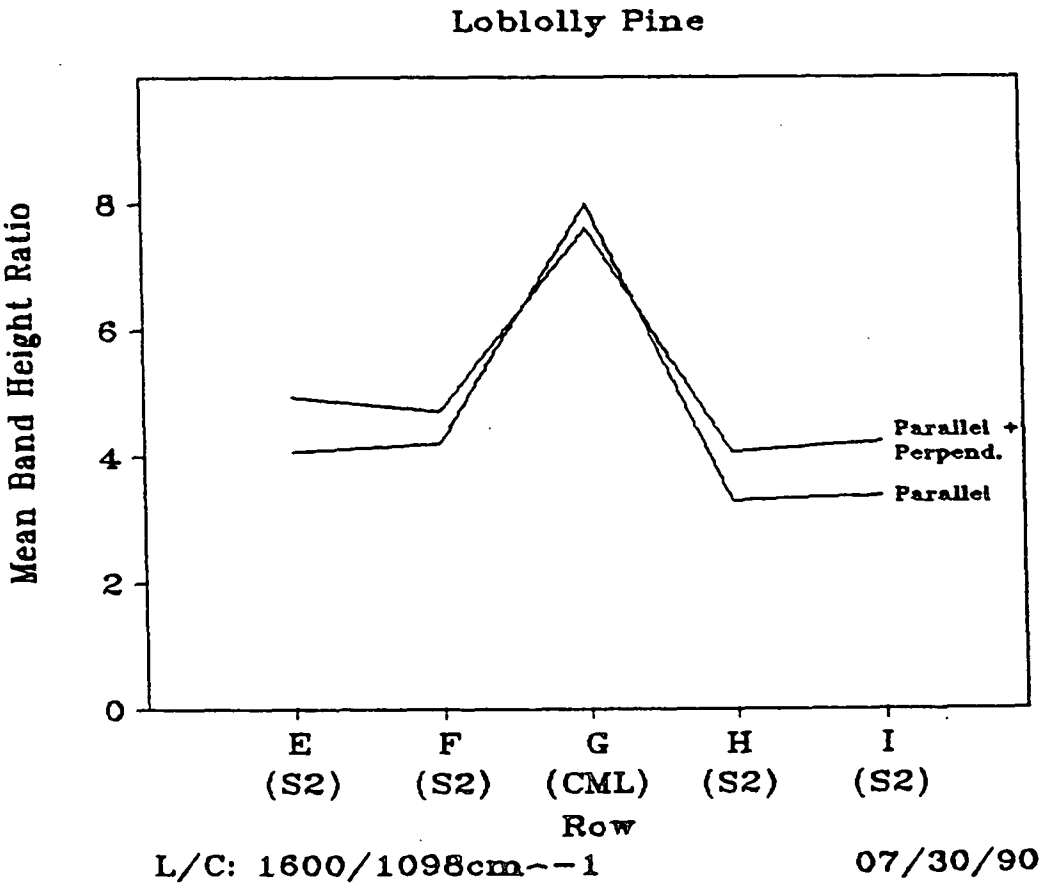

Figure 75. The variation of the lignin-to-cellulose ratio over different morphological regions in the latewood cell walls of loblolly pine tracheids.

The organization of cellulose and lignin in loblolly pine cell walls turned out to be more uniform (both along the fiber direction and within a particular cell wall layer) and the trends were more consistent with the literature than what was observed for black spruce. It may be that the cell wall organization in black spruce is more complex than the organization in loblolly pine. (Part of this complexity in black spruce may have been due to acid-chlorite pretreatment as was previously mentioned.)

Concluding Remarks

These Raman spectral mapping studies have provided direct evidence of molecular organization with respect to cellular morphological features, and suggest that the cell wall components are more highly organized than has been generally recognized. The evidence for the orientation of cellulose and lignin in woody plant cell walls was not unexpected. Atalla and coworkers have already established, although on a limited basis, that both of these biopolymers do show orientation.[10,125,222] What this present study has done is to extend their work by undertaking a more comprehensive investigation of the patterns of organization of cellulose and lignin in both black spruce and loblolly pine cell walls. One of the most significant findings, I believe, is not so much that a variation in molecular organization occurs between the various morphological cell wall regions, but rather that a variation in molecular order also occurs within these same regions. The problem which lies ahead in these cell wall architecture investigations is to understand the type

of order and organization which prevail in native plant tissue.

CONCLUSIONS

Raman microprobe studies of native woody tissues provided an opportunity for measurements of the macromolecular organization of cellulose and lignin across cell walls. These measurements were complicated by photo-induced changes in the lignin macromolecule that occurred during laser irradiation of the wet tissue. A considerable effort was spent in exploring this photomodification, both because it had to be adequately dealt with if the spectral mapping studies of the biopolymers were to reflect their native-state organization, and because of the new insights it provided about species which are constituents of native lignin, but which very likely become fugitive in the course of most preparative procedures.

There are a number of important findings that resulted from this thesis; the most significant ones are presented below. (Those pertaining to the photodecay of lignin are given first.)

Woody tissue, viz lignin, underwent a complex series of photochemical, degradative reactions which were initiated by the absorption of 514.5 nm photons. These reactions resulted in an imprinting of the incident intensity distribution on the secondary cell wall layer that became readily apparent during SEM visualization. During these reactions, lignin appeared to become solubilized as indicated by the almost complete disappearance of its 1595 cm^{-1} (ring breathing), 1620 cm^{-1} (C_α=C_β stretch), 1654 cm^{-1} (C_α=C_β and conjugated

carbonyl stretch), and 3070 cm^{-1} (aromatic CH stretch) Raman bands. Additionally, these reactions resulted in the formation of a yellowish-colored chromophore(s). GC/MS analysis suggested that these degradation products included quinonoid structures.

Lignin's 1600 cm^{-1} region bands were subject to two enhancement mechanisms, conjugation and preresonance Raman enhancement that arose from conjugated structural units in the lignin macromolecule. For black spruce, 49% of lignin's 1595 cm^{-1} band was found to be due to conjugation enhancement, 37% was due to preresonance Raman enhancement and the remainder due to nonenhanced Raman scattering from an idealized basic phenylpropane unit. For loblolly pine, these percentages were found to be 33%, 56%, and 11%, respectively. The difference in values between the species was thought to reflect differences in lignin make-up.

Lignin model compound studies revealed that the magnitude of both conjugation and preresonance Raman band enhancement was directly related to the degree of conjugation. The more conjugated the monolignol, the greater the conjugation/preresonance Raman enhancement of its ≈1600 cm^{-1} band. This observation, together with the finding that the contribution of preresonance Raman enhancement to the 1595 cm^{-1} band intensity was greater for loblolly pine lignin, suggested that loblolly pine lignin may have a larger number of ring conjugated structures (e.g., coniferaldehyde-type units) than does black spruce lignin.

The decay of lignin was found to be a multifaceted problem. Reduction, oxidation, and substitution reactions of the lignin macromolecule, as well as the use of fluorescence quenchers/radical scavengers, failed to stop lignin band decay. (The chemical pretreatment did, however, alter the percent contribution of conjugation/preresonance Raman enhancement to the 1595 cm^{-1} band intensity.) It is possible that other species present in woody tissue which are not sensitive to chemical attack may be the photochemistry initiators. These species could include polyphenolic flavanoid-type structures (extractives) or conceivably a charge-transfer complex between cellulose and lignin.

Lignin's 1595 cm^{-1} band decay appeared to involve two stages. The very rapid decline was thought to be primarily due to loss of band enhancement while the subsequent gradual decline probably reflected the loss of aromaticity. It is felt that phenoxy radical-type species are formed via secondary photochemical reactions and it is these species which degrade the aromatic ring.

Water was necessary for the photochemical reactions to occur. The lignin bands did not degrade when the section was dry and only a very slight degradation was seen to occur with a nonaqueous solvent (glycerol).

Although complete photostabilization of lignin was not achieved, a methodology that was thought to minimize the bias introduced by lignin modification was followed in the spectral mapping studies. The major findings resulting from this investigation are given below.

Analysis of the spectral mapping data confirmed that in loblolly pine, on the average, cellulose is not uniformly distributed in the three morphological regions (S_2/CML/S_2). The peak cellulose concentration occurred in the inner S_2 cell wall layer and declined to a minimum near the CML. This trend was also seen for the adjoining fiber, although the peak concentration differed slightly. The data also suggested that cellulose is more oriented parallel to the cell wall (in a radial section) in the inner S_2 layer and this became less pronounced closer to the CML.

Lignin also showed a nonuniform distribution. The 1595 cm^{-1} lignin peak intensity decreased from a high value near the lumen to a minimum in the outer S_2, and then increased in the CML region. This was paralleled in the adjoining fiber. It was unknown if the data reflected a true lignin concentration or whether the degree of lignin's 1595 cm^{-1} band enhancement varied over these regions. The data also suggested, in general, that the aromatic rings of the phenylpropane units in lignin are slightly more oriented parallel to the cell wall (in a radial section) in the inner S_2 regions, thus paralleling the trend seen for cellulose. These data taken together support the idea that during biogenesis, cellulose may act as a template for lignin organization.

The lignin-to-cellulose ratio was fairly flat for both S_2 regions but showed a strong peak in the CML. This peak reflected the lower cellulose concentration and the higher lignin concentration/degree of enhancement in this region.

In addition to these average trends across the three morphological regions, the molecular organization of cellulose and lignin was found to vary along these regions as well. This may be indicative of the occurrence of nodes in the organization of these components.

The interpretation of the black spruce data was more complex. The mirroring of the trends in organization for the adjoining fibers was not seen. For one fiber (A), on the average, the peak cellulose concentration occurred in the inner S_2 and declined to a minimum in the outer S_2 and remained at that level in the CML. The adjoining fiber (B) showed a flatter cellulose profile. For this fiber, only a slight peak in concentration was seen to occur in the middle of the S_2 cell wall layer. The data suggested that for one of the fibers (A), the chain axis of cellulose is more oriented parallel to the cell wall (radial section) in the inner S_2 and this orientation became less pronounced closer to the CML. This preferential orientation was not as apparent for the adjoining fiber (B).

The trends in the 1595 cm^{-1} band intensity of lignin paralleled those seen for cellulose. The intensification of this band in the CML region that occurred in the loblolly pine data was not seen. It was felt that specific subunits in the CML lignin may have been very sensitive to the acid-chlorite pretreatment and, consequently, the enhancement of the 1595 cm^{-1} in this region was disrupted.

The lignin-to-cellulose ratio was fairly flat throughout the S_2/CML/S_2 region. The strong peak seen in the loblolly pine data was not apparent; this most probably reflected the disruption of the 1595 cm^{-1} band enhancement mechanisms.

It is not known to what extent these black spruce data represented the actual native-state cell wall organization, but it was felt that the acid-chlorite pretreatment, as well as the sensitivity of black spruce lignin to 514.5 nm radiation may have biased the (lignin) data.

RECOMMENDATIONS

The results of this study have demonstrated that while polarized Raman microspectroscopy using 514.5 nm excitation is a viable technique to probe woody cell wall architecture, it is not without problems. The overriding difficulty is the photomodification of lignin that occurs during irradiation. Attempts to stabilize lignin to this radiation met with little success.

More fundamental work directed at understanding the photomodification of lignin in an aqueous environment will be required before in-depth mapping studies can be undertaken. These studies could involve further modification of the lignin macromolecule, i.e., acetylation of the phenolic hydroxyl groups, as well as the use of additional fluorescence quenchers/radical scavengers to stabilize lignin to 514.5 nm radiation.

The role of water in the lignin decay process needs to be elucidated. It may be possible to find a nonaqueous immersion medium which would function as well as water in regards to heat dissipation and fluorescence reduction, but without the unwanted lignin decay involvement.

An alternative approach would be to use longer wavelengths for Raman scattering. A FT-Raman microprobe is currently in the development stage. The use of 1064 nm excitation would effectively minimize both interfering fluorescence and lignin decay. Several shortcomings with this system are the high cost, the larger domain size, and the loss of orientation information. This

latter problem is due to a fiber optic coupling between the microscope and spectrometer which scrambles the electric vector. It may be overcome in later prototypes.

The custom built motorized stage used in this study will have to be modified to assure that its movements are accurate and reproducible. The present stage suffers from nonuniform stepping and its axes are not orthogonal. It may prove advantageous to custom design the stage and use piezoelectic translators.

ACKNOWLEDGEMENTS

The author would like to express his sincere appreciation for the guidance, encouragement and friendship provided by his thesis advisory committee: Drs. Rajai Atalla, Umesh Agarwal, Terrance Conners, and Ronald Dinus. A special thank you is extended to Dr. Rajai Atalla for his support and close friendship during the course of this thesis.

I would like to convey my sincere thanks to Drs. Earl Malcolm and Ronald Yeske for the valuable assistance they provided. I would especially like to thank Dr. Yeske for his continued support.

The research contained in this thesis was supported by The Institute of Paper Science and Technology and its member companies. Their contribution is gratefully acknowledged. The author would also like to express his deepest appreciation for the friendship of the many Institute faculty, staff, and students he has come to know during his student years.

The author is especially grateful to Lisa Sprister for her help in the preparation of this manuscript.

I am indebted to Chris Felix of The University of Wisconsin-Milwaukee's Biomedical Research Center (National Institute of Health grant RR-01008), Dr. Francis Purcell of Spex Industries, Integrated Paper Services - Appleton, Wisconsin, and Chris Duros of Electro Scan for providing instrumentation that

was invaluable during the course of this thesis.

Finally, I would like to express my heartfelt appreciation to my wife, Joan Marie, and children, Nathan James and Emily Elizabeth for their continued love, encouragement, sacrifices, and especially their ability to help me not to forget laughter during these thesis years.

LITERATURE CITED

1. Preston, R.D., In Dynamic Aspects of Plant Ultrastructure, A.W. Robards (ed.), McGraw-Hill, NY (1974).

2. Preston, R.D., Xylem Cell Development, J.R. Barrett (ed.), Academic Press, London (1981).

3. Clark, J.d'A., Pulp Technology and Treatment for Paper, 2nd ed., Miller Freeman Pub., Inc., San Francisco (1985).

4. Panshin, A.J. and C. deZeeuw, Textbook of Wood Techology, 4th ed., McGraw-Hill Book Co., NY (1980).

5. Smook, G.A., Handbook for Pulp and Paper Technologists, TAPPI Press, GA (1982).

6. Preston, R.D., The Physical Biology of the Plant Cell Wall, Chapman and Hall Ltd., London (1974).

7. Frey-Wyssling, A., The Plant Cell Wall, Gebruder Borntraeger, Berlin (1976).

8. Browning, B.L., Methods in Wood Chemistry, Interscience, NY (1967).

9. French, R.J., M.S. Dissertation, The Institute of Paper Chemistry, Appleton, WI (1984).

10. Agarwal, U.P. and R.H. Atalla, Planta 169:325(1986).

11. Calvert, J.G. and J.N. Pitts, Jr., Photochemistry, John Wiley and Sons, NY (1967).

12. Wells, C.H.J., Introduction to Molecular Photochemistry, Halsted Press, NY (1972).

13. Hon, D.N.-S., J. Polym. Sci. Polym. Chem. Ed. 13:1347(1975).

14. Hon, D.N.-S., Adv. Chem. Ser., 193:119(1981).

15. Launer, H.F. and W.K. Wilson, J. Res. Natl. Bur. Stand., 30:55(1943).

16. Van den Akker, J.A., H.F. Lewis, G.W. Jones, and M.A. Buchanam, Tappi, 32(4):187-192(1949).

17. Nolan, P., J.A. Van den Akker, and W.A. Wink, Pap. Trade J., 121(10):101(1945).

18. Norrström, H., Sven. Papperstidn., 72(2):32(1969).

19. Mechanical Pulping Manual, Tappi Monograph Series, No. 27, (1960) p. 22.

20. Nakano, J., K. Iiyama, H. Hatakeyama, and N. Migita, J. Jpn. Tappi, 20:369(1966).

21. Shriner, R.L., A Review of Nature Coloring Materials in Wood, Tappi Monograph Series, No. 6, NY (1948) p. 182.

22. Mayer, F., The Chemistry of Natural Coloring Matters, A.C.S. Monograph, No. 89, Reinhold, NY (1943).

23. Hon, D.N.-S, in Development in Polymer Degradation, N. Grassie (ed.), Vol. 3, Applied Science Publishers, Ltd., London (1981) p. 229.

24. Gierer, J.H., H. Norrström, and L. Stockman, Papier 27:469(1973).

25. Kondo, T., Jpn. Tappi, 26:499(1972).

26. Hon, D.N.-S., South. Pulp Pap. Manuf., 42(3):23(1979).

27. Freudenberg, K. in Constitution and Biosynthesis of Lignin, K. Freudenberg and H.C. Neish (eds.), Springer (1868).

28. Adler, E., Sven, Kem, Tidskr., 80:279(1968).

29. Adler, E., Pap. Puu, 11:634(1961).

30. Adler, E. and J. Marton, Acta Chem. Scand., 13:75(1959).

31. Pew, J.C. and W.J. Connors, Tappi, 54(2):245(1971).

32. Gellerstedt, G. and E.-L. Pettersson, Acta Chem. Scand. B, 29(10):1005(1975).

33. Kringstad, K.P. and S.Y. Lin, Tappi, 53:2296(1970).

34. Lin, S.Y., Ph.D. Dissertation, North Carolina State University, Raleigh (1970).

35. Lin, S.Y. and K.P. Kringstad, Nor. Skogind., 9:252(1971).

36. Lin, S.Y. and K.P. Kringstad, Tappi, 53:658(1970).

37. Harkin, F.M., Adv. Chem. Ser. 59:65(1966).

38. Imsgard, F., S.I. Falkehag, and K.D. Kringstad, Tappi, 54(10):1680(1971).

39. Rex, R.W., Nature, 188:1185(1960).

40. Ranby, B., K.P. Kringstad, E.B. Cowling, and S.Y. Lin, Acta Chem. Scand. 23:3257(1969).

41. Hon, D.N.-S., G. Ifju, and W.C. Feist, Wood Fiber, 12(2):121(1980).

42. Forrester, A.R., J.M. Hay, and R.H. Thomson, Organic Chemistry of Stable Free Radicals, Academic Press, NY (1968).

43. Hon, D.N.-S. and W. Glasser, Polym.-Plast. Technol. Eng., 12(2):159(1979).

44. Kringstad, K.P., Tappi, 52:1070(1969).

45. Leary, G.F., Tappi, 51:257(1968).

46. Hon, D.N.-S., J. Appl. Poly. Sci. : Appl. Poly. Symp., 37:845(1983).

47. Chang, S.-T., Ph.D. Dissertation, Virginia Polytechnic Institute and State University, Blacksburg (1982).

48. Rabek, J.F., Mechanisms of Photophysical Processes and Photochemical Reactions in Polymers - Theory and Applications, John Wiley and Sons, NY (1987).

49. Green, J.D., J. Wood Chem. Tech., 6:45(1986).

50. Leary, G.F., Tappi, 50:17(1967).

51. Sandermann, W. and F. Schlumbom, Holz Roh. Werkst., 20:245(1962).

52. Luner, P., Tappi, 43(10):819(1960).

53. Kalnins, M.A., C. Steelink, and H. Tarkow, U.S. Forest Service Research Paper, FPL-58(1966).

54. Hon, D.N.-S., Ph.D. Dissertation, Virginia Polytechnic Institute and State University, Blacksburg (1977).

55. Gierer, J. and S.Y. Lin, Sven. Papperstidn., 75:233(1972).

56. Brunow, G. and M. Sivonen, Paperi ja Puu, 57:215(1975).

57. Matsuura, T., N. Yoshimura, A. Nishinaga, and I. Satio, Tetrahedron 28:4933(1972).

58. Gellerstedt, G. and E.-L. Pettersson, Sven. Papperstidn., 80:15(1977).

59. Hon, D.N.-S. and S.-T. Chang, Wood Sci. Technol., 16:193(1982).

60. Roberti, P.C., R.F. York, and W.S. MacGregor, J. Am. Chem. Soc., 72:5760(1950).

61. Janson, J. and I. Forsskahl, Fourth Int. Symp. Wood Pulp. Chem., April 27-30, 1987, Paris, p. 313.

62. Peill, P.L.D., Nature, 158:554(1946).

63. Andrews, D.H. and P.D. Rosiers, Pulp Paper Mag. Can. 67(C):T119(1966).

64. Rudkin, A.W., Australian J. Appl. Sci., 1:270(1950).

65. Naragaramurti, D. and B.K. Handa, Das Papier, 7:87(1953).

66. Callow, H.J., Nature, 159:309(1947).

67. Manchester, D.F., J.W. McKinney, and A.A. Pataky, Sven. Papperstidn., 63:699(1960).

68. Lonas, V., Pulp Paper Mag. Can., 69(1):57(1968).

69. Callow, H.J. and J.B. Speaksman, J. Soc. Dyers and Colorists, 65:758(1949).

70. Stamm, A.J. and H. Tarkow, U.S. Patent 2,417,995(1947).

71. Ridgeway, W.B. and H.T. Wallington, British Patent 579,255(1946).

72. Tarkow, H., USDA FPL Office Report (1959).

73. Baird, B.R., Wood Fiber, 1:54(1969).

74. Clermont, L.P. and F. Bender, For. Prod. J., 7:167(1957).

75. Risi, J. and D.F. Arseneaw, For. Prod. J., 7:210(1957).

76. Ozolina, I. and K. Svalbe, Latr. Lauksaimn. Akad. Raksti:47(1972).

77. Arni, P.C., J.D. Gray, and R.K. Scougall, J. Appl. Chem. 2:163(1961).

78. Svalbe, K. and I. Ozolina, Plast. Modif. Drev.:145(1970).

79. Goldstein, I.S., E.B. Jeroski, A.E. Lund, J.F. Nielson, and J.M. Weater, For. Prod. J., 11:363(1961).

80. Tarkow, H.A., A.J. Stamm, and E.C.O. Erickson, USDA For. Serv. FPL Report, No. 1593(1950).

81. Singh, S.P., I. Dev., and S. Kumor, Wood Sci., 11(4):268(1979).

82. Singh, R.P., Tappi, 49(7):281(1966).

83. Mayer, W.C. and C.P. Donofrio, Tappi, 43(1):238A(1960).

84. Luner, P. and R. Supka, Tappi, 44(9):620(1961).

85. Tschirner, U. and C.W. Dence, Paperi ja Puu, 4:338(1988).

86. Friedman, J.M. and R.M. Hochstrasser, Chem. Phys. Lett., 33(2):225(1975).

87. Stoughton, R.W. and G.K. Rollefson, J. Am. Chem. Soc., 61:2634(1939).

88. Andrews-Wilberforce, D. and G. Patonay, Appl. Spect., 43(8):1450(1989).

89. Reineck, E.A., and H.F. Lewis, Paper Trade J., 121:27(1945).

90. Pivouarov, A.P., Y.A. Ershou, and A.F. Lukounikou, Sov. Plast., 10:11(1967).

91. Guillory, J.P. and C.F. Cook, J. Polym. Sci. A-1, 9:1529(1971).

92. Vink, P. and T.H.J. Van Veen, Eur. Polym. J., 14:533(1978).

93. Chakrabirty, K.B. and G. Scott, Eur. Polym. J., 13:1007(1977).

94. Behringer, J., in Raman Spectroscopy, Vol. 1, H.A. Szymanski (ed.), Plenum Press, NY (1967) p. 168.

95. Holzer, W., W.F. Murphy, and H.J. Bernstein, J. Chem. Phys., 52:399(1970).

96. Gillespie, R.J. and M.J. Morton, J. Mol. Spectrosc., 30:78(1969).

97. Shorygin, P.P., Pure Appl. Chem., 4:1(1962).

98. Shorygin, P.P., Russ. Chem. Rev. (Engl. Transl.), 40:367(1971).

99. Jesson, F.P. and H.W. Thompson, Proc. R. Soc. London, Ser. A, 268:68(1962).

100. Schmid, E.D. and B. Brosa, Berichte Bunsen Gesellschaft, 75(12):1334(1971).

101. Schmid, E.D., J. Chem. Phys., 56(12):6267(1972).

102. Schmid, E.D., J. Chem. Phys., 58(9):3871(1973).

103. Schmid, E.D., P. Schlenker, and R.R.M. Brand, J. Raman, Spect., 6(6):315(1977).

104. Schmid, E.D. and R.D. Topsom, J. Am. Chem. Soc., 103:1628(1981).

105. Schmid, E.D., J. Raman Spect., 14(3):191(1983).

106. Schmid, E.D. and B. Brosa, J. Chem. Phys., 58:637(1973).

107. Jones, D.W., O. Ellefsen, and B.A. Tonnessen, Cellulose and Cellulose Derivatives, Part IV, N.M. Bikales, and L. Segal (eds.), Wiley-Interscience, NY (1971).

108. Wardrop, A.B. and H. Harada, J. Exp. Bot., 16:356(1965).

109. Marx-Figini, M., Cellulose and Other Natural Polymer Systems, R.M. Brown, Jr. (ed.), Plenum, NY (1982).

110. Franke, W.W. and B. Ermen, Zeit. Naturforschung, 24b(7):917(1969).

111. Preston, R.D., E. Nicolai, R. Reed, and A. Millard, Nature, 162:665(1948).

112. Shafizadel, F. and G.D. McGinnis, Adv. Carbohydr. Chem. Biochem., 26:297(1971).

113. Bailey, I.W., Ind. Eng. Chem., 31:40(1938).

114. Page, D.H., J. Roy. Microscop. Soc., 90(2):137(1969).

115. El-Hosseiny, F. and D.H. Page, Wood and Fiber, 5(3):208(1973).

116. Muggli, R., R. Marton, and A. Sarko, J. Poly. Sci. (C), 36:121(1971).

117. Muggli, R., A. Sarko, and R. Marton, Wood Sci. Tech., 7:29(1973).

118. Sisson, W.A. and G.L. Clark, Ind. Eng. Chem. Anal. Ed., 5(5):296(1933).

119. Sisson, W.A., Ind. Eng. Chem., 27(1):51(1935).

120. Howsmon, J.A. and W.A. Sisson, Cellulose and Cellulose Derivatives, Part I, E. Ott, H.M. Sprulin, and M.W. Graffline (eds.), Interscience, NY (1954).

121. Kerr, A.J. and D.A.I. Goring, Cellulose Chem. Technol., 9:563(1975).

122. Scallan, A.M., Wood Sci., 6:266(1974).

123. French, A.D., Cellulose Chemistry and Its Applications, T.P. Nevell and S.H. Zeroniam (eds.), Eilis Horwood Rtd. Chichester (1985).

124. Morikawa, H., R. Hayashi, and M. Senda, Plant and Cell Physiol., 19(7):1151(1978).

125. Atalla, R.H. and U.P. Agarwal, Science 227(4687):363(1985).

126. Wiley, J.H., Ph.D. Dissertation, The Institute of Paper Chemistry, Appleton, WI (1986).

127. Northcote, P.H., Proc. Roy. Soc. Ser. B., 173:21(1969).

128. Nowak, M., E. Gruber, and J. Schurz, Das Papier, 28(7):273(1974).

129. Carpita, N.C., Cellulose and Other Natural Polymer Systems, R.M. Brown,, Jr. (ed.), Plenum, NY (1982).

130. Ray, P.M., Biochem. Biophys. Acta., 629:431(1980).

131. Ben-Hygylm, G. and I. Ohad, J. Cell Biol., 25:191(1965).

132. Millmann, B. and J.R. Colvin, Can. J. Microbiol., 7:383(1961).

133. Ohad, I., D. Danon, and S. Hestrin, J. Cell Biol., 12:31(1962).

134. Hopp, E.H., P.A. Romero, G.R. Daleo, and R. Pont-Lezica, Eur. J. Biochem., 84:561(1978).

135. Gestrin, S. and M. Schramm, Biochem. J., 53:345(1954).

136. Preston, R.D., Endeavour, 23:153(1964).

137. Roelofsen, P.A., Encyclopedia of Plant Anatomy, Part 4, W. Zimmerman and P.G. Ozenda (eds.), Gebruder Borntraeger, Berlin (1959).

138. Setterfield, G. and S.T. Bayley, Ann. Rev. Plant Physiol., 12:35(1961).

139. Colvin, J.R., The Formation of Wood in Forest Trees, M.H. Zimmermann (ed.), Academic Press, NY (1964).

140. Van Iterson, G., Chem. Weekbl., 24:165(1927).

141. Dunning, C.E., Ph.D. Dissertation, The Institute of Paper Chemistry, Appleton, WI (1968).

142. Heath, I.B., J. of Theoret. Biol., 48:445(1974).

143. Hardham, A.R., P.B. Green, and J.M. Lang, Planta, 149:181(1980).

144. Roelofsen, P.A. and A.L. Houwink, Acta Botanica Neerlandica, 2:218(1953).

145. Mueller, S.C. and R.M. Brown, Jr., Planta, 154:489(1982).

146. Marx-Figini, M., J. Polym. Sci., Part C, 28:57(1969).

147. Neville, A.C., D.C. Gubb, and R.M. Crawford, Protoplasma, 90:307(1976).

148. Gould, J.M., What's New Plant Physiol., 14:5(1983).

149. Bartuska, V.J. and G.E. Maciel, Holzforschung, 34:214(1980).

150. Goring, D.A.I., Lignins: Occurrence, Formation, Structure, and Reactions, K.V. Sarkanen and C.H. Ludwig (eds.), Wiley-Interscience, NY (1971) p. 695.

151. Levy, G.C., Topics in Carbon-13 NMR Spectroscopy, Vol. 2, John Wiley and Sons, NY (1976) p. 258.

152. Wardrop, A.B., Lignin: Occurrence, Formation, Structure, and Reactions, Wiley-Interscience, NY (1971) p. 19.

153. Mukoyoshi, S., Holzforschung, 35:233(1981).

154. Glasser, W.G. and H.R. Glasser, Pap. Puu, 63:71(1981).

155. Gibbs, R.D., The Physiology of Forest Trees, K.V. Thimann (ed.), Ronald Press, NY (1958) p. 269.

156. Ritter, G.J., Ind. Eng. Chem., 17:1194(1925).

157. Gailey, A.J., Ind. Eng. Chem., 8:52(1936).

158. Lange, P.W., Fundamentals of Paper Making Fibers, Tech. Section of the British Paper and Board Makers Association Inc. (1958) p. 147.

159. Frey-Wyssling, A., The Formation of Wood in Forest Trees, M.Z. Zimmermann (ed.), Academic Press, NY (1964).

160. Fergus, B.J., A.R. Procter, J.A.N. Scott, and D.A.I. Goring, Wood Sci. Technol., 3:117(1969).

161. Scott, J.A.N., A.R. Procter, B.J. Fergus, and D.A.I. Goring, Wood Sci. Technol., 3:73(1969).

162. Berlyn, G.P. and R.E. Mark, Forest Prod. J., 15:140(1965).

163. Saka, S., P. Whiting, K. Fukazawa, and D.A.I. Goring, Wood Sci. Technol., 16:269(1982).

164. Stone, J.E., A.M. Scallan, and D.A.V. Ahlgrean, Tappi, 54(9):1527(1971).

165. Kerr, A.J. and D.A.I. Goring, Cellulose Chem. Technol., 9:563(1975).

166. Sachs, I.B., I.T. Clark, and J.C. Pew, Poly. Sci. (C), 2:203(1963).

167. Heyn, A.J.N., J. Ultrastructural Res., 26:52(1969).

168. Scallan, A.M., Wood Sci., 6:266(1974).

169. Higuchi, T., Encyl. Plant Physiol., 133(1981) p. 194.

170. Vance, C.P., T.K. Kirk, and R.T. Sherwood, Ann. Rev. Phytopath, 18:259(1980).

171. Wardrop, A.B., Tappi, 40:225(1957).

172. Imagawa, H., K. Fukazawa, and S. Ishida, Bull. Hokkaido Univ. For., 33:127(1976).

173. Wardrop, A.B., Cellular Ultrastructure of Woody Plants, W.A. Cote, Jr. (ed.), Syracuse Univ. Press, NY (1965).

174. Hepler, P.K., D.E. Fosket, and E.H. Newcomb, Am. J. Bot., 57:85(1970).

175. Kutscha, N.P. and J.M. Schwarzmann, Holzforschung, 29:79(1975).

176. Saka, S., R.J. Thomas, and J.S. Gratzl, Wood Fiber, 11:99(1979).

177. Mollenhauer, H.H., J. Biophys. Biochem, Cytol., 6:431(1959).

178. Hoffmann, P. and N. Parameswaran, Holzforschung, 30:62(1976).

179. Saleh, T.M., I. Leney, and K.V. Sarkanen, Holzforschung, 21:116(1967).

180. Fujita, M. and H. Harda, Mokuzai Gakkaishi, 25:89(1979).

181. Saka, S. and R.J. Thomas, Wood Sci. Technol., 16:176(1982).

182. Takabe, K., Ph.D. Dissertation, Kyoto University, Japan (1984).

183. Pickett-Heaps, J.D., Protoplasma, 65:181(1968).

184. Fujita, M., H. Saiki, and H. Harada, Mokuzai Gakkaishi, 24:353(1978).

185. Goodwin, T.W. and E.I. Mercer, Intro. to Plant Biochem., 2nd ed., Pergamon Press, Oxford (1983).

186. Alberscheim, P., W.D. Bauer, K. Keegstra, and K.W. Talmadge, Biogenesis of Plant Cell Wall Polysaccharides, F. Loewus (ed.), Academic Press, NY (1973) p. 117.

187. Preston, R.D., Ann. Rev. Plant Physiol., 30:55(1979).

188. Monro, J.A., D. Penny, and W.B. Raymond, Phytochem., 15:1193(1976).

189. Hayashi, T., M.P.F. Marsden, and D.P. Delmer, Plant Physiol., 83:384(1987).

190. Varner, J.E. and L.-S. Lin, Cell, 56:231(1989).

191. Preston, R.D., Xylem Cell Development, J.R. Barnett (ed.), Castle House Publications Ltd. Kent (1981) p. 11.

192. Page, D.H., Wood and Fiber, 7:246(1976).

193. Hatfield, G.R., M. Sardashti, and G.E. Maciel, Anal. Chem., 59:1659(1987).

194. Ruel, K. and F. Barnoud, Comptes Rendus des Seances de l'Academie des Sciences, Series 3, 296(5):231(1983).

195. Terishima, N., Int. Symp. Wood Pulp. Chem., Raleigh, NC (1989) p. 359.

196. Terishima, N., J. Japan. Wood Res. Soc., 33(3):615(1987).

197. As cited by Terishima, N. in Reference 196, Atalla, R.H., private correspondence.

198. Tobin, M.C., Laser Raman Spectroscopy, Wiley-Interscience, NY (1971).

199. Long, D.A., Raman Spectroscopy, McGraw Hill, NY (1977).

200. Szymanski, H.A. (ed.), Raman Spectroscopy - Theory and Practice, Vols. 1 and 2, Plenum Press, NY (1967).

201. Tu, A.T., Raman Spectroscopy in Biology : Principles and Applications, Wiley-Interscience, NY (1982).

202. Gardiner, D.J. and P.R. Graves (eds.), Practical Raman Spectroscopy, Springer-Verlag, Berlin (1989).

203. Placzek, G., Rayleigh-Streung and Raman-Effekt, Handbuch der Radiologie, E. Marx (ed.), Leipzig (1934) p. 205.

204. Shorygin, P.P., as reported in J. Brand Muller and W. Kiefer, Physicist's View, Fifty Years of Raman Spectroscopy, Spex Speaker, 23:310(1978).

205. Shorygin, P.P., Usp, Khim., 19:419(1950).

206. Shorygin, P.P., Usp. Khim., 40:694(1971).

207. Hayes, W. and R. London, Scattering of Light by Crystals, Wiley and Sons, New York (1978) p. 26.

208. Kip, B.J. and R.J. Meier, Appl. Spect., 44(4):707(1990).

209. Strommen, D.P. and K. Nakamoto, Laboratory Raman Spectroscopy, Wiley-Interscience, NY (1984).

210. McMurry, J., Organic Chemistry, Brooks/Cole Publishing Co., CA (1984) p. 434.

211. Delly, J.G., Photography Through The Microscope, 9th ed., Eastman Kodak Company (1988).

212. Martin, L.C., The Theory of the Microscope, American Elsevier Publishing Co., NY (1966).

213. Rottenfusser, R., Personal Communication, Carl Zeiss, Inc., Thornwood, NY (1988).

214. Atalla, R.H. and U.P. Agarwal, in Microbeam Analysis, A.D. Romig Jr. and J.I. Goldstein (eds.), San Francisco Press, San Francisco, CA (1984) p. 125.

215. Inoue, S., Video Microscopy, Plenum Press, NY (1986).

216. Koch, P., Utilization of the Southern Pines, Vol. I, U.S. Dept. of Agric., Handbook No. 429 (1972).

217. Isenberg, I.H., Pulpwoods of the United States and Canada, Vol. I-Conifers (3rd ed. - revised by M.L. Harder and L.L. Louden), The Inst. of Paper Chem., Appleton, WI (1980).

218. Goetzler, M., Tappi, 65(3):149(1982).

219. Frieden, J., J. Opt. Soc. Am., 73:927(1983).

220. DeNoyer, L.K. and J.G. Dodd, Am. Laboratory, March (1990) p. 21.

221. Ehrhardt, S., Ph.D. Dissertation, The Institute of Paper Chemistry, Appleton, Wisconsin (1984).

222. Atalla, R.H., U.P. Agarwal, and J.S. Bond, in Methods in Lignin Chemistry, C. Dence and S.Y. Lin (eds.), Springer-Verlag, Berlin (to be published).

223. Lowrey, W.H. and W.H. Swantner, Laser Focus World, May (1989).

224. Born, M. and E. Wolf, Principles of Optics, 6th ed., Pergamon Press, Oxford (1980).

225. Optics Guide 3, Melles Griot Optics, 1770 Kettering Street, Irvine, California 92714, p. 29-33 (1985).

226. Oates, C.W. and M. Young, Appl. Optics, 26(11):2043(1987).

227. Lindstrom, T., in Paper - Structure and Properties, J.A. Bristow and P. Kolseth (eds.), Marcel Dekker, Inc., New York (1986) p. 99.

228. Irvine, G.M., CSIRO Division of Chemical Technology Res. Rev. (1980) p. 33.

229. Sadoh, T., Wood Sci. Technol., 15:57(1981).

230. Hoglund, H., U. Sohlin, and G. Tistad, Tappi, 59:144(1976).

231. Salmen, L. J. Material Sci., 19:3090(1984).

232. Hiemenz, P.C., Polymer Chemistry, Marcel Dekker, Inc., New York (1984) p. 631.

233. Gardon, J.L. and S.G. Mason, Can. J. Chem., 33:1477 (1955).

234. Nokihara, E., M.J. Tuttle, V.F. Felicetta, and J.L. McCarthy, J. Am. Chem. Soc., 79:4495(1957).

235. Yean, W.Q., A. Rezanowich, and D.A.I. Goring, in Chim., Biochim., Lignine, Cellulose, et Hemicellulose, Grenoble (1964) p. 327.

236. Favis, B.D., P.M.K. Choi, P.M. Adler, and D.A.I. Goring, Transactions of the Technical Section, Canadian Pulp and Paper Association, 7:TR35(1981).

237. Goring, D.A.I., Int. Symp. Wood Pulp Chem., Japan, May 23-27, 1983, p. 3.

238. Goring, D.A.I., Pulp Paper Mag. Can., 64:T517(1963).

239. Photomultiplier Manual PT-61 (Technical information for RCA photomultiplier tube type C31034A) RCA, Harrison, New Jersey.

240. Grating efficiency curve for Ramanor gratings (2000 grooves/mm blazed at 514.5 nm) J-Y Optical Systems/Instruments SA, Inc., Edison, New Jersey.

241. Polcin, J. and W.H. Rapson, Pulp Paper Mag. Can., T555, Dec. 19, 1969, p. 99.

242. Doub, L. and J.M. Vanderbelt, J. Am. Chem. Soc., 69:2714 (1947).

243. Doub, L. and J.M. Vanderbelt, J. Am. Chem. Soc., 71:2414(1949).

244. Agarwal, U.P. and R.H. Atalla, Proceedings, ICORS X, Eugene, Oregon, Paper 14-46 (1986).

245. Glasser, W.G. in Pulp and Paper - Chemistry and Chemical Technology, 3rd ed., Vol. 1, J.P. Casey (ed.) John Wiley and Sons, New York (1980).

246. Polcin, J. and W.H. Rapson, Tappi, 52(10):1960(1969).

247. Basham, H.G. and E.B. Cowling, Material and Organismen, Beihefte 3 (Org. Holz.):155(1976).

248. Streitwieser, A. and C.H. Heathcock, Introduction to Organic Chemistry, 2nd ed., MacMillan Publishing, New York (1981) p. 455.

249. Stifkin, M.A., Charge-Transfer Interactions of Biomolecules, Academic Press, Inc., New York (1971) p. 1.

250. Knowles, P.F., D. Marsh, and H.W.E. Raltle, Magnetic Resonance of Biomolecules, John Wiley and Sons, New York (1976).

251. Swartz, H.M., J.R. Bolton, and D.C. Borg, Biological Applications of Electron Spin Resonance, Wiley Interscience, New York (1972).

252. Borg, D.C., Applications of Electron Spin Resonance in Biology in Free Radicals in Biology, Vol. 1, W.A. Pryor (ed.) Academic Press, New York (1976), p. 69.

253. Wertz, J.E. and J.R. Bolton, Electron Spin Resonance Elementary Theory and Practical Applications, McGraw-Hill Book Co., New York (1972).

254. Alger, R.S., Electron Spin Resonance: Techniques and Applications, Interscience, New York (1967).

255. Hon, D.N.-S. and W.C. Feist, Wood Sci., 14(1):41(1981).

256. Birks, J.B., Photophysics of Aromatic Molecules, Wiley-Interscience, London (1970).

257. Dollish, F.R., W.G. Fateley, and F.F. Bentley, Characteristic Raman Frequencies of Organic Compounds, Wiley-Interscience, New York (1974) p. 162.

258. Nyquist, R.A., V. Chrizan, J. Houck, Appl. Spect., 43(6):981(1989).

259. Rapson, W.H. and G.B. Strumila, The Bleaching of Pulp, 3rd ed., R.P. Singh (ed.), Tappi Press, Atlanta, Georgia (1979) p. 152.

260. Barton, J.S., Tappi, 33(10):496(1950).

261. Levitin, N., N.S. Thompson, and C.B. Purves, Pulp and Paper Mag. Can., 56(5):117(1955).

262. Sarkanen, K.V., K. Kakehi, R.A. Murphy, and H. White, Tappi, 45(1):249(1962).

263. Dence, C.W., M.K. Gupta, and K.V. Sarkanen, Tappi, 45(1):29(1962).

264. Gianola, G., J. Meybeck, Assoc. Tech. Ing. Papetiere, Bull., No. 1, p.24 (1960).

265. Lindgren, B.O., Svensk Papperstidn, 74(3):57(1971).

266. Gierer, J., Wood Sci. Technol., 20:1(1986).

267. Masschelein, W.J., Chlorine Dioxide - Chemistry and Environmental Impact of Oxychlorine Compounds, Ann Arbor Science Publishers, Ann Arbor, Michigan (1979).

268. Lebo, S.E., Jr., Ph.D. Dissertation, The Institute of Paper Chemistry, Appleton, Wisconsin (1988).

269. Woitkovich, C., M.S. Dissertation, The Institute of Paper Chemistry, Appleton, Wisconsin (1988).

270. Medvecz, P., M.S. Disseration, The Institute of Paper Chemistry, Appleton, Wisconsin (1987).

271. Anderson, M.E. and R.Z. Muggli, Anal. Chem., 53:1772(1981).

272. Heazel, T. and T.J. McDonough, The Institute of Paper Chemistry Technical Paper Series, no. 216, January, 1987.

273. Parham, R.A. and W.A. Cote, Wood Sci. and Technol., 5:49(1971).

274. Saka, S., R.J. Thomas, and J.S. Gratzl, Proc. Int. Symp. on Wood and Pulping Chem., Stockholm, June 9-12, 1981, p. 35.

275. Hardell, H.-L., G.J. Leary, M. Stoll, and U. Westermark, Svensk Paperstid, 83(2):44(1980).

276. Whiting, P. and D.A.I. Goring, Paperi Puu, 64(10):592(1982).

277. Boutelje, J. and I. Eriksson, Holzforschung, 28:249(1984).

278. VanderHart, D.L. and R.H. Atalla, Preprints of the International Dissolving and Specialty Pulps Conference, Boston, 1983, p.207.

279. Atalla, R.H. and D.L. VanderHart, Science, 223:283(1984).

280. VanderHart D.L. and R.H. Atalla, Macromolecules, 17:1465(1984).

281. Atalla, R.H., Studies On The Structure Of Cellulose Using Raman Spectroscopy And Solid-State ^{13}C NMR, The Institute of Paper Chemistry Technical Paper Series, no. 217, January, 1987.

282. Sarkanen K.V. and C.H. Ludwig, Lignins: Occurrence, Formation, Structure, and Reactions, K.V. Sarkanen and C.H. Ludwig (eds.), Wiley-Interscience, NY (1971) p. 1.

283. Fengel, D., Tappi, 53:497(1970).

284. Agarwal, U., Personal Communication, The Institute of Paper Science and Technology, Appleton, WI (1986).

285. Spectra Calc Users Guide, Galactic Industries Corporation, Salem, NH (1990) p. 3-13.

APPENDIX 1. Selected Raman Spectra Of Black Spruce Tissue Used In The Local Temperature Determination At The Point Of Laser Focus.

(Radial section, latewood, secondary wall). The first spectrum shows cellulose's antiStokes 330 (D780) and 380 cm^{-1} (D740) bands, while the second spectrum shows the Stokes bands (330 cm^{-1}-D180, 380 cm^{-1}-D225). The large peak in the Stokes spectrum is cellulose's 1098 cm^{-1} band.

AntiStokes Raman Spectrum

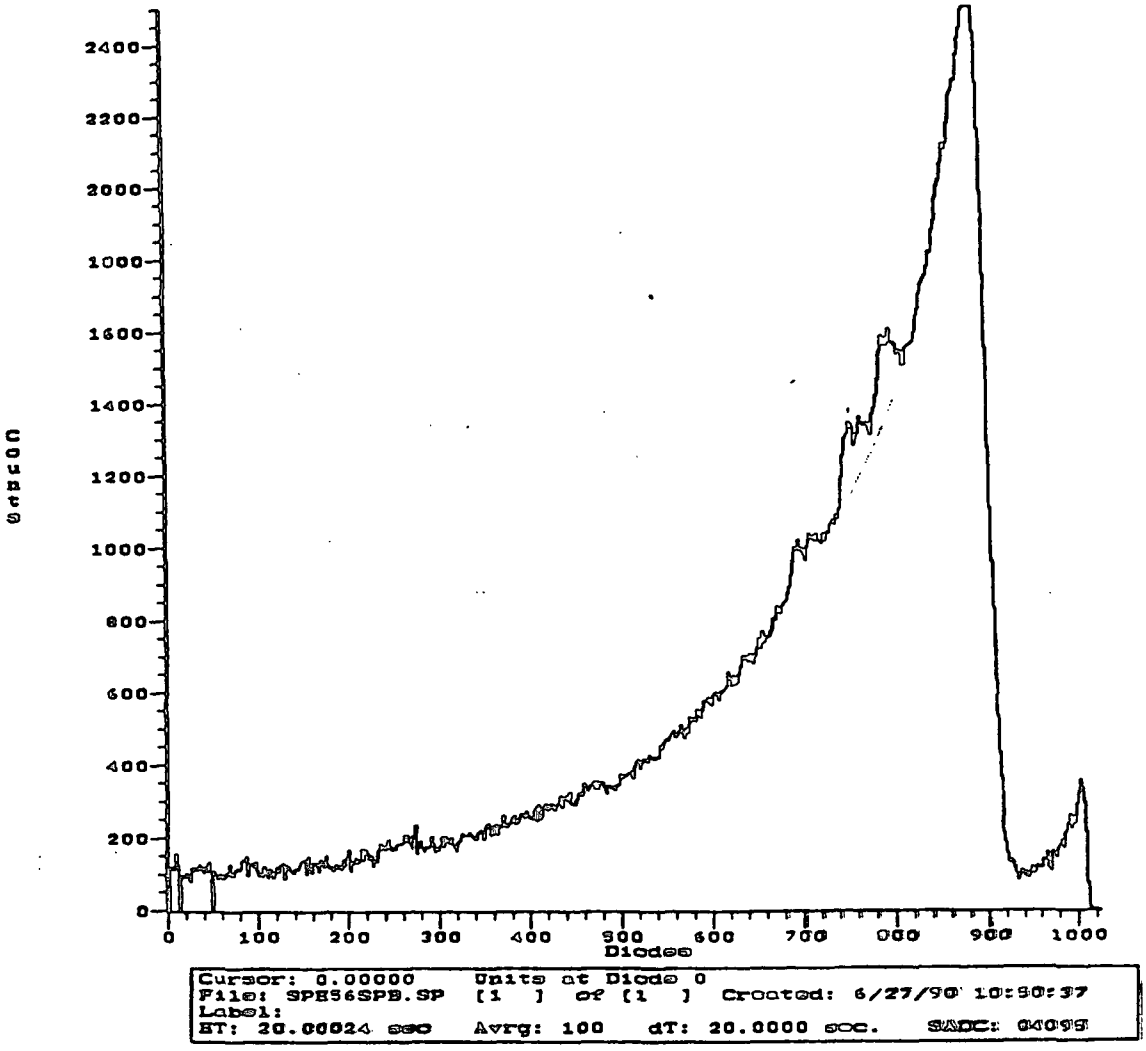

Stokes Raman Spectrum

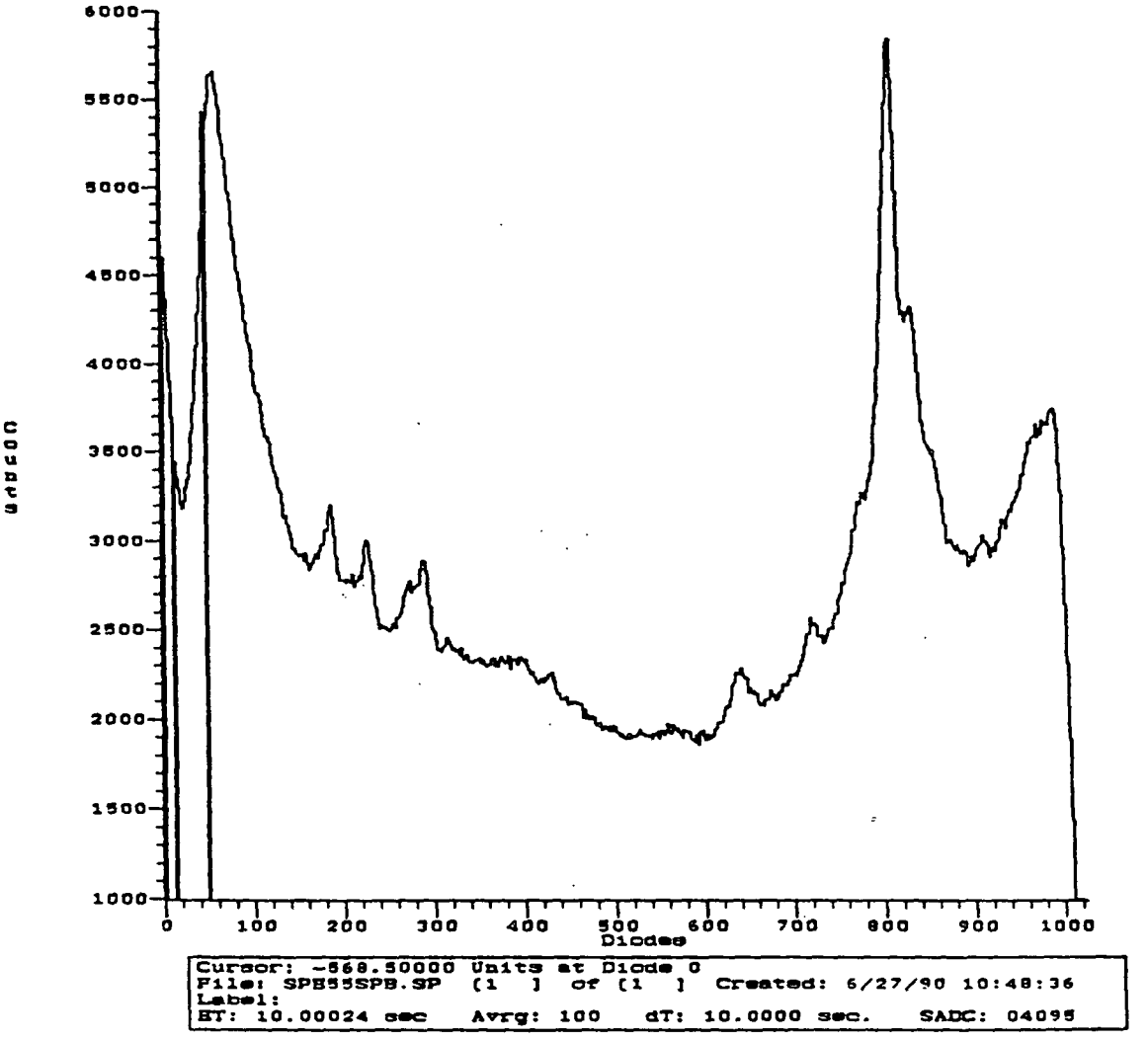

APPENDIX 2. GC/MS (SIMS) Spectra Of Controls And The Water In Which A Black Spruce Section Was Irradiated.

Control GC/MS Spectra

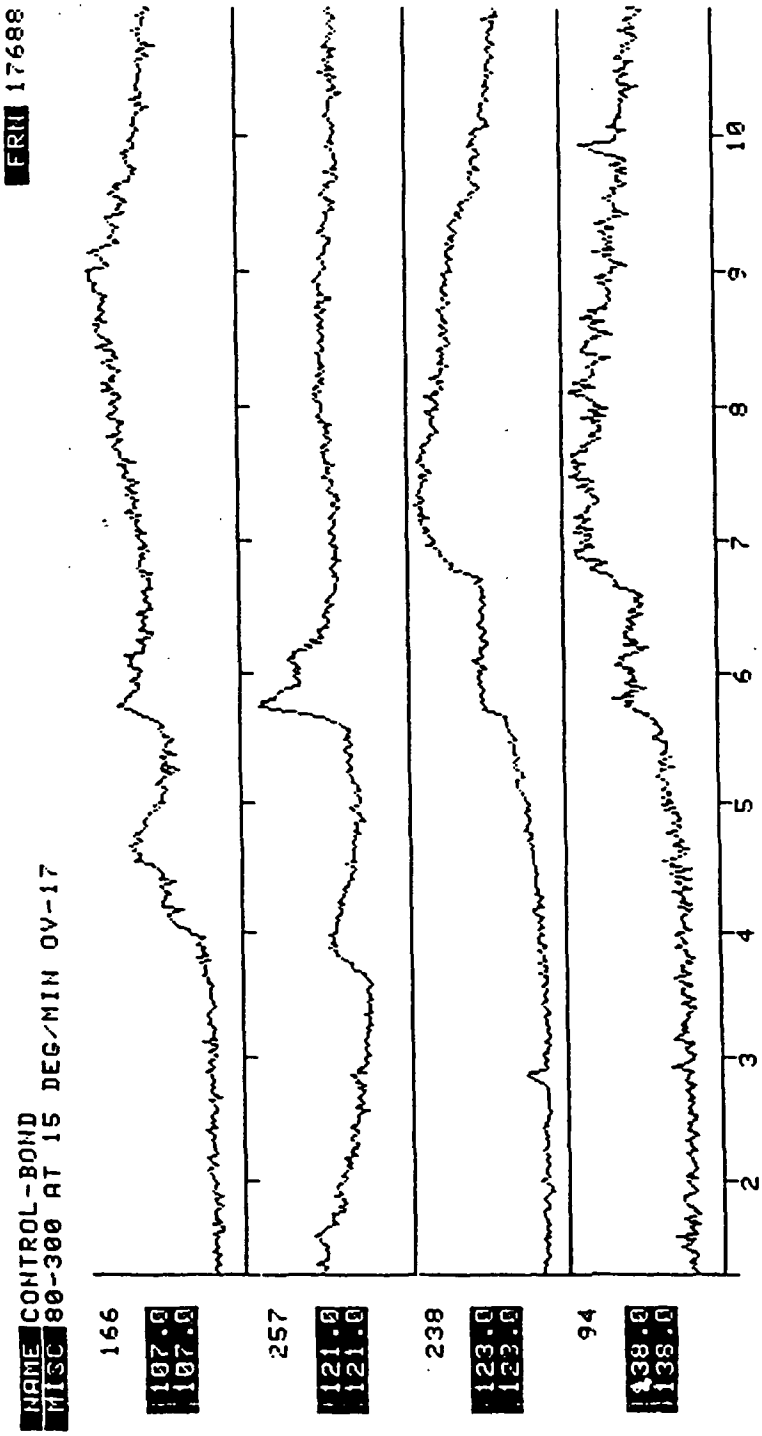

Control GC/MS Spectra

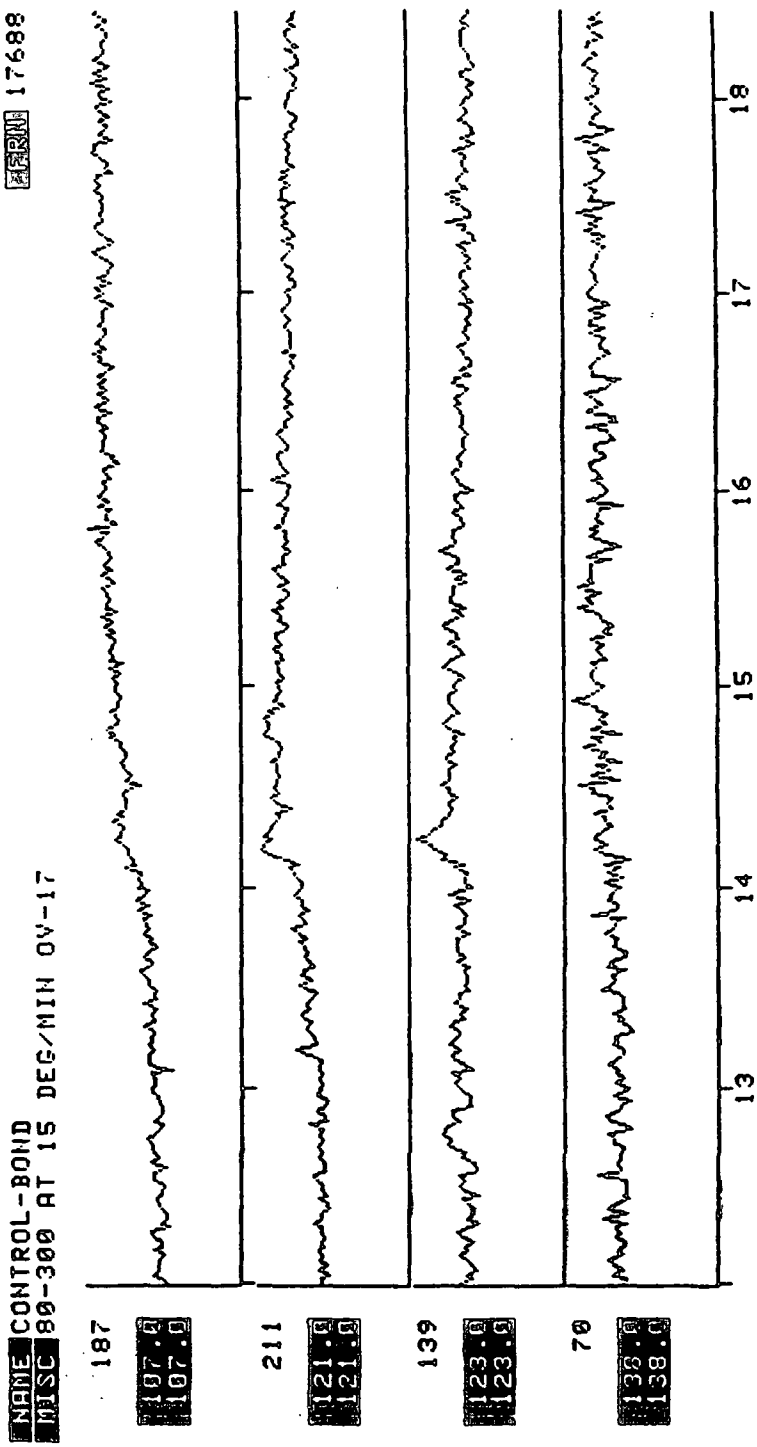

Control GC/MS Spectra

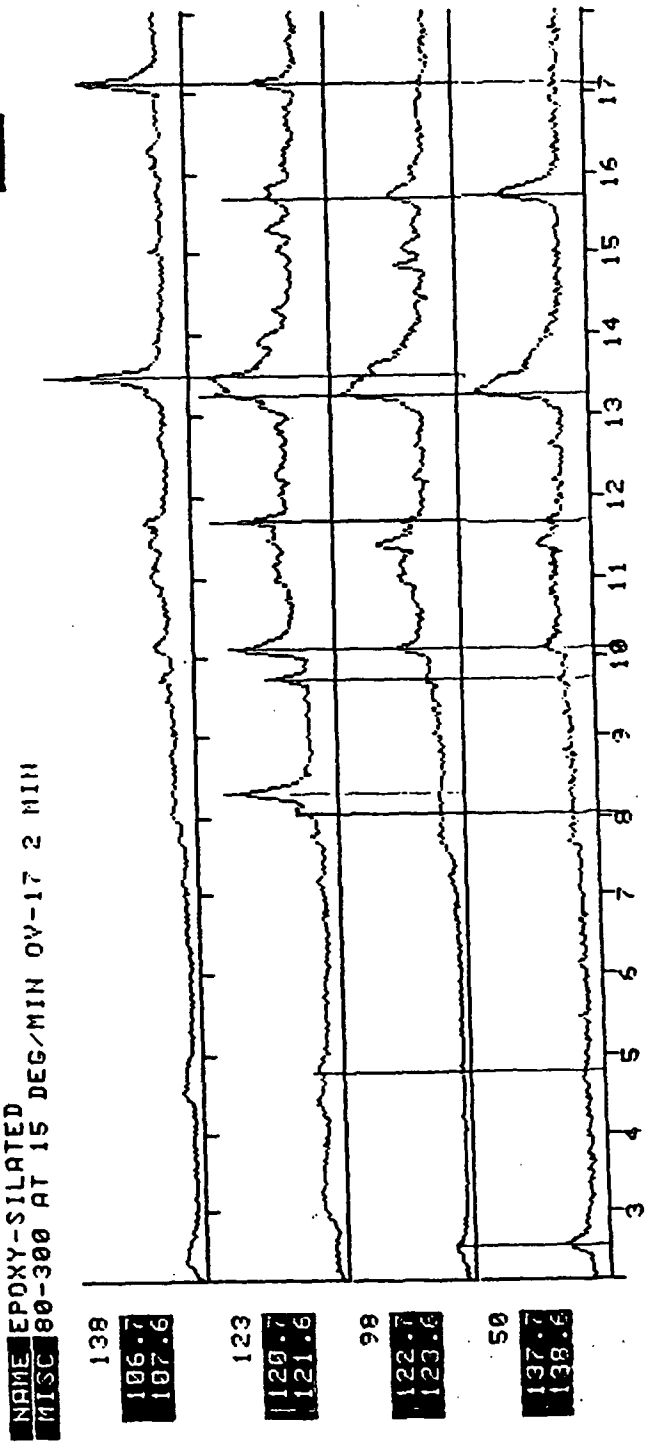

Sample GC/MS Spectra

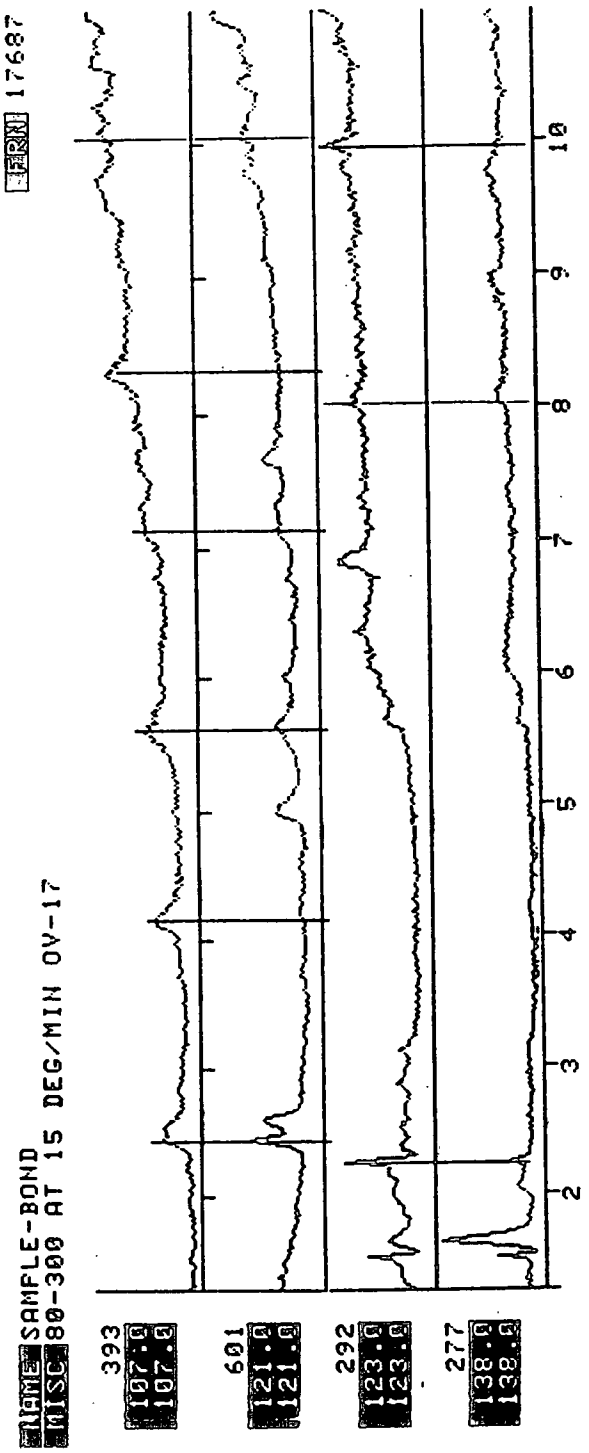

Sample GC/MS Spectra

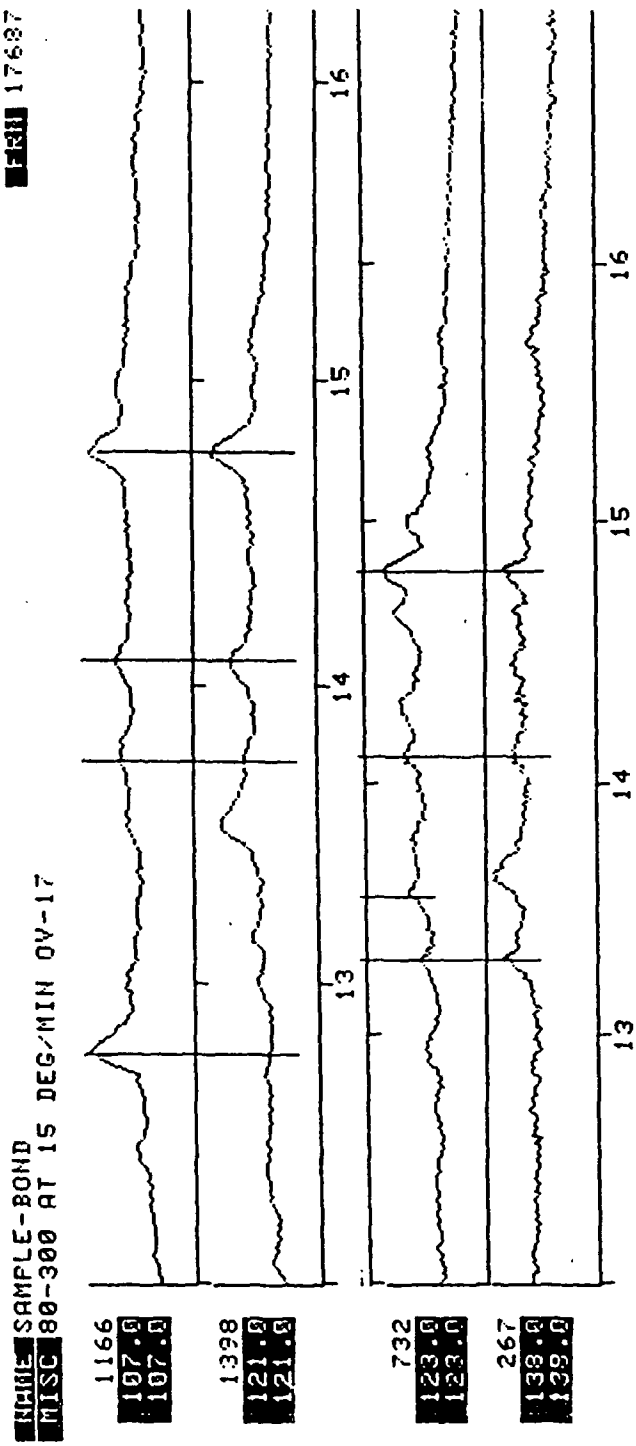

APPENDIX 3. Paper Presented At The 4th International Symposium On Wood And Pulping Chemistry, April 27-30, 1987, Paris, France.

RAMAN SPECTROSCOPIC STUDIES OF LIGNIN IN NATIVE WOODY TISSUE

R. H. Atalla, J. S. Bond, and C. P. Woitkovich
The Institute of Paper Chemistry
Appleton, WI 54912 U.S.A.

ABSTRACT

In previous reports we have described the use of Raman spectroscopy in studies of celluloses and chemical pulps. We are now extending the use of this technique to investigations of lignins. In the present report we describe experiments carried out to assess the feasibility of detecting the Raman spectra of native lignins. The approach is based on recording the spectra of groundwood, subjecting it to successive delignification treatments, and subtraction of the spectra of the final pulp to identify the spectral features associated with residual lignin at each stage.

BACKGROUND

We have discussed in detail elsewhere the advantages of using Raman spectroscopy in the study of pulp and woody tissue (1). The key factors are: 1. The possibility of recording spectra with little interference from moisture; 2. The clear possibility of separating effects due to Rayleigh scattering; 3. The high dependence on vibrational motions of covalent bond systems, making the spectra particularly sensitive to molecular architecture and conformational variation; 4. The greater convenience of working with frequencies in the visible and near infrared domains of the electromagnetic spectrum.

Experimentally, the acquisition of Raman spectra requires exposure of the sample under investigation to an intense source of exciting radiation, and examination of the spectral distribution of the scattered radiation. The intensity of light at frequencies shifted relative to the exciting radiation provides a measure of the exchange of vibrational spectral energy between

the sample and the exciting electromagnetic field. The information content is not unlike that of an infrared spectrum, except that the intensity associated with a particular vibrational mode is highest for the least polar motions; in this respect Raman spectra are complementary to infrared spectra.

Although detailed interpretation of the spectra of lignins is not possible without rather complex normal coordinate analyses, some spectral features can be informative when they are examined in conjunction with normal coordinate analyses of model compounds. Recent completion of such an investigation of lignin model compounds at our Institute (2) provides the background against which results of our present preliminary study are interpreted.

EXPERIMENTAL

The starting material consisted of air dried chips from loblolly pine (Pinus taeda L.). They were ground in a Wiley mill to pass through 40-mesh screen. The resulting wood meal was subjected to vacuum-assisted extraction in the following sequence: ethanol; chloroform:ethanol (2:1); ethanol; ethanol:water (1:1); water. It was then delignified by treatment with acid-chlorite at 70 deg. C (160 mL distilled water; 0.5 mL glacial acetic acid; 1.5 g $NaClO_2$ per 5 g air-dried wood meal). A small portion of wood meal (approximately 0.2 g) was removed after each hour of treatment, at which time pulping chemicals were replinished. The samples were extensively washed with distilled, deionized water immediately after removal.

The original groundwood and those treated for different periods of time were subjected to the following measurements: 1. Raman spectra; 2. FTIR diffuse reflectance spectra; 3. Klason lignin; 4. Acid soluble lignin. The Raman spectra were acquired using 514.5 nm excitation; all are the result of multiple scans. The infrared diffuse reflectance spectra were acquired with a Nicolet model 7199 spectrometer. Subtractions and integrations were carried out using the software of the dedicated computers for the respective instruments.

RESULTS AND DISCUSSION

The Raman spectra are shown in Figure 1. The spectrum of the untreated wood is clearly dominated by the 1595 cm^{-1} ring stretching mode of the aromatic rings in lignin, while that of the sample treated for 6 hours is typical of the celluloses from wood pulps, except for the small residue of the lignin peak at 1595 cm^{-1}. The spectra of intermediate samples show the changes resulting from the progressive removal of the lignin.

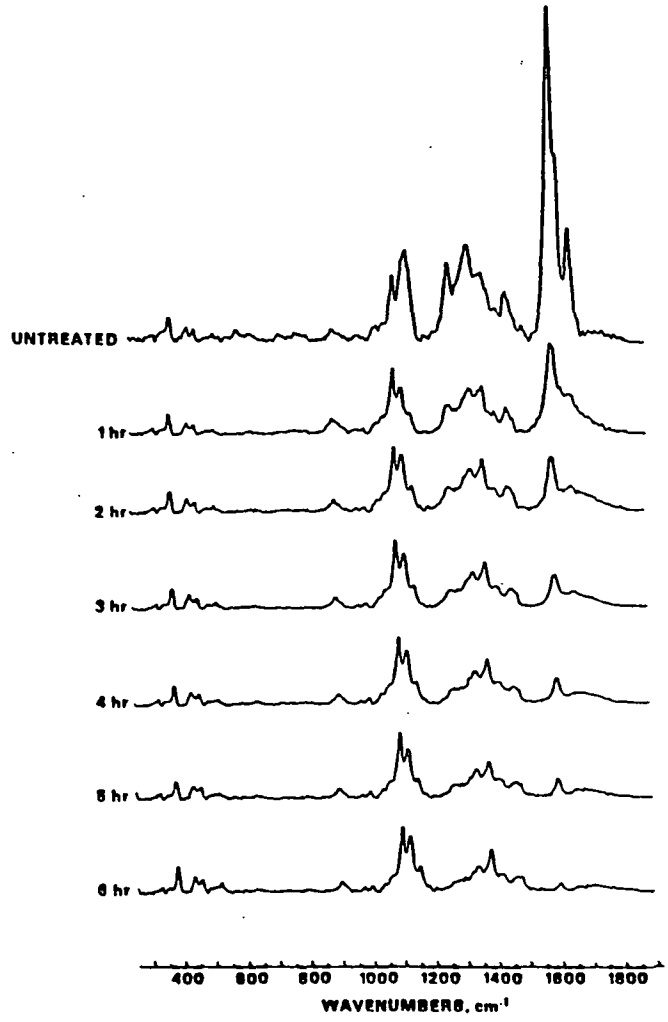

Figure 1. Raman spectra of wood meal from loblolly pine before and after delignification for 1 to 6 hours.

The changes in the spectra are highlighted more clearly in Figure 2, which represents the results of subtraction of the spectrum of the sample treated for 6 hours from all of the preceeding spectra. Clearly the most dramatic change occurs during the first hour of treatment. This is shown in Figure 3, where the intensity of the 1595 cm^{-1} band is plotted against lignin content. The intensity of the band in the original wood is a little over 4 times that of its intensity after the first period of treatment.

Another interesting feature which is obvious in Figure 2, is the total disappearance of the 1138 cm^{-1} band during this same interval. The other bands in the spectra appear to decay in proportion to the residue of the 1595 cm^{-1} band.

Finally, it is clear that the contribution of lignin to the low frequency portion of the spectrum is very limited indeed. This is consistent with the pattern observed by Ehrhardt (2) for the lignin model compounds, where, with regularity, the spectra were dominated by one or another of the symmetric stretching vibrations of the aromatic rings.

A discussion of all the features in the spectra are beyond the scope of this report, but two observations are worthy of note. The first is the rapid decline of the 1595 cm^{-1} band during the first interval, and the correlated decline of the 1138 cm^{-1} band. These suggest a common origin in aromatic rings with a distinctive pattern of substitution, which may be particularly sensitive to attack under the conditions of delignification. The studies on model compounds suggest that the 1138 cm^{-1} band has its origin in the stretching vibration between the aromatic ring and one of its substituent groups. If this is indeed the case, this substituent group must be one that has an effect on the scattering coefficient of the 1595 cm^{-1} band. We are actively assessing the validity of this interpretation.

The second interesting feature is the linearity of the plot in Figure 3, apart from the value for the original wood sample. The quality of this fit is superior to those derived from the 1510 and the 1590 cm^{-1} bands in the FTIR diffuse reflectance spectra. Though this observation

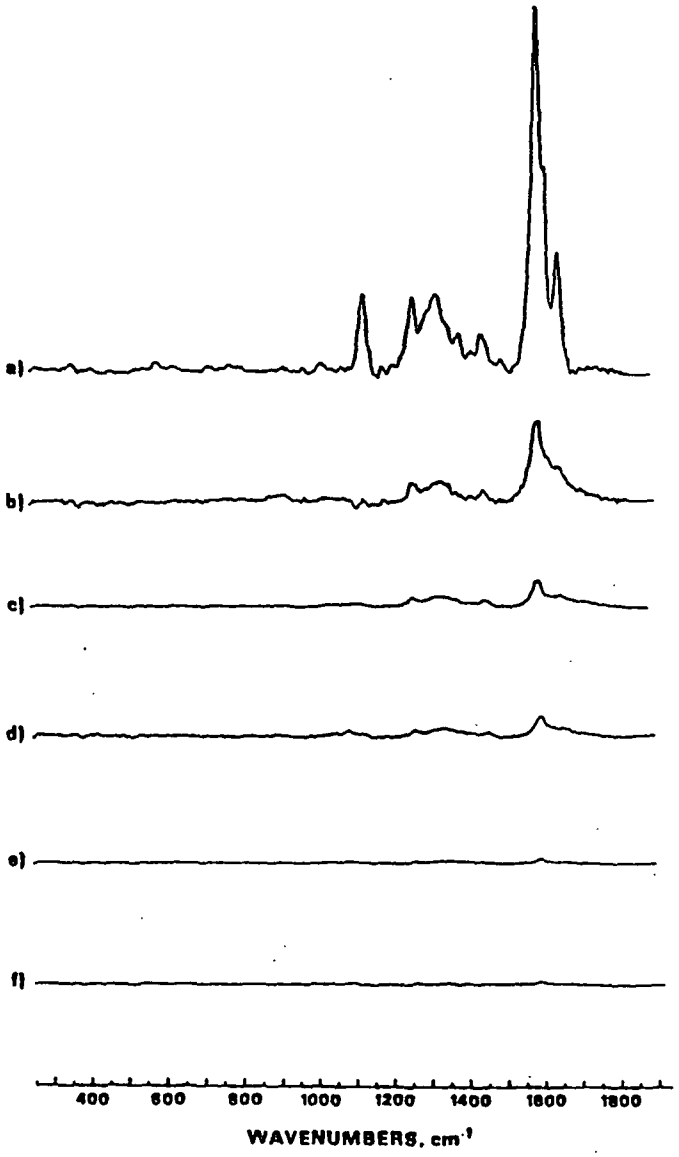

Figure 2. Difference spectra comparing the first six samples with the sample treated for six hours.

needs to be investigated further, it may reflect a lower sensitivity of the intensity of the aromatic ring stretching bands to substituents in the Raman effect than in infrared absorption. Thus, as the distribution of substituents on the aromatic rings varies during the progress of delignification, the absorption coefficients of

the infrared bands will change over a wider range than the scattering coefficients of the Raman bands.

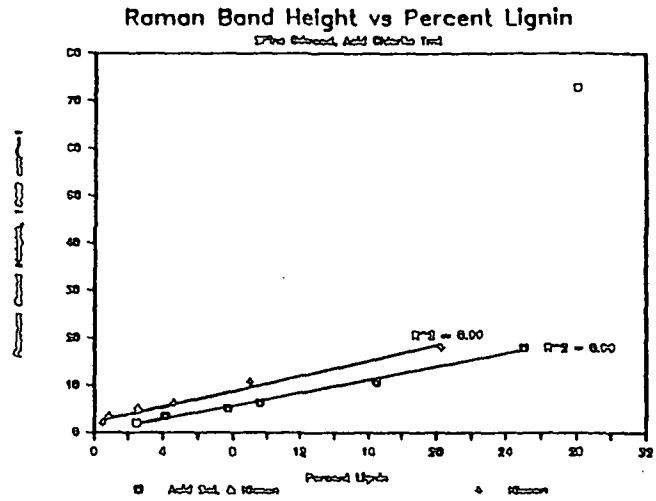

Figure 3. Variation of the intensity of the 1595 cm^{-1} band with lignin content.

REFERENCES

1. ATALLA, R. H. J. Wood Chem. and Tech., In press.

2. EHRHARDT, S. M. Doctoral Dissertation, The Institute of Paper Chemistry, Appleton, Wisconsin 1984.

APPENDIX 4. Specifics for Chemical Treatments.

Acid-chlorite (AC):

Recipe[8] - 0.083M solution ($NaClO_2$):

160 ml distilled water,

0.5 ml glacial acetic acid,

1.5 g sodium chlorite (80% active).

Monolignol - Treated with 10% excess ClO_2^-.

Woody section - Extracted with ethanol/toluene (1:2 v/v) at 25°C prior to treatment,

30 minutes contact time at 25°C,

Gentle agitation every 5 minutes,

Washed with distilled water 3 times.

Sodium borohydride (BH):

Recipe - 0.25M:

9.46 g $NaBH_4$/1000 ml distilled water.

Monolignol - Treated with 50% excess BH_4^-.

Woody section - Extracted with ethanol/toluene (1:2 v/v) at 25°C prior to treatment,

24 hour contact time at 25°C,

Gentle agitation throughout treatment,

Washed with distilled water 3 times.

AC/BH (BH/AC): After the initial treatment the woody section was stored in distilled water for 24 hours (4°C, dark), then subsequently treated with the second reagent.

Diethylenetriaminepentaacetic Acid (DTPA):

Recipe - 0.0025M:

1.0 g DTPA/1000 ml distilled water.

Woody section - Extracted with ethanol/toluene (1:2 v/v) at 25°C prior to treatment,

75 hour contact time at 25°C,

Solution changed after 22 and 52 hours,

Washed with distilled water 3 times.

Methylation: Extracted woody section solvent exchanged into methanol,

14 day contact time with DME (see below) at -18°C,

Washed with methanol,

Solvent exchanged into water.

DME reagent - 40% diazomethane and 10% methanol in anhydrous ether.

Trimethylphosphite (TMP): Extracted woody section solvent exchanged into methanol,

(Following done in nitrogen atmosphere)

Rinsed 6 times with dichloromethane (DCM),

Treated with 10 µL TMP in 10 ml DCM for 27.5 hours at 25°C (100 fold excess TMP relative to assumed number of quinone-type structures in native lignin - 3 per 100 C_9 units),

6 washes with 25 ml DCM,

2 washes with 25 ml DCM, 30 minute contact time stored in DCM under nitrogen.

Quenchers: Raman spectra were collected from wood sections immersed in 0.1M solutions of potassium iodide (KI) and copper (II) chloride ($CuCl_2$).

0.1M KI - 16.6 g/1000 ml distilled water.

0.1M $CuCl_2$ - 17.05 g/1000 ml distilled water (dihydrate).

APPENDIX 5. Raman Spectra Of Lignin Model Compounds (pure and 0.1M in methanol).

Pure Compound
α,4-Dihydroxy-3-Methoxyacetophenone

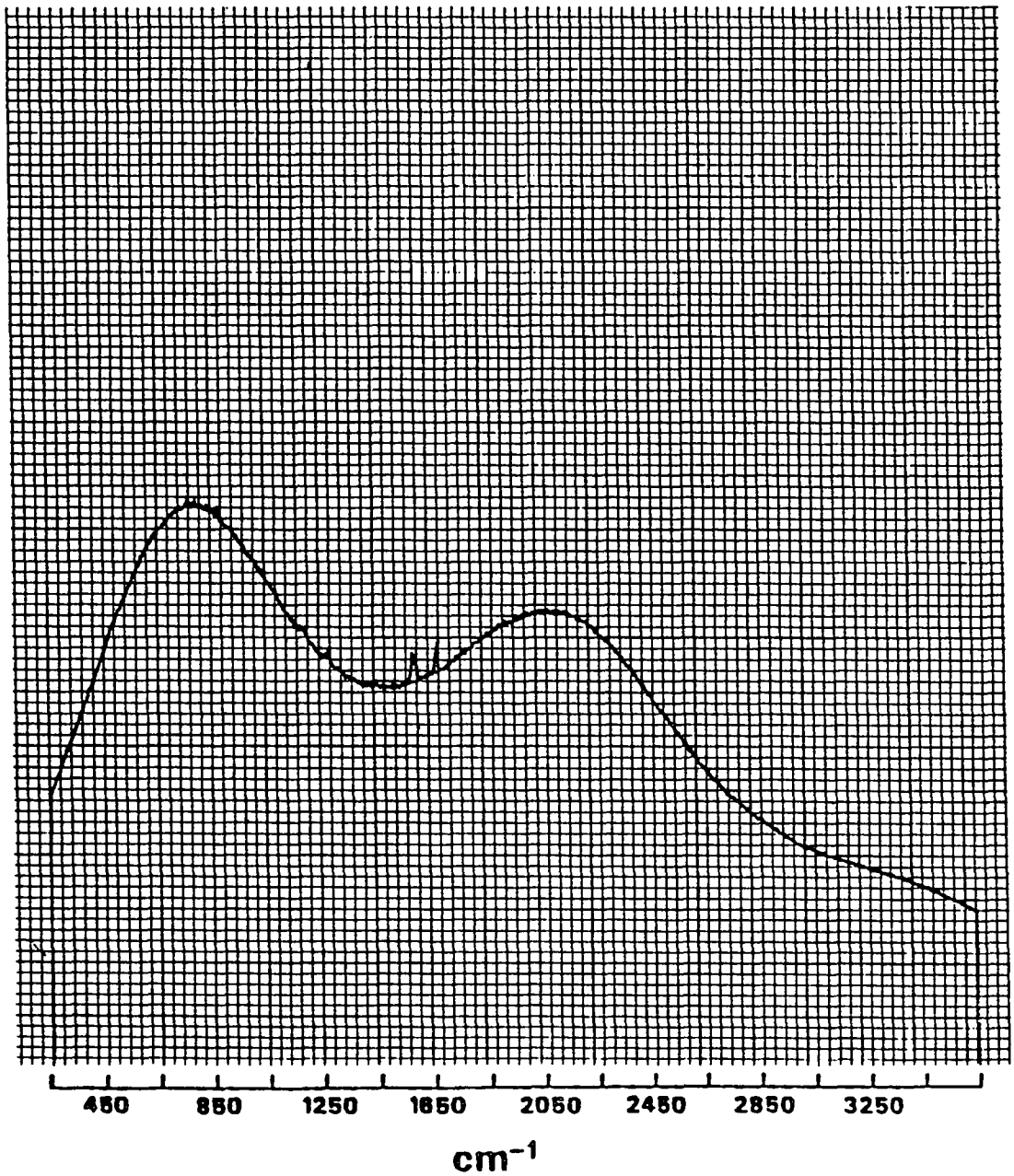

Pure Compound
Coniferaldehyde

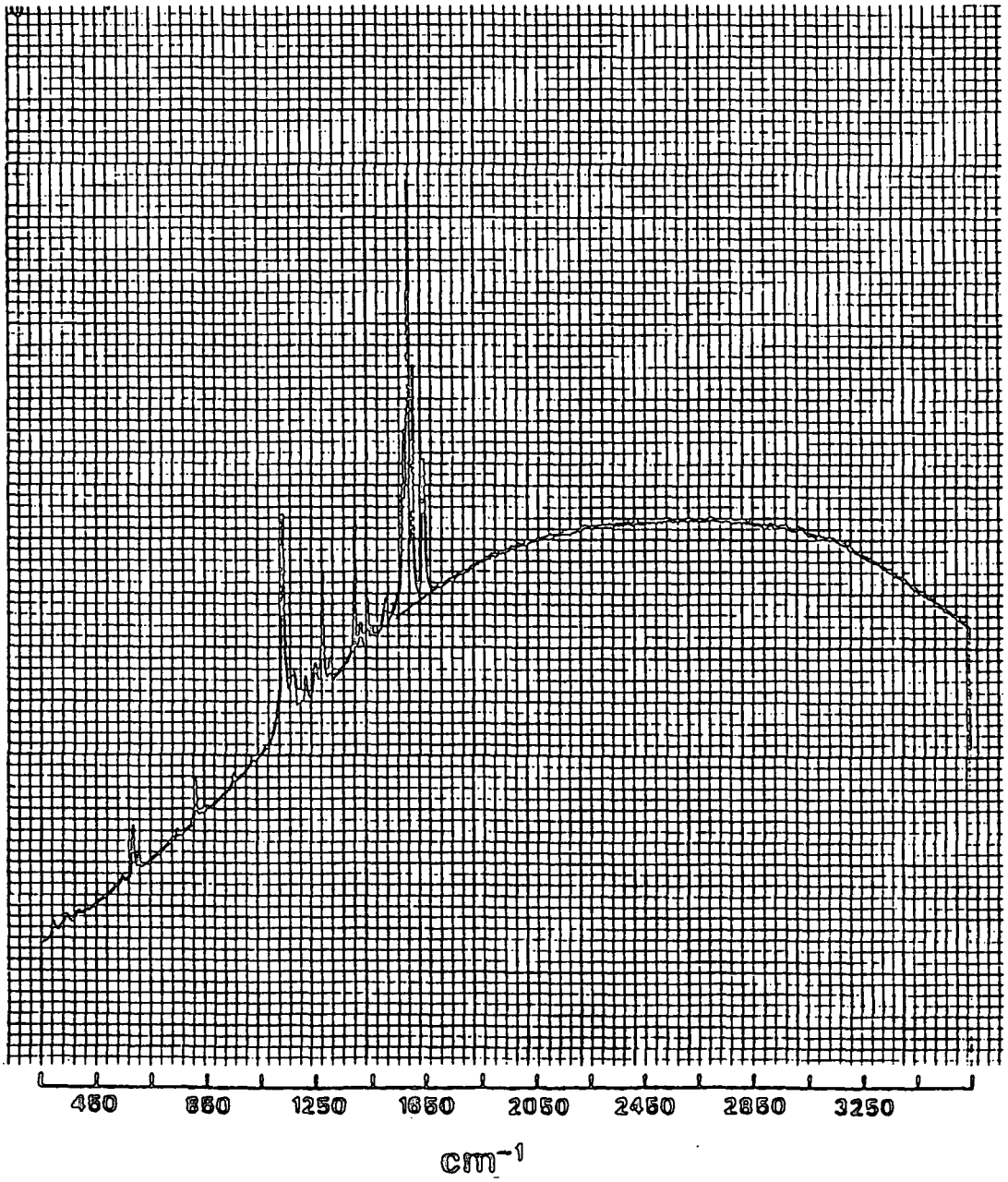

Pure Compound
Coniferyl Alcohol

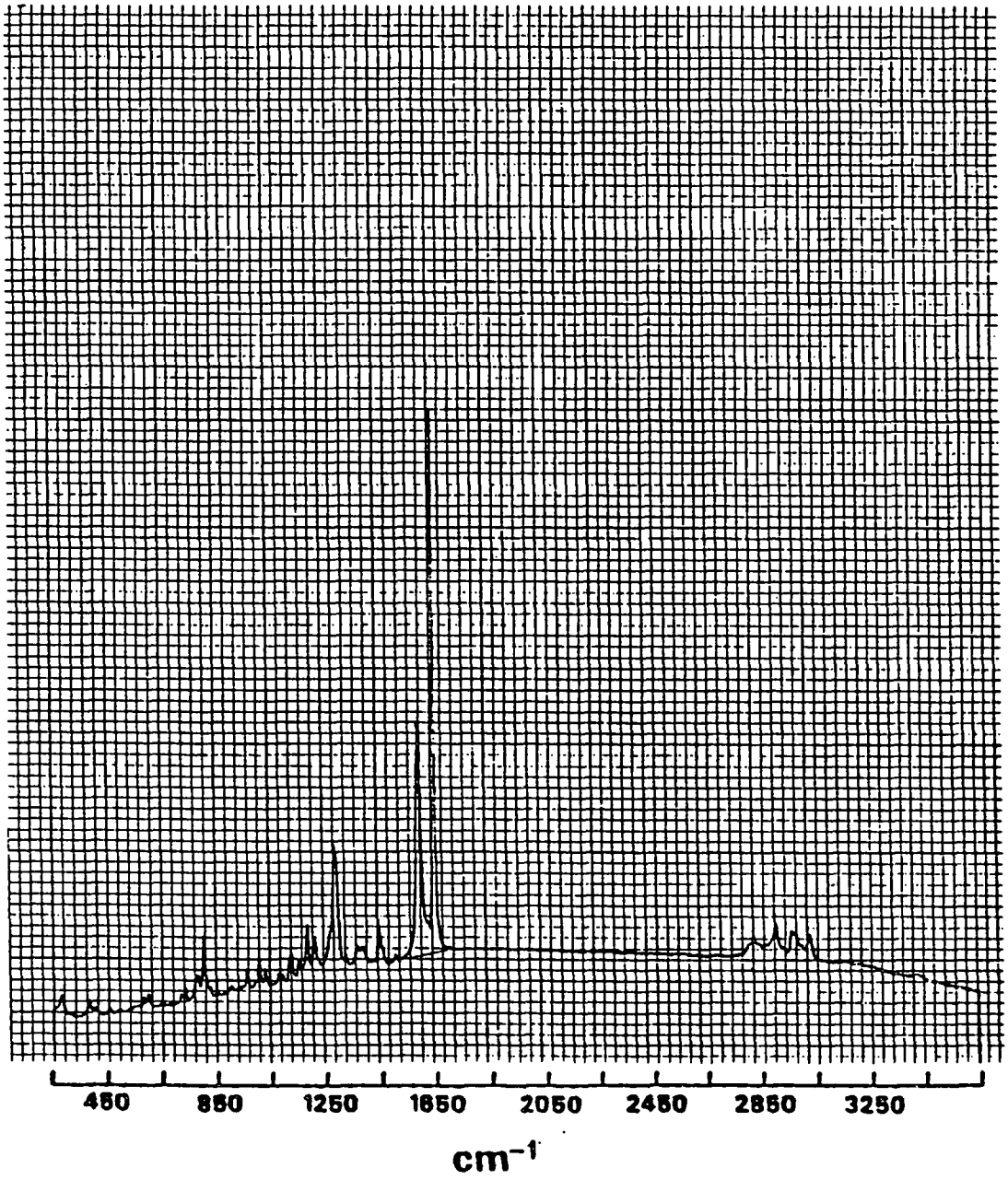

Pure Compound
Guaiacyl Propanol

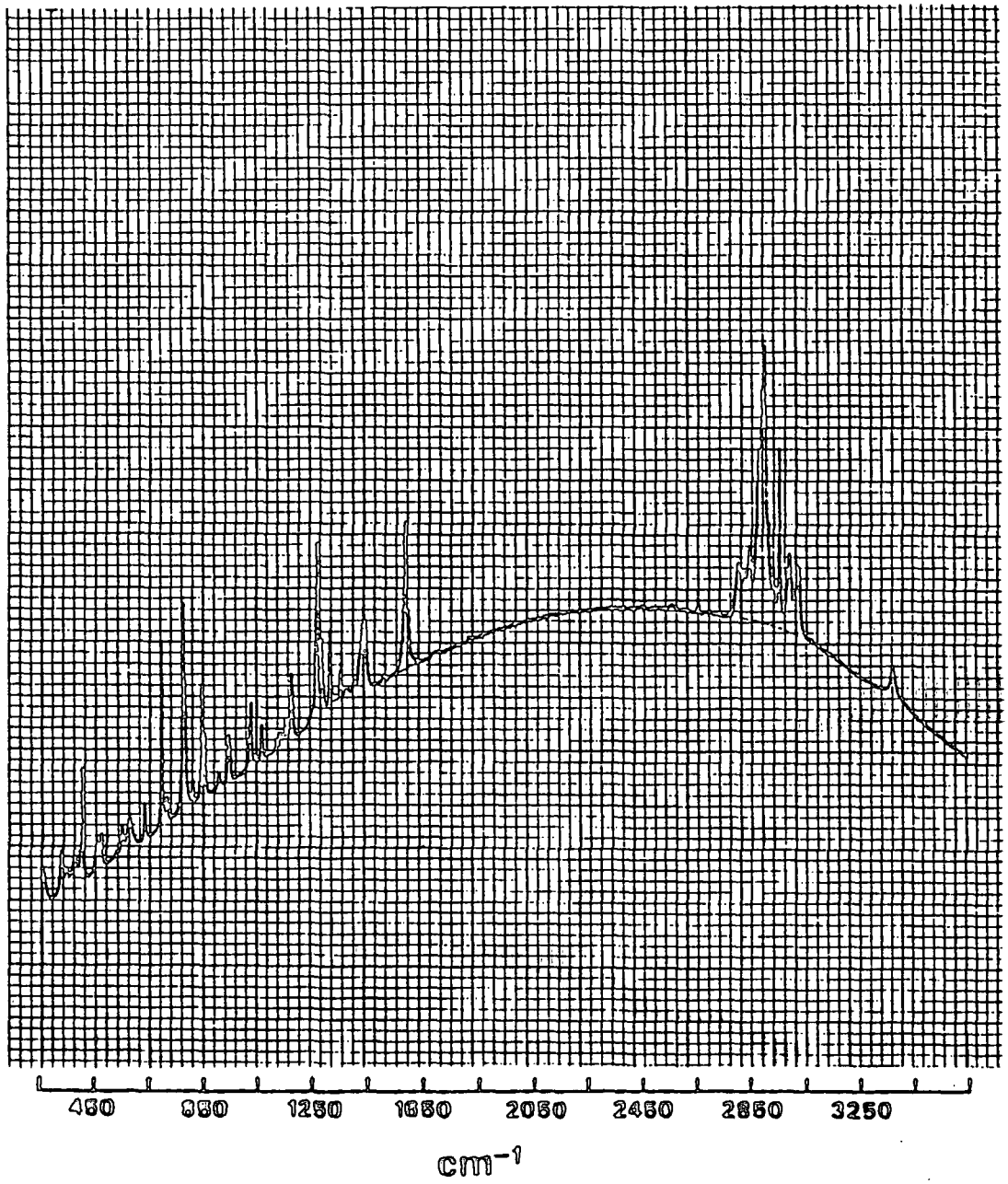

0.1M in Methanol
α,4-Dihydroxy-3-Methoxyacetophenone

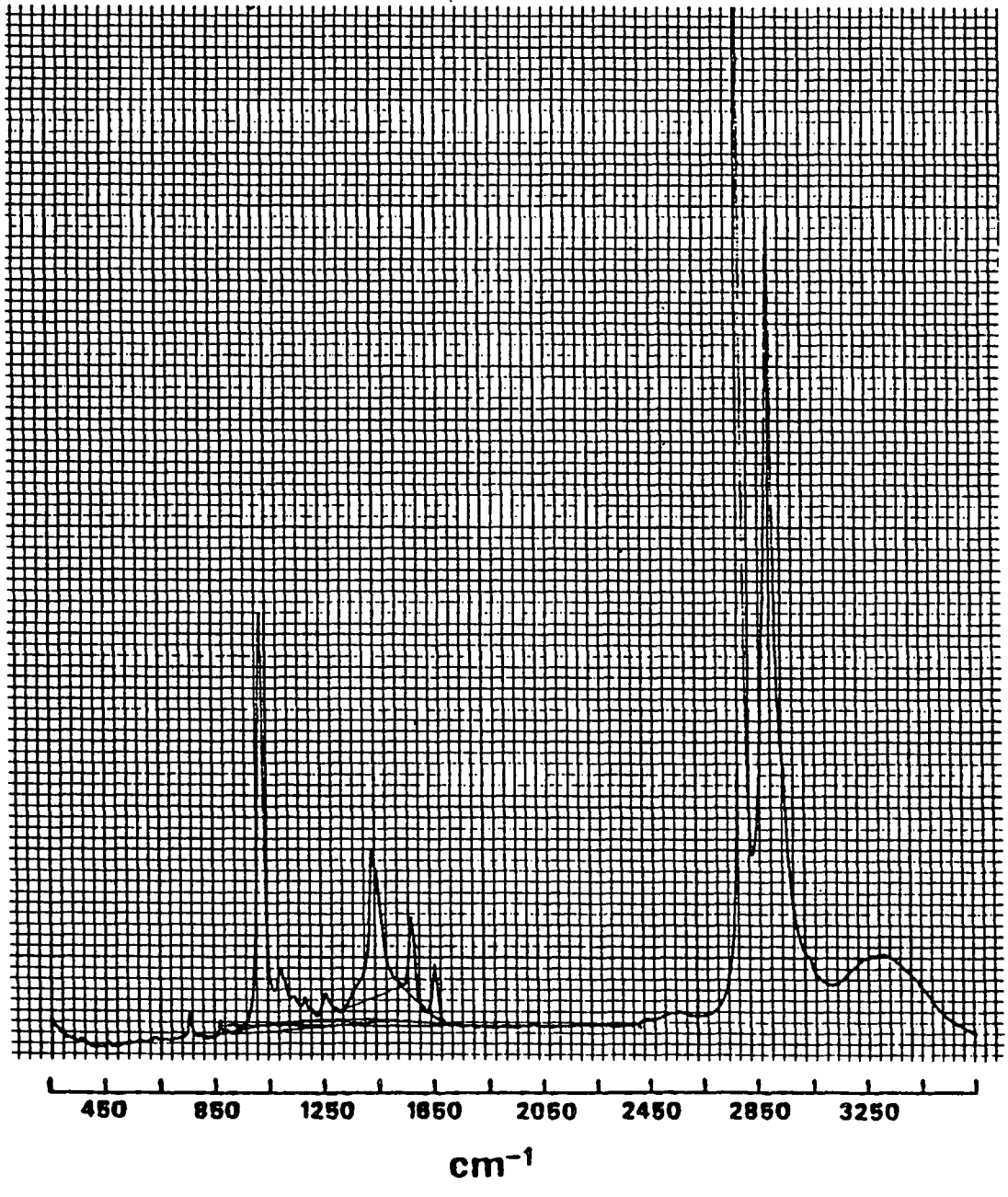

0.1M in Methanol
Coniferaldehyde

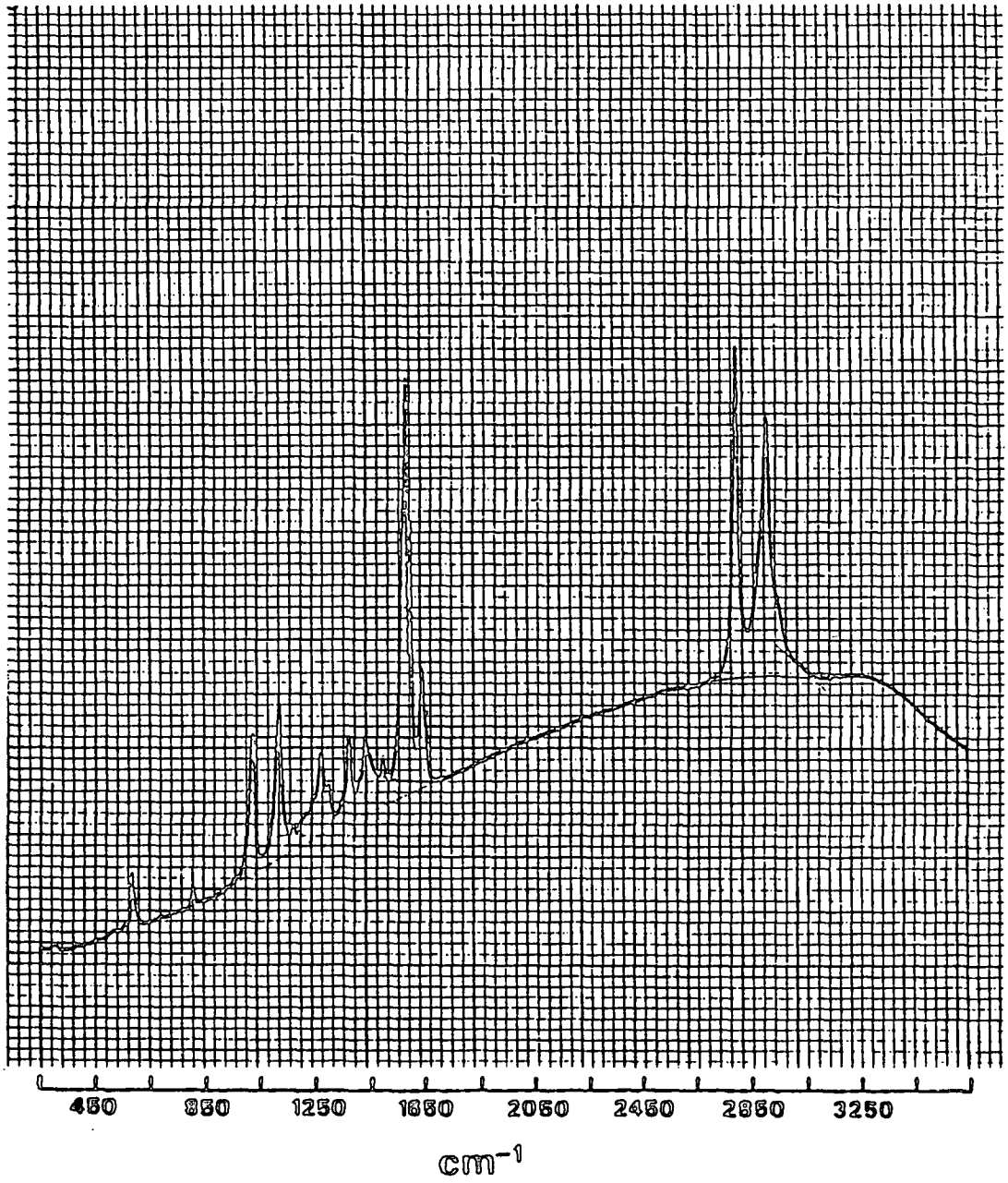

0.1M in Methanol
Coniferyl Alcohol

0.1M in Methanol
Guaiacyl Propanol

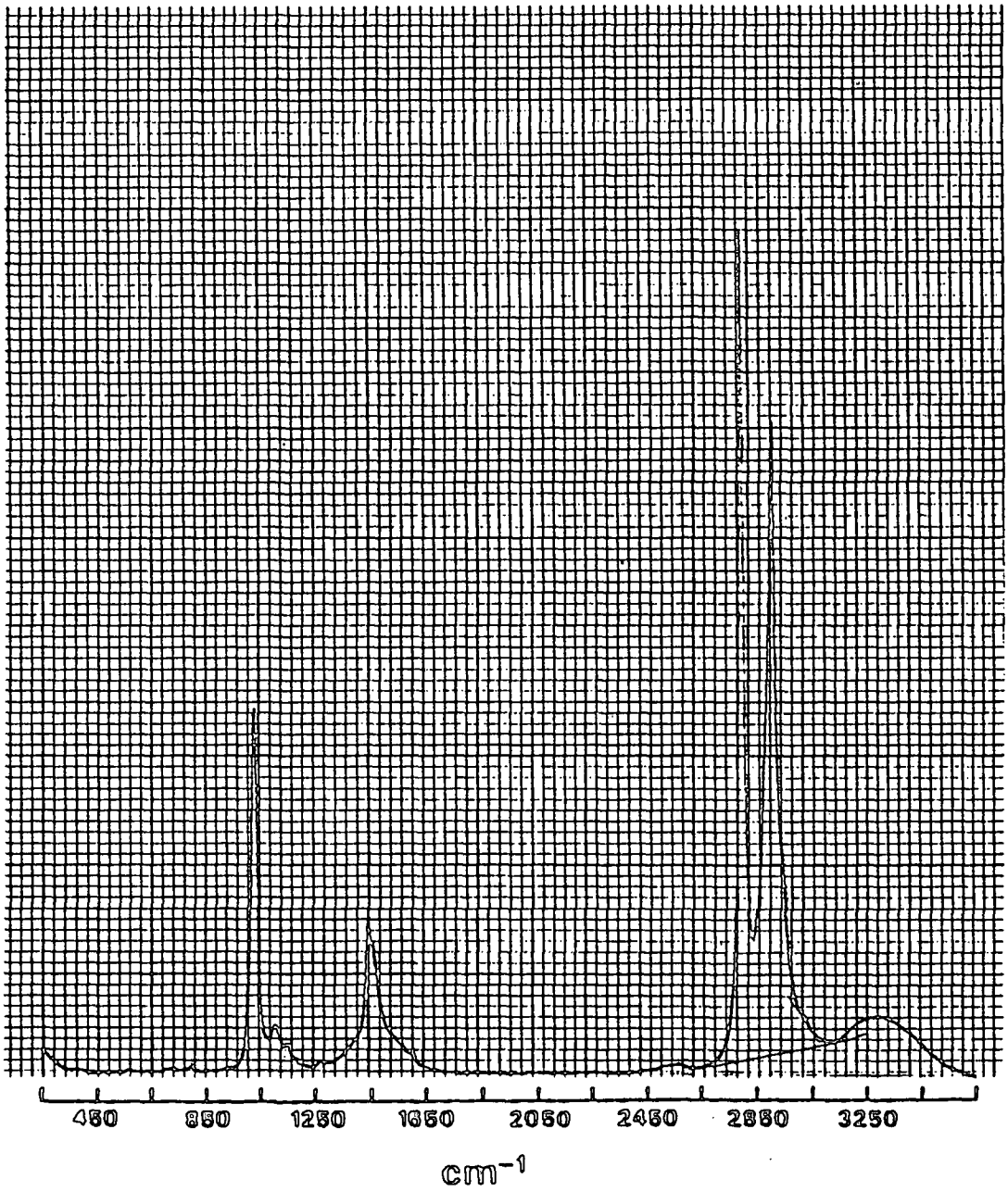

APPENDIX 6. Raman Spectra Of Lignin Model Compounds Treated With Acid-Chlorite (0.075M monolignol, 0.083M $NaClO_2$).

Acid-Chlorite Treatment
α,4-Dihydroxy-3-Methoxyacetophenone

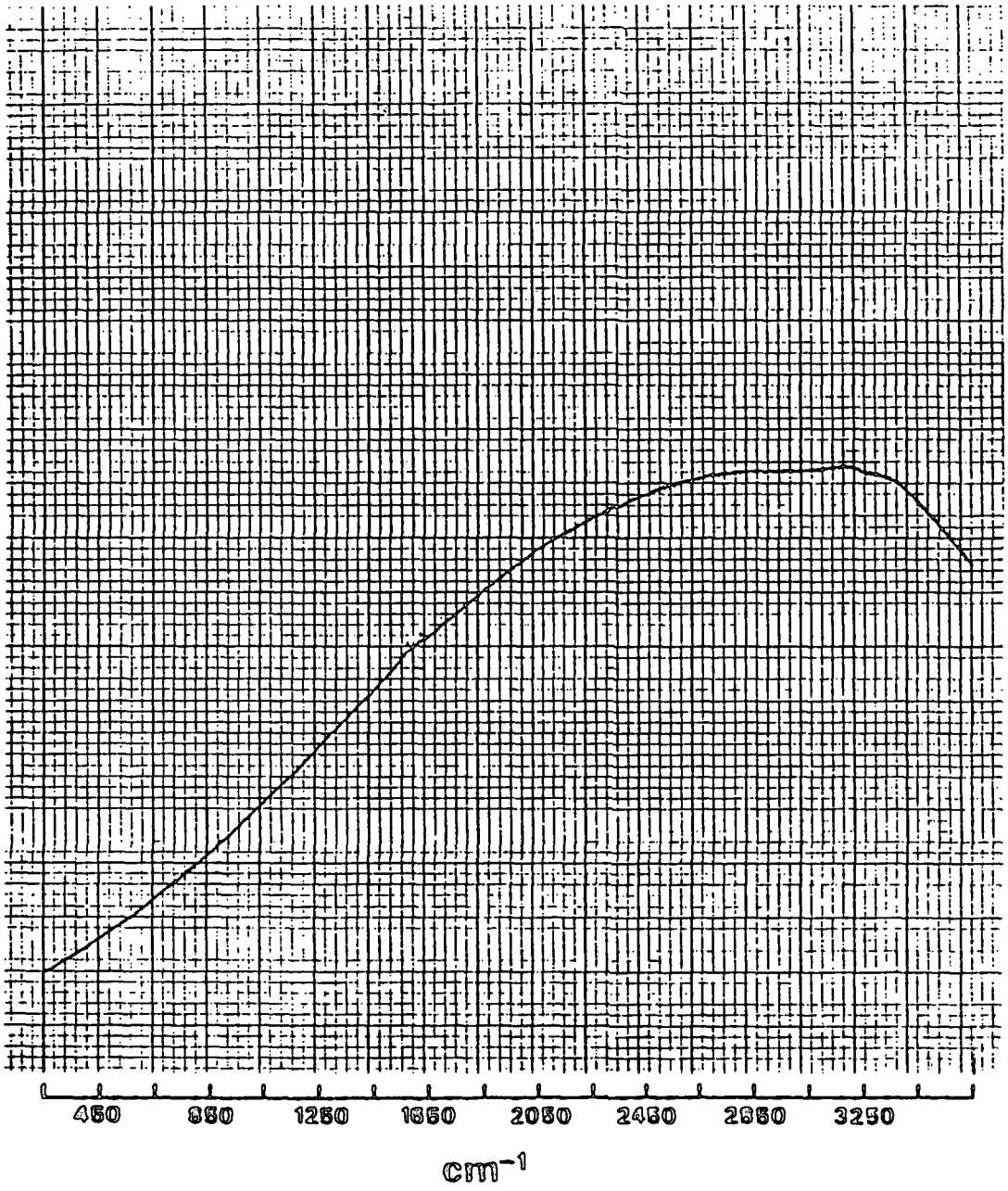

Acid-Chlorite Treatment
Coniferaldehyde

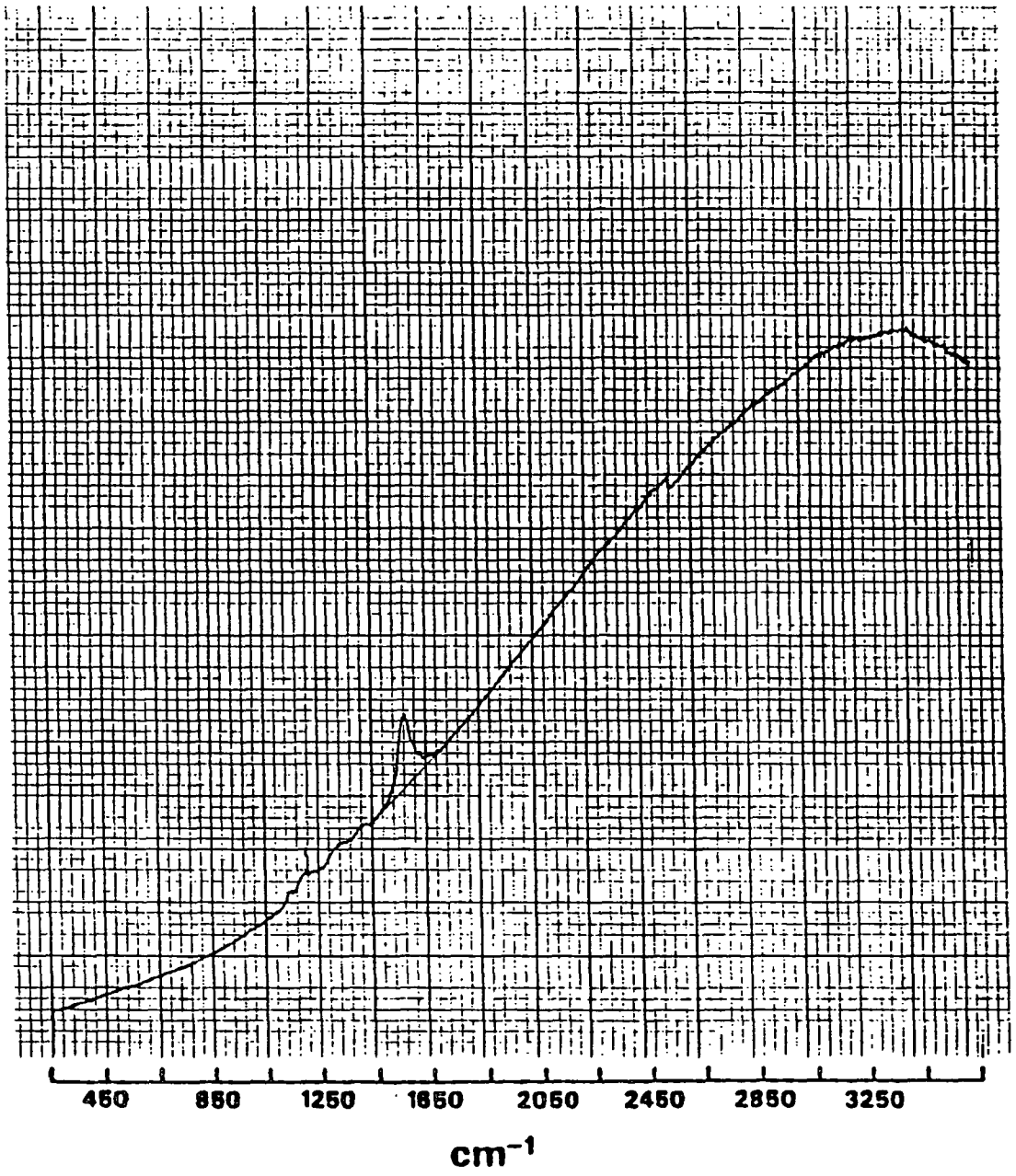

Acid-Chlorite Treatment
Coniferyl Alcohol - 6 hour

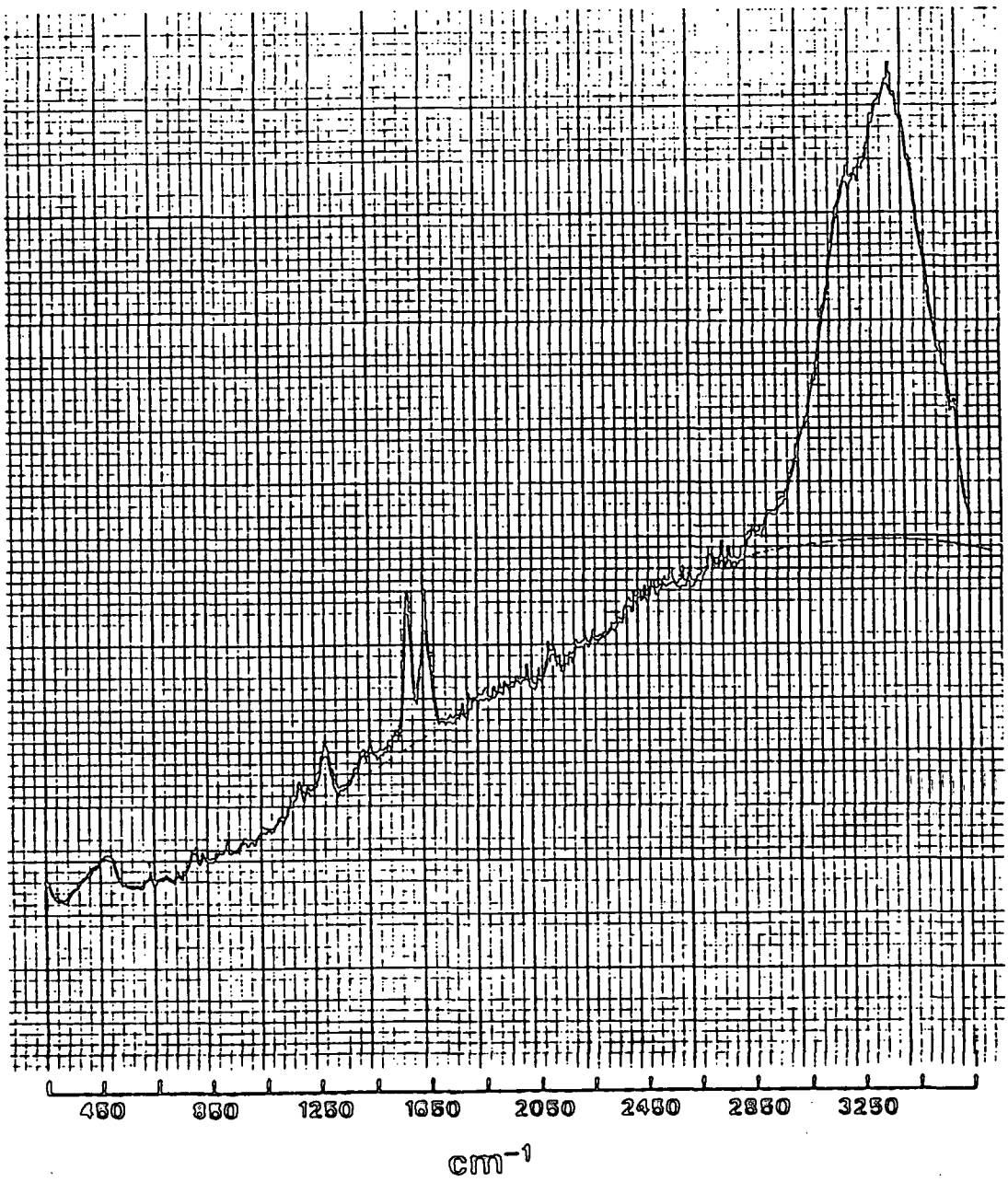

Acid-Chlorite Treatment
Coniferyl Alcohol - 16 day

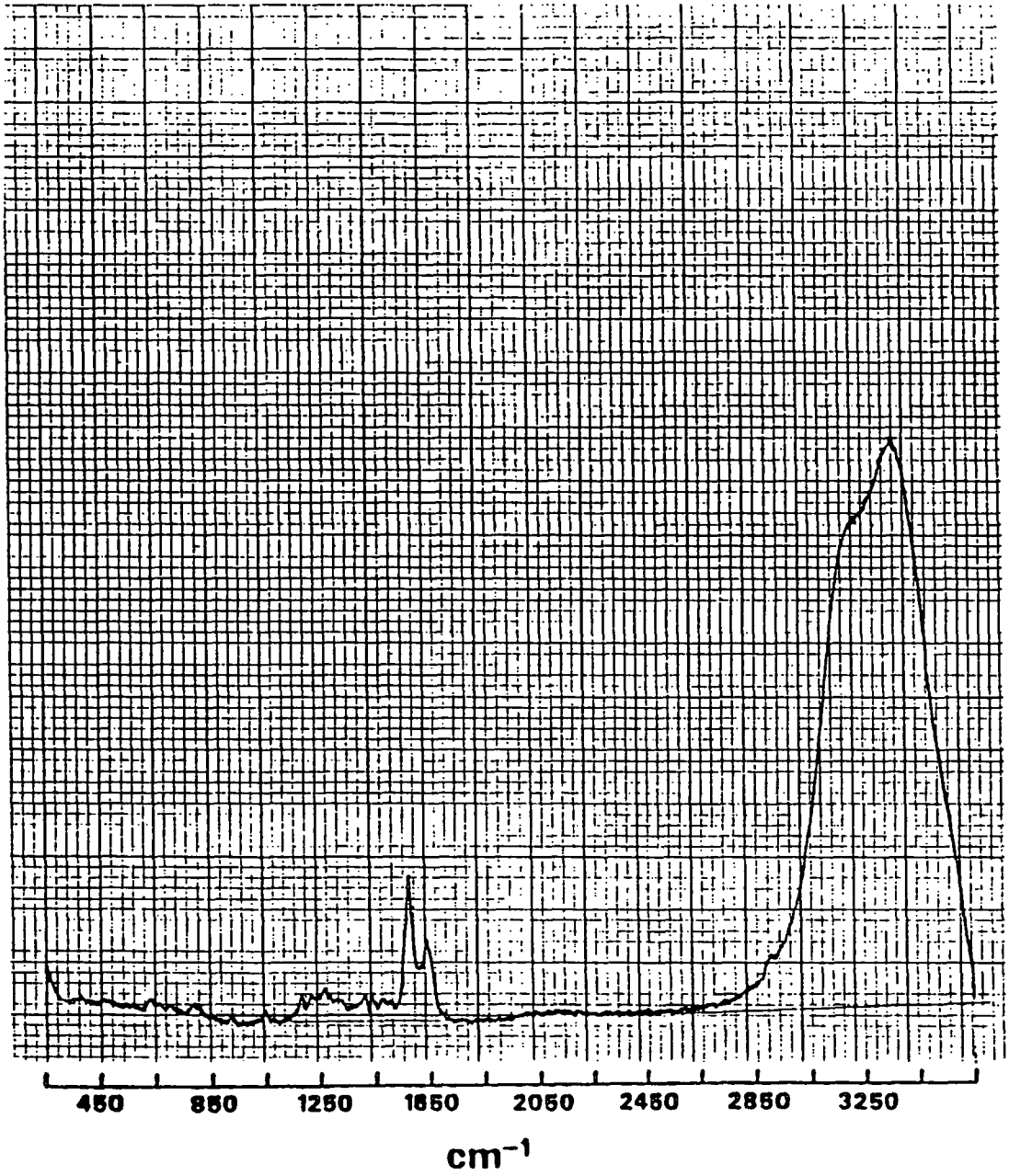

Acid-Chlorite Treatment
Guaiacyl Propanol - 6 hour

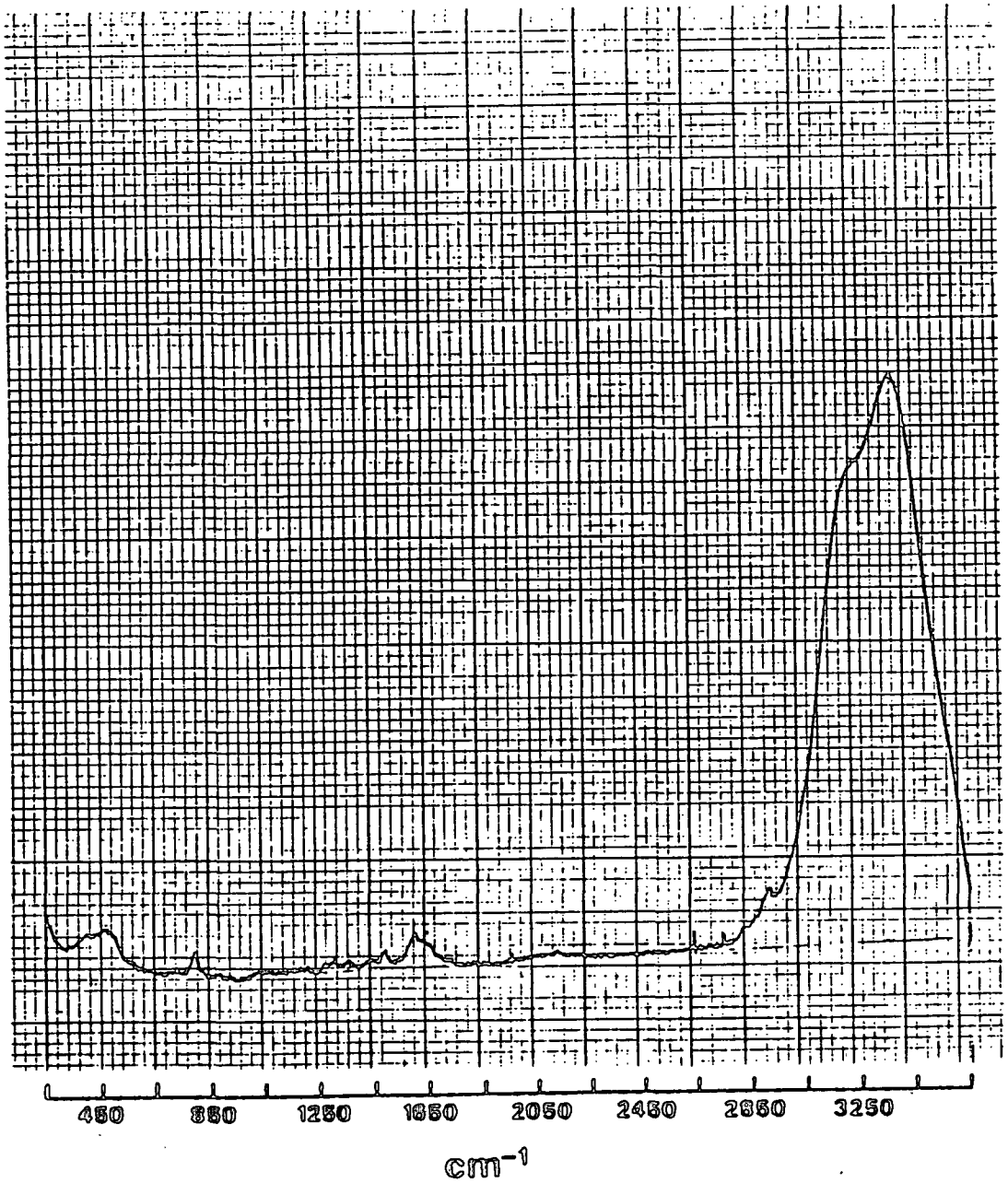

Acid-Chlorite Treatment
Guaiacyl Propanol - 26 day

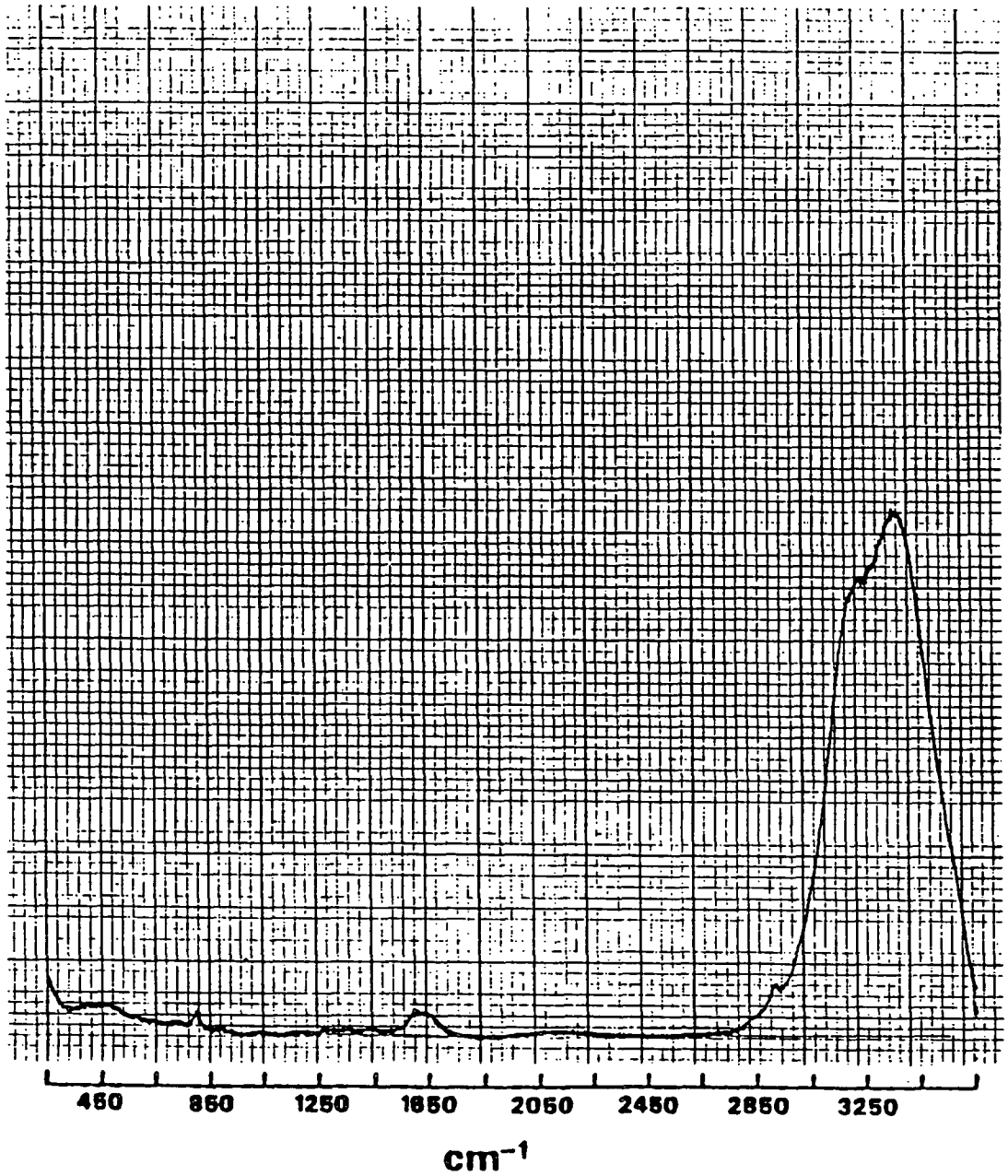

APPENDIX 7. Raman Spectra Of Lignin Model Compounds Treated With Sodium Borohydride (0.167M monolignol, 0.250M $NaBH_4$).

Sodium Borohydride Treatment
α,4-Dihydroxy-3-Methoxyacetophenone

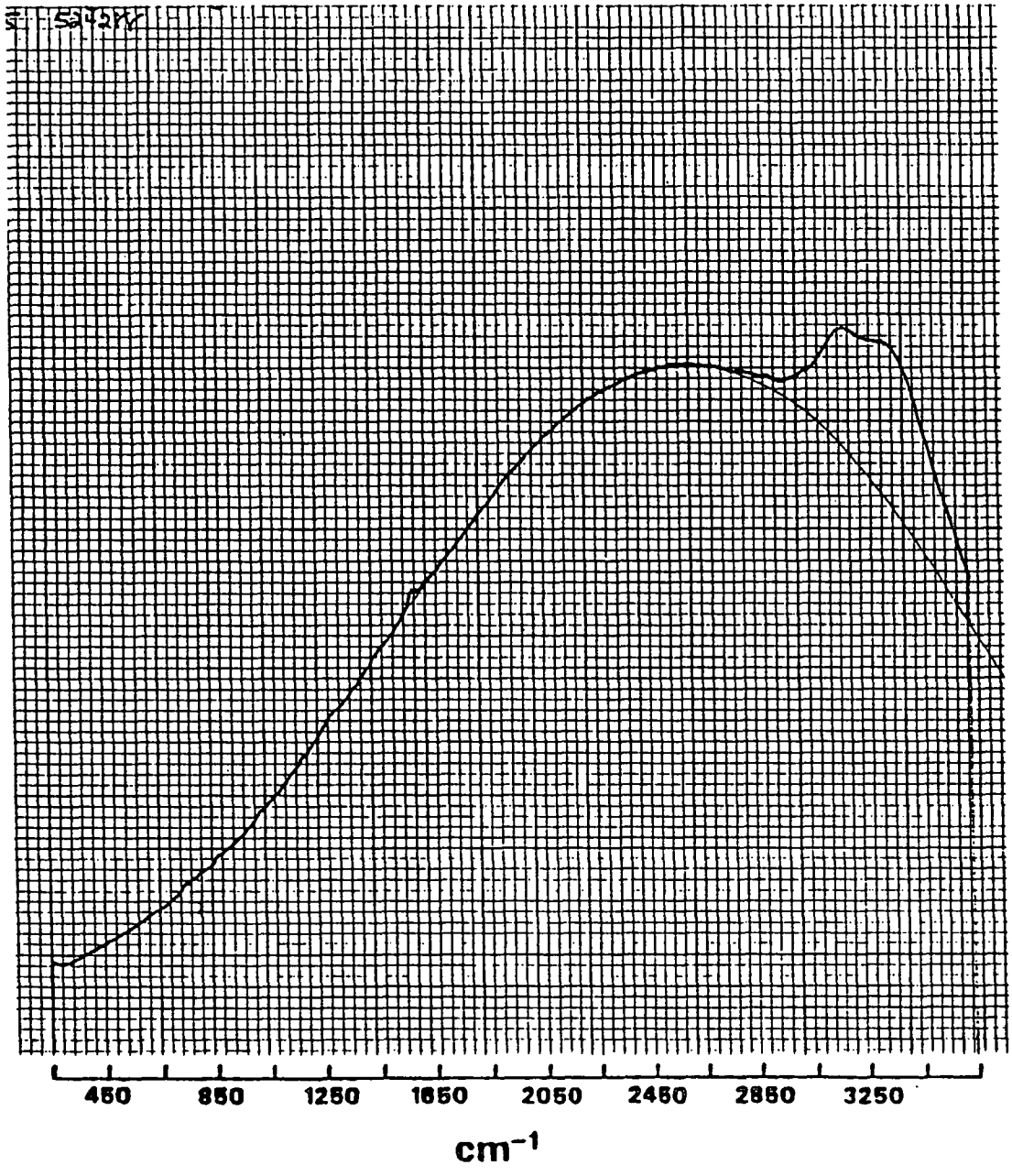

Sodium Borohydride Treatment
Coniferaldehyde

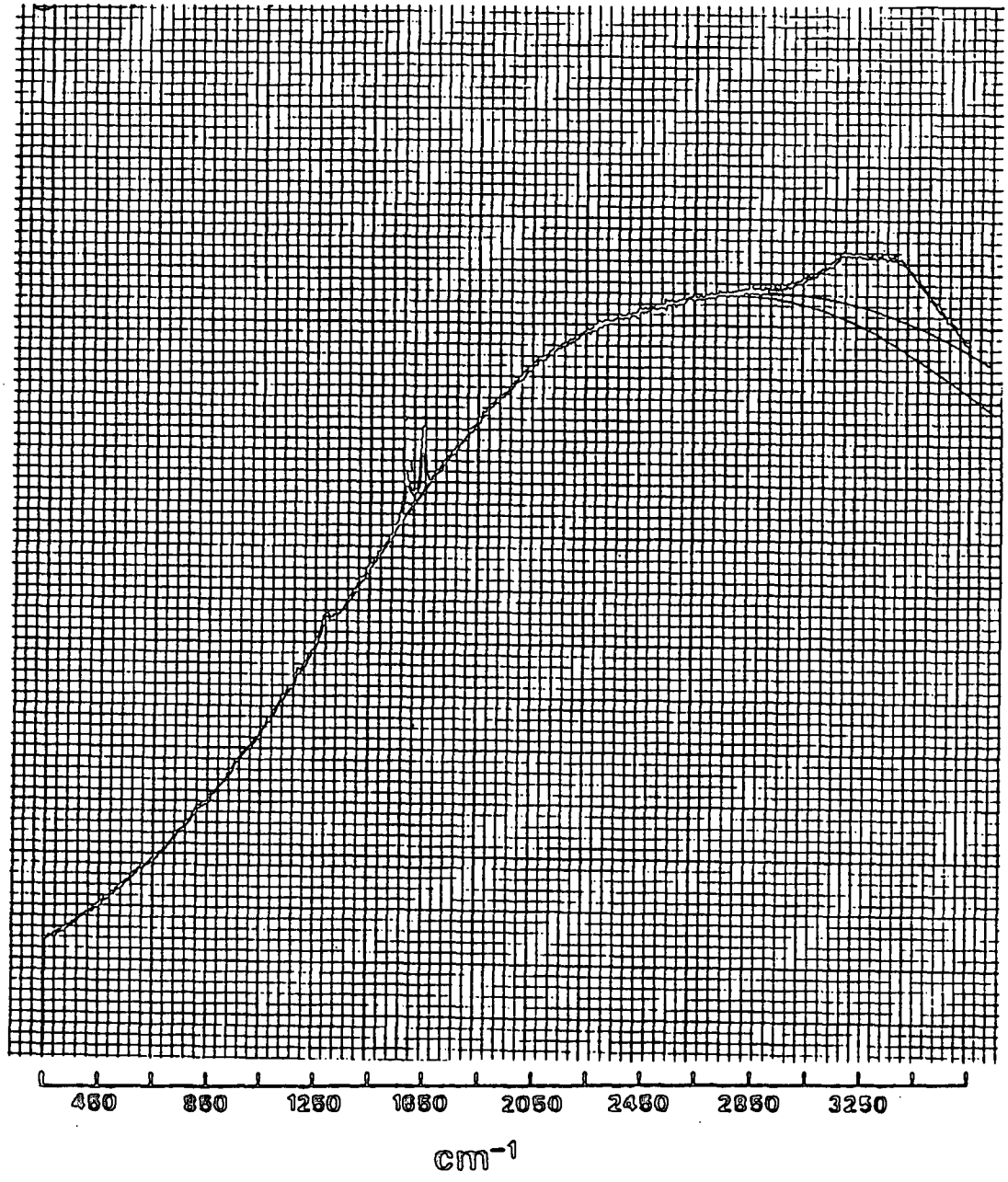

Sodium Borohydride Treatment
Coniferyl Alcohol

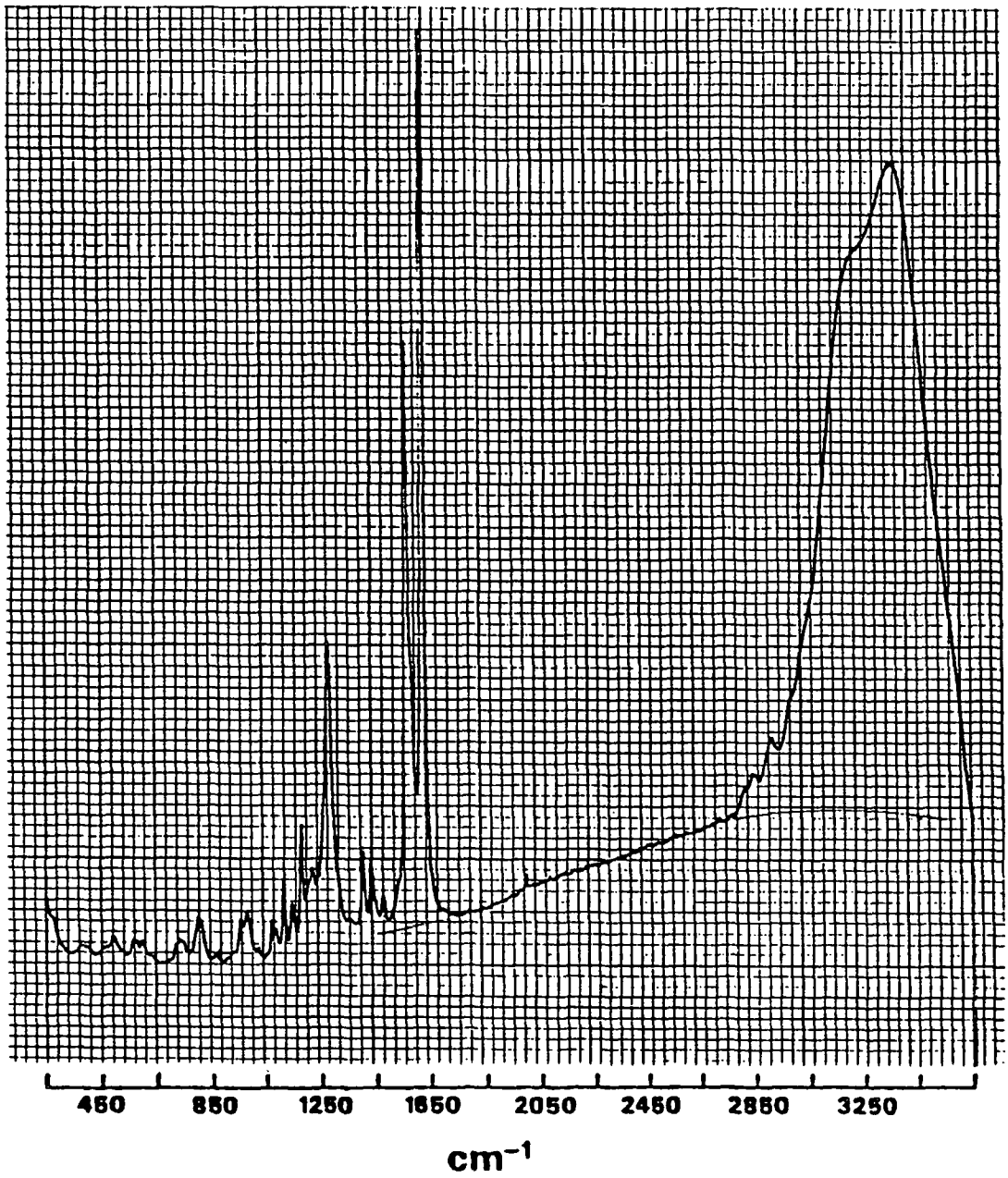

Sodium Borohydride Treatment
Guaiacyl Propanol

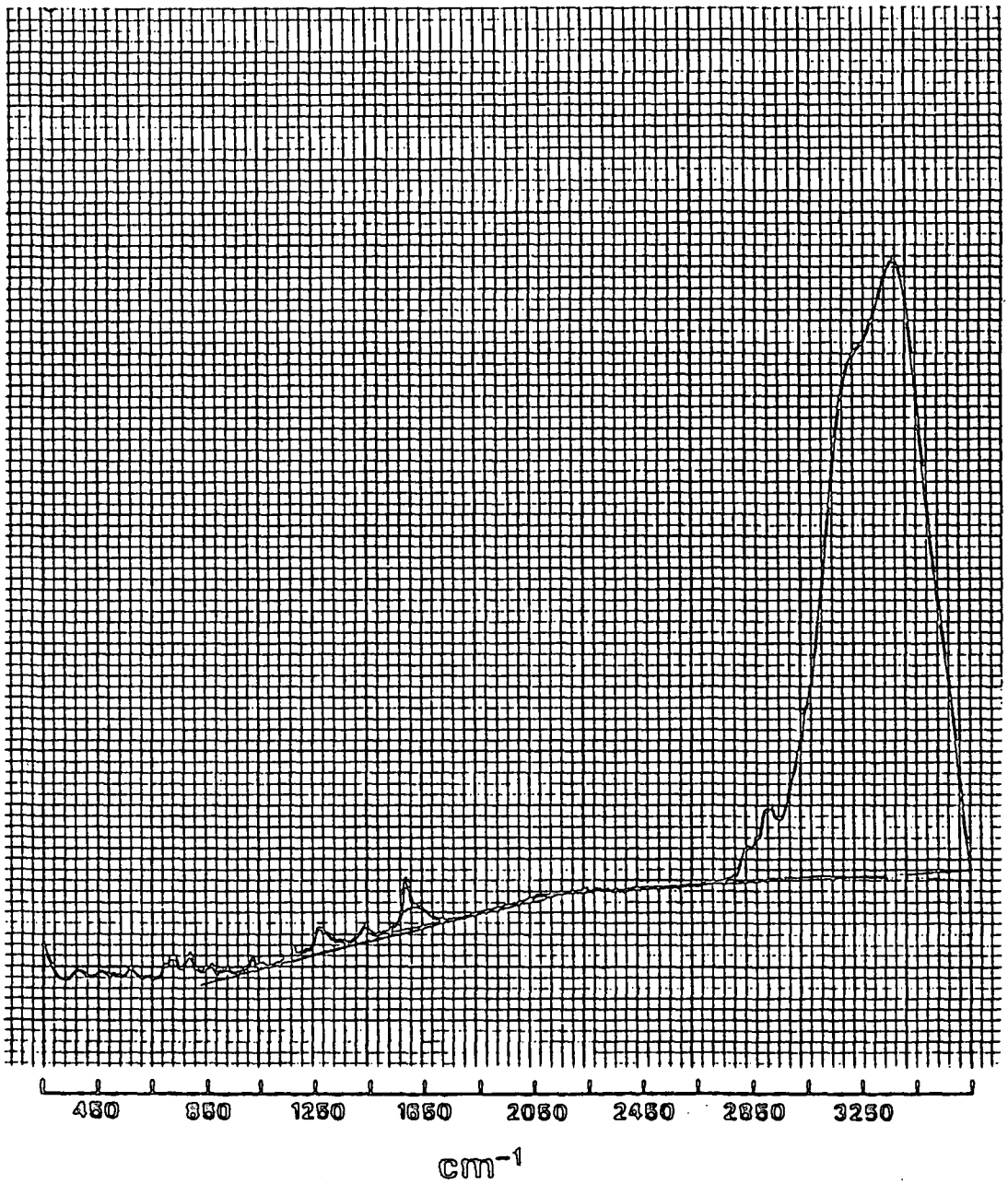

APPENDIX 8. Raman Spectra Of Chemically Modified Black Spruce Radial Thin Sections.

Control - 514.5 nm Excitation

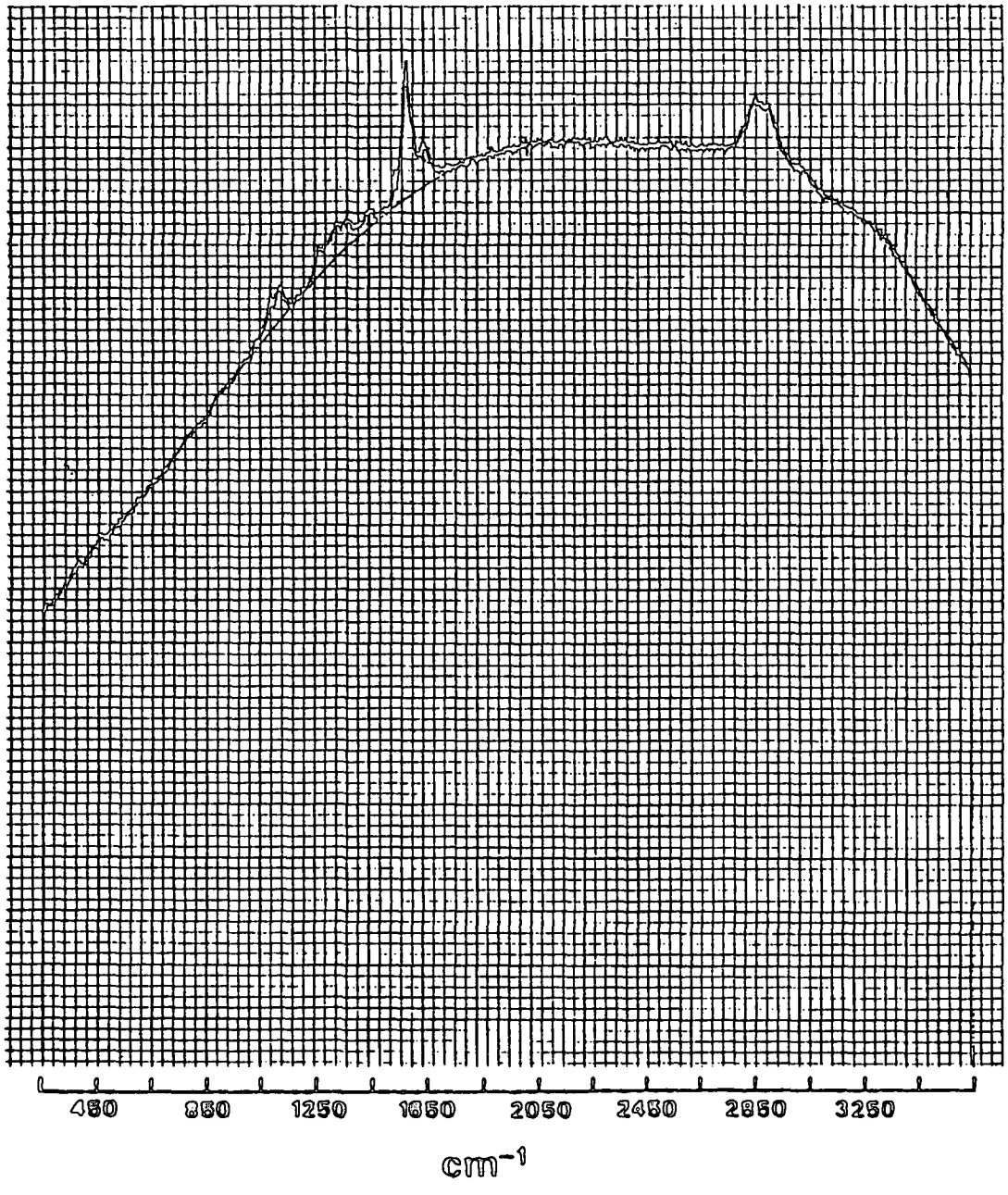

Control - 647.1 nm Excitation

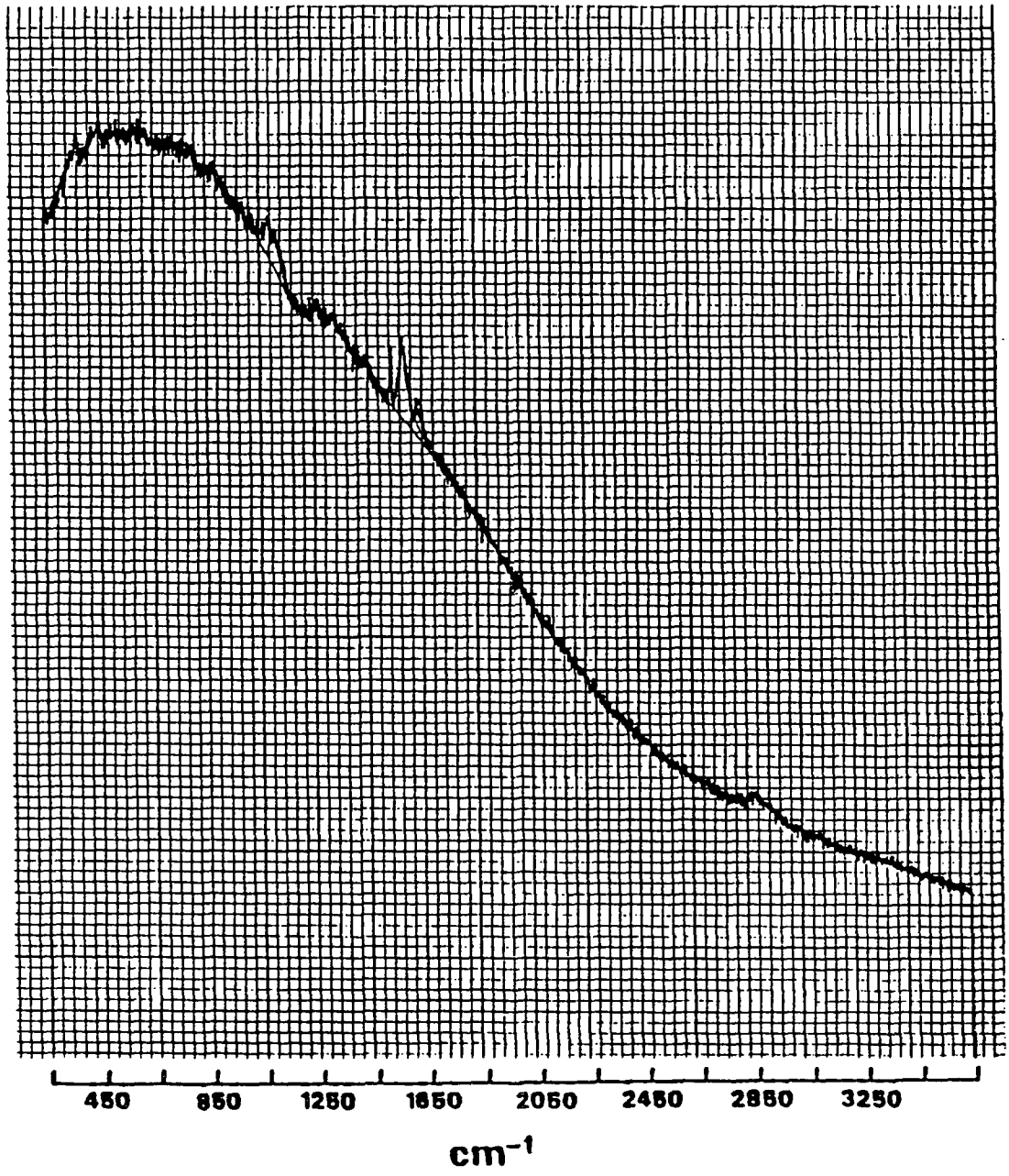

Acid-Chlorite Treatment
514.5 nm Excitation

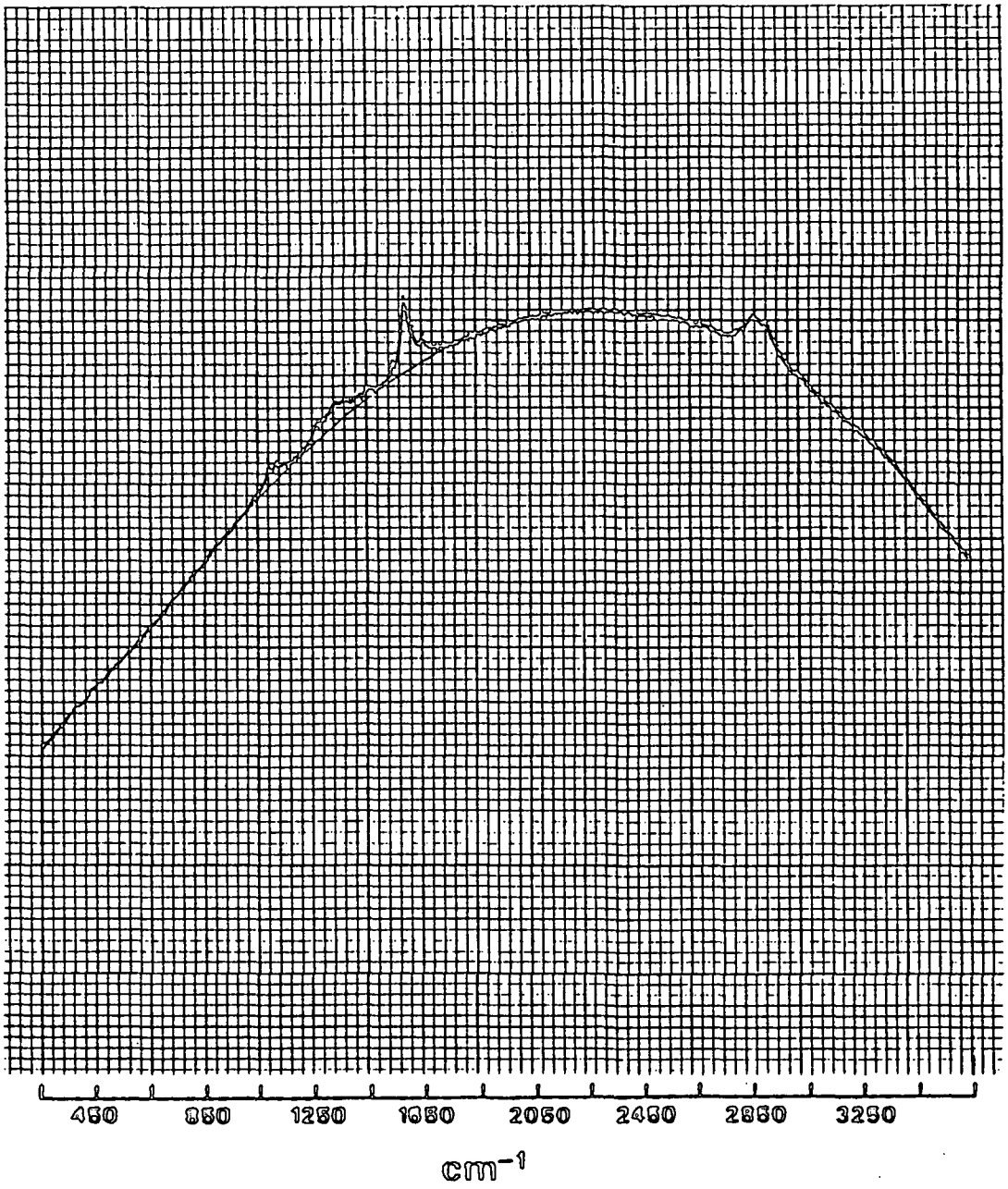

Acid-Chlorite Treatment
647.1 nm Excitation

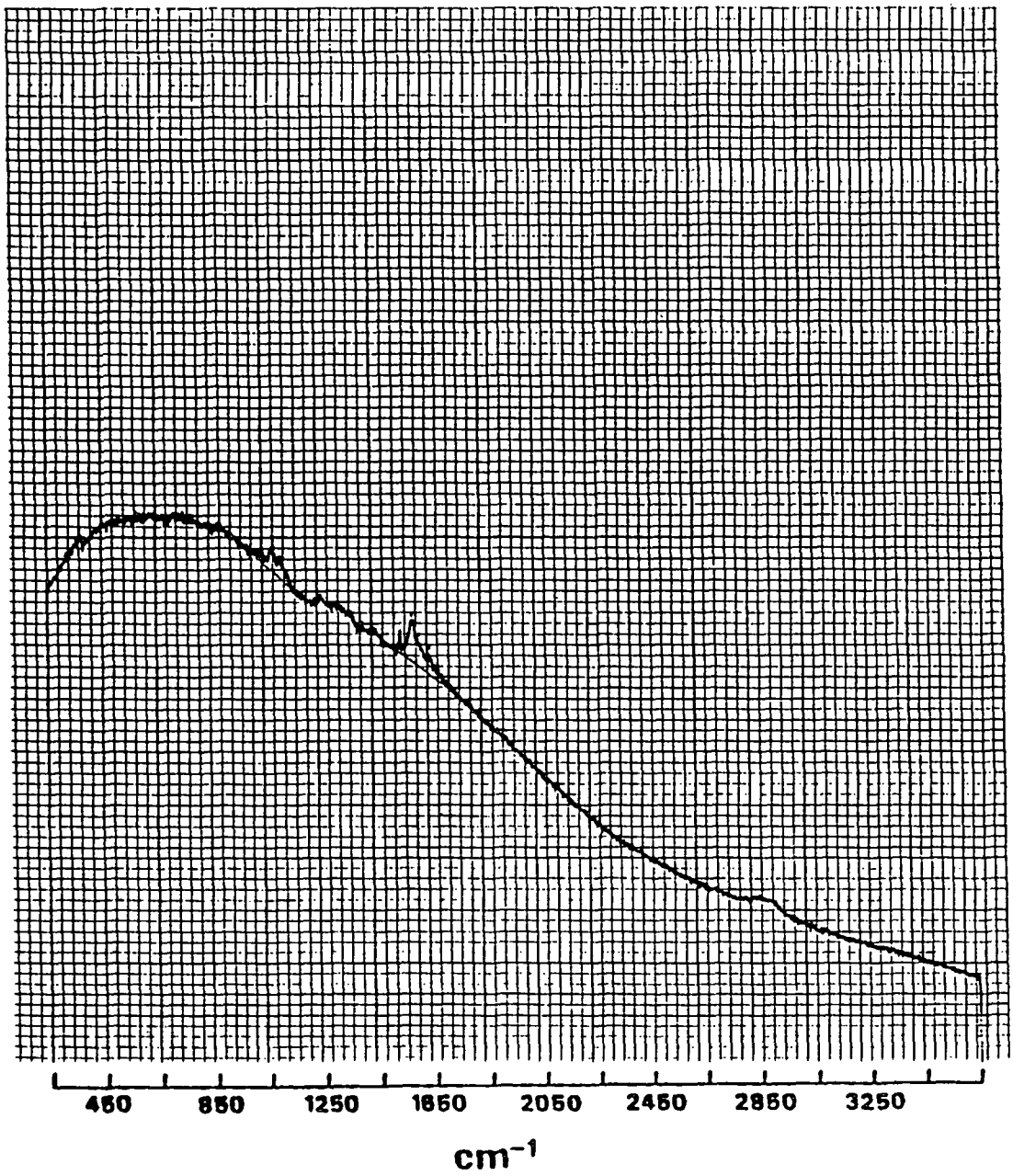

Sodium Borohydride Treatment
514.5 nm Excitation

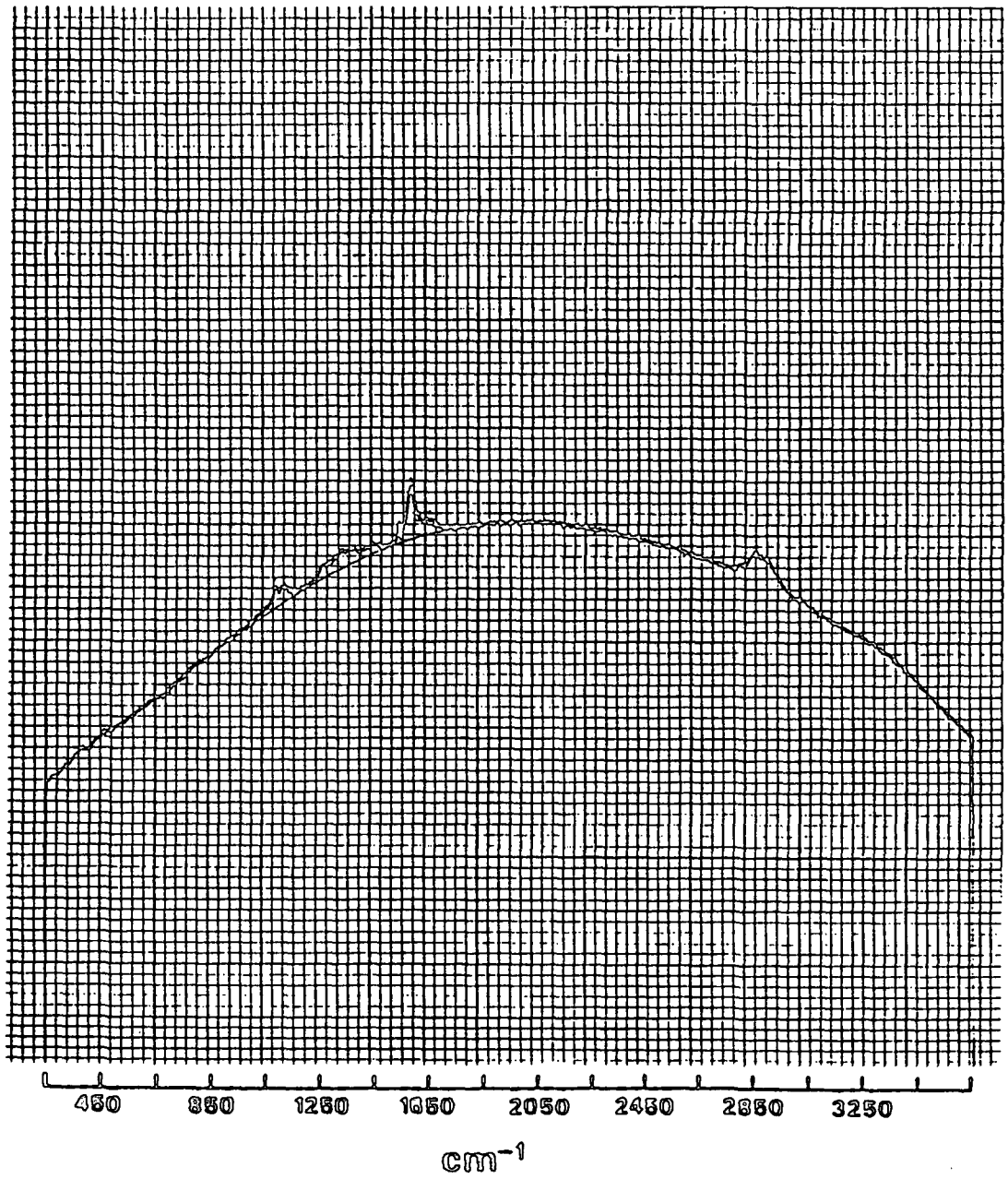

Sodium Borohydride Treatment
647.1 nm Excitation

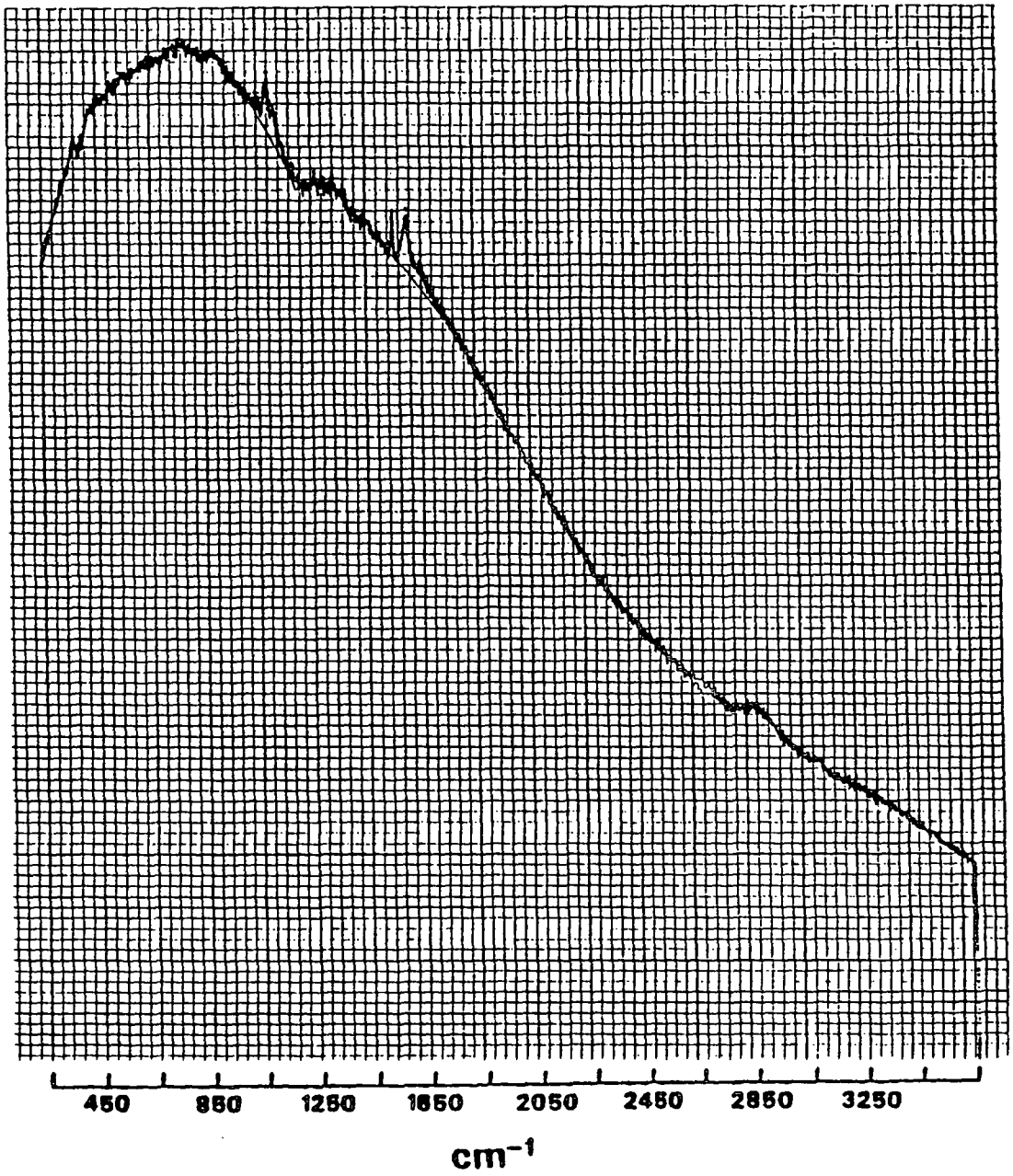

AC/BH Treatment
514.5 nm Excitation

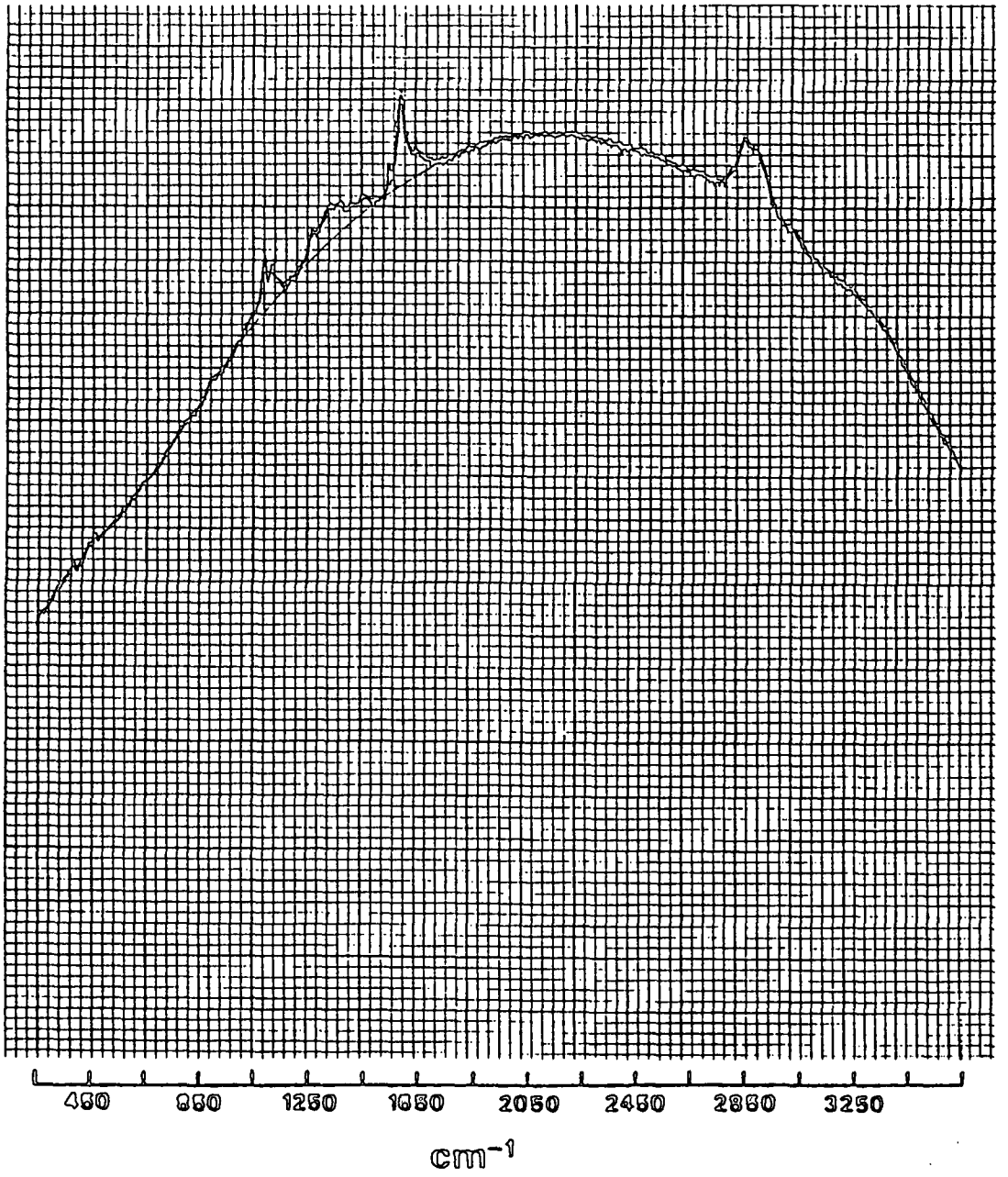

AC/BH Treatment
647.1 nm Excitation

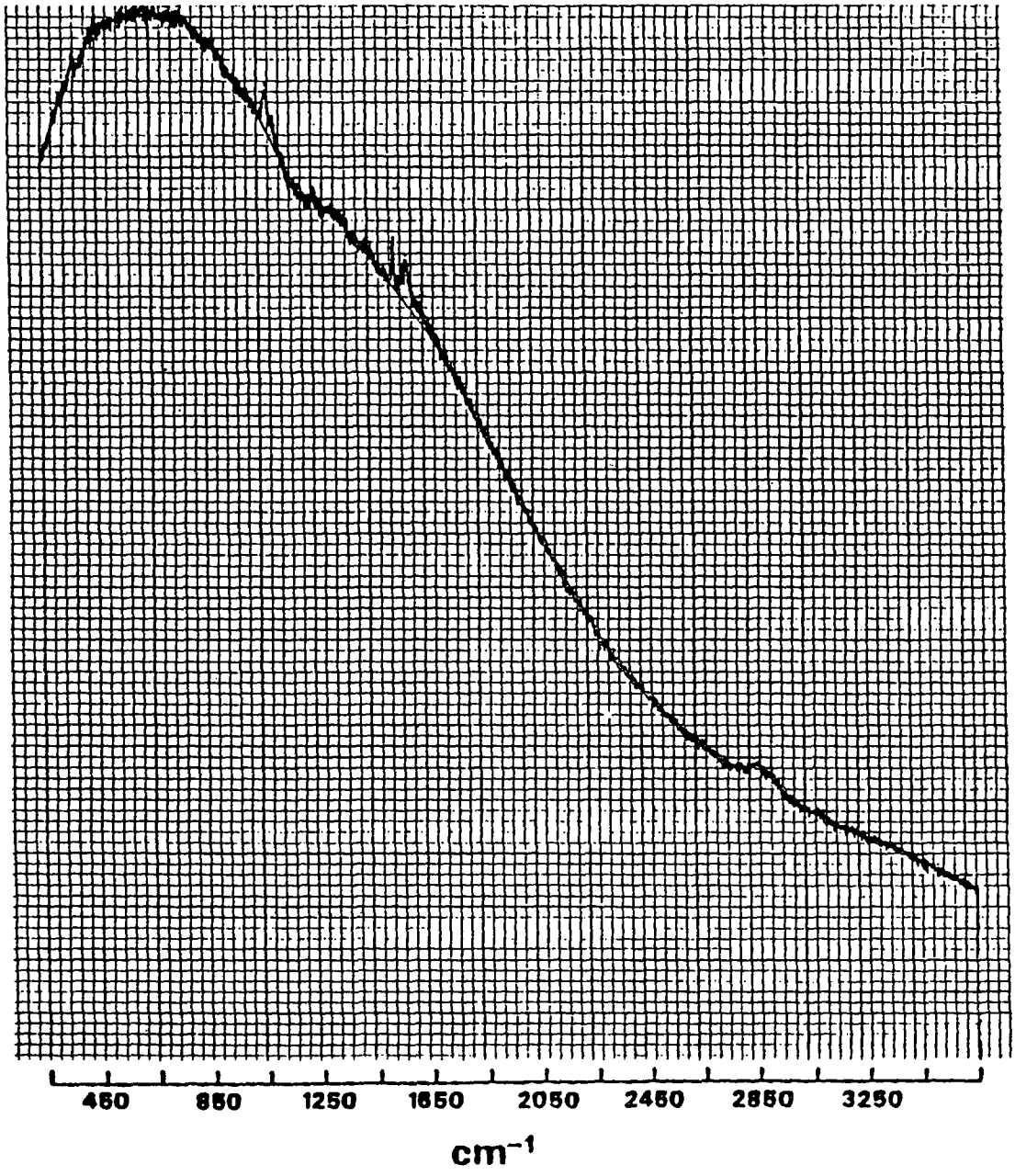

BH/AC Treatment
514.5 nm Excitation

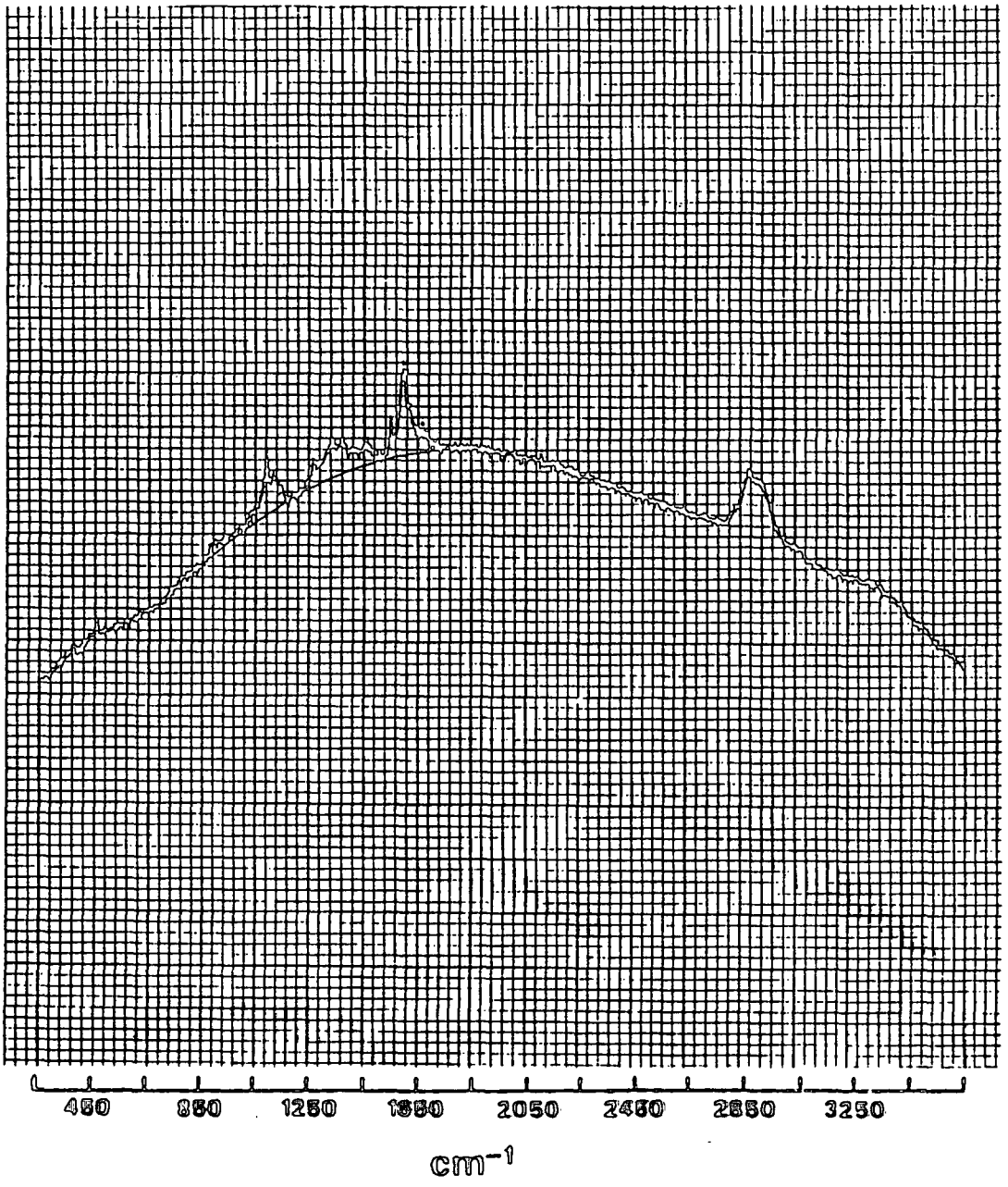

BH/AC Treatment
647.1 nm Excitation

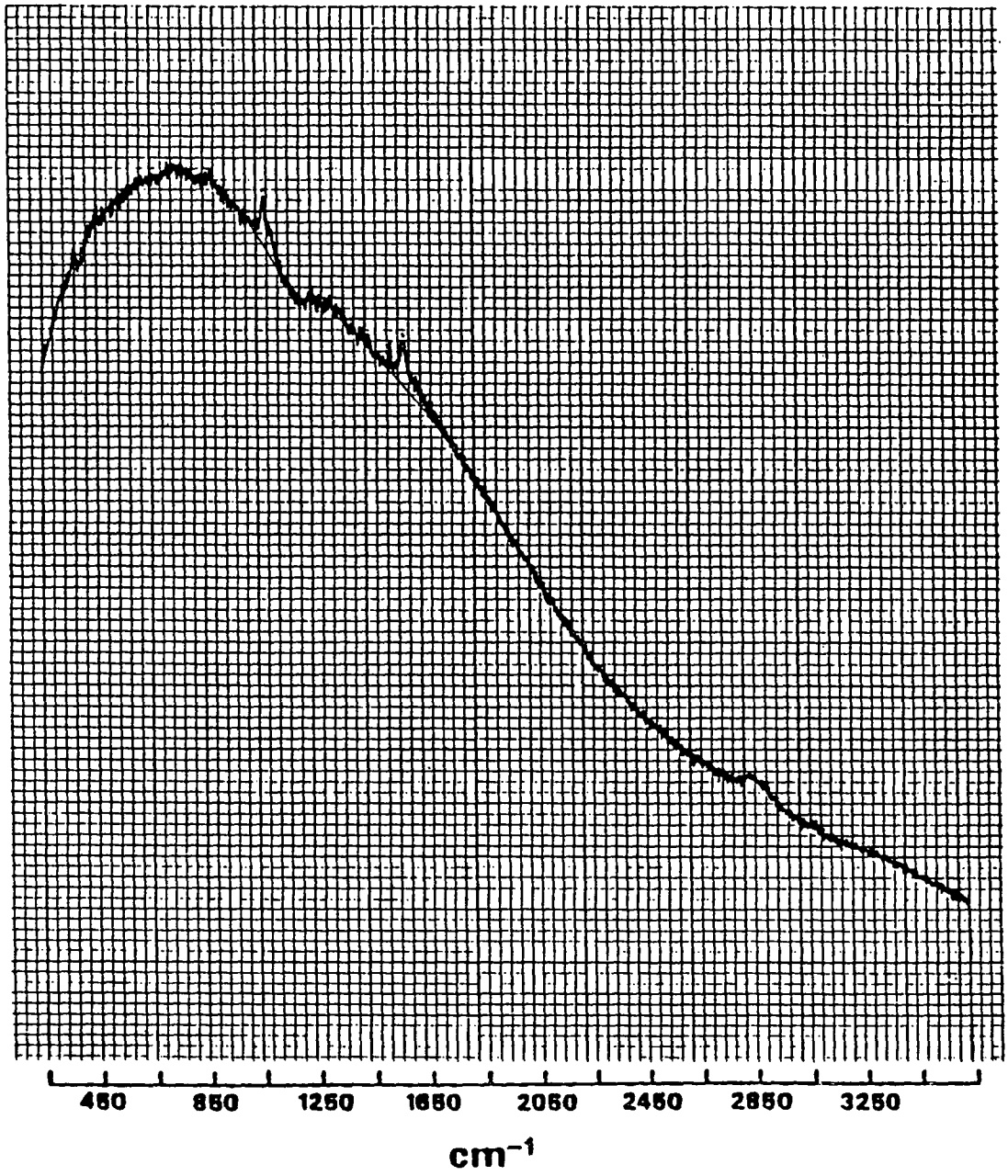

APPENDIX 9. Acid-Chlorite Treated Black Spruce Spectral Mapping Data.

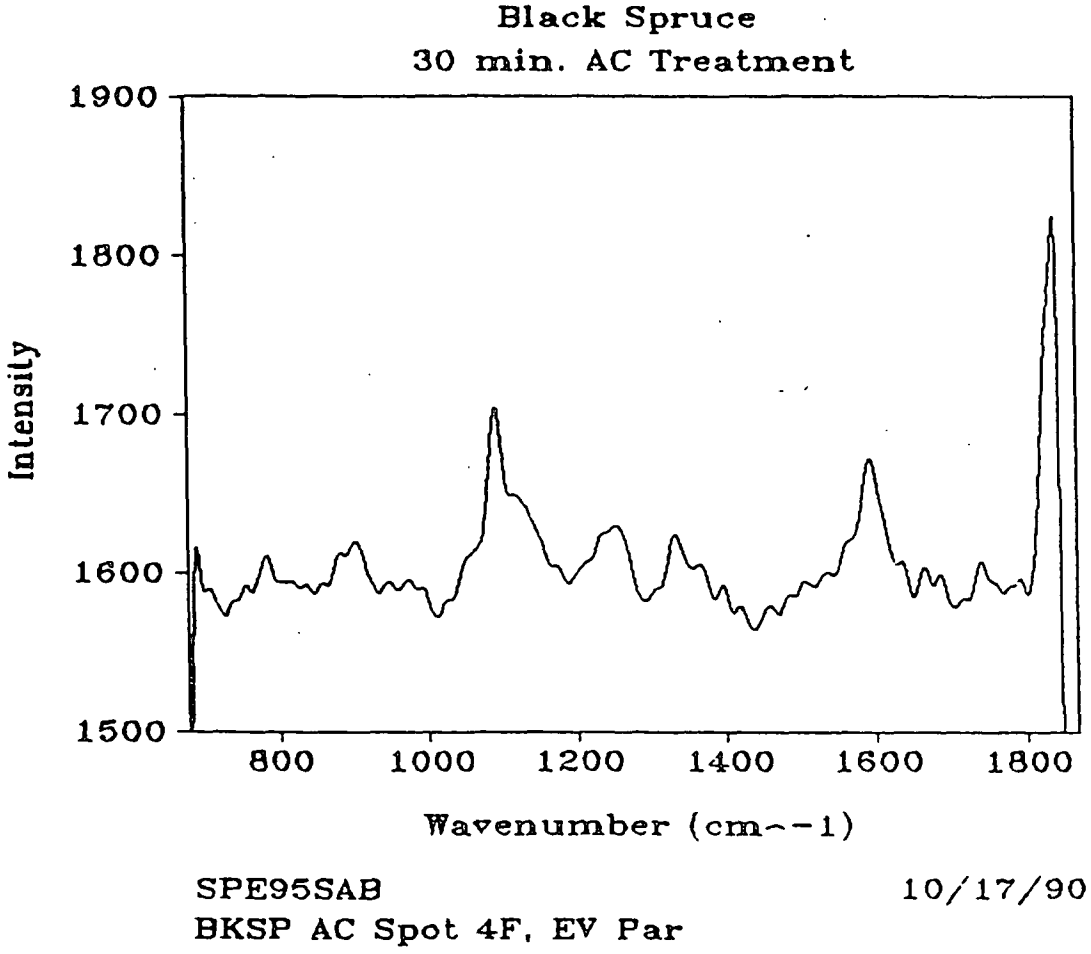
Black Spruce
30 min. AC Treatment
1900
1800
1700
1600
1500
Intensity
800
1000
1200
1400
1600
1800
Wavenumber (cm--1)
SPE95SAB
10/17/90
BKSP AC Spot 4F, EV Par

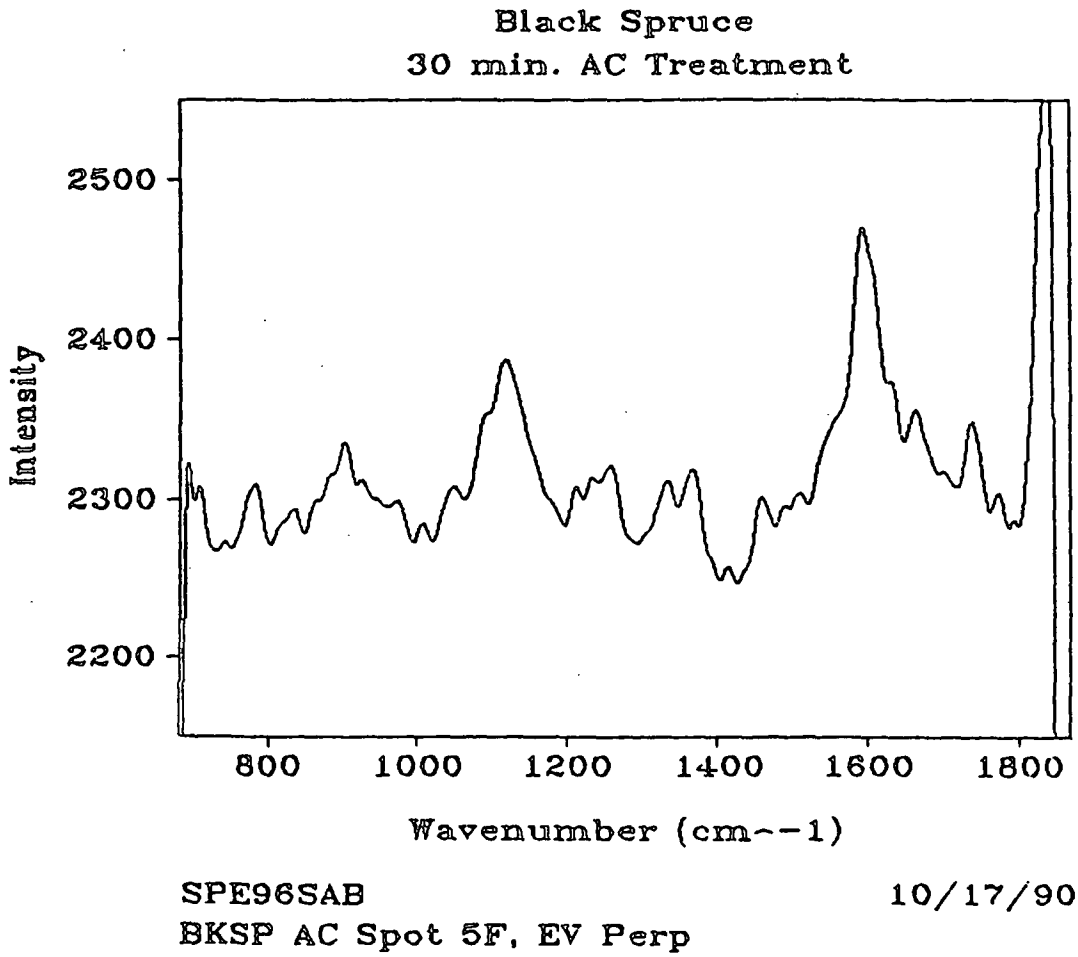
Black Spruce
30 min. AC Treatment
2500
2400
2300
2200
Intensity
800
1000
1200
1400
1600
1800
Wavenumber (cm--1)
SPE96SAB
10/17/90
BKSP AC Spot 5F, EV Perp

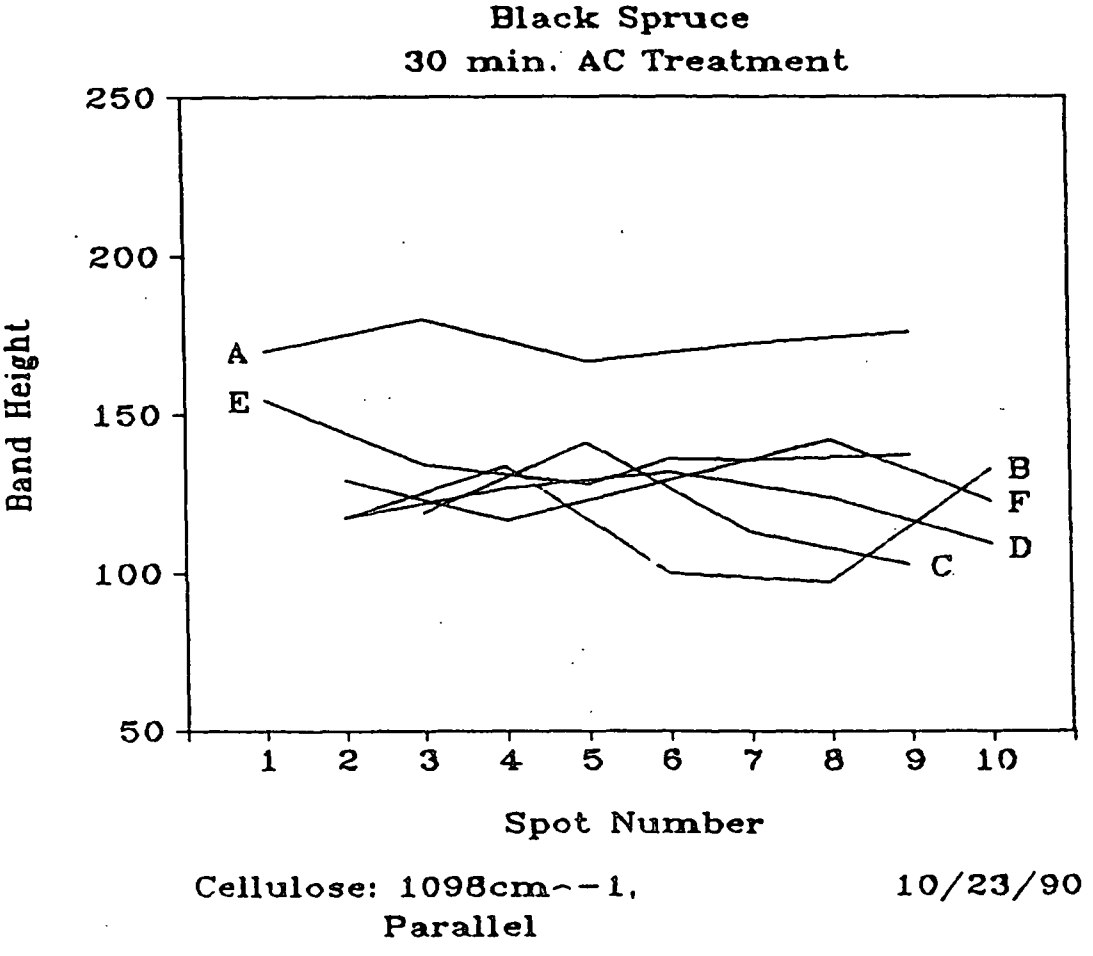
Black Spruce
30 min. AC Treatment
250
200
150
100
50
Band Height
A
E
B
F
D
C
1
2
3
4
5
6
7
8
9
10
Spot Number
Cellulose: 1098cm^-1,
Parallel
10/23/90

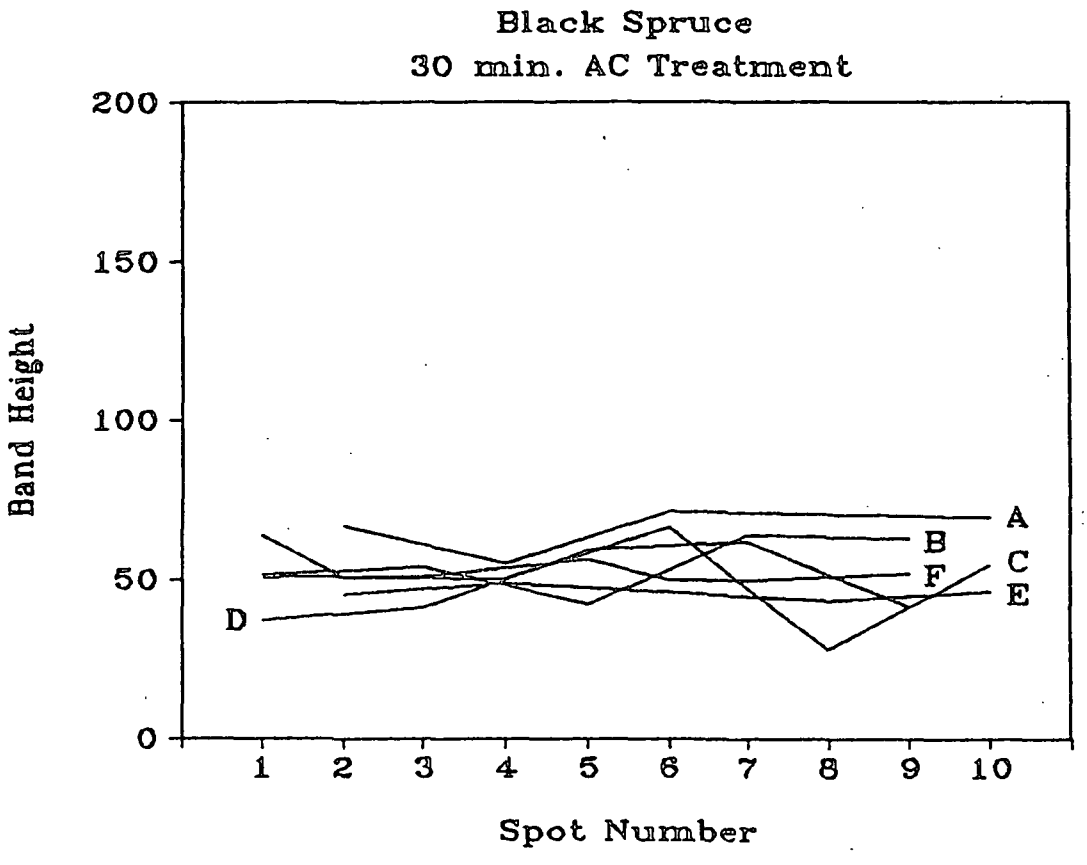

Cellulose: 1098cm--1, 10/23/90
Perpendicular

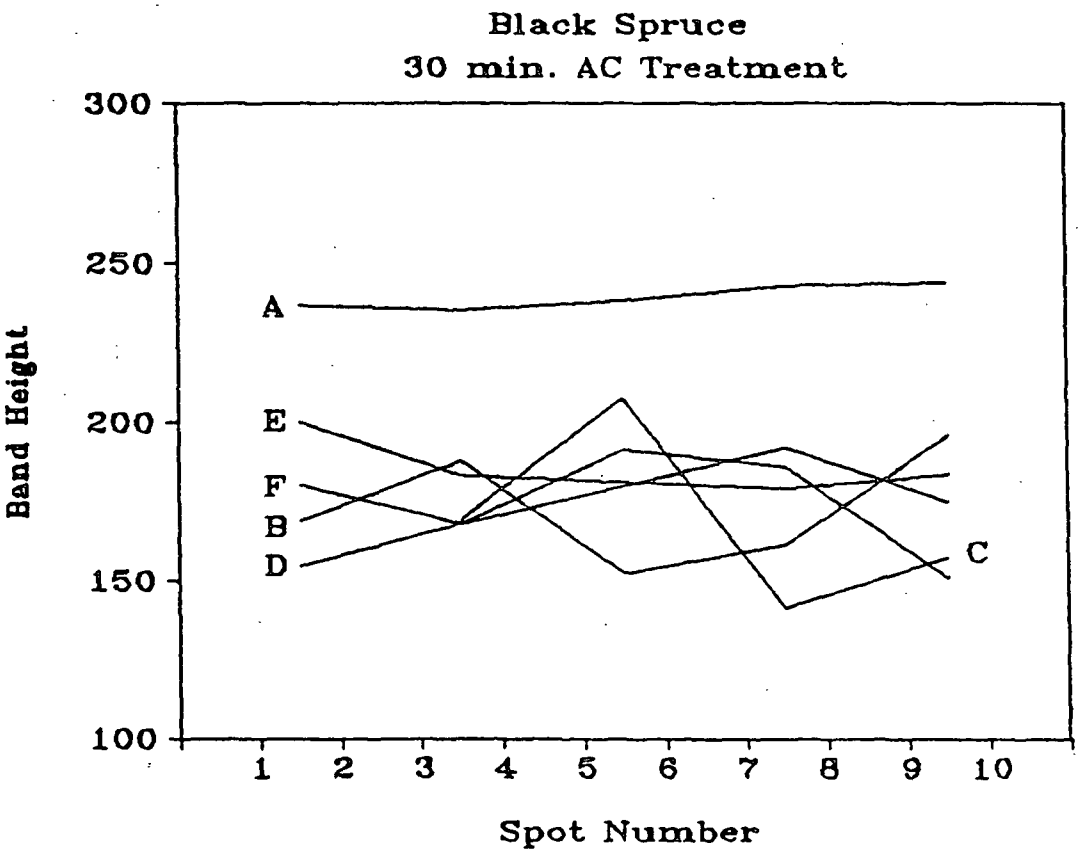

Cellulose: 1098cm^{-1}, 10/23/90
Parallel + Perpendicular

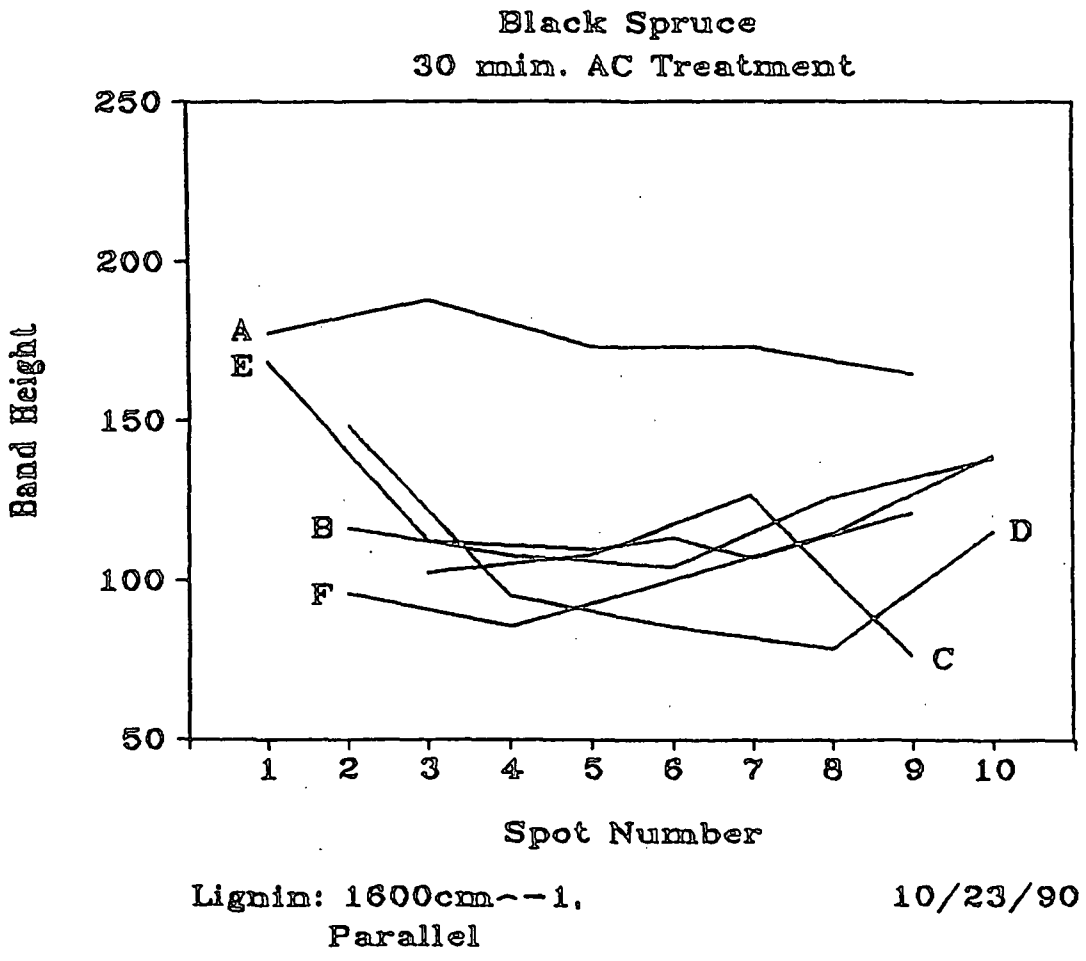
Black Spruce
30 min. AC Treatment
250
200
150
100
50
Band Height
A
E
B
F
C
D
1
2
3
4
5
6
7
8
9
10
Spot Number
Lignin: 1600cm--1,
Parallel
10/23/90

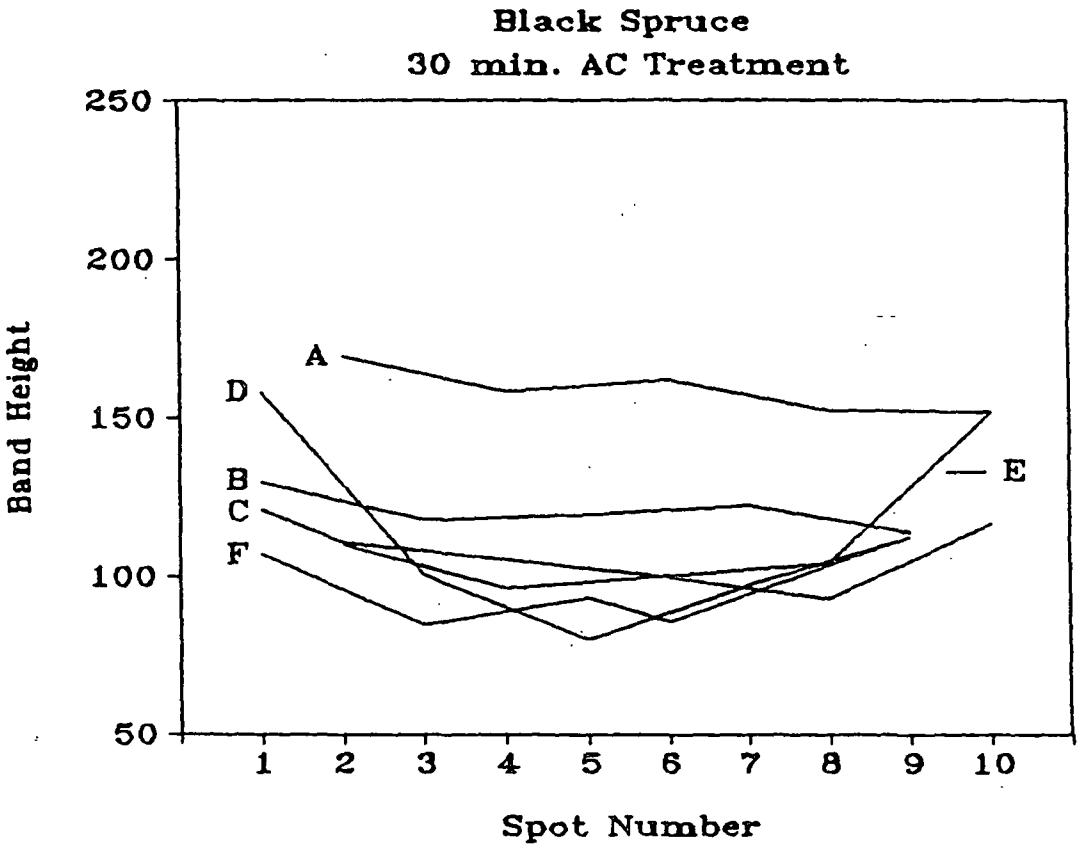
Black Spruce
30 min. AC Treatment
250
200
150
100
50
Band Height
A
D
B
C
F
E
1
2
3
4
5
6
7
8
9
10
Spot Number
Lignin: 1600cm--1,
Perpendicular
10/23/90

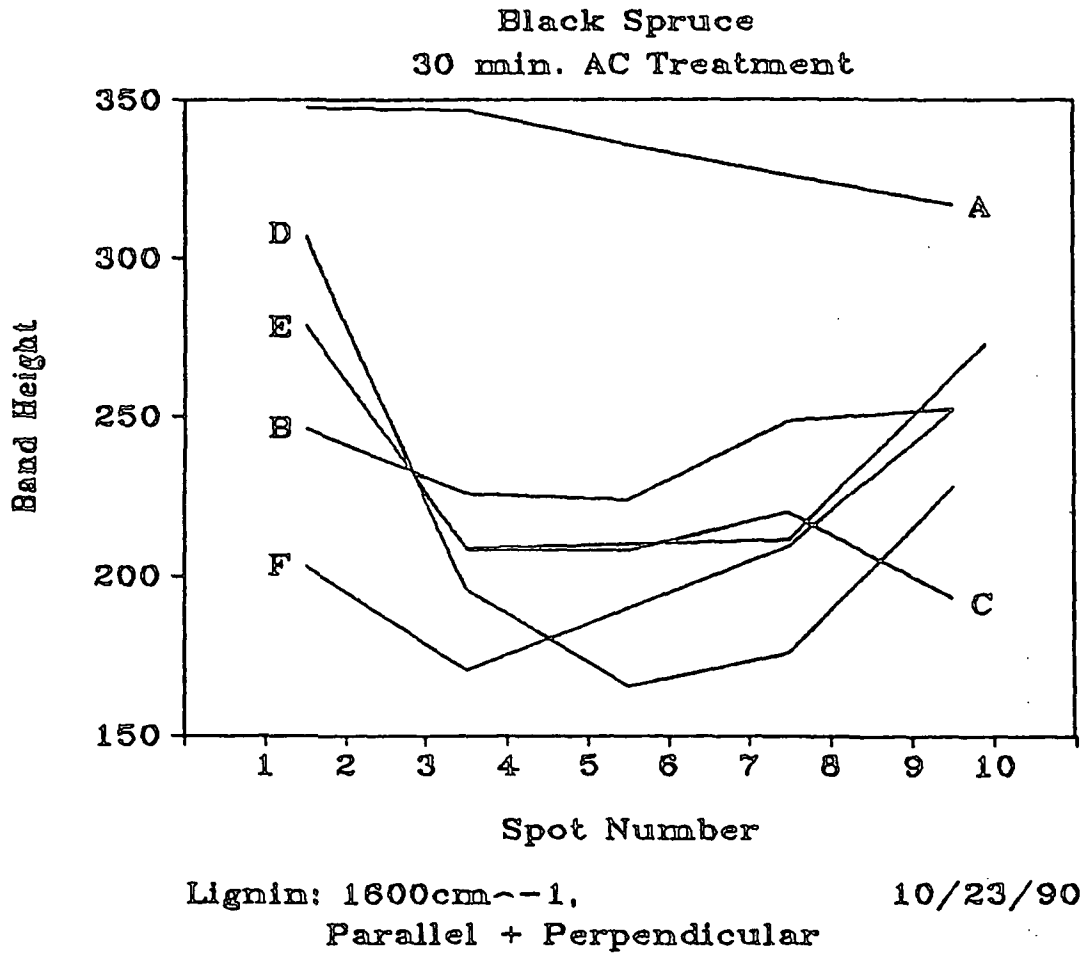
Black Spruce
30 min. AC Treatment
350
300
250
200
150
Band Height
A
D
E
B
F
C
1
2
3
4
5
6
7
8
9
10
Spot Number
Lignin: 1600cm--1,
Parallel + Perpendicular
10/23/90

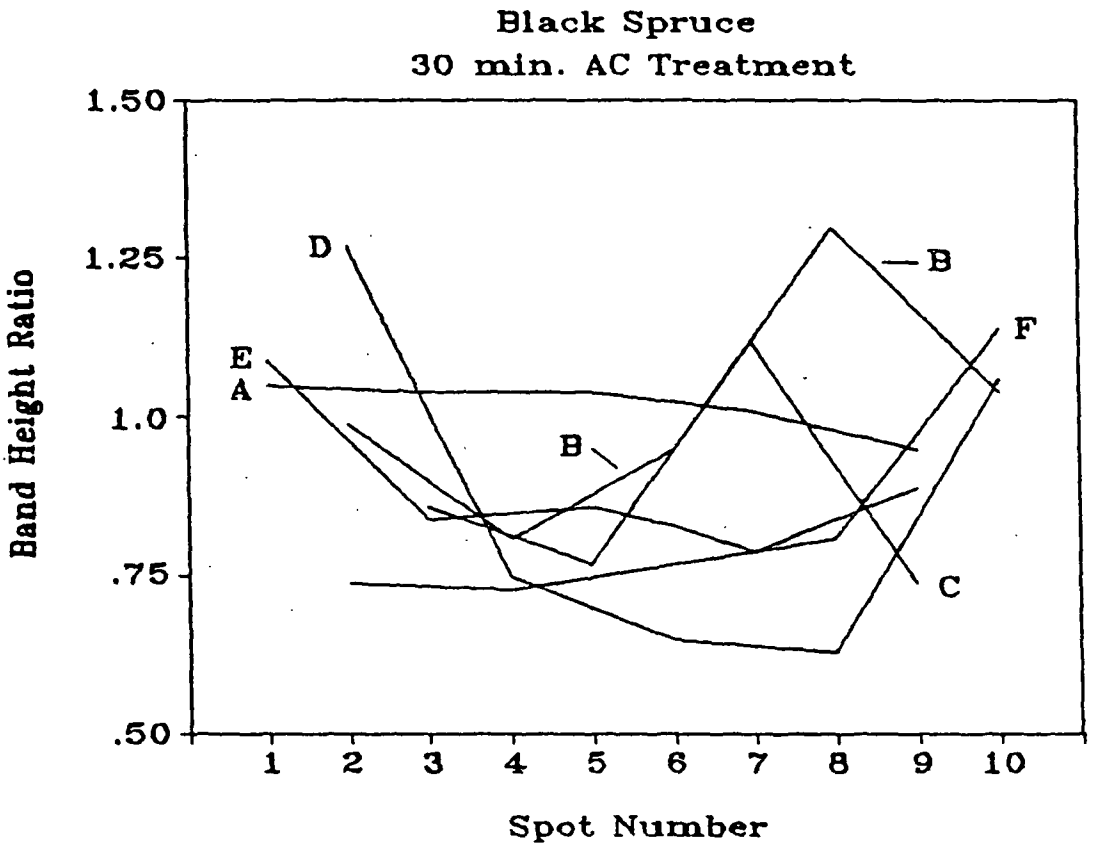

L/C: 1600/1098cm--1 10/23/90
Parallel

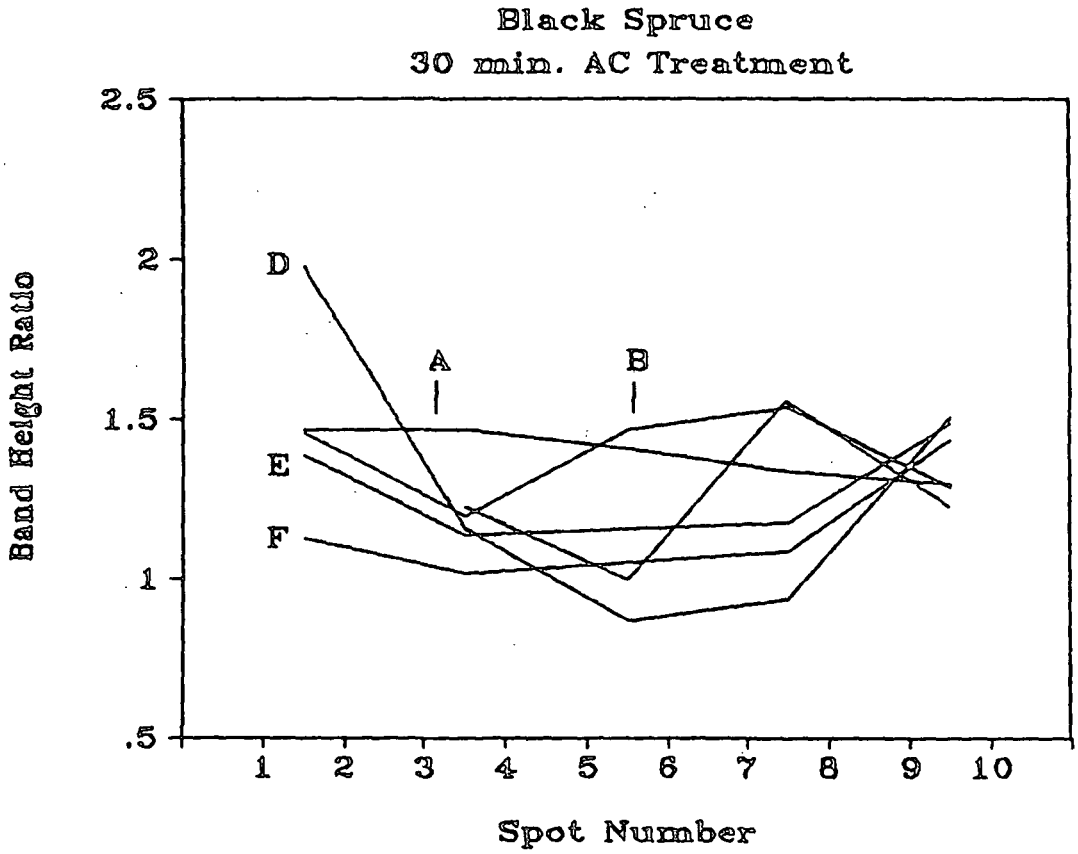
Black Spruce
30 min. AC Treatment
Band Height Ratio
2.5
2
1.5
1
.5
D
A
B
E
F
1
2
3
4
5
6
7
8
9
10
Spot Number
L/C: 1600/1098cm--1
10/23/90
Parallel + Perpendicular

APPENDIX 10. Loblolly Pine Spectral Mapping Data.

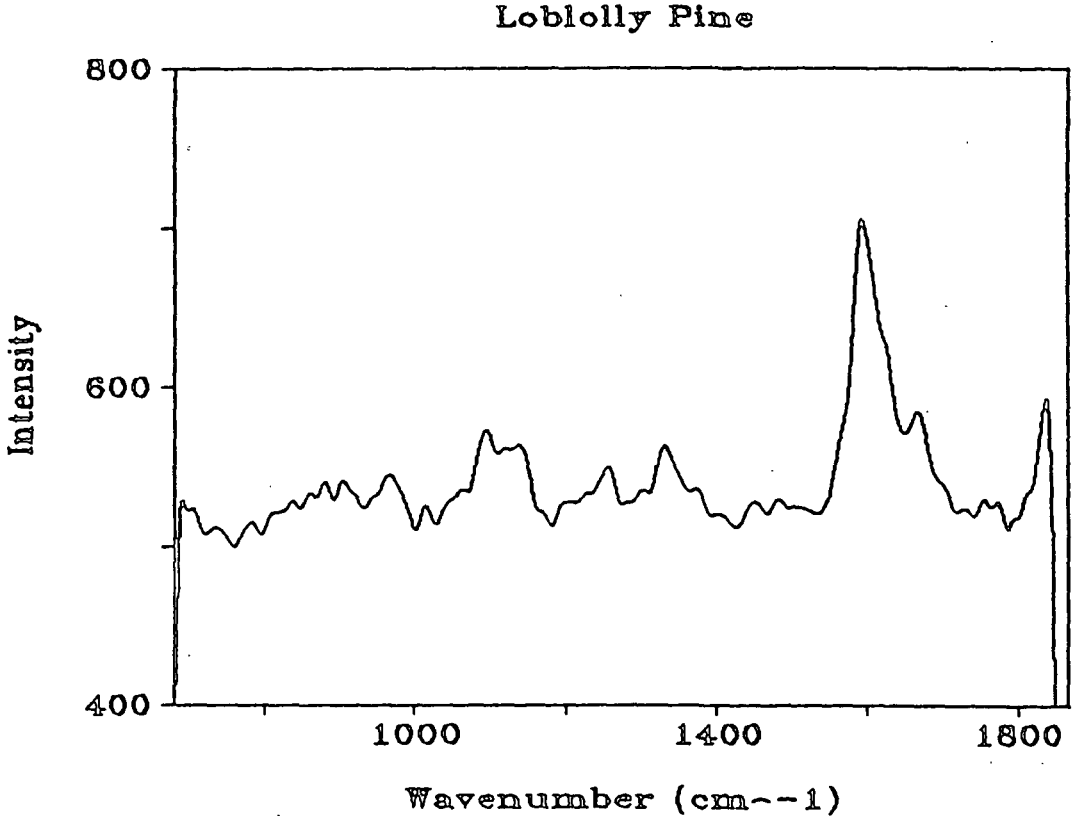
Loblolly Pine
800
600
400
Intensity
1000
1400
1800
Wavenumber (cm--1)
48
06/21/90
Lob Pine Spot 3E Par

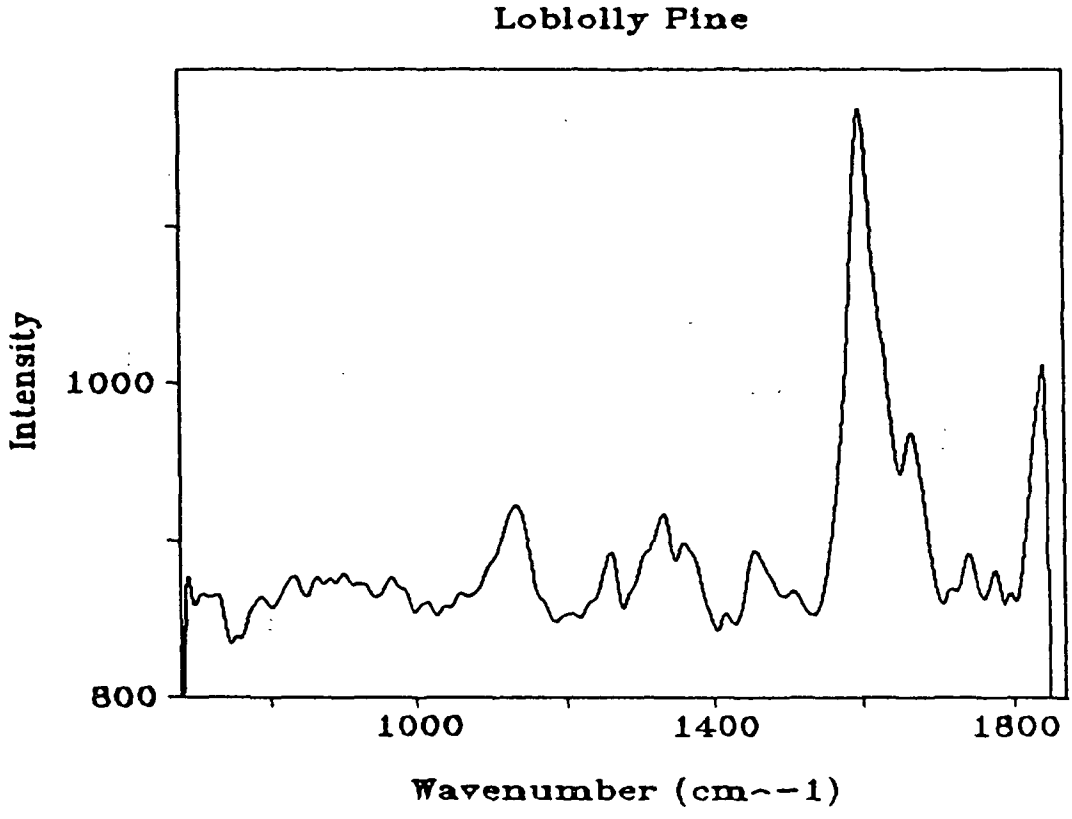
Loblolly Pine
Intensity
1000
800
1000
1400
1800
Wavenumber (cm--1)
49
06/21/90
Lob Pine Spot 4E Perp

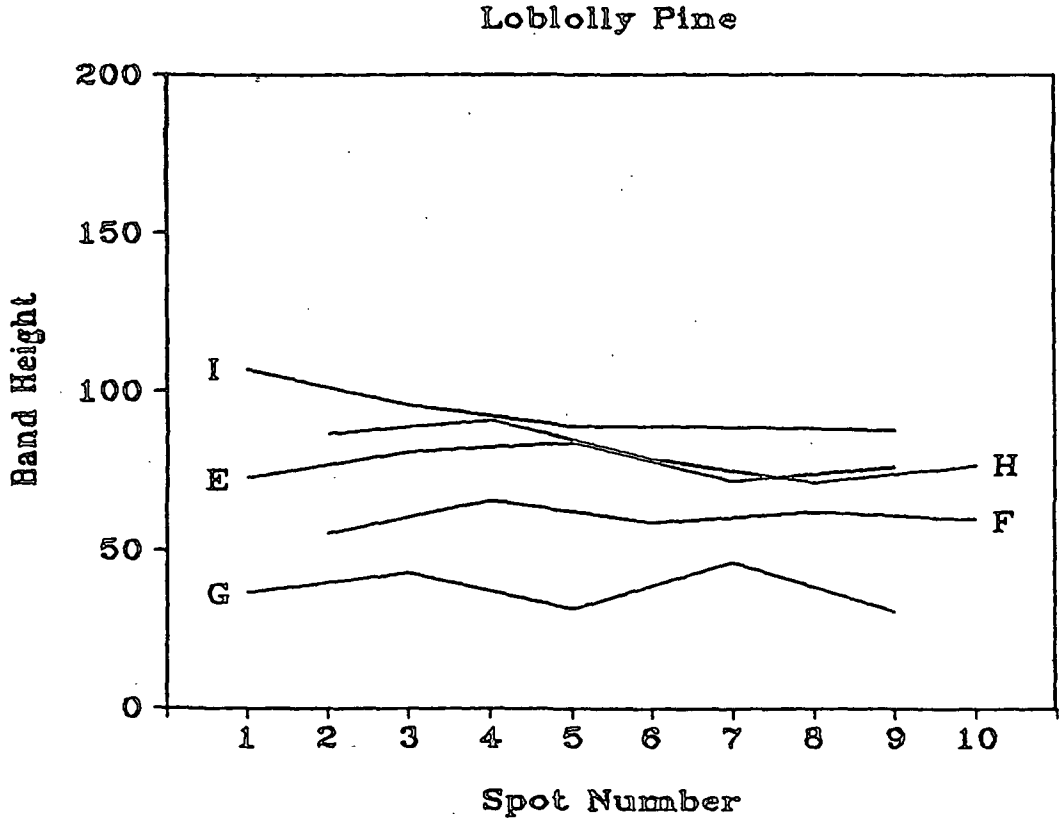
Loblolly Pine
200
150
100
50
0
Band Height
I
E
G
H
F
1
2
3
4
5
6
7
8
9
10
Spot Number
Cellulose: 1098cmm--1,
Parallel
07/24/90

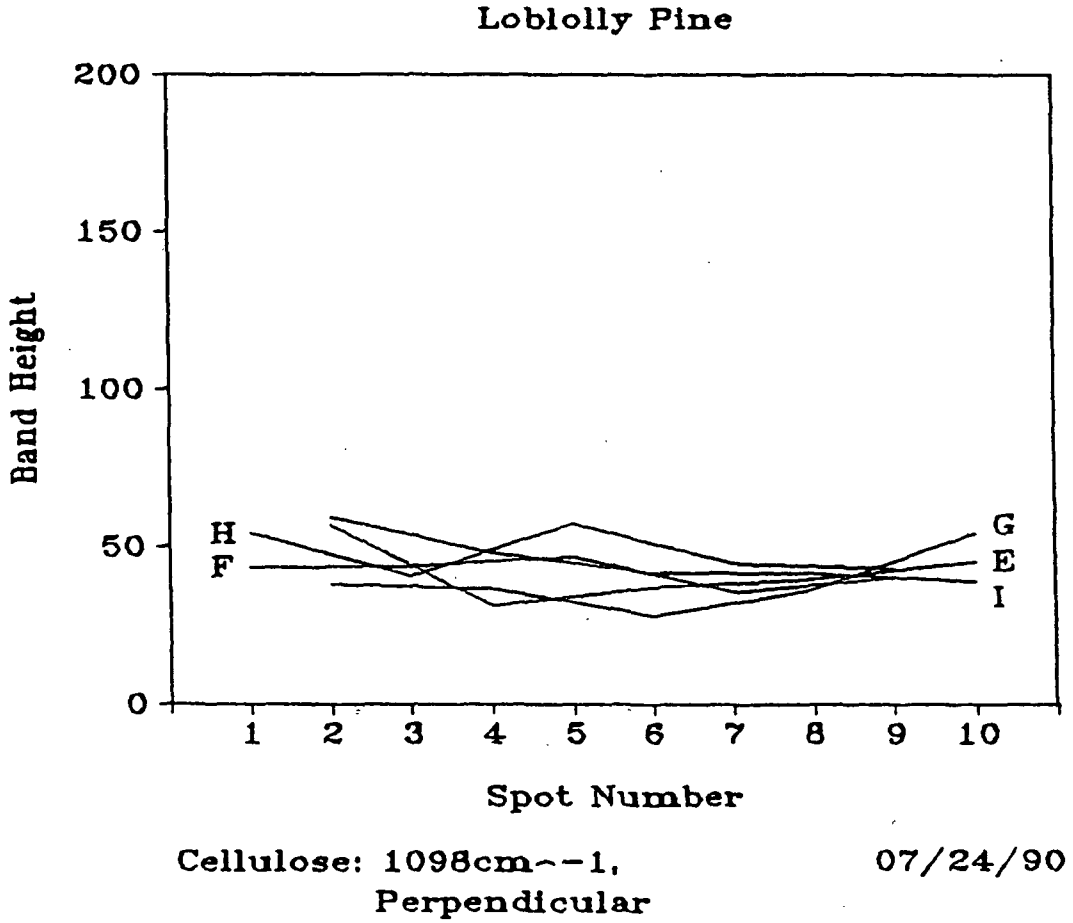
Loblolly Pine
200
150
100
50
0
Band Height
H
F
G
E
I
1
2
3
4
5
6
7
8
9
10
Spot Number
Cellulose: 1098cm--1,
Perpendicular
07/24/90

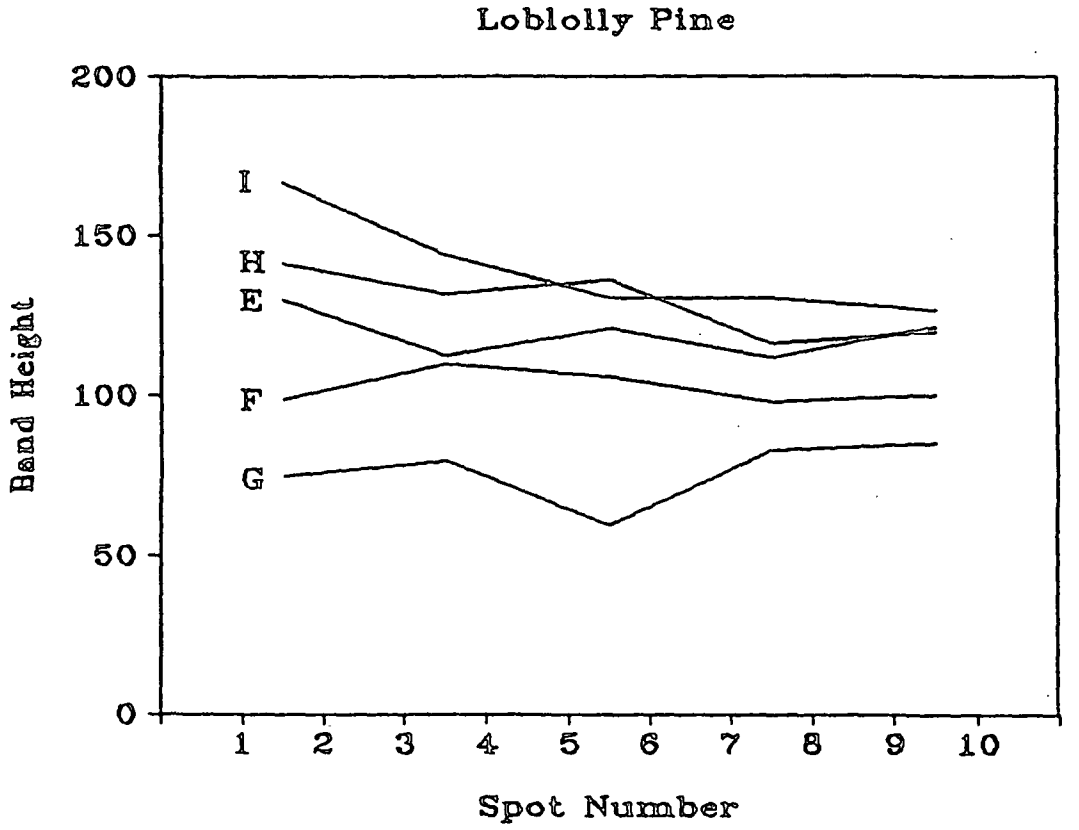
Loblolly Pine
200
150
100
50
0
Band Height
I
H
E
F
G
1
2
3
4
5
6
7
8
9
10
Spot Number
Cellulose: 1098cm~-1,
07/24/90
Parallel + Perpendicular

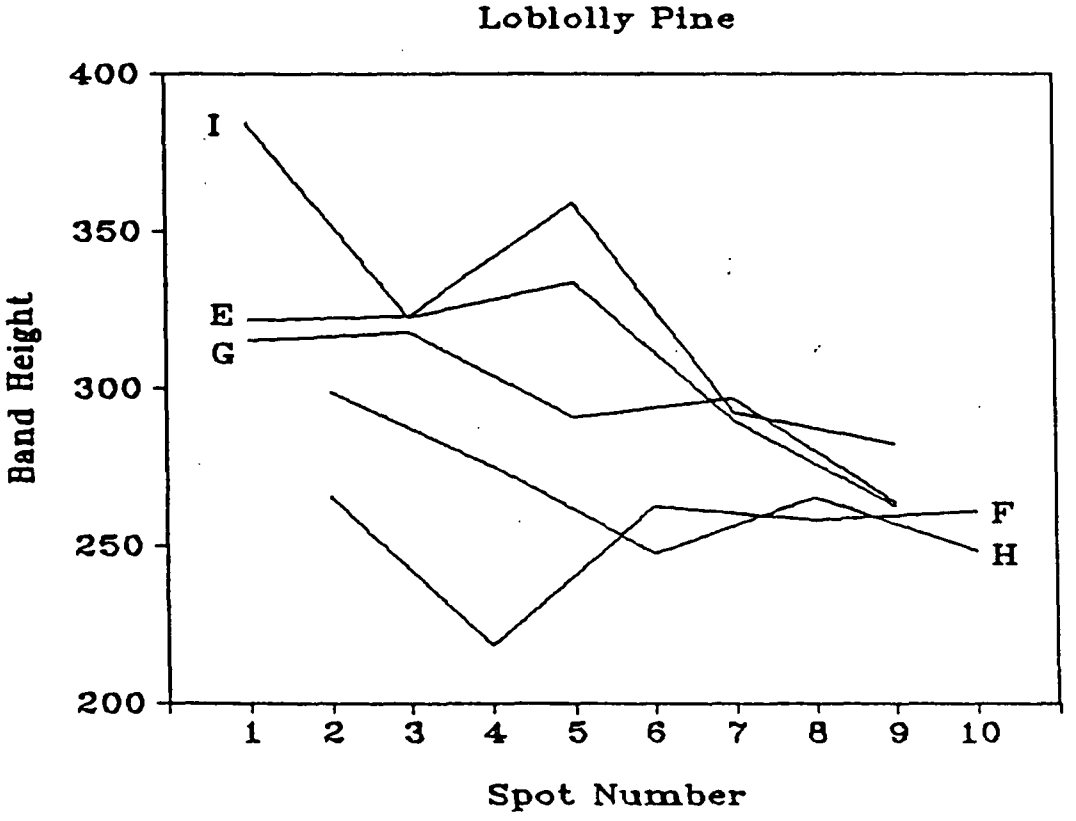

Lignin: 1600cm--1, 07/24/90
Parallel

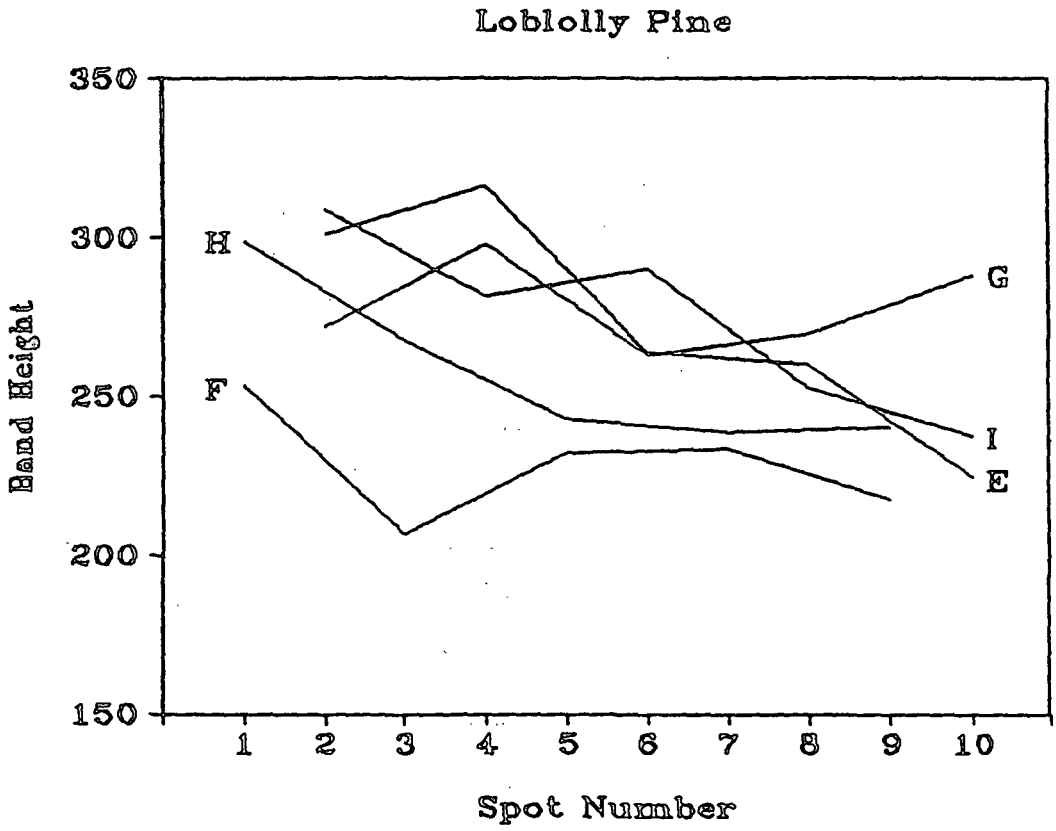
Loblolly Pine
350
300
250
200
150
Band Height
H
F
G
I
E
1
2
3
4
5
6
7
8
9
10
Spot Number
Lignin: 1600cm--1,
Perpendicular
07/24/90

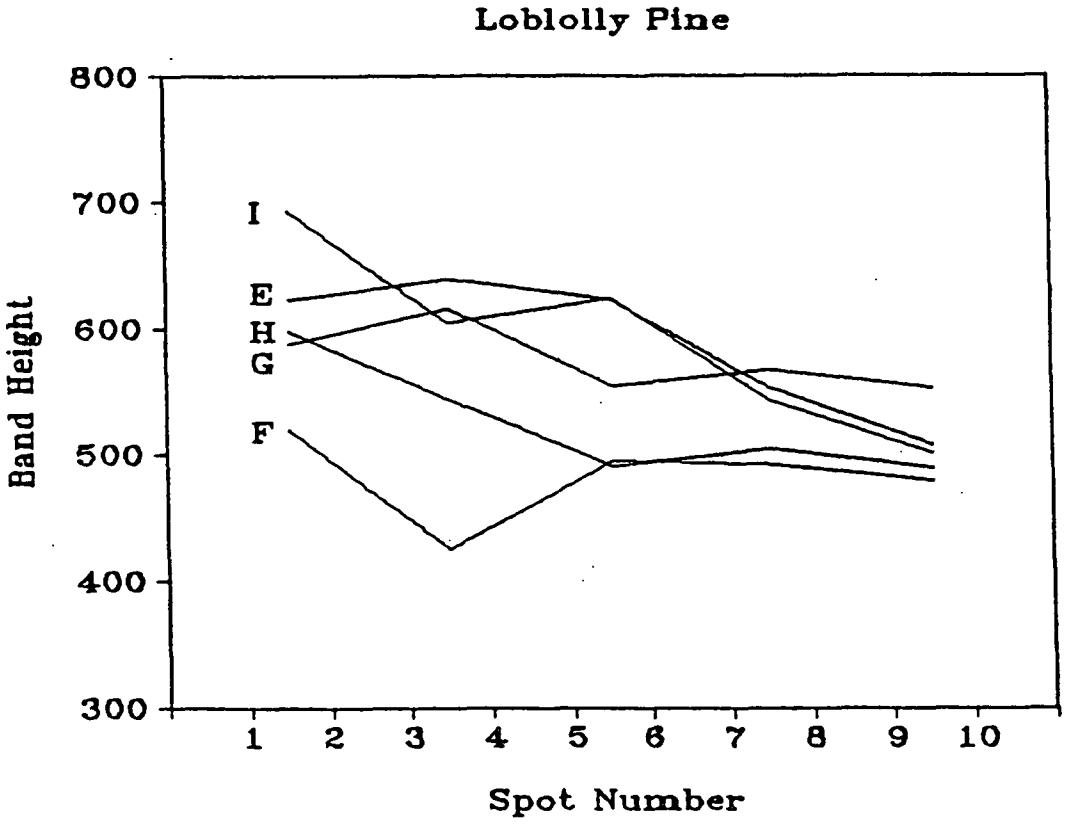

Lignin: 1600cm^-1, 07/24/90
Parallel + Perpendicular

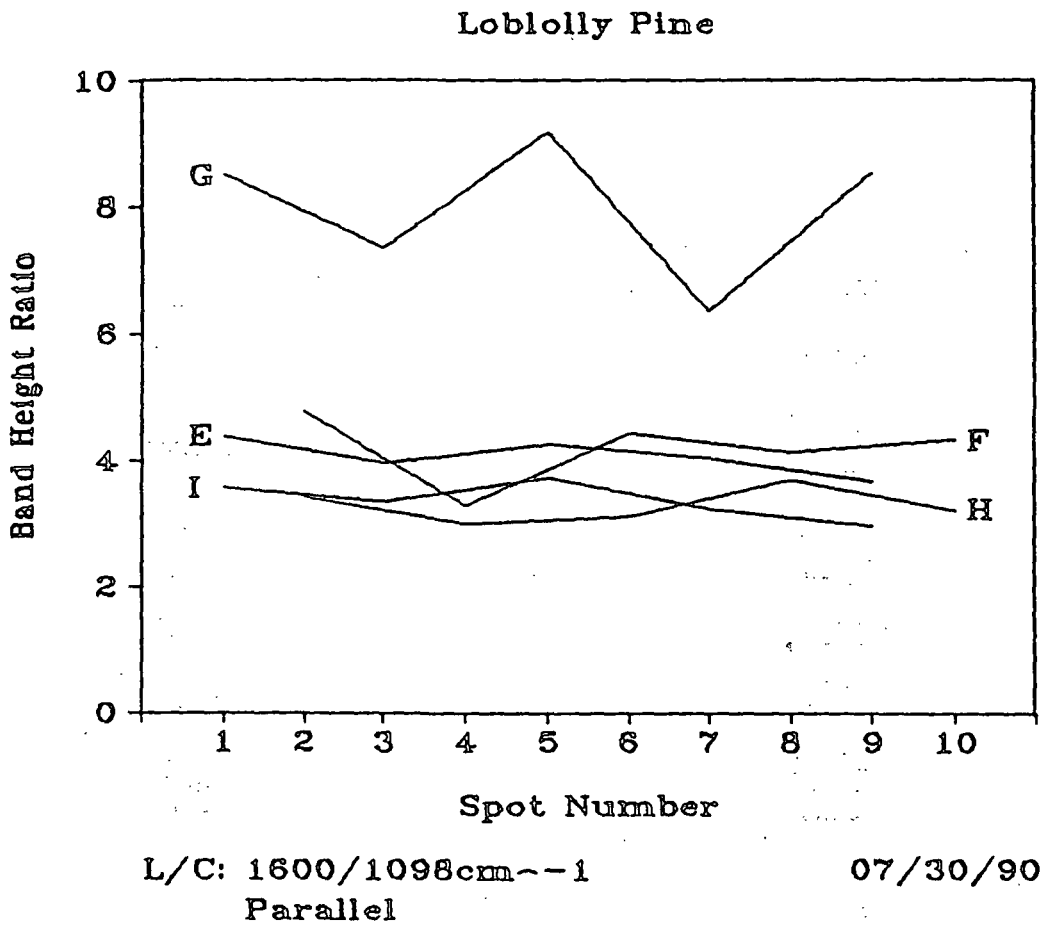
Loblolly Pine
Band Height Ratio
10
8
6
4
2
0
G
E
I
F
H
1
2
3
4
5
6
7
8
9
10
Spot Number
L/C: 1600/1098cm--1
Parallel
07/30/90

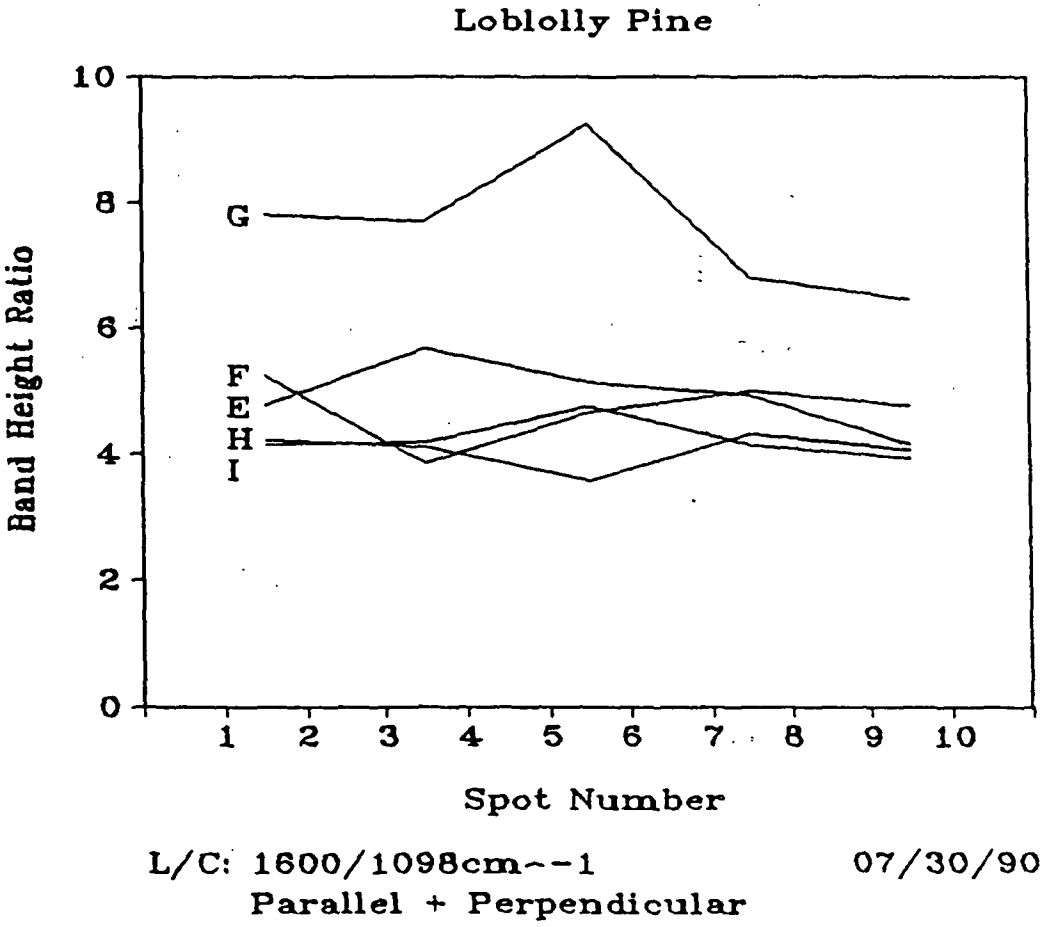
Loblolly Pine
Band Height Ratio
10
8
6
4
2
0
G
F
E
H
I
1
2
3
4
5
6
7
8
9
10
Spot Number
L/C: 1600/1098cm--1
07/30/90
Parallel + Perpendicular